IKE Institut für Kernenergetik
und Energiesysteme

Coolability of Corium Debris under Severe Accident Conditions in Light Water Reactors

Saidur Rahman

November 2013 IKE 2 -155

Universität Stuttgart

IKE Institut für Kernenergetik
und Energiesysteme

Coolability of Corium Debris under Severe Accident Conditions in Light Water Reactors

von der Fakultät Energie-, Verfahrens- und Biotechnik der Universität Stuttgart zur Erlangung der Würde eines Doktor-Ingenieurs (Dr.-Ing.) genehmigte Abhandlung

vorgelegt von

Saidur Rahman

geboren in Faridpur / Bangladesch

Hauptberichter: Prof. Dr.-Ing. habil. Eckart Laurien

Mitberichter: Prof. Dr.-Ing. habil. Manfred Piesche

Tag der mündlichen Prüfung: 07.Oktober 2013

ISSN –0173– 6892

November 2013 IKE 2 -155

Universität Stuttgart

I Abstract

The debris bed which may be formed in different stages of a severe accident will be hot and heated by decay heat from the radioactive fission products. In order to establish a steady state of long-term cooling, this hot debris needs to be quenched at first. If quenching by water ingression into the dry bed is not rapid enough then heat-up by decay heat in still dry regions may again yield melting. Thus, chances of coolability must be investigated considering quenching against heat-up due to decay heat, in the context of reactor safety research. As a basis of the present investigations, models for simulation of two phase flow through porous medium were already available in the MEWA code, being under development at IKE. The objective of this thesis is to apply the code in essential phases of severe accidents and to investigate the chances, options and measures for coolability. Further, within the tasks, improvements to remove weaknesses in modeling and implementation of extensions concerning missing parts are included. An emphasis with this respect is posed to qualify the friction and heat transfer models which are decisive for determining the cooling process (flow conditions) inside the debris bed.

It was identified previously that classical models without explicit considering the interfacial friction, can predict dryout heat flux (DHF) well under top fed condition but under-predict DHF values under bottom flooding conditions. Tung & Dhir introduced an interfacial friction term in their model, but this model has deficits for smaller particles considered as relevant for reactor conditions. Therefore, some modification of Tung & Dhir model is proposed in the present work to extent it for smaller particles. A significant improvement with the new friction description (Modified Tung & Dhir, MTD) is obtained considering the aim of a unified description for both top and bottom flooding conditions and for broad bandwidth of bed conditions. Concerning heat transfer, it has been found from validation calculations that, except in cases with large forced bottom injection, water moves into the debris bed in a slowly propagating front due to high friction, and the quenching is rapid enough to occur in a thin front (few mm). Thus, a detailed modeling of thin heat transfer regimes is less important, rather an appropriate description for the friction is essential.

Calculations for reactor conditions are carried out in order to explore whether or to which degree coolability can be concluded, how strong the trend to coolability is and where major limits occur. The general result from the various calculations in this work is that there exist significant cooling margins and strong trends to coolability which is achieved due to multidimensional cooling options, especially lateral and bottom ingression of water, established in the core region through an intact rod or bypass region, in the lower head through the wall and in the cavity due to the shape (heap) of the bed. These cooling options together with cooling effects of steam flow through a hot dry zone provide mechanisms to facilitate and support quenching processes. Limits also have been obtained, mainly with significant piling up of particles, cake parts with very low porosities and bed with very small particles. Calculations results on in-vessel reactor conditions show that much larger amount of debris bed can be coolable in the core region (up to 100 tons) than in the lower head (up to 40 tons). This is due to the different bed configurations which delayed the establishment of bottom quenching and subsequent steam cooling in the lower head

as compared to the core, where it starts immediately. Nevertheless, the lower head still has significant cooling potential for conditions of limited melt release. Compared to the relocated molten mass of ~20 t in the TMI-2 accident, the amount of coolable debris mass is still significant. For ex-vessel configurations, deep water pool indicates good chances of coolability for thin diameter melt jet due to complete breakup of melt. For thicker melt jet, melt jet breakup is incomplete. In this case, injection of water from below may be combined with deep water pool for the improvement of melt/debris coolability.

The initial temperature distribution inside the bed has a major influence on the coolability behavior of the bed, no matter if the bed is located in the lower head or in the flooded cavity. Previously, quenching calculations were only possible for given debris configurations starting from assumed initial temperatures. However, assuming the whole bed at a uniform initial temperature strongly misses the real process in which settling of partly solidified melt drops occurs simultaneously with water inflow and quenching. Therefore, in the frame of this work, the MEWA models have been extended i.e. coupled to jet breakup and mixing model (JEMI) to treat the combined process. This improved the capabilities of realistic analysis significantly and showed significant effects on cooling in the calculations. Another important step for the improvement of overall modeling of coolability is undertaken by introducing the porosity formation in liquid melt layers through the supply of water from the bottom (COMET concept) in the MEWA model. The related modeling is implemented for situations where liquid melt arrives un-fragmented at the cavity floor due to incomplete breakup of melt.

II Zusammenfassung

Im Verlauf eines schweren Reaktor-Unfalls kann es dazu kommen, dass der Reaktorkern sich bei unzureichender Kühlung aufgrund der freigesetzten Nachzerfallswärme weiter aufheizt und schmilzt. Während verschiedener Stadien eines solchen Unfallablaufs können sich Schüttbetten bilden. Zum Beispiel kann bei der Wiedereinspeisung von Wasser in den Reaktordruckbehälter ein zuvor trocken gefallener, überhitzter Kern aufgrund von thermischen Spannungen zu einem Schüttbett zerfallen. Eine andere Möglichkeit ist die Bildung eines Schüttbetts durch die Fragmentierung geschmolzenen Kernmaterials („Corium“, ein Gemisch aus Kernbrennstoff, Hüllrohrmaterialen und Kernstrukturen) beim Einfließen in eine Wasservorlage, entweder in das mit Restwasser gefüllte untere Plenum des Reaktordruckbehälters (RDB) oder, nach Versagen des RDBs, in die mit Wasser gefüllte Reaktorgrube.

Eine auf diese Weise gebildete Schüttung ist zunächst trocken und heiß und setzt durch den Nachzerfall der darin enthaltenen radioaktiven Spaltprodukte weiterhin Wärme frei. Um eine stetige und langfristige Kühlung zu erreichen, muss das heiße und trockene Schüttbett zunächst abgeschreckt, d.h. mit Wasser geflutet und abgekühlt werden („quenchen“ des Betts). Falls das Eindringen von Wasser in das Bett zu langsam erfolgt, werden trockene Regionen innerhalb des Betts aufgrund der Nachzerfallswärme sich soweit aufheizen, dass sie wieder schmelzen. Durch die hierbei erfolgende Kompaktierung ist in der Folge die Kühlbarkeit in Frage gestellt. Im Kontext der Reaktorsicherheitsforschung muss deshalb die Frage nach einer möglichen Kühlbarkeit hinsichtlich der konkurrierenden Prozesse des Flutens und des Wiederaufheizens untersucht werden.

Aufgrund der sensiblen Wärme des Betts (Temperatur oberhalb der Sättigungstemperatur) und der Nachzerfallswärme, verdampft darin eindringendes Wasser. Der gebildete Dampf strömt nach oben durch die obere Grenzfläche des Betts. Auf diese Weise bildet sich ein Zweiphasen-Strömungsmuster aus eindringendem Wasser und abströmendem Dampf innerhalb des Schüttbetts aus, das letztendlich die Kühlbarkeit bestimmt. Als Grundlage der vorliegenden Untersuchungen wurden Modelle zur Simulation von Zweiphasenströmungen in porösen Medien benutzt, die bereits im am IKE der Universität Stuttgart entwickelten Rechenprogramm MEWA vorlagen.

Ein Ziel dieser Arbeit ist die Anwendung dieses Programms auf wesentliche Phasen des Unfallablaufs, um Chancen, Optionen und Maßnahmen zur Kühlbarkeit in Schüttbetten auszuloten. Darüber hinaus wurden innerhalb der Zielsetzung der Arbeit Schwachstellen in der Modellierung beseitigt und Verbesserungen und Erweiterungen bezüglich fehlender Modellteile implementiert. Ein Schwerpunkt in dieser Hinsicht liegt in der Qualifizierung der Reibungs- und Wärmeaustauschs-Modellierung, die entscheidend für die genaue Beschreibung der Abkühlprozesse (Strömungsbedingungen) innerhalb des Betts sind.

In früheren Arbeiten wurde schon festgestellt, dass klassische Modelle zum Druckverlust in porösen Medien ohne die explizite Berücksichtigung der Reibung zwischen Wasser und Dampf (Interphasenreibung) nicht ausreichen. Mit diesen kann zwar für den Fall eines von oben

gefluteten Betts der sogenannte Dryout Heat Flux (DHF), das ist der pro Flächeneinheit aus dem Bett abführbare Wärmestrom, oberhalb dessen es zur Austrocknung im Bett kommt, korrekt bestimmt werden. Allerdings wird damit der DHF für von unten geflutete Betten stark unterschätz. Tung und Dhir führten einen Interphasenreibungsterm in ihrem Modell ein, allerdings wies dieses Modell ein Defizit bei kleineren, unter Reaktorbedingungen als relevant betrachteten Partikelgrößen (1-6 mm) auf. Deshalb werden in dieser Arbeit einige Änderungen des Tung & Dhir Modells für kleinere Partikel vorgeschlagen. Diese Änderungen betreffen Korrekturen der relativen Permeabilitäten und Passabilitäten für die Reibung zwischen Partikeln und Fluiden, die im originalen Modell überschätzt wird. Darüber hinaus wird ein Reduktionsfaktor für die Interphasenreibung in Abhängigkeit der Partikelgröße eingeführt, um den DHF unter von oben gefluteten Bedingungen korrekt zu beschreiben. In der originalen Modellierung war die Interphasenreibung zu hoch.

Mit der neuen Reibungsbeschreibung (Modifizierter Tung & Dhir, MTD) wurde eine bedeutende Verbesserung erzielt hinsichtlich des Ziels einer einheitlichen Reibungs-Modellierung bei von oben und unten gefluteten Schüttbetten. Das MTD Modell wurde über eine große Bandbreite von Bedingungen validiert, für verschiedene Schüttungs-Konfigurationen von Betten mit einheitlichen Partikeldurchmessern bis zu Betten mit unregelmäßig geformten Partikeln. Die wichtigsten experimentellen Trends hinsichtlich des Flutungs-Verfahrens und der Effekte von Partikelgröße, Systemdruck und Geometrie konnten gut reproduziert werden. Die Erweiterungen und die damit verbundene Validierung stellen eine gute Basis für die Anwendung der Analysen zum Fluten dar.

Hinsichtlich des Wärmeübergangs beim Fluten zeigten die Validierungsrechnungen, außer für Fälle bei Zwangseinspeisung von Wasser mit hoher Rate von unten, dass das Wasser innerhalb des Betts aufgrund der hohen Reibung hinter einer sich langsam durch das Bett ausbreitenden Front strömt, und dass dabei das Abschrecken der Partikel schnell in einem schmalen Abschnitt innerhalb der Front stattfindet (wenige mm). Aus diesem Grund ist eine detaillierte Modellierung des Wärmeübergangs im Vergleich zur Reibungsmodellierung weniger wichtig. Darüber hinaus wird gezeigt, dass das Fluten von unten aufgrund der Ausbildung einer Gleichstrom-Konfiguration eine höhere Effektivität hinsichtlich des Kühlpotentials aufweist als das Fluten von oben, bei dem sich ein antiparalleles Strömungsmuster von Wasser und Dampf einstellt. Allerdings ermöglichen in Fällen mit Fluten von oben Inhomogenitäten (besonders laterale Unterschiede in der Permeabilität) oder Downcomer dem Wasser zunächst zum Boden durchzudringen, um in der Folge das übrige Bett von unten abzuschrecken. Dies stellt einen effektiven Mechanismus für eine schnellere Kühlung dar.

Rechnungen zu Reaktorbedingungen wurden durchgeführt um die Möglichkeiten des MEWA-Rechenprogramms als Werkzeug zur Untersuchung der Kühlbarkeit während verschiedener Phasen eines schweren Störfalls im Allgemeinen bewerten zu können und um zu sondieren, ob und bis zu welchem Grad von Kühlbarkeit ausgegangen werden kann, wie stark der Trend zur Kühlbarkeit ist und wo die Limitierungen liegen. Die Kühlbarkeit eines heißen Schüttbetts, d.h. ein erfolgreiches Abschrecken, hängt stark von den anzunehmenden Eigenschaften der Schüttung ab. Die in dieser Hinsicht wichtigen und berücksichtigten Parameter sind die Porosität, der Partikeldurchmesser, die anfängliche Temperaturverteilung im Schüttbett, die

Masse im Bett, der Systemdruck, Inhomogenitäten im Bett, usw. Mit diesen Parametern wurden Variationsrechnungen durchgeführt, um eine grundsätzliche Übersicht zu den Chancen und kritischen Bereichen zu bekommen. Ein allgemeines Ergebnis dieser Variationsrechnungen ist die Existenz bedeutender Spielräume und starker Trends zur Kühlbarkeit, die durch multidimensionale Kühlungsoptionen erreicht werden können. Dazu zählen speziell lateral und von unten zugeführtes Wasser, was im Kernbereich durch intakte Stab- oder Bypass-Regionen etabliert werden kann, im unteren Plenum durch die Wand und in der Reaktorgrube aufgrund der Form des Schüttbetts (Haufen). Diese Prozesse fördern die Kühlbarkeit zusammen mit der Möglichkeit des Dampfes, Wärme aus einer heißen und trockenen Zone abzuführen und stellen auf diesem Wege Mechanismen zur Verbesserung und Unterstützung des Abkühlprozesses zur Verfügung. Begrenzungen der Kühlbarkeit bestehen in der Anhäufung der Partikel über eine bestimmte Höhe, in verbackenen Anteilen mit sehr niedrigen Porositäten und in Schüttbetten mit sehr kleinen Partikeln.

Im Bereich des Reaktorkerns sind nach den Ergebnissen der Untersuchungen zu Reaktorbedingungen Schüttbetten mit weit größeren Partikelmassen (bis zu 100 Tonnen) kühlbar als im unteren Plenum (bis zu 40 Tonnen). Dies liegt an den verschiedenen Bettgeometrien, die im unteren Plenum die Ausbildung einer Wasserzuströmung von unten mit anschließender Dampfkühlung des noch trockenen Betts im Vergleich zur im Kern vorliegenden Situation verzögern. Dennoch besitzt das untere Plenum ein bedeutendes Kühlungspotential für begrenzte Schüttbettmassen. Im Vergleich mit der beim Unfall von Three Mile Island (TMI2) verlagerten Schmelzemasse von ~20 Tonnen, ist die Höhe der darüber hinaus noch kühlbaren Schüttbettmasse bedeutend. Andere Anteile der Schmelze, die im Kern zurück bleiben, können dort gekühlt werden, wenn die Wassereinspeisung wieder rechtzeitig fortgesetzt wird, was prinzipiell die in TMI erreichte Kühlung erklärt.

Die anfängliche Temperaturverteilung innerhalb des Schüttbetts hat einen entscheidenden Einfluß auf das Bettverhalten, egal ob sich das Bett im unteren Plenum oder in der mit Wasser gefüllten Grube unter dem Reaktor befindet. Bisher wurden Rechnungen zum Fluten nur für eine vorgegebene Schüttbett¬kon¬fig¬urat¬ion mit einer angenommenen, initialen Temperaturverteilung durchgeführt, die aus den mittleren Temperaturwerten der sich absetzenden Partikel abgeleitet wurde. Unter der Annahme einer einheitlichen initialen Temperaturverteilung im Bett werden jedoch die realen Prozesse des gleichzeitigen Absetzens der heißen Partikel auf der Schüttbettoberfläche und des Abschreckens nicht berücksichtigt. Deshalb wurde im Rahmen dieser Arbeit eine einfache Kopplung zwischen MEWA und dem ebenfalls am IKE entwickelten Rechenprogramm JEMI zur Modellierung von Strahlfragmentations- und Vermischungsvorgängen erstellt, um Schüttungsaufbau und gleichzeitiges Abschrecken beschreiben zu können. Dadurch wurden die Möglichkeiten einer realistischen Analyse erheblich verbessert und es konnten in den Rechnungen deutliche Einflüsse auf die Kühlbarkeit der so gebildeten Betten aufgezeigt werden. Vergleichsrechnungen wurden durchgeführt für das Fluten eines bereits existierenden Schüttbetts mit einer mittleren Anfangstemperatur und dem Fluten eines gleichzeitig entstehenden Schüttbetts. Im ersten Fall trat in großen Bereichen des Betts Aufschmelzen auf, während im Fall mit simultanen Bettaufbau und Fluten komplettes Abschrecken bei erheblichem Sicherheitsspielraum aufgezeigt

werden konnte. Dies lässt sich auf die realistischere Modellierung zurückführen. Aus diesem Grund und um eine realistische Perspektive zum Flutungs-Prozess und damit zur Kühlbarkeit in Reaktor-Szenarien zu erhalten, wird die Modellierung des gleichzeitigen Bettaufbaus und Abschreckens, wie sie durch die implementierte Kopplung von JEMI und MEWA ermöglicht wurde, als unerlässlich erachtet. Ohne Berücksichtigung des simultanen Abschreckens während des Bett-Aufbaus, d.h. ausgehend von einem schon fertigen Bett wie in früheren Studien, wird die Kühlbarkeit beträchtlich unterschätzt.

Sogar mit tieferen Wasserpools in der Reaktorgrube (7-10 m bei Schwedischen Siedewasserreaktoren), können Probleme aufgrund eines unvollständigen Aufbruchs von dickeren Schmelzestrahlen auftreten (Strahldurchmesser > 20 cm). Dabei können Konfigurationen mit Schmelzeschichten am Boden auftreten, die mit den gegenwärtig vorgesehenen SAM (Severe Accident Measures) nicht mehr kühlbar sind. In diesen Fällen würde die Schmelzeschicht nur durch oben aufliegendes Wasser gekühlt werden, was nur bei relativ dünnen Schmelzeschichten funktioniert. Deshalb sollten bei diesen SAM-Konzepten Verbesserungen berücksichtigt werden. Eine Lösung könnte darin bestehen, dem Wasser den Zustrom von unten in die Schmelze zu ermöglichen, wie sie im COMET Konzept vorgesehen ist. Die Möglichkeit Wasser von unten einzuspeisen könnte als Backup-Maßnahme für das gegenwärtig vorgesehene Konzept der Bereitstellung tiefer Wasserpools angesehen werden, falls flüssige Schmelze aufgrund unzureichender Strahlfragmentation den Boden der Reaktorgrube erreicht. In diesem Fall kann die Wassereinspeisung von unten zur Porositätsbildung in der entstandenen Schmelzeschicht und folgend zu einem schnellen Abschrecken führen.

Ein weiterer wichtiger Schritt für die Gesamtmodellierung zur Kühlbarkeit wurde durch die Einführung einer Option unternommen, die Porositätsbildung in flüssigen Schmelzeschichten durch die Einspeisung von Wasser von unten (COMET-Konzept) im MEWA-Modell zu beschreiben. Die diesbezügliche Modellierung der Situationen, bei denen unfragmentierte Schmelze aufgrund unzureichender Strahlfragmentierung den Boden der Reaktorgrube erreicht, wurde implementiert.

In dieser Arbeit werden einige dieser Prozesse generisch betrachtet und die Optionen kombinierter SAM bestimmt. Die im Rahmen dieser Arbeit durchgeführten Rechnungen mit MEWA-COMET zeigten, dass eine Schmelzeschicht innerhalb eines Schüttbetts bis zu einer Höhe von 26 cm (sehr wahrscheinlich auch höher) sicher durch eine Einspeisung von Wasser von unten gekühlt werden kann. Daher kann die Kombination der Wassereinspeisung von unten mit dem Konzept der gefluteten Reaktorgrube das Potential zur Kühlung und Rückhaltung von Kernschmelzen erheblich verbessern. Diese Resultate bedürfen jedoch weiterer Absicherung, da das gegenwärtige Modell zur Porositätsbildung Effekte gegen die Porositätsbildung wie z.B. Verstopfen der Porosität durch erstarrende Schmelze im Kontakt mit kalten Partikeln nicht ausreichend berücksichtigt.

III Table of Contents

IV Nomenclature

a	m^2/m^3	interfacial area concentration
A	m^2	area
c_p	J/(kg K)	isobaric heat capacity
D	m	diameter
e	J/kg	specific internal energy
g	m/s^2	gravitational acceleration
h	$W/(m^2 K)$	heat transfer coefficient
H	m	height
i	J/kg	specific enthalpy
K	$kg/(m^3 s)$	friction coefficient
L	m	length
M	kg	mass
$\dot{m}$	kg/s	mass flux
p	Pa	pressure
P	W	power
$\dot{q}$	W/kg	specific power
Q	W/m^3	heat flux density
r	m	radial coordinate
R	m	radius
s	m^3/m^3	saturation, fraction of fluid in porous space
t	s	time
T	K	temperature
$\vec{u}$	m/s	superficial velocity

V	m^3	volume
$\vec{w}$	m/s	velocity
x	m	x-coordinate
z	m	z or axial coordinate

Greek symbols

ε	m^3/m^3	porosity
Γ	$kg/(m^3\ s)$	mass transfer rate, evaporation rate
η	Pa s	dynamic viscosity
κ	m^2	permeability
μ	m	passability
ρ	kg/m^3	density
σ	N/m	surface tension
θ	°	angle of repose, angle of cone

Indices

0	initial, constant
A	annular flow regime
b	debris bed
B	bubble, bubbly
BST	Bubbly / slug transition
cav	cavity
eff	effective
evap	evaporation
FB	film boiling
g	gas
HB	high void bubbly flow regime

GC	gas continuous regime
l	liquid
LB	low void bubbly flow regime
LC	liquid continuous regime
LGT	Liquid / gas transition
LP	lower plenum
lam	laminar
M	melt
P	particles
NB	nucleate boiling
rel	relative
sat	saturation, gas/liquid interface
s	solid, particles
S	slug flow
SAT	Slug / annular transition
trans	transition
turb	turbulent

Mathematical symbol

∂	partial derivative
Δ	difference
∇	Nabla operator, gradient or divergence
$\overrightarrow{(\cdot)}$	Vector

Dimensionless numbers

Ja	Jacob number, $Ja = \frac{c_p \cdot \Delta T}{\Delta i}$
Nu	Nusselt number, $Nu = \frac{h \cdot D}{\lambda}$
Pr	Prandtl number, $Pr = \frac{\eta \cdot c_p}{\lambda}$
Re	Reynolds number, $Re = \frac{\rho \cdot w \cdot D}{\eta}$

Abbreviations

AMM	Accident Management Measure
ATHLET-CD	Analysis of Thermal-Hydraulics of LEaks and Transients-Core Degradation
BWR	Boiling Water Reactor
CATHARE	Code for Analysis of THermalhydraulics during an Accident of Reactor and safety Evaluation
CCM	Corium Coolant Mixing
CEA	Commissariat à l'Energie Atomique
COMET	Coolability of Melt
COOLOCE	Coolability of Cone
DEFOR	DEbris bed FORmation
DHF	Dryout Heat Flux
EPR	European Pressurized Water Reactor
FARO	Fuel melt And Release Oven
FCI	Fuel Coolant Interaction
FZK	Forschungszentrum Karlsruhe
ICARE	Interprétation des Coeurs Accidentés pour les Réacteurs à Eau
IKE	Institut für Kernenergetik und Energiesysteme
IRSN	Institut de Radioprotection et Sûreté Nucléaire
JEMI	JEt fragmentation and preMIxing
KTH	Royal Institute of Technology, Sweden

LWR	Light Water Reactor
MC-3D	Multi Componet-3D
MESOCO	MElting/SOlidification COde
MEWA	Melt Water
POMECO	Porous Medium Coolability
PRELUDE	Préliminaire sur le Renoyage ExpérimentaL d'Un Lit de Debris
PREMIX	PREMIXIng phase of melt coolant interaction
PWR	Pressurized Water Reactor
RPV	Reactor Pressure Vessel
SAM	Severe Accident Management
TMI-2	Three Miles Island Unit 2 reactor in Harrisburg, PA, USA
VTT	Technical Research Centre of Finland
WABE	WAter BEd

1 Introduction

1.1 Motivation

Worldwide, a significant part of electrical energy (about 14 % of world electricity [1]) comes from nuclear reactors. In nuclear reactors, controlled nuclear fission is taken place to generate heat, which is used to boil water, produce steam, and drive a steam turbine to produce electricity. Producing electricity in this way has some significant benefits. In this process a huge amount of energy can be produced from small amounts of fuel, without CO_2 emission, which is the key issue considering the consequences of global warming. In spite of this benefit, larger commercial use and prolongation of the use of nuclear energy are suppressed due to controversial discussions about potential risk of nuclear reactors for the public and the environment. In order to assess the risk accurately and to prevent the accidents with an adverse effect to the environment, reactor safety is of paramount importance for the construction and operation of nuclear plants.

In case of an accident the reactor will shut down automatically. But, even after shutdown of the reactor, heat will still be produced (decay heat) inside the core due to ongoing radioactive decay by fission products. The heat that is produced by this radioactive decay has to be removed at the same rate as it is produced, otherwise the reactor core (fuel elements made of UO_2 cladded by Zircaloy) will heat up. Depending on the type of reactor, there exist various reactor core cooling systems for the removal of this heat. These core cooling systems provide water flow through the reactor core and then reject the heat elsewhere. High quality standards are maintained to ensure the proper operation of these core cooling systems in normal operation as well as in case of emergency. However, in case of a very unlikely severe accident, in spite of high safety standards, a failure may occur which exceeds the range of design. This may be caused by simultaneous failure of all core cooling systems due to an event for which the plant was not designed, as the tsunami in Fukushima, or by operator errors as in the Three Mile Island-2 (TMI-2) accident. The probability of such an event in a nuclear power plant is very low but the consequences of such an accident may be enormous. Due to decay heat and a missing heat sink (water), the core will melt. If melting of corium (molten UO_2+ZrO_2+ structure materials) and its progression cannot be stopped it will damage the plant extensively by breaking all the safety barriers and finally release the radioactive material to the environment, which gives a deep impact on individual and social health risks.

Fukushima and TMI-2 are the two major core melt accidents in Light Water Reactors (LWRs) of Western type technology. The Fukushima accident occurred in March 11, 2011 in four reactors (units 1 to 4) as a result of an extreme natural event: the earthquake and tsunami caused a Station Black-Out and loss of water cooling systems. So, core cooling functions were lost. There were some small contributions by the emergency cooling systems, but they were also lost when the batteries were used up. After that, the fuel encountered dry-out, heat-up and fuel damage processes. Hydrogen gas was generated by chemical reaction between hot cladding material and steam. This caused hydrogen explosions in the reactors (see also Omoto [2], Yoshioka and Lino [3]). Presently, the actual status of core damage is not known, but it can be presumed that debris and melt came down to the bottom of the reactor pressure vessel (RPV) and due to vessel failure,

may be to the bottom of the primary containment also (see Tanabe [4] and the technical report by L'Institut de Radioprotection et de Sûreté Nucléaire (IRSN) [5]).

The other core melt accident occurred in the nuclear power plant TMI-2 in Harrisburg (USA), on March 28, 1979 (see Broughton et al. [6], Kemeny [7]). This accident has been caused by a coincidence of unfavorable factors and operator misjudgment (see Buck [8]). Before the examinations of the accident, it was mostly thought that only a small part of the core was damaged. But the post-accident examinations clearly showed that large fractions of the core had melted and some 20 tons of the molten cores had reached the lower head (see Sehgal [9]). If the operators had not succeeded to fill the reactor vessel with water, or if a larger quantity of melt had dropped into the lower head, the lower head would not have survived and the melt would not have been retained in the vessel. Melt-through of the RPV and release of melt to the containment and melt-concrete interaction at the basement would have created much greater damage to the plant. The conditions and mechanisms which enabled cooling of the relocated core material and melt are still not fully clarified.

These accidents posed challenges to severe accident research to evaluate whether and by which means even such events can be managed and terminated. This means to reach a safely cooled state of corium, whether it is still intact as rods or in the form of particulate debris, i.e. broken solidified structure of molten corium (UO_2+ZrO_2+ structure materials) or in the form of liquid melt. Coolability of hot corium and finally even of molten corium is a key issue in a severe accident.

Emphasis of the present work is put on debris cooling because debris beds may form in essential phases of an accident and therefore may play a significant role in retention and accident mitigation. Debris beds are generally produced due to breakup of corium melt. Depending on accident progression and water supply, the bed formation process by breakup of core material and melt may be different. In the degrading hot core, a debris bed may be formed due to thermal stresses during re-flooding. It may be formed by breakup of melt jets due to contact with water in the lower head when melt from the core flows into water in the lower head, and in the cavity (space below the reactor pressure vessel) by melt flow out of a failing RPV into a cavity with water. Further, particulate debris formation by breakup processes is also considered in dedicated AMM (accident management measure) of evolutionary reactor concepts, as e.g. the deep water concept (see Chu et al. [10]) in BWRs (boiling water reactors). Another concept is the COMET (COolability of MElT) concept (see Alsmeyer et al. [11], and Alsmeyer and Tromm [12]), where injection of water from below into a melt layer is considered to break up the melt and produce a porous structure.

As mentioned above, debris beds may be formed in different stages of a severe accident and may support coolability due to their open pores. A debris bed is considered coolable when a steady state temperature can be reached by removing the heat. This steady state condition may be at saturation temperature when water flow is sufficient to remove the heat from debris bed without any dry zone or may be higher than saturation temperature when steam flow makes the dry zone stable (temperature does not increase with time). On the other hand, a non-coolable debris bed is defined by the rise in temperature due to the residual decay heat. Non-coolable debris would

ultimately yield melting and form a large molten pool which is a huge threat for the integrity of the plant. Therefore, knowledge about coolability of such debris and relocated core material is a key in evaluation of safety margins in case of severe accidents. This knowledge will help with the planning and application of appropriate measures for stopping an accident.

It is important to evaluate the chances of coolability during the progression of an accident. This is in line with the safety philosophy of defense-in-depth, which means to analyze the options and chances to stop an accident at every stage. Ex-vessel melt retention concepts appear to be largely independent of the in-vessel development and may be considered as ultimate measures. However, not considering the chances of coolability of corium before such ex-vessel situations neglects the possibility to get safe states before, i.e. in the RPV (Bürger et al. [13]). Therefore, mitigating measures and options and their chances of success as well as adverse effects are to be analyzed for both in- and ex-vessel situations. Such analyses contribute to the overall assessment of the reliability of the plant.

1.2 Severe reactor accidents with core melting and investigations of coolability-state of the art

1.2.1 Possible accident scenarios leading to debris bed in Light Water Reactors

Two major reactor designs of Light Water Reactors (LWRs), Pressurized Water Reactor (PWR) and the Boiling Water Reactor (BWR) are the most common types of nuclear reactors operated nowadays worldwide. According to the place of occurrence, the description of a severe accident in LWRs can be roughly divided into in-vessel and ex-vessel scenarios. The formation of particulate debris both in and ex-vessel scenarios are expected by breakup of core materials due to contact with water. This breakup of corium may occur as a consequence of severe accidents or may be induced by severe accident measures as described details in below.

1.2.1.a In-vessel scenarios

During a severe accident, if the core is not sufficiently cooled due to loss of water, the decay heat of the fission products in the fuel heats up the reactor core. This heat up causes evaporation of cooling water in the core region and decreases the water level in RPV. The time period of core dryout depends on the accident development and specific reactor design, but the usual time ranges are considered from two to several hours. The decay heat yields a continued heat-up of the fuel rods and the other core materials. Zirconium of the fuel rod cladding at temperatures higher than ~1500 K reacts with superheated steam in a highly exothermic manner. This exothermic reaction further accelerates the temperature rise and core degradation process. Further, by this reaction, also large amounts of hydrogen are produced, which may arrive in the reactor containment, either through a leak or through the safety valves of the reactor cooling system. High concentrations of hydrogen in the containment can there lead to explosive combustion of the gas mixture, which may damage the containment. The oxidation of core metal and hydrogen generation processes can be found details in Chikhi et al. [14] and Ederli et al. [15].

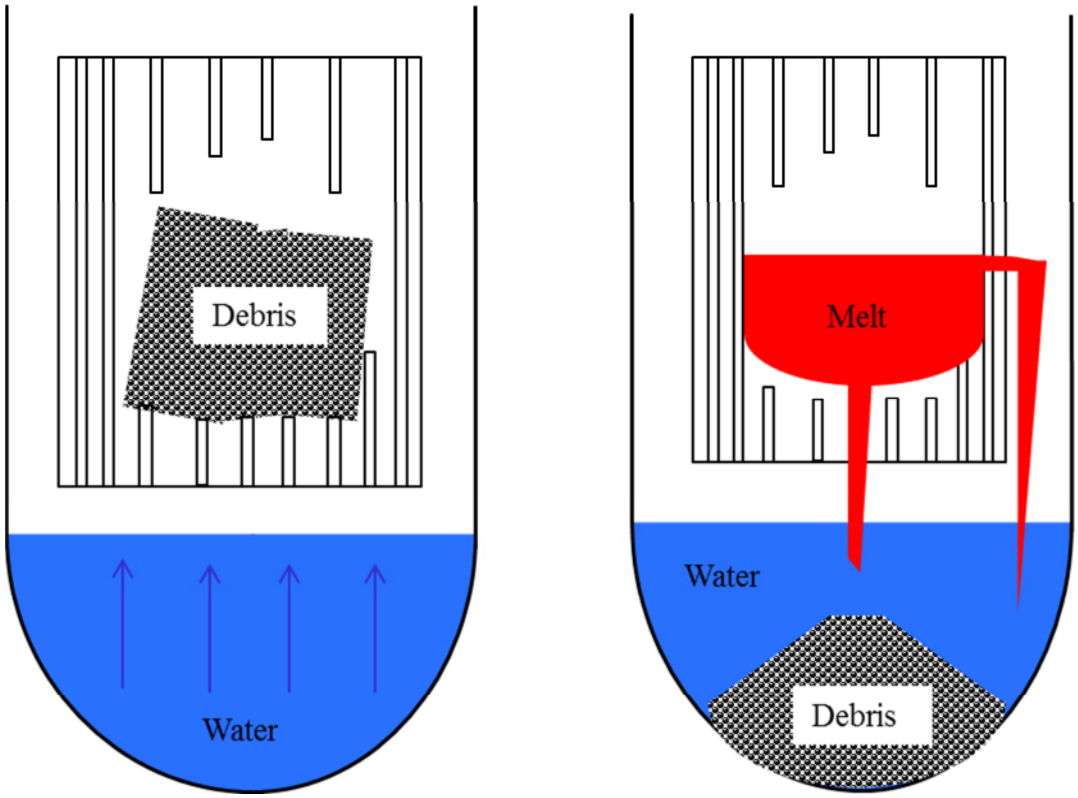

Figure 1.1: Configurations with particulate debris in the core (left) and in the lower head (right) during in-vessel accident scenario.

The continued temperature increase due to decay heat will lead to melting of other core materials. If water supply can be reestablished in this stage of accident, the hot rods will be in direct contact with cold water. This will give a thermal shock to the hot rods. Due to this thermal stress some of the rods may crumble, and form a configuration with particulate debris surrounded by intact core regions, as shown in Figure 1.1. Analysis of the debris generated during the TMI-2 accident showed that the fuel was fragmented to particles in a size range of 1 to 5 mm (see Akers et al. [16] and Akers and McCardell [17]). The high temperatures (more than 2000 K) and small hydraulic diameters (few millimeters) in a debris bed make the coolability more difficult than for intact fuel rods. Termination of accident in this stage or further progression largely depends on the stabilization (steady state condition i.e. temperature of the bed does not change with time) of such debris. To reach a stable cooling condition, the hot and dry debris bed needs to be quenched (cool down to saturation temperature by flooding with cooling water) before reaching melting due to decay heat. Elaboration the chances of quenching of such core debris against heat up due to decay heat is one of the major objectives of the present work.

If water supply cannot be reestablished, the temperature of the dry portions of the core will continue to increase, resulting in the melting of the core materials. The components with low melting temperatures such as control rod materials (silver, indium, cadmium, boron) and steel from mounting structures will be melted first. Later with increasing temperature also the ceramic parts of oxidized ZrO_2 and UO_2 fuel will start melting. Several other processes, such as candling

of melt or the dissolution of fuel by metallic melt are involved in this stage but these are not described here. Details can be found in Buck [8] and Bürger et al. [18].

Due to gravity, the molten materials will relocate in the lower core regions. The temperatures in the lower core parts are expected to be significantly smaller in comparison with the upper parts of the core due to later dryout during decreasing water level. Because of this smaller temperature in the lower parts, the relocated molted materials will solidify and form a crust structure there. The stability of such crust configuration depends on the cooling conditions from below e.g. conduction, radiation and steam flow. Two different extreme scenarios may be considered. Scenario with no cooling from below will prevent stable crust formation. As a result there will be no large accumulation of pools and molten materials will gradually relocate in the lower plenum. In the other extreme, good cooling of crust from below provides the potential for accumulation of large quantities of melt in the core region (i.e. a melt pool will be formed), supported by a crust, as observed TMI-2 accident (see Reinke et al. [19]) . The stability of the supporting crust depends on the heat flux distribution at the pool inner boundaries and the extent of external heat removal. If the thermal loads are high enough to fail the support of melt pool, melt will release in the lower head. Different modes of melt release may be possible. Melt may flow out in the form of several jets through the lower grid plate due to crust failure in the bottom central part or it may release sideways due to crust failure in the upper region, provided by natural convection in the melt pool, yielding highest temperatures at the top of the pool.

When melt is released from the core, it interacts with residual water in the lower head resulting in melt fragmentation. The kind of melt release is important for the interaction of the melt with water. Small melt mass fluxes yield good fragmentation of melt jet when pouring into water. On the other hand, larger melt fluxes produce limited interaction with water. As a result, the relocated melt will remain largely liquid. Details of this fragmentation process can be found in Bürger et al. [20], Pohlner et al. [21] and also Speis and Basu [22]. Steam explosions can also occur in this phase. The strength of a potential steam explosion is directly linked to the amount of pre-fragmented liquid melt mixed with water. This requires sufficiently large melt mass flow rate, coarse breakup and melt superheat. Steam explosion is discussed in details by Fröhlich and Unger [23], Vujic [24] and Schröder [25].

However, as described above, generally small melt fluxes from the core to the lower head are expected. Additionally, if the reactor pressure vessel is intact, the lower head will be filled with residual water. When the melt pours into this water, the jet will break up and fragment into droplets that solidify and settle as particulate debris as shown in Figure 1.1. Evidences from TMI-2 (Rekine et al. [19]) as well as FARO (Fuel melt And Release Oven) experiments (see Magallon [26], Magallon and Hohmann [27]) show that corium melt jets with diameters of few centimeters will be fragmented in water into droplets with average size of few millimeters. The so formed particle bed still includes the decay heat. Further, initially, the settling particles are so hot that water will be driven out of the forming bed. To enable long term coolability and maintain in-vessel retention, this debris bed of nuclear material has to be re-flooded and quenched afterwards fast enough such that heat-up (rise in temperature due to decay heat) of the particles, while they are dry, does not lead to re-melting. Investigation of the quenching process

of such debris configurations against heat-up due to decay heat is the major interest of the present study and will be performed in the present work.

If the corium cannot be cooled inside the reactor pressure vessel e.g. due to large melt mass or non-availability of cooling water, it will re-melt and relocate, resulting in a melt pool. In the extreme case, when all water in the vessel is evaporated, a large melt pool develops in the lower head. This hot melt will attack the vessel wall and weaken it. If no counter measures can be taken, e.g. flooding of the reactor cavity and thereby cooling of the Reactor Pressure Vessel (RPV) from outside "in-vessel retention" as proposed for some Westinghouse Advanced Pressurized Water reactors , AP-600 (see Theofanaous et al. [28]), the lower head will fail leading to melt outflow from the RPV.

1.2.1.b Ex-vessel scenarios

RPV failure initiates scenarios of melt release into the cavity i.e. the volume below the RPV in a LWR. The melt has to be cooled or retained in the cavity, otherwise melt-through of the containment basement would occur and containment integrity would be in danger. In order to avoid the occurrence of such events, especially to avoid melt-through and finally to mitigate the consequences, AMM (accident management measures) or SAM (severe accident management) measures, in addition to emergency cooling systems, are being provided in nuclear power plants and improved as per requirements. The ultimate purpose of these AMM is to prevent the release of radioactive materials and thus to reduce the consequences of severe accidents to the environment. To achieve this, a safely cooled state of corium has to be reached. Two basic concepts of devices and measures for ex-vessel melt cooling can be distinguished:

- Enclosure of melt within cooling boundaries,
- Quenching of melt based on significant surface increase by breakup processes.

The Tian Wan core catcher and European Pressurized Reactor (EPR) core catcher (see Seiler et al. [29], Sehgal [30], Fischer [31]) can be classified as enclosure concepts, applied for ex-vessel melt retention. Both core catchers are being implemented in so-called Generation 3 reactors. Tian Wan core catcher (see Tian Wan [32]) provides an enlarged and diluted melt pool (by addition of sacrificial material) and then cooled from outside. The latter core catcher is being realized at Olkiluoto in Finland. The EPR contains a core catcher in a lateral spreading compartment where melt is collected, conditioned with sacrificial concrete and subsequently spread over a large surface area at about 170 m^2. Due to this large surface area, a relatively thin melt layer (~ 30-40 cm) is expected. It is considered that by top cooling, via addition of water from top, and cooling from bottom by a cooling circuit, the melt is safely enclosed and retained within these cooling boundaries (see Fischer et al. [33], Bittermann et al. [34]). This prevents further progression of the accident as well as fission product release. A disadvantage also of this concept may be that the melt partly stays liquid for a long time (months). Due to the low heat conductivity of corium, high temperatures and a partly liquid state are within these concepts required to extract the power from nuclear decay to the cooling boundaries by natural convection, as long as decay heat has not decreased sufficiently.

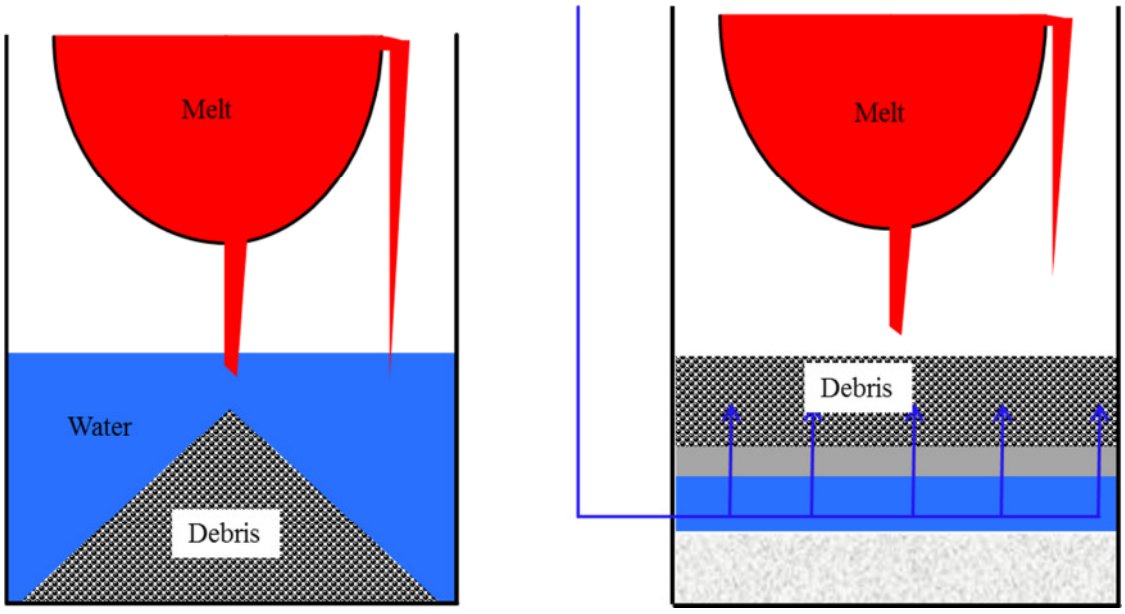

Figure 1.2: Ex-vessel particulate debris in a deep water pool (left) and in the COMET core catcher (right).

In other concepts (see Sehgal [30]) cooling of corium based on significant surface increase by breakup of melt due to contact with water is considered. Breakup of the corium melt in conjunction with quenching is considered to yield rapid cooling. The open porosities and much larger surface of melt are created during the breakup process. The subsequent formation of porous and solidified debris then facilitates the coolant ingression inside the bed. As a result, such debris beds provide much better chances to remove the heat than a compact molten corium pool or layer where coolant access is limited.

With the aim of particulate debris formation, cavity (volume below the reactor pressure vessel) flooding with water is established as AMM or SAM in Finnish and Swedish BWRs. The melt flowing out of the broken vessel and pours into this water as a jet. As described above for the lower head, the melt jet will break up and create particulate debris due to interaction with water. A deep water pool favors the formation of coolable particle debris. In the AMM concepts for BWRs, water pools of 7-10 m height are foreseen, while in existing PWRs only about 1-2 m (or even less) cavity depth are available. Further, the kind of melt release is important. A large melt pour can generally be considered as less favorable for breakup than a limited diameter of outflow from the RPV. Depending on vessel breach size and depth of water pool different bed configurations may be envisaged. If a melt jet with limited diameter falls in a deep water pool, significant break-up of melt and formation of debris bed is expected. A sketch of such configuration is shown in Figure 1.2. On the other hand, breakup of melt will be greatly reduced with thicker melt jets and also with shallow water pools. This may result in bed configurations containing molten parts mixing with debris bed in the cavity floor.

Another concept is the COMET concept (see Alsmeyer et al. [11], and Alsmeyer and Tromm [12]), where injection of water from below into a melt layer is considered to break up the melt. This concept is originally based on the dry cavity situation. Here, the melt flowing out of the vessel is collected in the dry reactor pit and let spread over the available cavity area. To provide water supply into the melt from the bottom a sacrificial layer including nozzles with plugs is

installed in the cavity basement. These nozzles are connected to a water pool at higher-placed level. The spreading melt attacks the sacrificial layer, as well as the plugs, and opens the water path. Due to the hydrostatic head, the water is injected through the nozzles into the melt. The water will force up through the melt and evaporate. The resulting high volume steam generation process yields a rapid breakup of the melt and by this creates a porous, solidified structure (see Widmann et al. [35]) as shown in Figure 1.2, from which heat can be removed.

Thus, particulate debris may be formed by the consequence of a severe accident or may be induced by the AMM. Without achieving the coolability of debris, a severe accident cannot be characterized as stabilized and terminated. Investigation of coolability of debris is therefore paramount importance in severe accident research. The fundamental problem linked to removal of heat from the bed. The efficiency of heat removal depends on the bed properties. In the following the important bed properties and their effect on coolability investigated in different experiments are summarized.

1.2.2 Investigations of debris bed properties and cooling behavior

The important properties of particle beds concern the particle morphology (size distribution, shape), porosity (free space inside the debris bed) range, multi-dimensionality (shape of the bed), bed inhomogeneity (more porous or less porous region) etc. The bed properties from breakup of melt jets penetrating into water pools have been investigated experimentally with corium melt in FARO (Magallon [26]) and CCM (Corium - Coolant Mixing) experiments (Wang et al. [36], Spencer et al. [37]), with corium stimulant materials in DEFOR (DEbris bed FORmation) experiments (Kudinov et al.[38], Kudinov et al. [39] and Karbojian et al. [40]) and with aluminum melt in PREMIX (PREMIXIng phase of melt coolant interaction) experiments (Kaiser et al. [41], Huber et al. [42]). These experiments focus especially particulate debris formation and the underlying physical mechanisms that determine the debris bed. The results of these experiments suggest that irregular bed geometry with non-homogeneous internal structure is possible. Irregular bed geometry e.g. heap shaped bed (see Figure 1.3) is obtained in DEFOR experiments [38]. This indicates multidimensional flooding of coolant is typical for debris bed. Internally less porous regions, re-agglomerated drops of melt or un-fragmented melt forming so-called cake parts, and also of regions with higher porosity may occur. All experiments show particle size ranges from 1 to 10 mm. Very high porosity (50 to 60%) is obtained in DEFOR experiments. Unfortunately, bed porosities have not been analyzed in others experiments.

To investigate the behavior of a debris bed, several experiments and analyses have been performed. The most important cooling behavior inside the debris beds are dryout and quenching. The dryout behavior is mainly related to long-term cooling which means how much heat can be removed from a water-filled debris bed without any dry zone formation inside the debris bed i.e. bed remains steady state at saturation condition. On the other hand quenching behavior related to removal of heat from hot and dry debris (liquid saturation zero and bed temperature higher than saturation temperature), i.e. the question whether the debris bed can be flooded and cooled to saturation conditions before the further heat-up (rise in temperature due to decay heat) of still dry parts leads to re-melting.

Figure 1.3: Debris bed from DEFOR 07 experiments [40].

Previous investigations of debris cooling mainly focused on dryout behavior under one-dimensional top flooding conditions (Marshall and Dhir [43], Catton et al. [44], Stevens and Trenberth [45]). The objective of most of these investigations had been to determine the DHF (dryout heat flux) which is the maximum heat flux that can be removed under steady-state conditions from the debris bed through the upper surface (by transport of the latent heat: internal power is converted by evaporation of cooling water), without occurrence of dry spots inside the bed. Water inflow from above results in the spatially averaged two-phase flow approach against the upward steam flow and dryout occurs when the escaping steam prevents water inflow into the bed (counter-current flooding limit).

Much higher DHF i.e. better coolability is expected if there is a water supply from the bottom where the water flows into the bed via water-rich regions and co-current with up flowing steam. Indeed, experiments showed a much better coolability with bottom than with top flooding. More than twice the dryout heat flux (DHF) was obtained with bottom injection from a lateral water column of the same height as the bed (see Hofmann [46], Rashid et al. [47]).

An important aspect of realistic debris concerns the local distribution of particle sizes of non-spherical shape obtained from a few fuel-coolant interaction (FCI) experiments. This has been addressed by STYX (Lindholm et al. [48]) and DEBRIS experiments (Rashid et al. [49], Kulkarni et al. [50]). Mixtures of particles (alumina sands) of different sizes and irregular shapes are used in the STYX experiments performed at VTT (Technical Research Centre of Finland). They applied a broad particle size distribution based on the data from different international fragmentation tests, especially the FARO experiments (Addabbo et al. [51], Silverri and Magallon [52]). Most tests were done with top flooding conditions. Small dryout heat flux values (200 kW/m^2 for 1 bar system pressure) resulted in these top flooding experiments due to significantly small effective particle diameter (less than 1 mm). The question remains whether the well-mixed particles in the experiment correspond to the local bed structure obtained in reality under settling conditions. Intense mixing of particles as employed in these experiments

may be doubted under postulated severe accident conditions where the bed is formed in a settling process. In the DEFOR experiments (Karbojian et al. [40]) of KTH (Royal Institute of Technology, Sweden) surprisingly high porosities resulted which also indicate the effect of settling versus mixing of particles. In the DEBRIS experiments at IKE (Institut für Kernenergetik und Energiesysteme), mixtures of irregularly shaped alumina particles from PREMIX experiments (Keiser et al. [41]) and spherical steel particles have been included. Higher dryout heat flux value (800 kW/m^2 for 1 bar system pressure) results compared to STYX experiments due to higher effective particle diameter (3 mm).

The particulate bed employed in coolability studies has to be characterized by an averaged diameter (effective diameter) and it plays an important role in coolability analysis. However, the identification of such effective particle diameter is not straightforward. Several mean diameters are in use to characterize this effective particle diameter e.g. mass mean $D_{p,mm}$ used by Konovalikhin [53], surface mean $D_{p,sm}$ used by Dhir [54] and Kaviany [55] or number of particle mean diameter $D_{p,nm}$ used by Zeisberger & Mayinger [56]. All are based on the major assumption that each of the particles has the same shape and defined as follows

$$D_{p,mm} = \frac{\sum_{\text{all particles}} D_{p,i} W_i}{\sum_{\text{all particles}} W_i} \tag{1.1}$$

$$D_{p,sm} = \frac{\sum_{\text{all particles}} W_i}{\sum_{\text{all particles}} \frac{Wi}{D_{p,i}}} \tag{1.2}$$

$$D_{p,nm} = \frac{\sum_{\text{all particles}} \frac{Wi}{D_{p,i}^2}}{\sum_{\text{all particles}} \frac{Wi}{D_{p,i}^3}} \tag{1.3}$$

Where W_i is the volume fraction of particle $D_{p,i}$. The effective diameter should ideally be chosen by the "friction loss" diameter, i.e. such that it would reproduce the measured pressure drop (from single-phase experiments) when inserted in the Ergun friction model (Ergun [57]). Single-phase pressure loss experiments performed at KTH (Li et al. [58]) and IKE (Rashid et al. [47], [49]) with several particulate debris beds suggest that the effective diameter lies between surface and number of particle mean diameter.

In relation to reactor safety concepts, downcomers are considered as a possible accident management measures (AMM) in debris cooling (Konovalikhin et al. [59]). Moreover, in debris beds, internally less porous (porosity < 30%) or more porous region (porosity > 50%) may occur, the latter even as downcomer-like structures are considered to favor supply of water to the bed and thus coolability. In this respect, DEBRIS experiments at IKE [49] and POMECO (POrous MEdia COolability) experiments at KTH ([53], [59]) with downcomers have been

performed to investigate the downcomer effect on debris bed cooling. Experimental results suggest that the bottom inflow via downcomer tube improves the coolability of debris bed significantly. Compared to top flooding alone, DHF increased 2 times in DEBRIS experiments and 1.5 times in POMECO experiments. Downcomer channels the water from top water pool to the bottom of the bed and develop a natural circulation flow loop, providing larger mass flow rate (compared to mass flow rate of top flooding bed only) in the bed and thus increase coolability compared to top flooding bed.

In COOLOCE (Coolability of Cone) experiments (Takasuo et al. [60]) the dryout power is measured for two different geometries: a conical debris (heap like) bed and a cylindrical (evenly distributed) debris bed. The main focus of these experiments is to investigate the 2D effect as well as effect of the debris bed geometry on its coolability. The cylindrical debris bed configuration is top-flooded, i.e. it represents a scenario in which the core debris is evenly distributed against the walls of the spreading area. In the conical geometry, the surface of the cone is open to lateral infiltration of water. The results suggest that if the two debris bed configurations have equal height, the coolability of the conical bed is improved compared to the cylindrical bed due to the lateral infiltration of water through the surface of the cone. However, in case the conical and cylindrical debris beds have equal diameter and volume, the dryout power density of the conical configuration is lower than that of the cylindrical configuration due to taller bed height of the conical configuration [60].

The available knowledge about quenching of hot particulate debris comes from few experiments although quenching versus heat-up by decay heat mostly determines the coolability question in reactor scenarios. Among the available quenching experiments, the classical experiments of Tutu et al. [61] provide valuable data on the progression of the quench front and the production of steam during quenching. These experiments are performed with bottom injection of water into hot particulate debris at fixed flow rates. A major finding in the experiments is the transition heat transfer phenomenon: Cases of smaller water flows result plateau-like (constant) steam fluxes and cases of larger water flows result peaks of steam fluxes. The difference is mainly related to a more rapid quenching than water progression (thin quenching front, mm range) versus the opposite i.e. water progression is rapid enough than quenching (thick quenching front, centimeter range). A similar behavior as shown in Figure 1.4 is also observed in the PRELUDE (Préliminaire sur le Renoyage ExpérimentaL d'Un Lit de Debris) experiments (Repetto et al. [62], [63]) performed recently at IRSN (Institut de Radioprotection et de Sureté Nucléaire). However, peak behavior is concluded here due to multidimensional effects i.e. simultaneous quenching over extended bed regions which is different from the consideration of [61] where peak behavior is considered due to a thick quenching front.

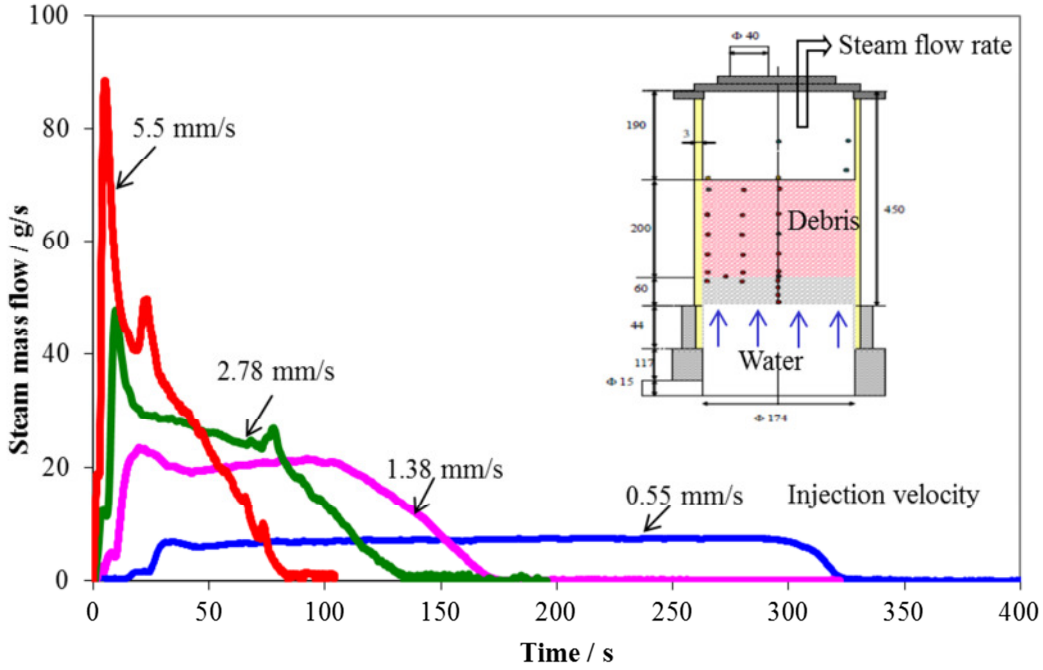

Figure 1.4: Steam mass outflow measured in PRELUDE experiments [62] for different fixed water injection rates from bottom.

In the reactor configurations, water access to the debris bed is governed by pressure difference not by fixed inflow. E.g. in the core region the water access inside the bed is achieved via a downcomer i.e. water flow is driven by a hydrostatic head of lateral water column. In a heap like debris in the lower head or cavity, water infiltration along the heap is driven by the lateral pressure differences caused by the radial increase of water content, due to less steam production with less height. Quenching behavior of hot debris driven by lateral water column is addressed in DEBRIS experiments (Rashid et al. [64]). Differing from [61] or [62] experiments (fixed water flow rate at bottom), here water inflow is determined by feedback with internal processes in the bed, i.e. the pressure build up due to friction with the water flow, evaporation, limited release of steam etc. Experiments were carried out for different initial bed temperatures .With the lower particle temperatures higher quench front velocities were obtained in the experiments.

The cool-down behavior of superheated particles under top flooding condition is investigated by Schäfer et al. [65]. It was observed that the quenching front never covered the whole cross section of the bed during downward progression but penetrated the bed always in individual flow streaks (also observed in the top flooding experiments of Ginsberg [66] and Cho and Bova [67]). Once a streak reached the bottom of the bed, an upward filling process of the bed started. While filling up the bed, the remaining superheated regions were quenched.

Cooling conditions of hot debris with variable permeability (flow resistance of porous medium due to friction) in the axial and radial direction were investigated by Tung and Dhir [68]. The beds were flooded either from the top or the bottom. In the bottom flooding experiments, the water entered through a pipe connected to a large reservoir, which provided a constant hydrostatic pressure head. It is found that the quench front velocity decreases with decreasing driving pressure and increasing initial temperature during bottom quenching. The experimental results of the top flooding of a radially stratified bed (outer region with 6 mm particle has higher

permeability than that of inner region with 3 mm particles) suggest that the quench front progresses much faster downwards in the outer region with high permeability. The lower permeability region (inner region) is quenched mostly from the bottom due to the inflow of liquid from the quenched high-permeability region.

1.2.3 Modeling approaches for debris coolability analysis codes

In order to analyze the coolability of debris bed several computational codes have been built by different institutions e.g. MEWA (MElt WAter) code (Buck et al. [69]) developed at IKE, ICARE/CATHERE Fichot et al. [70]) and MC-3D (Multi Component-3D, Berthoud [71]) codes developed by IRSN. These codes are still under development to improve the understanding of basic processes related to debris cooling. Here, overviews of the models used by the computational codes to simulate the key processes of debris cooling are given.

For an analysis of long-term coolability i.e. assuming an initially water filled bed heated by decay heat, the modeling of heat transfer between the phases is of minor importance, due to only small deviations from saturation conditions. In this case it is sufficient to assume thermal equilibrium between the phases (solid / liquid). Usually, only small superheats of the particles of few degrees will be required to transfer decay heat to surrounding water. Thus, limitations of cooling do not occur by this process but by limitations of steam removal and especially water access (Bürger and Berthoud [72]). For this condition, the friction forces are decisive; determining how much water can enter into the heat generating bed and how fast the produced steam can be removed.

Two phase friction models are generally based on Ergun's law [57] which is originally proposed for single phase flow through porous media. Ergun's friction law has been extended to two phase flows by introducing relative permeabilities and passabilities which are the volume parts of the fluids inside the pore. In classical models like the model of Lipinski [73], Reed [74] and Hu & Theofanous [75] interfacial friction is not considered explicitly. In these approaches interfacial friction between steam and water is considered in the relative friction contributions of the phases with the solid depending on the volume parts. This is not sufficient in general, if interfacial friction between steam and water plays a role. It is not possible to tune the particle fluid drag in the models without interfacial friction to fit the top (counter-current flow) as well as bottom fed (co-current flow) configuration. A unified description for co- and counter-current flows requires a separate interfacial friction term since its influence is in opposite directions (against in counter-current or favor in co-current flow). In fact, calculations on the experiments of Hofmann [46] failed to reproduce DHF values of the bottom-fed beds with the description adapted to top-flooding i.e. without interfacial friction (see also Schmidt [76] and Bürger et. al. [77]). The obtained DHF values for bottom flooding were significantly too low. For multi-dimensional situations it is essential that the model can cover both cases.

The need of an interfacial friction term has also been shown by Schäfer et al.[65] and Tutu et al. [78]. Measurement of pressure loss in axial segments of the debris bed have demonstrated, that classical friction laws of Lipinski [73], Reed [74] or Hu &Theofanous [75] not including explicitly interfacial friction terms can in principle not reproduce these pressure drops in a large range of conditions. Including an interfacial friction term as e.g. in the Schulenberg & Müller

[79] and Tung & Dhir [80] friction laws, at least the qualitative behavior can be reproduced ([65], [77]).

Schulenberg & Müller [79] used the isothermal air/water experimental pressure drop measurement data to deduce a formulation for the interfacial friction. The major limitation of this model is that the interfacial friction term is dependent on the relative permeabilities and passabilities i.e. the correlations chosen for friction between fluids and solid. Further, its influence vanishes in the model rapidly with increasing void. Therefore, the physical meaning of the interfacial friction, that yields the limitation of water inflow and steam release, does not appear clearly in this model (see also [70], [77]).

A completely different approach was proposed by Tung & Dhir [80]. Based on visual observation in air/water experiments they introduced three different flow regimes, namely bubbly, slug and annular flow regimes. They distinguished the flow regime depending on void fraction as seen in Figure 1.5. For each flow regime and transition particle fluids friction and interfacial friction are derived from geometric considerations.

Tung & Dhir compared their model with the measured pressure gradient and they found a fair agreement with the experiment. But they compared their model with the experiments which are performed with relative large particle diameter. For smaller particle the model results are unsatisfactory (Schmidt [76], Bürger et al. [77]). The range of most interest for reactor applications with respect to severe accidents in LWR lies rather within 1–6 mm diameters. While the values from the Tung & Dhir model lie significantly below the measured dryout heat flux (DHF) data, especially for sphere diameters smaller than 6 mm.

Some attempts have already been taken by Schmidt [76] to extend the Tung & Dhir model for smaller particles. In his approach the transition between the flow patterns of bubbly, slug and annular flow have been modified to yield a more rapid transition towards slug and annular flows with smaller particle diameters. Besides the correction of flow patterns the reduction of

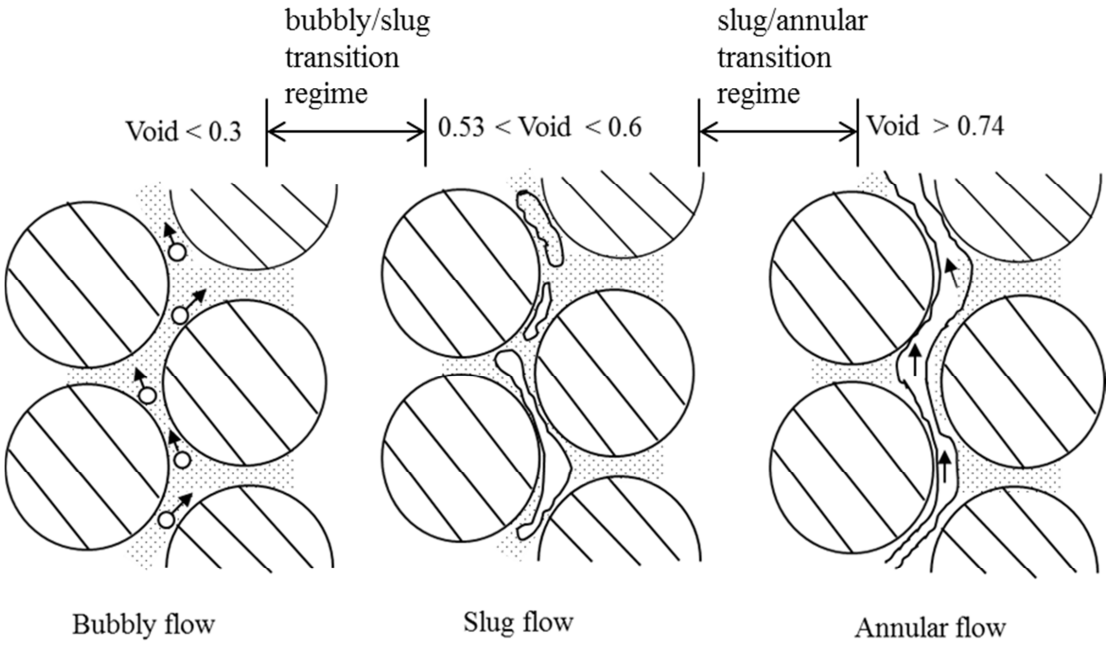

Figure 1.5: Flow pattern in different flow regime inside the debris bed according to Tung & Dhir [80].

interfacial friction for the annular flow regime has also been introduced in his approach. But considering these modifications in the Tung & Dhir model, deficit is still detected especially for capturing the DHF results in both top and bottom flooding situations. Thus, the present status of the Tung and Dhir model requires some modifications to extend it for both top and bottom flooding conditions.

Earlier debris cooling analyses in reactor conditions (e.g. Schmidt [76], Bürger et al. [77]), mainly the case of a water- filled saturated bed has been considered and limits of coolability have been addressed with respect to decay heat removal, i.e. long term coolability. Long-term coolability of a given debris bed configuration is a necessary, but not sufficient condition for the cases when the bed is initially hot and dry. In case of hot and dry debris bed, in order to achieve long term coolability, the bed has to be quenched (from higher temperature to saturation temperature) at first. Quenching of hot debris is the first problem as expected in most of the accident scenarios. Even in an ex-vessel accident scenario with a deep water pool where a debris bed is formed by settling of particles from breakup of melt jets flowing into the water pool, it cannot be assumed to be initially filled with water at saturated conditions. Rather, a hot and dry debris bed is to be expected, at first. Then, in addition with decay heat, sensible heat of the particles has to be removed which is much higher than the decay heat. If quenching of the dry bed is not rapid enough then heat-up by decay heat in still dry regions may again yield melting. It is important to notice that there is a competition between quenching and heat-up. Therefore, quenching is the main problem because quenching versus heat-up by decay heat mostly determines the coolability question in reactor scenarios. Adequate analysis of quenching of hot debris in reactor conditions is required to evaluate the safety margin of debris cooling which has not been done before. Therefore, an emphasis is laid on quenching analyses in the present work.

In case of quenching of hot debris in addition with friction, the modeling of heat transfer is also important. In porous medium, heat transfer and evaporation are in principle based on a thermal non-equilibrium between the phases. Superheated particles, sub-cooled water and superheated steam are taken into account. To calculate the heat transfer between the phases different approaches are presently used. E.g. in ICARE/CATHARE model [70], the heat transfer coefficients are obtained analytically as a function of the local geometry of the porous medium. In this approach geometrical configurations of the porous medium and the local phase distribution are represented by the stratified cell. In this cell, two typical phase repartitions are considered, namely solid–liquid–gas or solid–gas–liquid. Further, it has been assumed that one phase will be wetting (attached to the wall) and the second phase will eventually flow in the remaining pores in the form of bubbles or slugs. For each configuration, macroscopic conservation equations are obtained together with local closure relations from which the effective heat transfer coefficients are determined analytically. However, analytical solutions for these heat transfer coefficients are rather complex due to the complicated formulation.

In the present status of modeling quenching calculations are only possible for given debris configurations starting from assumed initial temperatures (e.g. see calculation in reactor condition by ICARE/CATHERE model [70] or by MEWA model [69]). However, assuming the whole bed at a uniform initial temperature strongly misses the real process in which settling of partly solidified melt drops occurs simultaneously with water inflow and quenching. This real

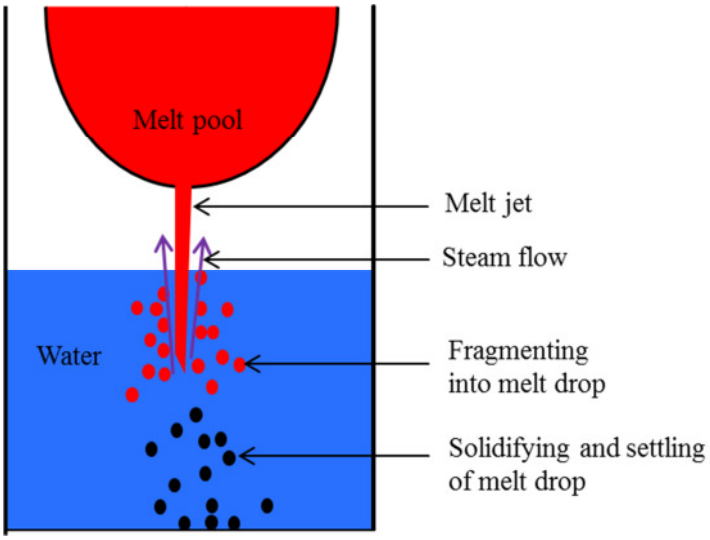

Figure 1.6: Sketch of jet break up process modeled in JEMI [81] code.

process of bed formation by settling and simultaneous quenching is considered strongly favor cooling. Thus, the analyses and the modeling have to be extended to this combined treatment.

The existing codes JEMI (JEt fragmentation and preMIxing, Pohlner [81]) and MEWA [69] serve as the basis for the coupled and integrated simulation. For jet breakup in JEMI [81], it is assumed that the dominant process is stripping of melt from the surface of the jet due to shear flow instabilities. These are produced by the steam flowing upwards along the jet (see Figure 1.6). Growth and wavelength of the instabilities is modeled based on the Kelvin-Helmholtz approach. This approach yields locally varying fragmentation rates and fragment diameters along the jet, developing with time according to the development of the jet and surrounding mixture. The fragmenting upwards vapor flow is driven by the hydrostatic head of the surrounding water and exchanges momentum with particles from the fragmentation process, i.e. feedback between the resulting mixture and jet breakup is taken into account. The local particle diameter yielded by the fragmentation process is superposed by a probability density function in order to obtain a drop size spectrum.

Up to now, these two models concentrate on the individual thermal-hydraulic processes, e.g. JEMI treats the processes of melt jet fragmentation and settling of particles under mixing of melt with water, MEWA describes the debris bed behavior and coolability. Coupling of these two models is required in order to treat the combined simultaneous quenching during debris build up process and will be performed in the present work.

1.3 Aim of the present work

The major aim of the present work is to investigate the options and chances of coolability in key phases of a severe accident with core melting and debris formation, depending on various accident scenarios. The emphasis is on particulate debris or porous structures forming or being induced by AMM (Accident Management Measure). Such porous structures are considered to offer in principle a high potential for coolability due to their open pore. Options and chances of coolability are to be investigated related to the key question i.e. the question whether the hot and dry debris bed can be flooded and cooled by water ingression before further heat-up (rise in temperature due to decay heat) of still dry parts leads to re-melting.

As a basis for these investigations, a model for simulation of two phase flow through porous medium is already available with the MEWA code [69], being under development at IKE. Within the present task the aim is to check the applicability of the MEWA code as a tool to give answers to the above key questions as well as to explore the extent to which generalized conclusions can be drawn about the coolability in each phase and situation.

More than checking and evaluating the adequacy of this existing tool i.e. MEWA, further development to remove weaknesses in modeling and to extent it concerning missing parts (or not sufficient detailed modeling) is envisaged in the present work. This includes also corrections due to specific validation analyses on available experiments. An emphasis with this respect is posed on further qualifying the friction and heat transfer models which are considered as decisive for determining the cooling process. Concerning friction, it will be checked whether the model can sufficiently describe different flow conditions. In view of the importance of 2D/3D flows, various constellations, especially co- as well as counter-current flow patterns of water and steam have to be considered, including the relevance of interfacial friction.

Concerning heat transfer, slow water progression (few mm/s) and a thin quenching front (up to few centimeters) is considered in the present approach for hot beds. Thus, the need for detailed modeling of this thin heat transfer zone (see Figure 1.7) is not important. However, if the water would move a large distance into the debris bed without significant quenching, i.e. with a thick quenching front (several centimeters), then the detailed description of this large heat transfer zone would become important for determining quenching. Therefore the heat transfer zone which is relevant for reactor related cases (thick or thin) needs to be determined in order to justify the present modeling approach. Support has to be taken from the quenching experiments performed in different international laboratories, especially PRELUDE experiments by Repetto et al. [62] with fixed injection rate from bottom and DEBRIS experiments by Rashid et al. [64] with external downcomer. Further, in the validation process, it will especially be checked, whether the most important features of quenching front propagation inside the bed for different configurations and conditions can sufficiently be captured by the code.

In the reactor applications, the aim is to analyze accident scenarios over a wide range of conditions and to seek general conclusions on this basis. In a sequence of a severe accident, a first area is to investigate chances of quenching a hot and degraded core or trends towards melt pool formation. Strong trends (i.e. trends not modified strongly by variations of conditions) in either direction, are to be explored. Supporting options to reach coolability of hot debris as well

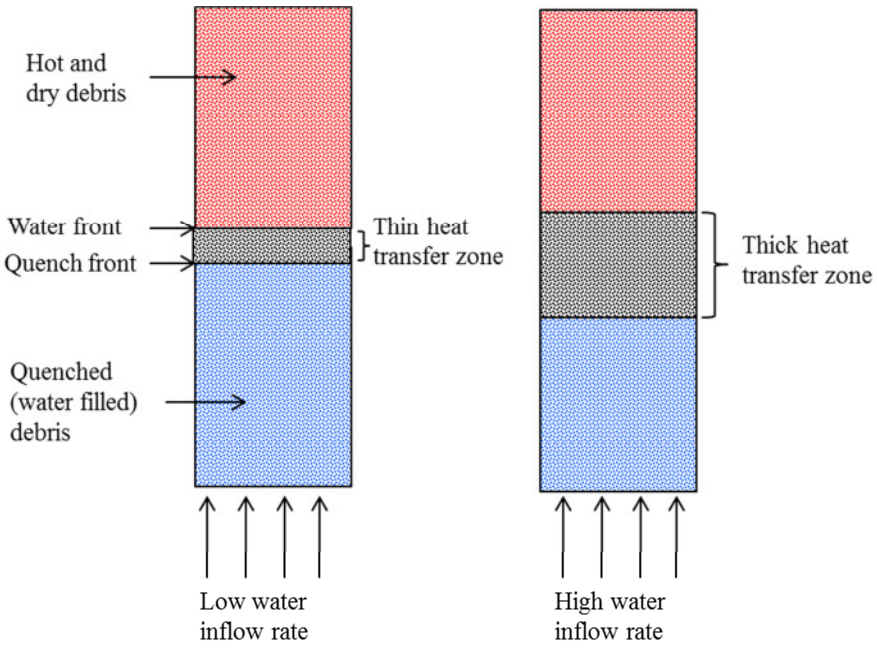

Figure 1.7: Different zone during quenching of hot debris from bottom.

as hindering effects are to be evaluated in this stage of an accident. E.g. lateral water inflow supports the cooling; on the other hand small particle size makes the coolability difficult.

In the lower head, conditions and limits of coolability of hot debris beds are to be examined in order to evaluate options and chances of water injection into the vessel, even in such progressed states of an accident. As for the hot core, the competition of heat-up by decay heat in the dry debris vs. quenching by water ingression decides the final success of cooling. This success of quenching strongly depends on assumed initial parameters. The important parameters considered in this respect are porosity, particle diameter, initial bed temperature, mass of debris bed, system pressure, bed heterogeneities, etc. Variations of calculations with these parameters are to be performed in order to explore up to which conditions and configurations (degradation level) the bed is still coolable. An emphasis will lie on bed heterogeneities, including “cake” regions, i.e. regions with agglomerated, compacted material, but also variations of porosities which may facilitate downcomer-like access of water to bottom regions. The mechanisms to reach the coolable situation will be in the focus in order to provide understanding

In this situation as well as in a debris bed in the flooded cavity, a major influence is the initial temperature of particles, to be assumed if not calculated by a model on jet breakup (e.g. by JEMI [81]). However, assuming the whole bed at a uniform or even non-uniform initial temperature, as normally done in previous analyses (see Fichot et al. [70]) , may strongly miss the real process in which settling of partly solidified melt drops is combined with simultaneous water inflow and quenching. This real process of bed formation by settling and simultaneous quenching is considered strongly favor cooling. Thus, the aim is to extend the existing JEMI and MEWA model to treat and analyze this combined debris bed formation and quenching process.

Only scarce information is available concerning geometries of debris beds formed during inflow of large corium melt into deep water pools. It may be heap-like (conical) or flat shaped due to

spreading of particles on the large surface of a cavity floor caused by strong convective flows. Experimental evidence regarding bed porosity is also poor. Therefore, in order to get an impression on the overall coolability of the debris bed in possible reactor scenarios the calculations are to be carried out by variation of geometry and porosity of the bed.

Even with deep water pool in the cavity (7-10 m for Swedish BWRs), a problem remains that incomplete breakup of melt may occur for thick melt jet (jet diameter > 20 cm, Pohlner [81]). This can lead to configurations with liquid melt at the bottom which may not be coolable with the present SAM (Severe Accident Measures). In this case, the melt would have to be cooled only by water from top which is strongly limited to rather thin melt layers (Allelein and Bürger [82], Sehgal [83]). Thus, improvements should be considered for the SAM concept. One solution may be to provide bottom injection of water into the melt to create porosity inside the melt as considered in COMET concept (Alsmayer and Tromm [12], Journeau et al. [84]). The application of bottom injection of water as a backup measure for this remaining liquid parts needs further investigations. E.g., it is to be examined whether sufficient porosities for effective cooling can be produced in the remaining molten parts. Therefore, some emphasis is posed here on these processes as generic ones and as determining options of combined SAM.

2 Description of the model

The MEWA (MElt and WAter) code (Buck et al. [69]) is being developed at IKE, University of Stuttgart, for the description of the in- and ex-vessel behavior of corium during the late phase of severe accidents. The MEWA code is a combination of the modules MESOCO (MElting/SOlidification COde, Buck [8]), describing the processes in the core with massive melting, melt relocation, molten pool formation and behavior, and the WABE (WAter and BEd) module (Schmidt [76], Bürger et al. [77]), which describes the thermal-hydraulics of water and steam in a porous medium. As the investigations in the present work concentrate on the behavior of particulate or porous debris beds under boil-off or quenching conditions, emphasis here is given to the modeling which is relevant for the two-phase flow of water and steam in a solid debris bed. The full MEWA model is presently only available in the German system code ATHLET-CD (Analysis of Thermal-Hydraulics of LEaks and Transients-Core Degradation, Trambauer et al. [85]). For the present study, a stand-alone version is applied, which contains only a simplified version of MESOCO (no description of melt).

In MEWA, three separate phases, solid particles, liquid coolant (water) and gas (vapor) are considered. The basic assumption is that each phase is considered as a continuum. So, each phase fills only a fraction of the whole control volume V. Volume fractions of solid ($\frac{V_s}{V}$), liquid ($\frac{V_l}{V}$) and gas ($\frac{V_g}{V}$) in a control volume are defined as follows

$$\frac{V_s}{V} = 1 - \varepsilon \tag{2.1}$$

$$\frac{V_l}{V} = s_l \varepsilon \tag{2.2}$$

$$\frac{V_g}{V} = s_g \varepsilon \tag{2.3}$$

Where V_s , V_l and V_g are the solid, liquid and gas volume respectively and these are related to the whole control volume V via $V = V_s + V_l + V_g$.

And ε is the porosity, s_g and s_l are the volume fractions of gas and liquid in porous space, respectively. These quantities are related by

$$s_g + s_l = 1 \tag{2.4}$$

The solid particles are assumed to be in a fixed matrix, which is passed by the flow of the fluids (liquid and vapor). The system is determined by the conservation equations for mass, momentum and energy. Additionally, constitutive laws for heat transfer and friction between the liquid, gas and solid phase are necessary for closure of the equation system.

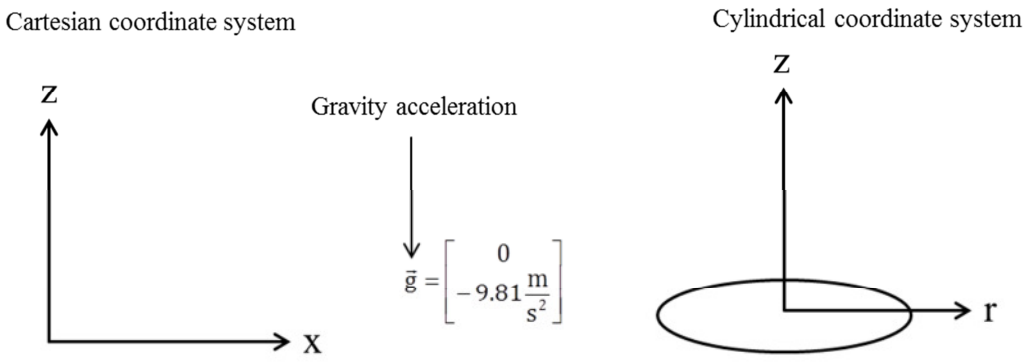

Figure 2.1: Two dimensional Cartesian (left) and cylindrical (right) coordinates systems with the direction of gravity acceleration $\vec{g}$.

2.1 Conservation equations

In MEWA, the cooling behavior of the debris bed is modeled in two dimensions. Either Cartesian or cylindrical geometry may be chosen as shown in Figure 2.1.

The mass conservation equations for gas and liquid are

$$\varepsilon \frac{\partial}{\partial t}(s_g \rho_g) + \nabla .\ (\rho_g \varepsilon s_g \vec{w}_g) = \Gamma^{evap} \tag{2.5}$$

$$\varepsilon \frac{\partial}{\partial t}(s_l \rho_l) + \nabla .\ (\rho_l \varepsilon s_l \vec{w}_l) = -\Gamma^{evap} \tag{2.6}$$

Where, ρ_g and ρ_l are the gas and liquid densities respectively; $\vec{w}_g$ and $\vec{w}_l$ in equation (2.5) and (2.6) are the actual velocities of gas and liquid which related to superficial velocities $\vec{u}_g$ and $\vec{u}_l$ with

$$\vec{u}_g = \varepsilon s_g \vec{w}_g \ , \quad \vec{u}_l = \varepsilon s_l \vec{w}_l \tag{2.7}$$

And Γ^{evap} is the mass transfer rate due to evaporation. The Del operator nabla ∇ and its operations (gradient and divergence) in Cartesian and cylindrical coordinates are defined in Table 2.1.

Table 2.1: Del operator nabla ∇ and its operations in Cartesian and cylindrical coordinates.

Operator / Operations	Cartesian coordinates (x, z)	Cylindrical Coordinates (r, z)
Nabla ∇	$\hat{x}\frac{\partial}{\partial x} + \hat{z}\frac{\partial}{\partial z}$ $\{\hat{x}, \hat{z}\}$ are the unit vectors	$\hat{r}\frac{\partial}{\partial r} + \hat{z}\frac{\partial}{\partial z}$ $\{\hat{r}, \hat{z}\}$ are the unit vectors
Gradient ∇f Where f is a scalar	$\frac{\partial f}{\partial x}\hat{x} + \frac{\partial f}{\partial z}\hat{z}$	$\frac{\partial f}{\partial r}\hat{r} + \frac{\partial f}{\partial z}\hat{z}$
Divergence $\nabla \cdot \vec{v}$ Where $\vec{v}$ is a vector	$\frac{\partial v_x}{\partial x} + \frac{\partial v_z}{\partial z}$	$\frac{1}{r}\frac{\partial (r v_r)}{\partial r} + \frac{\partial v_z}{\partial z}$

In the porous medium, momentum conservation of gas and liquid is assumed to be governed by friction forces, pressure gradient and buoyancy (or weight). Thus, temporal and spatial derivatives of the velocities do not appear. These leads to simplified momentum conservation equation

$$K_{gs}\vec{u}_g + \frac{K_{gl}}{s_g}\left(\vec{w}_g - \vec{w}_l\right) = -\nabla p_g + \rho_g \vec{g} \tag{2.8}$$

$$K_{ls}\vec{u}_l - \frac{K_{gl}}{s_l}\left(\vec{w}_g - \vec{w}_l\right) = -\nabla p_l + \rho_l \vec{g} \tag{2.9}$$

Where, p_g and p_l are the gas and liquid pressure respectively. Liquid pressure will be different than gas pressure if capillary force is considered. Capillary force is important when the particle diameter is very small (< 1 mm). For the present study capillary force is not considered, i.e. $p_g = p_l = p$. In the momentum equations the frictions coefficients are symbolize by K. The dominating forces on the fluids in the porous structures are the particle- fluid drags (friction coefficients K_{gs}, K_{ls}) and the interfacial drag (friction coefficient K_{gl}). The interfacial friction between the fluids has to be the same but with opposite sign.

It is considered that each of the three phases has its own temperature i.e. T_s (solid temperature), T_g (gas temperature) and T_l (liquid temperature). So, three energy conservation equations are considered for each phase separately. For the solid, energy conservation yields

$$(1-\varepsilon)\frac{\partial}{\partial t}\left(\rho_s e_s\right) = \nabla\cdot\left(\lambda_s^{eff}\nabla T_s\right) + Q_{s,decay} - Q_{s,sat} - Q_{s,g} - Q_{s,l} \tag{2.10}$$

Where ρ_s and e_s are the density and specific internal energy of the solid particle. Here all Q are per unit volume $\left(\frac{W}{m^3}\right)$. Heat conduction in the solid (first term on the right hand side), the volumetric heat source, $Q_{s,decay}$ from radioactive decay (or electrical heating in experiments) and the heat going to the vapor-liquid interface, $Q_{s,sat}$ (leading to evaporation) are considered. Direct heat transfer between solid and gas, $Q_{s,g}$ is mainly important in dry regions ($s_l = 0$), while heat transfer between solid and liquid, $Q_{s,l}$ is only considered under sub-cooled conditions i.e. $T_l < T_{sat}$, where T_{sat} is the saturation temperature. The conductive heat transfer in the solid phase is expressed by an effective conduction coefficient λ_s^{eff}, where $\lambda_s^{eff} = \lambda_s(1-\varepsilon)$ and λ_s is the thermal conductivity of solid. The radiation heat transfer in the solid phase is implicitly considered through this effective thermal conductivity.

The energy conservation for the gas phase is given by

$$\varepsilon\frac{\partial}{\partial t}\left(s_g\rho_g e_g\right) + \nabla\cdot\left(\varepsilon s_g\rho_g\vec{w}_g\, i_g\right) = \nabla\cdot\left(\lambda_g^{eff}\nabla T_g\right) + Q_{s,g} + \Gamma^{evap} i_{g,sat} \tag{2.11}$$

Where e_g and i_g are the specific internal energy and enthalpy of gas and $i_{g,sat}$ is the specific gas enthalpy at saturation. The respective terms on the right hand side of the equation denote

conduction, heat transfer between flowing gas and the solid as well as the enthalpy fluxes associated with the mass transfer (evaporation). The conductive heat transfer in the gas phase is expressed by an effective conduction coefficient λ_g^{eff}, where $\lambda_g^{eff} = \lambda_g \varepsilon s_g$ and λ_g is the thermal conductivity of gas.

The energy conservation for the liquid phase yields

$$\varepsilon \frac{\partial}{\partial t}(s_l \rho_l e_l) + \nabla \cdot (\varepsilon s_l \rho_l \vec{w}_l\, i_l) = \nabla \cdot (\lambda_l^{eff} \nabla T_l) + Q_{s,l} - \Gamma^{evap} i_{l,sat} \tag{2.12}$$

Where e_l and i_l are the specific internal energy and enthalpy of liquid and $i_{l,sat}$ is the specific liquid enthalpy at saturation. Here, heat conduction, heat transfer between flowing liquid and the solid as well as the enthalpy fluxes associated with the mass transfer (evaporation) are considered. The conductive heat transfer in the liquid phase is expressed by an effective conduction coefficient λ_l^{eff}, where $\lambda_l^{eff} = \lambda_l \varepsilon s_l$ and λ_l is the thermal conductivity of liquid.

2.2 Constitutive laws

For closure of the equation system several additional relations (constitutive laws) are necessary. These constitutive laws are mainly empirical correlations which are deduced from experiments. Details of these constitutive laws used in the present work are given below.

2.2.1 Equation of state

The equations of state are defined by the thermodynamic properties of water and steam. In order to define the state, the water and steam properties package of ATHLET is used. It calculates the density ρ and enthalpy i of water and steam as functions of pressure p and temperature T, i.e.

$$\rho_l = \rho_l(p, T_l) \qquad i_l = i_l(p, T_l) \tag{2.13}$$

$$\rho_g = \rho_g(p, T_g) \qquad i_g = i_g(p, T_g) \tag{2.14}$$

Saturation properties T_{sat} (saturation temperature), $\rho_{l,sat}$ (liquid density at saturation), $\rho_{g,sat}$ (vapor density at saturation), $i_{l,sat}$ (liquid enthalpy at saturation), $i_{g,sat}$ (vapor enthalpy at saturation) are calculated as a function of pressure p, i.e.

$$\begin{aligned} T_{sat} &= T_{sat}(p) \\ \rho_{l,sat} &= \rho_{l,sat}(p) \quad \rho_{g,sat} = \rho_{g,sat}(p) \\ i_{l,sat} &= i_{l,sat}(p) \quad i_{g,sat} = i_{g,sat}(p) \end{aligned} \tag{2.15}$$

Further, the steam/water properties package provides the calculation of the transport properties dynamic viscosity (η_l, η_g), heat conductivity (λ_l, λ_g) and surface tension (σ).

2.2.2 Heat and mass transfer

Heat transfer and evaporation are based on thermal non-equilibrium between the phases. Superheated particles, sub-cooled water and superheated steam are taken into account. A

conceptual sketch for heat and mass transfer mechanisms is shown in Figure 2.2. In a single phase configuration with either liquid or gas a continuous fluid, direct heat transfer between the solid particles and the fluids can occur. In a two-phase configuration, heat is transferred from the solid to the gas/liquid interface, where it produces evaporation. The mass transfer rate is then given by the heat fluxes directed from solid to the gas/liquid interface $Q_{s,sat}$, divided by the latent heat of evaporation ($i_{s,sat} - i_{l,sat}$).

$$\Gamma_{evap} = \frac{Q_{s,sat}}{i_{g,sat} - i_{l,sat}} \tag{2.16}$$

The respective heat fluxes and mass transfer rates are specified in more detail below.

2.2.2.a Heat transfer between solid particles and interface (the boiling heat transfer)

The heat flux between the solid particles and the gas/liquid interface ($Q_{s,sat}$) is calculated as

$$Q_{s,sat} = a_{s,sat} h_{s,sat} (T_s - T_{sat}) \tag{2.17}$$

Where $h_{s,sat}$ is the heat transfer coefficient between solid particles and the gas/liquid interface and the interfacial area density $a_{s,sat}$ is given by

$$a_{s,sat} = \frac{6 \cdot (1-\varepsilon)}{D_P} \cdot F(s_l) \tag{2.18}$$

$$F(s_l) = \begin{cases} 1 & \text{if} \quad s_l \geq 0.3 \\ \dfrac{s_l}{0.3} & \text{if} \quad s_l < 0.3 \end{cases} \tag{2.19}$$

Boiling at the surface of solid particles is calculated by using correlations, assuming film or nucleate boiling, depending on the solid temperature. A minimum film boiling temperature T_{min}^{FB} is defined as

$$T_{min}^{FB} = T_{sat} + 17.0 \tag{2.20}$$

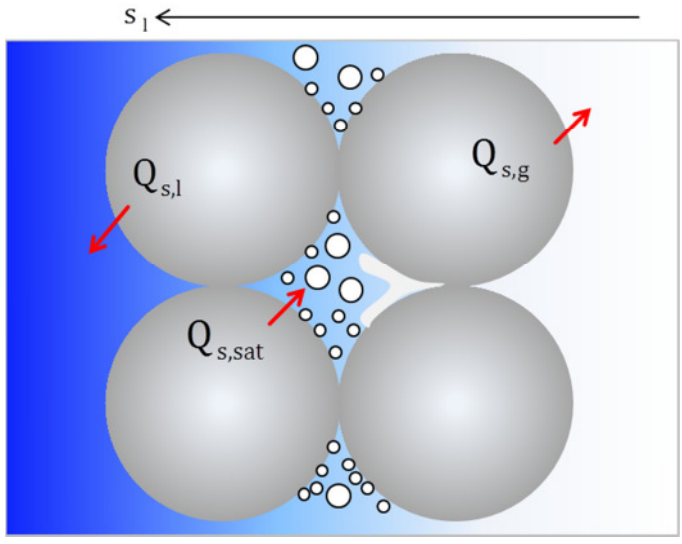

Figure 2.2: Conceptual sketch of heat transfer between phases

If the solid temperature T_s is below the minimum film boiling temperature, i.e. $T_s \le T_{min}^{FB}$, pure nucleate boiling is assumed and the heat transfer coefficient for nucleate boiling $h_{s,sat}^{NB}$ is calculated according to the correlation of Rhosenow [86],

$$h_{s,sat}^{NB} = \frac{c_{p,l}^3 \cdot \eta_l \cdot (T_s - T_{sat})^2}{(i_{g,sat} - i_{l,sat})^2 \cdot (1.2 \cdot 10^{-2} \cdot Pr_l)^3 \cdot \sqrt{\frac{\sigma}{g(\rho_l - \rho_g)}}} \tag{2.21}$$

Where Prandtl number, $Pr_l = \frac{\eta_l c_{p,l}}{\lambda_l}$ and $c_{p,l}$ is the specific heat capacity of liquid.

Above a maximum nucleate boiling temperature

$$T_{max}^{NB} = T_{min}^{FB} + \Delta T_{trans} \quad (\Delta T_{trans} = 100\,K) \tag{2.22}$$

pure film boiling is assumed. The heat transfer coefficient for film boiling $h_{s,sat}^{FB}$ is calculated from the correlation of Lienhard [87], given by

$$h_{s,sat}^{FB} = \frac{Nu_{s,sat}^{FB} \cdot \lambda_g}{D_P} \tag{2.23}$$

With Nusselt number

$$Nu_{s,sat}^{FB} = 0.67 \cdot \left(\frac{\rho_g \cdot g \cdot (\rho_l - \rho_g) \cdot \Delta i'_{sat} \cdot D_P^3}{\eta_g \cdot \lambda_g \cdot (T_s - T_{sat})} \right)^{1/4} \tag{2.24}$$

Where D_p is the particle diameter and the modified latent heat i'_{sat} is a function of the Prandtl and Jacob numbers,

$$\Delta i'_{sat} = (i_{g,sat} - i_{l,sat}) \cdot \left[1 + \left(0.968 - \frac{0.163}{Pr_g} \right) \cdot Ja \right] \tag{2.25}$$

With

$$Ja = \frac{c_{p,g} \cdot (T_s - T_{sat})}{(i_{g,sat} - i_{l,sat})} \tag{2.26}$$

and $Pr_g = \frac{\eta_g c_{p,g}}{\lambda_g}$ where $c_{p,g}$ is the specific heat capacity of liquid. In a transition region between T_{min}^{FB} and T_{max}^{NB}, the heat transfer coefficient is obtained by linear interpolation between the nucleate boiling heat transfer coefficient, calculated at T_{min}^{FB} from Equation (3.21) and the film boiling coefficient, calculated at T_{max}^{NB} from Equation (3.23)

$$h_{s,sat}^{trans} = [1 - W(T_s)] \cdot h_{s,sat}^{NB}(T_{min}^{FB}) + W(T_s) \cdot h_{s,sat}^{FB}(T_{max}^{NB}) \tag{2.27}$$

$$W(T_s) = \frac{T_s - T_{min}^{FB}}{T_{max}^{NB} - T_{min}^{FB}} \tag{2.28}$$

2.2.2.b Heat transfer between solid and gas

Heat transfer between solid and gas bulk is assumed to occur only if the solid temperature is above saturation temperature and gas is the continuous phase ($s_g \geq 0.7$). The heat flux from solid to gas $Q_{s,g}$ is given by

$$Q_{s,g} = a_{s,g} h_{s,g} (T_s - T_g) \tag{2.29}$$

The interfacial area density is given by

$$a_{s,g} = \frac{6 \cdot (1-\varepsilon)}{D_P} \cdot F(s_g) \tag{2.30}$$

$$F(s_g) = \begin{cases} 0 & \text{if} \quad s_g < 0.7 \\ \dfrac{s_g - 0.7}{0.3} & \text{if} \quad s_g \geq 0.7 \end{cases} \tag{2.31}$$

The heat transfer coefficient for solid to gas bulk $h_{s,g}$ is calculated according to

$$h_{s,g} = \frac{Nu_{s,g} \cdot \lambda_g}{D_P} \tag{2.32}$$

with Nusselt number

$$Nu_{s,g} = 2 + 0.6\sqrt{Re_g} \tag{2.33}$$

and Reynolds number

$$Re_g = \frac{\left|\vec{w}_g \rho_g D_P\right|}{\eta_g} \tag{2.34}$$

2.2.2.c Heat transfer between solid and liquid

Heat transfer between solid and liquid is assumed to occur only if the liquid temperature is below saturation temperature and liquid is the continuous phase ($s_l \geq 0.7$). The heat flux from solid to liquid $Q_{s,l}$ is given by

$$Q_{s,l} = a_{s,l} h_{s,l} (T_s - T_l) \tag{2.35}$$

and the interfacial area density by

$$a_{s,l} = \frac{6 \cdot (1-\varepsilon)}{D_P} \cdot F(s_l) \tag{2.36}$$

$$F(s_l) = \begin{cases} 0 & \text{if} \quad s_l < 0.7 \\ \dfrac{s_l - 0.7}{0.3} & \text{if} \quad s_l \geq 0.7 \end{cases} \tag{2.37}$$

The same Equations (2.32-2.34) apply also for the solid/liquid heat transfer, with the index g replaced by l, throughout.

2.2.3 Friction laws

Two phase friction models are generally based on Ergun's law [57] which is originally proposed for single phase flow through porous medium.

The coefficients K used in Equations (2.8) and (2.9) are assumed to have the form

$$K_{gs} = K_{gs}^{lam} + K_{gs}^{turb}\left|\vec{w}_g\right|, \quad K_{ls} = K_{ls}^{lam} + K_{ls}^{turb}\left|\vec{w}_l\right|, \quad K_{gl} = K_{gl}^{lam} + K_{gl}^{turb}\left|\vec{w}_g - \vec{w}_l\right| \tag{2.38}$$

Where K_{gs} and K_{ls} are the friction coefficients for gas particle and liquid particle drags and K_{gl} is the friction coefficient for the interfacial drag, taking into account laminar and turbulent contributions to friction.

Classical models for friction in porous particulate debris, like those of Lipinski [73], Reed [74] and Hu &Theofanous [75], are based on an extension of the single-phase friction law of Ergun. They do not explicitly consider the interfacial fiction between steam and liquid water. Models like those of Schulenberg & Müller [79] and Tung & Dhir [80] explicitly consider the interfacial friction terms.

2.2.3.a Models without consideration of interfacial friction (Lipinski, Reed and Hu/Theofanous models)

These friction models do not explicitly consider interfacial friction between gas and liquid. Rather, they take into account the presence of a second fluid through relative permeabilities (κ_{rel}) and passabilities (μ_{rel}) which are exponents of the saturation (s_g, s_l). Specifically,

$$K_{ls} = \underbrace{\frac{\varepsilon s_l \eta_l}{\kappa \kappa_{rel,l}}}_{K_{ls}^{lam}} + \underbrace{\frac{\varepsilon^2 s_l^2 \rho_l}{\mu \mu_{rel,l}}}_{K_{ls}^{turb}} \cdot \left|\vec{w}_l\right| \tag{2.39}$$

$$K_{gs} = \underbrace{\frac{\varepsilon s_g \eta_g}{\kappa \kappa_{rel,g}}}_{K_{gs}^{lam}} + \underbrace{\frac{\varepsilon^2 s_g^2 \rho_g}{\mu \mu_{rel,g}}}_{K_{gs}^{turb}} \cdot \left|\vec{w}_g\right| \tag{2.40}$$

$$K_{gl} = 0 \tag{2.41}$$

with the relative permeabilities and passabilities of the liquid

$$\kappa_{rel,l} = s_l^m, \qquad \mu_{rel,l} = s_l^n \tag{2.42}$$

and of the gas

$$\kappa_{rel,g} = s_g^m, \qquad \mu_{rel,g} = s_g^n \tag{2.43}$$

where $m = 3$ and n equals 3 (Lipinski), 5 (Reed) or 6 (Hu and Theofanous) and η_l, η_g dynamic viscosity of liquid and gas respectively.

The single phase permeability κ and the passability μ are given according to Ergun [57] by

$$\kappa = \frac{\varepsilon^3 D_P^2}{150 \cdot (1-\varepsilon)^2}, \quad \mu = \frac{\varepsilon^3 D_P}{1.75 \cdot (1-\varepsilon)} \tag{2.44}$$

2.2.3.b Models with consideration of interfacial friction (Schulenberg & Müller and Tung & Dhir models)

Model of Schulenberg and Müller

In the model of Schulenberg & Müller, the coefficient for gas/solid friction is given by Equation (2.40), with relative permeabilities and passabilities

$$\kappa_{rel,g} = s_g^3, \quad \mu_{rel,g} = s_g^4 \cdot f(s_g), \quad f(s_g) = \begin{cases} 0.09 & \text{if } s_g < 0.3 \\ s_g^2 & \text{if } s_g \geq 0.3 \end{cases} \tag{2.45}$$

The coefficient for liquid/solid friction is given by Equation (2.39), with relative permeabilities and passabilities the coefficient for liquid/solid friction by

$$\kappa_{rel,l} = s_l^3, \quad \mu_{rel,l} = s_l^3 \tag{2.46}$$

The coefficient for interfacial friction is given by

$$K_{gl} = \underbrace{350 \cdot \varepsilon^2 \cdot \rho_l \cdot \frac{\kappa}{\mu} \cdot \frac{g(\rho_l - \rho_g)}{\sigma} \cdot s_l^7 \cdot s_g \cdot |\vec{w}_{rel}|}_{K_{gl}^{lam}} \tag{2.47}$$

Model of Tung & Dhir

In the model of Tung & Dhir, several flow regimes are distinguished, depending on the void

Table 2.2: Flow regime according to friction model of Tung & Dhir [80].

Flow regime		**Void fraction range**
Low void bubbly flow	liquid continuous	$s_g \leq s_{g,0}$ $s_{g,0} = \max\left\{0, \frac{\pi}{3} \cdot \frac{(1-\varepsilon)}{\varepsilon} \cdot \gamma \cdot (1+\gamma) \cdot [6\beta - 5 \cdot (1+\gamma)]\right\}$ $\gamma = \frac{D_B}{D_P}$, Bubble diameter $D_B = 1.35\sqrt{\frac{\sigma}{g(\rho_l - \rho_g)}}$, $\beta = \left(\frac{\pi\sqrt{2}}{6(1-\varepsilon)}\right)^{1/3}$
High void bubbly flow		$s_{g,0} < s_g \leq s_{g,1}$ $s_{g,1} = \min\{0.3, 0.6 \cdot (1-\gamma)^2\}$
Transition from bubbly flow to slug flow		$s_{g,1} < s_g \leq \frac{\pi}{6}$
Slug flow		$\frac{\pi}{6} < s_g \leq 0.6$
Transition from slug flow to annular flow	transition	$0.6 < s_g \leq \frac{\pi\sqrt{2}}{6}$
Annular flow	gas continuous	$s_g > \frac{\pi\sqrt{2}}{6}$

fraction (gas saturation), see Table 2.2.

The coefficients for friction between the liquid and the porous matrix are given by Equation (2.39). The relative permeabilities and passabilities for liquid/solid friction are, independent of the flow regime and are given by

$$\kappa_{rel,l} = s_l^3, \quad \mu_{rel,l} = s_l^3 \tag{2.48}$$

The coefficient for gas/solid friction is given by Equation (2.40). Concerning the friction between the gas phase and the porous matrix, it is distinguished with respect to the continuous fluid. For the liquid continuous (LC) region, which is assumed to hold up to $s_g < 0.6$, the relative permeabilities and passabilities for the gas/solid friction are

$$\kappa_{rel,g}^{LC} = s_g^3 \cdot \left(\frac{1-\varepsilon}{1-\varepsilon s_g} \right)^{4/3}, \quad \mu_{rel,g}^{LC} = s_g^3 \cdot \left(\frac{1-\varepsilon}{1-\varepsilon s_g} \right)^{2/3} \tag{2.49}$$

For the gas continuous region (GC) with $s_g > \frac{\pi\sqrt{2}}{6}$,

$$\kappa_{rel,g}^{GC} = s_g^2 \cdot \left(\frac{1-\varepsilon}{1-\varepsilon s_g} \right)^{4/3}, \quad \mu_{rel,g}^{GC} = s_g^2 \cdot \left(\frac{1-\varepsilon}{1-\varepsilon s_g} \right)^{2/3} \tag{2.50}$$

In the transition between liquid continuous and gas continuous region (LGT), where $0.6 < s_g < \frac{\pi\sqrt{2}}{6}$, the gas/particle friction coefficient is obtained by interpolation between the coefficients of the respective regime,

$$K_{gs}^{LGT} = \left[1 - W(s_g, 0.6, \pi\sqrt{2}/6) \right] \cdot K_{gs}^{LC} + W(s_g, 0.6, \pi\sqrt{2}/6) \cdot K_{gs}^{GC} \tag{2.51}$$

using the weighting function

$$W(s, s_{min}, s_{max}) = 3 \cdot \left(\frac{s - s_{min}}{s_{max} - s_{min}} \right)^2 - 2 \cdot \left(\frac{s - s_{min}}{s_{max} - s_{min}} \right)^3 \tag{2.52}$$

For the interfacial friction between liquid and gas, several flow regimes are distinguished. In the *low void bubbly flow regime* (LB), the interfacial friction coefficients are given by

$$\begin{aligned} K_{gl}^{LB} = & \underbrace{18 \cdot s_g \cdot s_l \cdot \frac{1+\gamma}{2} \cdot \ln\left(1 + \frac{2}{\gamma}\right) \cdot \frac{\eta_l}{D_B^2}}_{K_{gl}^{lam}} \\ & + \underbrace{0.34 \cdot s_g \cdot s_l^5 \cdot \left[\left(\frac{1+\gamma}{2} \right) \cdot \ln\left(1 + \frac{2}{\gamma}\right) \right]^2 \frac{\rho_l s_l + \rho_g s_g}{D_B} \cdot \left| \vec{w}_{rel} \right|}_{K_{gl}^{turb}} \end{aligned} \tag{2.53}$$

In the *high void bubbly flow regime* (HB), the friction coefficients are

$$K_{gl}^{HB} = \underbrace{18 \cdot \left[s_{g,0} \cdot \frac{1+\gamma}{2} \cdot \ln\left(1+\frac{2}{\gamma}\right) + s_g - s_{g,0} \right] \cdot s_l \cdot \frac{\eta_l}{D_B^2}}_{K_{gl}^{lam}}$$
$$+ \underbrace{0.34 \cdot \left\{ s_{g,0} \cdot \left[\left(\frac{1+\gamma}{2}\right) \cdot \ln\left(1+\frac{2}{\gamma}\right) \right]^2 + s_g - s_{g,0} \right\} \cdot s_l^5 \cdot \frac{\rho_l s_l + \rho_g s_g}{D_B} \cdot \left|\vec{w}_{rel}\right|}_{K_{gl}^{turb}} \tag{2.54}$$

In the *slug flow regime* (S), the friction coefficients are

$$K_{gl}^{S} = \underbrace{5.21 \cdot s_g \cdot s_l \cdot \frac{\eta_l}{D_B^2}}_{K_{gl}^{lam}} + \underbrace{0.92 \cdot s_g \cdot s_l^5 \cdot \frac{\rho_l s_l + \rho_g s_g}{D_B}}_{K_{gl}^{turb}} \cdot \left|\vec{w}_{rel}\right| \tag{2.55}$$

For the *annular flow regime* (A),

$$K_{gl}^{A} = K_{gs}^{GC} \cdot s_l = \underbrace{\frac{\varepsilon s_l \eta_g}{\kappa s_g^2} \cdot \left(\frac{1-\varepsilon}{1-\varepsilon s_g}\right)^{-4/3}}_{K_{gs}^{lam}} + \underbrace{\frac{\varepsilon^2 s_l \rho_g}{\mu s_g} \cdot \left(\frac{1-\varepsilon}{1-\varepsilon s_g}\right)^{-2/3}}_{K_{gs}^{turb}} \cdot \left|\vec{w}_g\right| \tag{2.56}$$

For the interfacial friction coefficients in the transition regions between the bubbly and slug flow regimes (BST), as well as between the slug and annular flow regimes (SAT), a weighting between the respective regimes is applied:

$$K_{gl}^{BST} = \left[1 - W(s_g, s_{g,1}, 0.3)\right] \cdot K_{gl}^{HB} + W(s_g, s_{g,1}, 0.3) \cdot K_{gl}^{S} \tag{2.57}$$

$$K_{gl}^{SAT} = \left[1 - W(s_g, 0.6, \pi\sqrt{2}/6)\right] \cdot K_{gl}^{S} + W(s_g, 0.6, \pi\sqrt{2}/6) \cdot K_{gl}^{S} \tag{2.58}$$

2.2.4 Modified Tung and Dhir friction model

When applied to cases with pure top-flooding (counter-current flow of water and steam) the model of Tung and Dhir [80] gives unsatisfying results compared to experimental results for dryout in particulate debris beds with smaller particle size. Therefore some modification of Tung and Dhir model are necessary to extend it for smaller particles. An attempt has already been taken by Schmidt [76] especially concerning the modification of flow pattern range for smaller particles. Besides the correction of flow pattern the reduction of interfacial friction for the annular flow regime has also introduced in his approach. But with his modification deficit is still detected especially for capturing the DHF for both top and bottom flooding situations . Correction of gas particle and liquid particle drag might also necessary which was missing in his approach. The following modifications are presently considered in the Tung & Dhir friction model to extend it for both top and bottom flooding situations over the whole bandwidth of particle size .

Modification of the flow pattern range

In the original Tung & Dhir model, the annular flow regime establishes for void fraction $s_g > 0.74$, for all particle sizes. But according to Schmidt [76], for smaller particles, channel flow is expected to establish for smaller void fractions than the prescribed void fraction in original Tung & Dhir model. This is physically plausible because of the thinner flow channels. Therefore, Schmidt [76] modified the flow patterns transition regime of bubbly, slug and annular flow to yield a more rapid transition towards slug and annular flows with smaller particle diameters. Consequently, the bounds for the bubbly and slug flow regimes have also modified . However, to yield earlier transition with smaller particle diameter, a sharp linear decrease of void fraction is considered by Schmidt (see blue solid line in Figure 2.3) which is not realistic. Instead, in the present approch a gradual decrease of void fraction is taken to yield more rapid transition with smaller particles as shown in Figure 2.3 with black solid lines. This appears more plausible as also confirmed by the flow regime measurement by Haga [88]and Stürzel [89]. Haga who performed experiments with 2 and 1 mm particles and conclude that for 2 mm particle annular flow established with 32% void and for 1 mm particle it established with 25% void. Stürzel performed isothermal air / water experiments for the debris bed with different particle diameter and found that transition between slug and annular flow start with 60% void fraction for 10 mm particle, 55 % void for 7 mm particle and 48 % void for 5 mm particle. The proposed modified flow pattern range is given in Table 2.3.

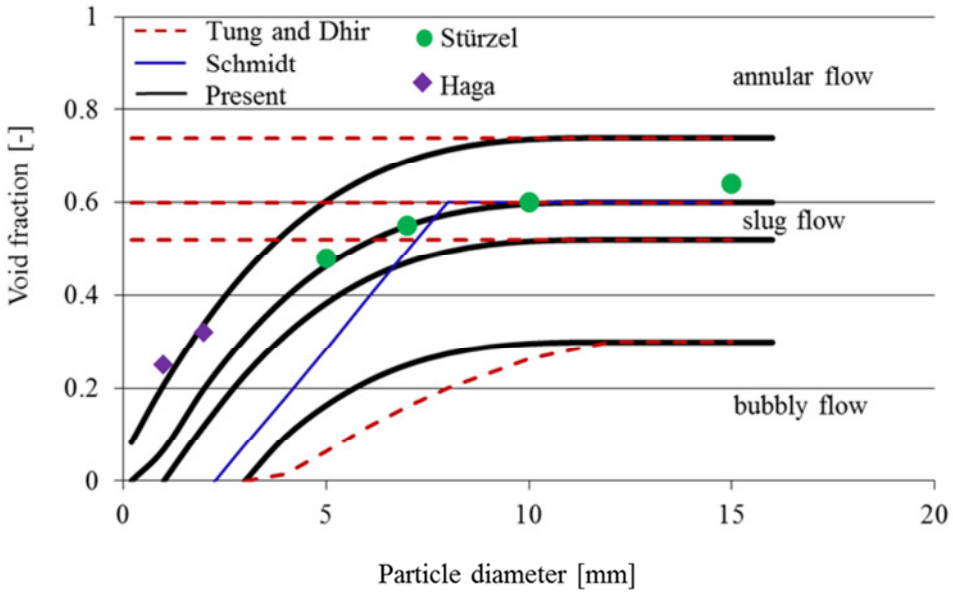

Figure 2.3: Flow pattern map for modified Tung and Dhir model

Table 2.3: Flow regime according to modified Tung & Dhir.

Flow regime		**Void fraction range**
Low void bubbly flow	liquid continuous	$s_g \le s_{g,0}$ $s_{g,0} = \max\left\{0, \frac{\pi}{3}\cdot\frac{(1-\varepsilon)}{\varepsilon}\cdot\gamma\cdot(1+\gamma)\cdot[6\beta-5\cdot(1+\gamma)]\right\}$ $\gamma = \frac{D_B}{D_p},\ D_B = 1.35\sqrt{\frac{\sigma}{g(\rho_l-\rho_g)}},\ \beta = \left(\frac{\pi\sqrt{2}}{6(1-\varepsilon)}\right)^{1/3}$
High void bubbly flow		$s_{g,0} < s_g \le s_{g,1}$ $s_{g,1TD} = \min\{0.3, 0.6\cdot(1-\gamma)^2\}$ $s_{g,1} = \min\left(s_{g,1TD},\ 4\cdot10^5\cdot(D_p - D_{p0})^3 + s_{g,1TD}\right),\ D_{p0} = 1.2\cdot10^{-2}$ [m]
Transition from bubbly flow to slug flow		$s_{g,1} < s_g \le \min\left(\frac{\pi}{6},\ 4\cdot10^5\cdot(D_p - D_{p0})^3 + \frac{\pi}{6}\right)$
Slug flow		$\min\left(\frac{\pi}{6},\ 4\cdot10^5\cdot(D_p - D_{p0})^3 + \frac{\pi}{6}\right) < s_g \le \min\left(0.6,\ 4\cdot10^5\cdot(D_p - D_{p0})^3 + 0.6\right)$
Transition from slug flow to annular flow	transition	$\min\left(0.6,\ 4\cdot10^5\cdot(D_p - D_{p0})^3 + 0.6\right) < s_g \le \min\left(\frac{\pi\sqrt{2}}{6},\ 4\cdot10^5\cdot(D_p - D_{p0})^3 + \frac{\pi\sqrt{2}}{6}\right)$
Annular flow	gas continuous	$s_g > \min\left(\frac{\pi\sqrt{2}}{6},\ 4\cdot10^5\cdot(D_p - D_{p0})^3 + \frac{\pi\sqrt{2}}{6}\right)$

Modification of gas particle and liquid particle drag

The second point to be modified concerns the relative permeabilities of gas-particle and liquid-particle friction. In the Tung & Dhir model, the system of particles and liquid is considered for the gas-solid friction as an isotropic porous layer with porosity εs_g . Due to the presence of the liquid layer at the solid, they correct the particle diameter, yielding extra terms $\left(\frac{1-\varepsilon}{1-\varepsilon s_g}\right)^{4/3}$ and $\left(\frac{1-\varepsilon}{1-\varepsilon s_g}\right)^{2/3}$ for the relative permeabilities and passabilities in the gas and liquid continuous regimes (equations 2.49 and 2.50). The contribution of these extra terms to gas/ particle drag may be more relevant for isothermal air/ water system but for heated particle their contribution can be neglected due to intermittent contact of liquid with water. Therefore, in the modified Tung & Dhir model relative permeabilities and passabilities for gas particle drag simply become

$$\kappa_{rel,g}^{LC} = s_g^3, \quad \mu_{rel,g}^{LC} = s_g^3 \tag{2.59}$$

for the liquid continuous region (LC), and

$$\kappa_{rel,g}^{GC} = s_g^2, \quad \mu_{rel,g}^{GC} = s_g^2 \tag{2.60}$$

for the gas continuous region (GC).

The liquid-particle drag is also modified. It is reduced for laminar flow regime and increased for turbulent flow regime. The proposed relative permeabilites and passabilities are

$$\kappa_{rel,l} = s_l^2, \quad \mu_{rel,l} = s_l^5 \tag{2.61}$$

Modification of interfacial friction

The third point to be modified is the interfacial friction in different flow regimes. The original Tung & Dhir model predicts too low dryout heat fluxes under top flooding condition. A too high interfacial friction may be considered acting against the water inflow from top. So some reduction to the interfacial drag in the bubbly, slug and annular flow regime is necessary. Additionally, for smaller particles, annular flow is established. As a result interfacial area between gas and liquid is now reduced for annular flow. So an additional reduction factor for the interfacial friction term in annular flow has been introduced to meet top flow DHF. It is modeled to decrease below particle diameters of 3 mm. The modified formulation of the interfacial friction is for the *bubbly and slug flow*

$$K_{gl}^{S} = K_{gl,TD}^{S} \cdot \min\left(1, \frac{d_p}{1.2 \cdot 10^{-2}}\right) \tag{2.62}$$

and for the *annular flow*

$$K_{gl}^{A} = K_{gl,TD}^{A} \cdot 0.25 \cdot \min\left(1, \left(\frac{d_p}{0.3 \cdot 10^{-2}}\right)^3\right) \tag{2.63}$$

2.3 Numerical solution method

The mass, momentum and energy conservation equations are given in the form of partial differential equations. These coupled differential equation systems are solved numerically in MEWA (see Buck [8]). For the spatial discretization of the partial differential equations a finite volume method (Patankar [90]) is applied. Cylindrical or Cartesian coordinates and an orthogonal, staggered grid are used for discretization. Scalar quantities (like pressure, temperature and volume fractions) are defined at cell centers and vector quantities (like velocity and mass flux) at cell faces. For the temporal discretization, implicit scheme based on backward differences are used. The non-linear coupled system of equations resulting from the discretized conservation equations is solved with a segregated procedure as described below.

Due to the implicit time discretization, the mass and momentum conservation equations (and also the energy conservation equations) have to be solved iteratively. This is done in MEWA as follows: First, the momentum equations for gas and liquid are solved for the gas and liquid velocities, using actual values of saturation and pressure. Then, the velocities are inserted in the mass conservation equations of gas and liquid. By applying a Newton type method, the mass

conservation equations are used to calculate corrections to the pressure and saturation, such that the mass flow rates calculated with the corrected pressures and saturations satisfy the discrete mass conservation equations. This involves the linearization of the terms in the mass conservation equations with respect to saturation and pressure, including the dependence of the velocities on these. After the update of pressure and void fractions, the energy equations of liquid and vapor are solved separately. Linearization with respect to the respective temperatures yields linear systems, from which temperature corrections are calculated. Due to non-linearity and coupling between equations, an iterative procedure is required. The above steps of the segregated solution procedure are therefore repeated within the actual time step until sufficient convergence is reached.

2.4 Extension of the model: debris bed formation from melt jet breakup and particle settling

The Initial temperature of particles has a strong influence in the evaluation of quenching of hot debris. In the present status of modeling, quenching analysis is only possible with an established debris bed starting from assumed uniform initial temperatures. However, assuming the whole bed at a uniform temperature may strongly miss the real process in which settling of partly solidified melt drops is combined with simultaneous water inflow and quenching. This real process of bed formation by settling and simultaneous quenching is considered as strongly favorable for cooling. Thus, the modeling has to be extended to this combined treatment. The existing codes of IKE, JEMI (Pohlner[81]) and MEWA (Buck et al.[69]) are considered as the basis to treat this coupled process.

The JEMI code treats the processes of melt jet fragmentation and mixing of melt with water and MEWA described the debris bed behavior and coolability. For jet breakup in JEMI, it is assumed that the dominant process is stripping of melt from the surface of the jet due to shear flow instabilities. These are produced by the steam flowing upwards along the jet. Growth and wavelength of the instabilities is modeled based on the Kelvin-Helmholtz approach [81]. This approach yields locally varying fragmentation rates and fragment diameters along the jet (see Figure 2.4), developing with time according to the development of the jet and surrounding mixture. The fragmenting upwards vapor flow is driven by the hydrostatic head of the

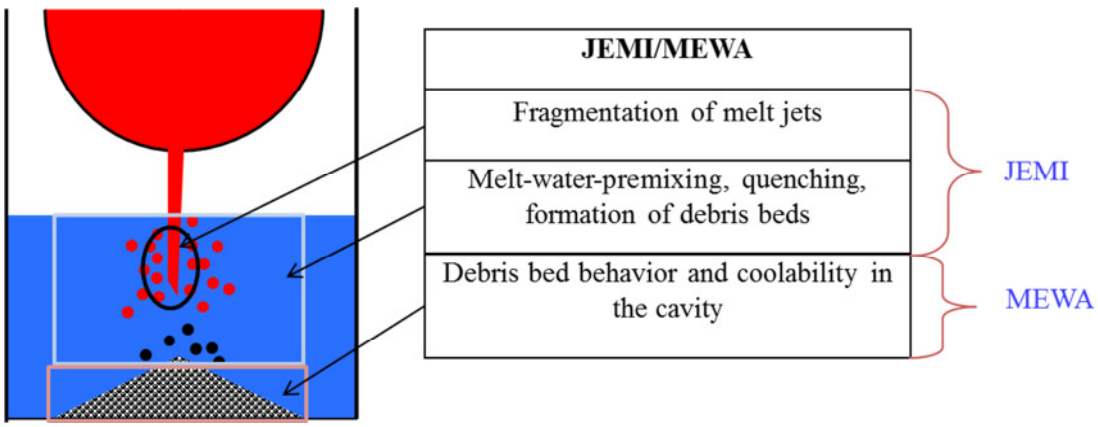

Figure 2.4: Sketch of debris bed build up from jet breakup during falling into water pool

surrounding water and exchanges momentum with particles from the fragmentation process, i.e. feedback between the resulting mixture and jet breakup is taken into account. The local particle diameter yielded by the fragmentation process is superposed by a probability density function (log-normal or Weibull) in order to obtain a drop size spectrum.

The JEMI model treats the mixing zone outside the debris bed, while MEWA treats the processes inside the debris bed. This now allows the combined simulation of jet breakup, quenching, solidification of droplets, settling as debris bed and the quenching of the debris bed already during the buildup. A conceptual sketch for jet breakup and debris bed formation is given in Figure 2.4. The coupling of the model regions takes place at the surface of the debris bed. It must be noted that the boundaries of the debris bed are temporally and spatially not fixed. They change according to the continuous addition of debris to the bed, either in the form of (coherent) melt or of particles.

The mixing zone (treated by the JEMI model) yields the local mass flow rates and state (composition, temperature) of coherent melt or local mass flow rates and state of particles across the actual bed boundaries, thus the deposition of mass on top of the debris bed. From this information the formation of the debris bed is derived. The development of the debris region is treated within the MEWA model, including the development of the actual bed boundaries (local function of height versus coordinates of the base plane) based on the continuous addition of debris mass from the mixing zone.

3 Validation of the model

3.1 Important aspects

The emphasis here is to capture the most important features for the final aim, i.e. understanding of cooling processes inside the debris bed sufficiently. Key areas in this respect are to check the processes of lateral and bottom inflow of water into the debris beds. These modes have been considered as most effective in cooling (see also Schmidt [76] and Bürger et al. [77]). E.g. heap-like, heterogeneous beds are to be expected in realistic multidimensional configurations. Due to this shape of the bed, the inflow of water from top will be more favorable for the smaller heights at the sides. The inflow from the sides, especially via bottom regions, is further promoted by the lateral pressure gradients inherently produced between central regions with high steam content and water-rich outer regions. As a result, a two-phase natural convection loop is established. Water inflow into bottom regions may also occur via preferable paths where water penetration is easier e.g. due to larger particles, higher porosity, unheated parts etc.

An emphasis for validation with this respect is posed on further qualifying the friction and heat transfer laws which are considered as decisive for determining the flow conditions inside the debris bed. With boil-off under release of decay heat, starting with an initially quenched and water-filled bed, the modeling of heat transfer between the phases is of minor importance, due to only small deviations from saturation conditions. Usually, only small superheats of the particles of few degrees will be required to transfer the decay heat to surrounding water. Thus, limitations of cooling do not occur by this process but by limitations of steam removal and especially water access. In such conditions friction effects are decisive; determining how much water can enter into the heat generating bed and how fast the produced steam can be removed. In other words, friction determines the occurrence of dryout inside the debris bed.

In view of the importance of 2D/3D flows indicated by the lateral water inflow as described above, it is important to capture the different flow conditions by the model, especially, the gravity driven flow. It was identified that classical models without considering the interfacial friction explicitly, like the model of Reed can predict DHF (dryout heat flux – DHF – as maximum cross-sectional heat flux) well under top fed condition after adaption for this case but it fails to predict DHF values driven by a lateral water column yielding inflow of water into the bed from bottom. The lack of an interfacial water/ steam friction term in the Reed model is considered as possible cause for yielding lower DHF values under bottom flooding than obtained experimentally (Bürger [77]). Interfacial friction decreases DHF for top flooding (counter-current flow of water and steam) but increases it for bottom flooding (co-current flow). Then, a unified approach requires an explicit interfacial friction term accounting for this difference.

In realistic accident scenarios, debris beds cannot be expected to have a homogeneous structure. Internally more porous and less porous regions with irregularly shaped particles of different sizes, distributed as well as mixed on a more local level are to be expected. Compared to spherical particles higher friction is expected with prototypic, irregularly shaped particles. Also, higher friction is generally obtained with particles of different sizes, locally mixed, due to reduced porosity if smaller particles take the free space between larger ones. However, the

irregular shape counteracts and may even yield increased porosity. This process is different from intense mixing as usually performed for construction of debris beds in experiments. It appears not to favor local mixing, as also indicated by high porosities in the DEFOR experiments aiming at debris bed formation from breakup and settling. Further, such processes provide stratification, either vertically or horizontally, and in general heterogeneities in the bed as a whole. This may increase or decrease the coolability, depending on the given configuration. Therefore, a broad bandwidth of conditions with different debris configurations ranging from beds with uniform particle diameters to beds with irregularly shaped particles and stratification is to be considered.

For the validation of MEWA, to be oriented at prototypic beds, it is then not sufficient to check constitutive laws and integral behavior for specific, idealized conditions, but in view of the uncertainties- to consider a broad spectrum of conditions. The major aim must be to explore the effects and their strength in order to be able to conclude in an overall way on coolability in reactor scenarios. A realistic view has to be envisaged in this process (modeling and validation fitting for reactor safety purpose), allowing to limit variations already from scenario aspects (as e.g. concerning porosity of beds formed by settling).

Experiments with fully quenched, water-filled beds addressed the limit of coolability with respect to decay heat removal, i.e. long-term coolability. Long-term coolability of a given debris bed configuration is a necessary, but not sufficient condition to determine whether debris beds created from melt jet breakup and settling of particles will finally lead to a stabilized configuration. Initially, the settling particles are so hot that water will be driven out of the forming bed. It has to be re-flooded and quenched afterwards.

The need for respective modeling and checking increases if initially hot debris is considered. In case of quenching of hot debris, the heat transfer description becomes important, in addition to friction. However, slow water progression and a thin quenching front, as expected under reactor conditions, may relax the need for detailed modeling of the heat transfer zone. But, if the water would move a larger distance into the debris bed without significant quenching, i.e. with a thick quenching front, then the detailed description of this enlarged heat transfer zone would become important for determining quenching. This could happen with increased water velocity and stable vapor film boiling at high temperatures. Therefore, in order to clarify to which degree details have to be described in an adequate model, it is important to determine the characteristic of quenching in debris beds under reactor conditions, especially concerning the thickness of the quenching regions. It has to be checked, whether quench-front propagation inside the bed is sufficiently described by the model for different configurations and conditions.

3.2 Validation with respect to dryout heat flux (long term coolability aspects)

3.2.1 Spherical particles under top and bottom flooding

As describe above, an explicit interfacial friction term has to be introduced into the friction model in order to describe DHF under top and bottom flooding (counter and co-current flow) conditions. Tung and Dhir [80] as well as Schulenberg and Müller [79] have introduced such interfacial terms. Schmidt [76] has introduced modification on the basis of the model of Tung and Dhir, especially concerning a reduction factor for the interfacial term and modification of

the flow pattern transitions depending on the particle diameter. Further modifications have been performed here, due to remaining deficits (see section 2.2.4). The main overall objective of these modifications is to reach a unified description of friction for different flow configurations which can be used in the multi-dimensional codes in order to analyze adequately the coolability under reactor conditions. For this purpose, the various flow configurations under 2D/3D situations must in principle be captured, especially the most determining conditions of counter and co-current flows of steam and water connected with top and bottom flooding situations.

In order to validate the friction model, equations (2.51) to (2.63), an extended number of experiments from the literature have been calculated here with MEWA comparing the different modeling approaches. These experiments mostly serve to determine the maximum heating power (dryout power, dryout heat flux), that can be removed from a debris bed with different flow conditions, especially for top and bottom flooding. With the model, the DHF is determined in a similar way as in the experiments: the volumetric heat flux is increased in small steps and kept constant for a sufficiently long period (10 to 15 minutes). First occurrence of a dry spots is in both top and bottom flooding cases taken as DHF criterion and the corresponding power is considered as the dryout power.

Under top flooding, the counter-current flow situation yields limitations to water inflow from top (see Figure 3.1). With bottom flooding, in addition to an overlying pool, the water inflow from bottom prevails over the whole bed height when the heating power is small enough (mass inflow > evaporation within height). However, with a lateral water column providing water inflow at the bottom, this depends in a self-regulating way on the feedback with the development in the bed, especially the void buildup there, which determines the driving pressure difference. If, with higher bed power, the water inflow is not sufficient, additional water inflow from top may support the cooling in upper regions. Then, DHF is determined under the mixed influences of top and bottom water inflow and correspondingly by friction in counter as well as co-current configurations (see Figure 3.1). Thus, since friction determines DHF, as already outlined above, these experiments on DHF, especially with various flow configurations, serve to check the friction laws in an integral way.

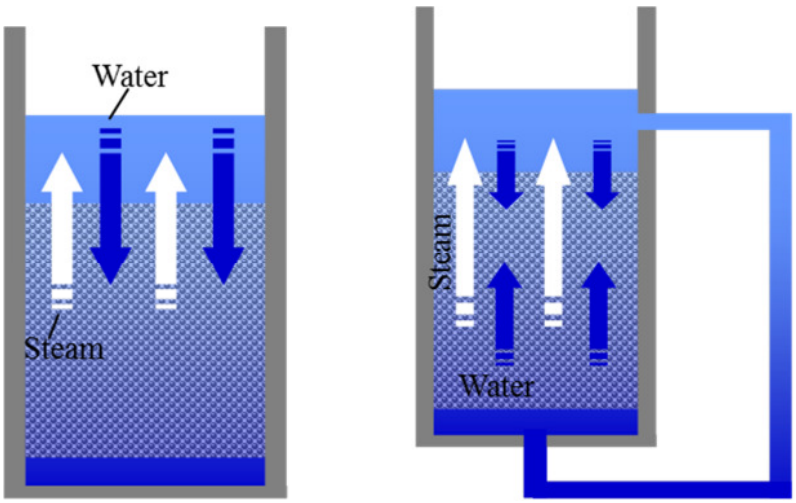

Figure 3.1: Water and steam flow under top (left) and bottom (right) flooding experiments.

3.2.1.a Hofmann top and bottom flooding experiments [46]

In these experiments, an inductively heated bed with porosity, $\varepsilon = 0.405$, spherical particles of diameter, $D_p = 3$ mm at ambient pressure (p =1 bar) was used. These well-documented experiments are still outstanding since in contrast to most other earlier experiments, they have been performed for both top and bottom flooding conditions, where the water could enter only from the pool above the bed, and for conditions where the bottom of the bed was connected by an external pipe to the pool on top. The latter configuration is denoted by "bottom flooding" in the following, although water access is possible from both top and bottom in this case.

Table 3.1shows the results for the dryout heat flux calculated with the MEWA code using different friction models. A significant improvement with the new friction description, modified Tung & Dhir (MTD) model (see equations (2.51) to (2.63)), can be observed considering the aim of a unified description, here for both top and bottom flooding. A rather good agreement with the experimental DHF results is achieved with the MTD description. The other models fail to reproduce the experimental result either for top or bottom flooding. Especially, the Reed correlation (equations (2.39) to (2.44)), adapted to top flooding, yields lower DHF for bottom flooding. Since interfacial friction acts supporting for water inflow from bottom and subsequent upwards flow but hindering for inflow from top (i.e. different in co- and counter-current flow) the Reed correlation, without explicit interfacial friction term, cannot be adapted to both situations. The Schulenberg & Müller (SM) improves Reed concerning bottom flooding but not sufficiently. The lower dryout heat flux prediction with the original Tung & Dhir (TD) model including interfacial friction indicates that the effect of interfacial friction for inflow of water from top in a counter-current flow is too strong, while the correlation is adapted to bottom flooding. Werner Schmidt (WS) improves the Tung & Dhir model concerning top flooding but not sufficient for bottom flooding while yielding to strong reduction for bottom flooding case. The new approach (MTD) introduced in the present study by considering weak supporting effect for bottom flooding (increase of DHF) and too strong reduction for top flooding (see equation (2.63)) appears as the best compromise for both top and bottom flooding.

Table 3.1: Dryout heat flux (DHF) calculation with different friction laws on Hofmann top and bottom flooding experiments.

	DHF [kW/m2]	
	Top flooding	Top + Bottom flooding
Experiment	**910**	**2088**
Reed	952	1284
Schulenberg & Müller (SM)	861	1665
Tung & Dhir (TD)	595	2089
Werner Schmidt (WS)	950	1535
Modified Tung & Dhir (MTD)	**886**	**2000**

3.2.1.b DEBRIS top and bottom flooding experiments with poly-disperse spherical particles [47]

The bed is composed of 6/3/2 mm particles (mass composition: 50 % 6 mm, 30 % 3 mm , 20 % 2 mm). In this bed the measured porosity is 0.36. From single phase pressure drop measurements, taking this porosity, the effective particle diameter, calculated by means of the Ergun law is 2.9 mm (surface average value 3.50 mm). The experiments have been performed for both top and bottom flooding conditions. The bottom flooding is provided by a lateral water column of the height of the bed.

Figure 3.2 shows the comparison of the DHF calculated by MEWA using different friction models with the measured experimental results. The comparison again confirms the MTD approach, especially against those of Reed and original Tung and Dhir (TD), but again also with advantages concerning the other correlations. These DEBRIS results confirm the strong increase (about twice) of the DHF with bottom versus top flooding also for the poly-dispersed debris. In

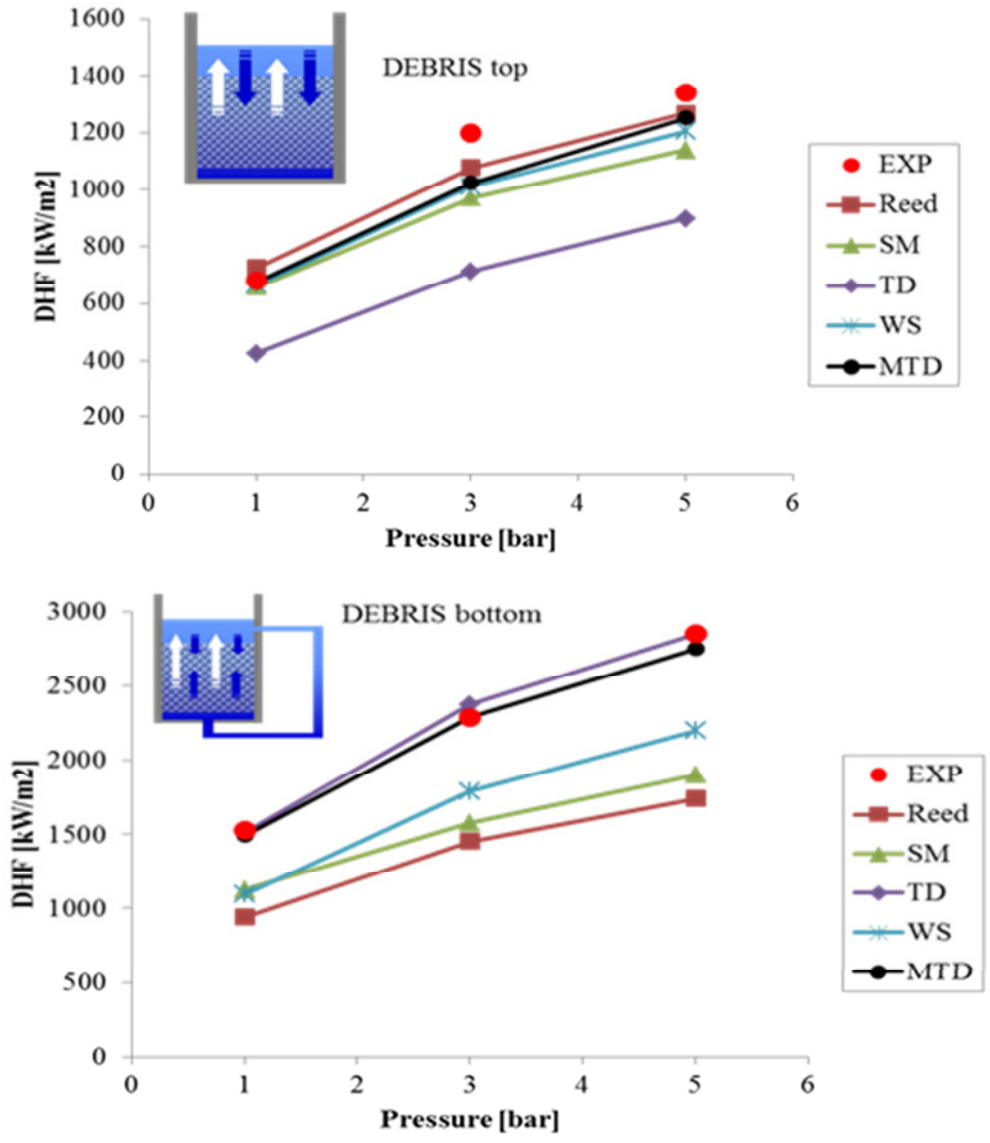

Figure 3.2: Dryout heat flux measured in DEBRIS top and bottom flooding experiments with debris bed composed of poly-dispersed spheres at different system pressures and corresponding MEWA results using different friction models.

case of bottom flooding, a natural circulation loop is established due to the lateral pressure difference between the pure water column and the water/steam column in the bed. This natural circulation driven cooling supports water inflow in the bottom bed regions and alleviates the counter-current flow limitation and therefore increases the DHF value.

In order to confirm the adequacy of the friction model over a large bandwidth of conditions, MEWA is applied to further experiments. Since the Reed, TD, SM or WS friction models fail to reproduce the experimental results either for top or bottom flooding conditions (see Table 3.1 and Figure 3.2) and the new MTD correlation yielded best results, only the latter are further applied.

3.2.2 Mixed and irregular particles

3.2.2.a DEBRIS experiments with irregular particles [49]

In these experiments, the bed was composed of 48 volume % irregularly shaped alumina particles and 52 % steel spheres. The alumina particles resulted from PREMIX melt-water interaction experiments [41] performed at FZK (Forschung Zentrum Karlsruhe), in which molten alumina was poured into a water pool. It was considered to use typical particles from breakup and settling experiments in the DEBRIS experiments especially in view of character shapes. However, this approach is limited due to the need of a large amount of steel particles to enable induction heating. Further, the breakup process with alumina is typical concerning high temperature, but especially not with respect to the melt density tending to yield larger particles. Nevertheless, these experiments can at least be taken as an approach to more realistic irregular debris which has some link to the real process. The particle sizes from the melt-water interaction ranged from 2 to 5 mm in diameter and the additional spherical steel particles were composed of 19 volume % with 3 mm and 33 volume % with 6 mm diameter. For this bed, produced by mixing of the particles, the measured porosity was 0.38. From single phase pressure drop measurements, taking this porosity, the effective particle diameter, calculated with Ergun correlation is 3.2 mm. In these experiments, the dryout heat flux was measured for different system pressures (1, 3 and 5 bar).

A comparison between the experimental dryout heat flux and MEWA prediction with the MTD model is shown in Figure 3.3. From Figure 3.3, one can conclude that the MTD model gives good agreement in predicting the DHF also for beds with mixtures of irregular particles using the effective particle size calculated from the single-phase flow measurements of pressure drop in the bed. This shows that determining the bed characteristics by single phase flow through the bed is sufficient to get good results also for the two-phase flow using the related MEWA-model. But, determining the bed characteristics directly from fragment-size distributions is more difficult. From experimental experience it appears that effective sizes are in the range of surface averaged values or even smaller. On the other hand, porosities appear to be higher with debris from settling processes than from mixing of particles in counteracting experimental debris. Thus, this indicates the need for extended experiments in order to better evaluate realistic quantities and also for the model application to reactor conditions, to check effects over a sufficient variety of conditions.

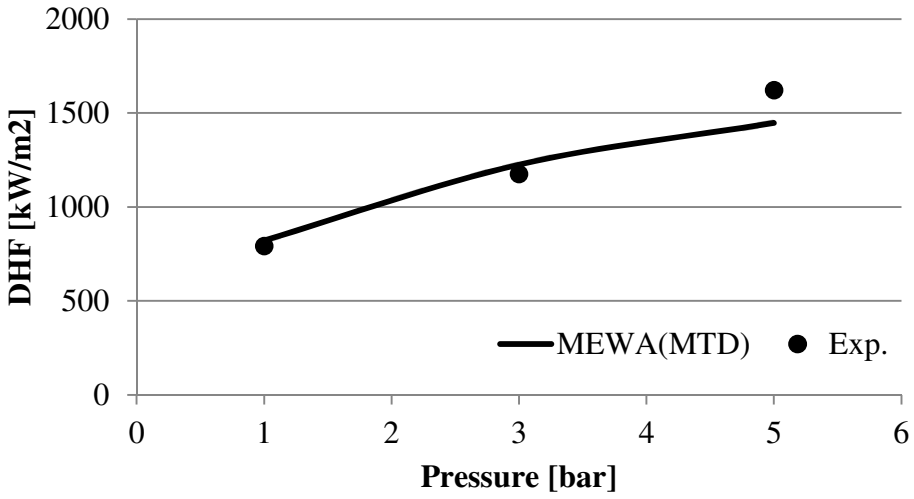

Figure 3.3: Dryout heat flux measured in DEBRIS experiments with the debris bed composed of irregular mixed particles at different system pressures and corresponding MEWA results using modified Tung & Dhir (MTD) friction model.

From Figure 3.3, it can be seen that the DHF increases with increasing system pressure. This can be explained by the increasing density of steam. With higher pressure the produced steam fills up less volume fraction due to the higher density. Therefore, more steam can escape from the bed.

3.2.2.b STYX experiments at VTT (Finland)

In prototypic situations, mixtures of particles of different sizes and irregular shapes are expected, as e.g. obtained in the FARO (Magallon [26]) and DEFOR (Karbojian et al. [40]) experiments. In the STYX experiments (Lindholm et al. [48]) performed at VTT, Finland, a broad particle size distribution based on the data from different international fragmentation tests, especially the FARO experiments. Alumina sands have been used as particles.

The porosity of the STYX bed has been determined in a separate test bed as 0.37 and measurements of the single-phase pressure drop in this bed yielded an effective particle diameter (friction loss diameter) of 0.8 mm by use of the classical Ergun laws. Whereas surface mean diameter is 1.9 mm. Thus, effective particle diameter (friction loss diameter) is smaller compared to surface mean diameter. Resistance heaters embedded in the gravel are applied to simulate decay heat. A local dryout is determined as a sustained temperature rise at a thermocouple location and that is taken as the criterion for the DHF.

Figure 3.4 show the results of STYX test series and calculations with MEWA applying MTD friction laws. Compared to DEBRIS experiments, the DHF values are low. The low experimental DHF in STYX experiment can be understood by the smaller effective particle diameter. The MTD model gives again rather good agreement with experimental value, especially for high system pressure (7 bars), while some under prediction for low system pressure.

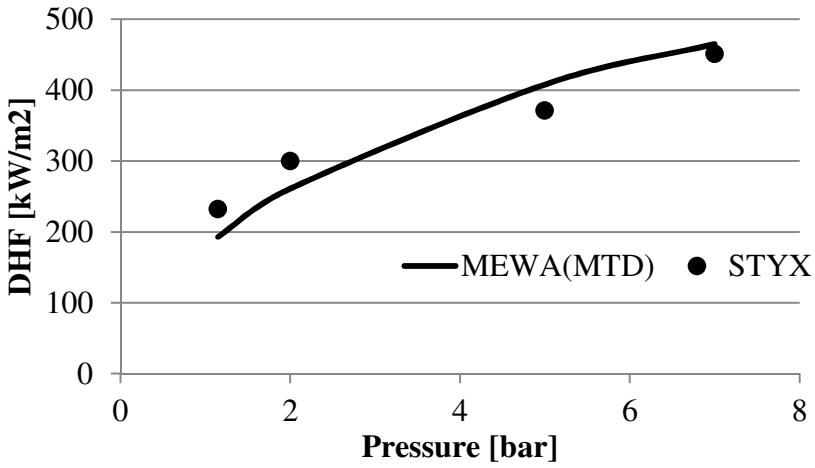

Figure 3.4: STYX experimental DHF versus MEWA prediction under top flooding conditions using MTD friction model.

3.2.3 Experiments with two dimensional cooling effects

3.2.3.a POMECO experiments with central downcomer

The POMECO experiments (Konovalikhin [53]) were carried out at KTH Stockholm. The focus is placed on the enhancement of the dryout heat flux by using downcomers considered as possible AMM measure for reactors. A central downcomer is built in the debris bed which enables to flow from the top water pool to the bottom of the bed and develop a two phase natural circulation flow loop, driving water into the bed from bottom.

The bed is composed of sand particles with mean particle size of 1 mm and porosity 0.36. The cross-sectional area of the test section is 350x350 mm rectangular. The maximum height of the sand bed is 450 mm. The bed is placed on a perforated plate which is 50 mm above the bottom water pool. A pipe with 30 mm inside diameter is placed in the middle of the debris bed in order to serve as a downcomer of water flow. Electric heaters are uniformly embedded in the bed to provide internal heating. A schematic diagram of the POMECO experiment is shown in Figure 3.5.

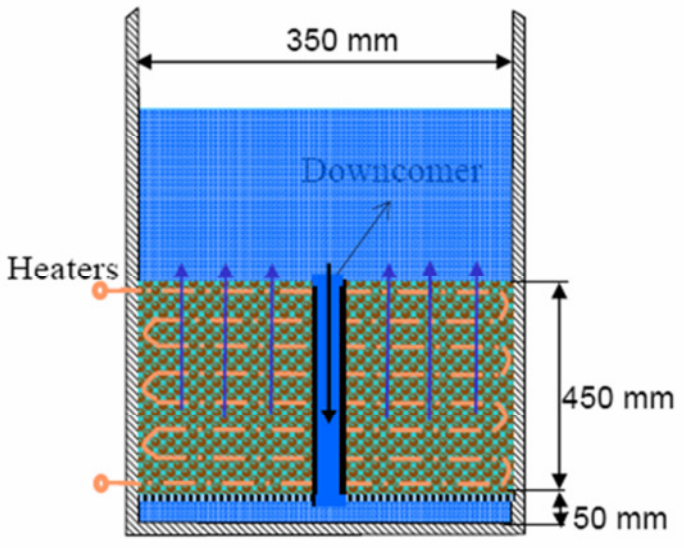

Figure 3.5: Schematic of POMECO experiments.

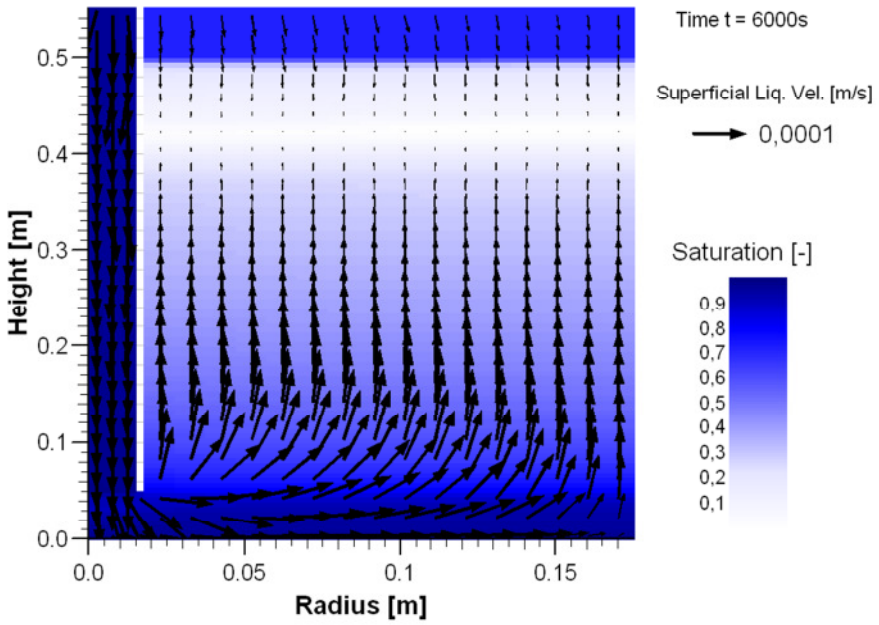

Figure 3.6: MEWA calculation for POMECO (half bed section: axisymmetry): heat load 355 kW/m^2 (heat flux to be released at the top surface of the bed).

Calculations have been performed with MEWA applying the MTD friction model. Results of MEWA calculations are given in Figure 3.6. In this Figure, natural-circulation-driven cooling due to the lateral pressure difference between the hydrostatic heads of pure water (in downcomer) and the water/steam mixture (in the bed) is demonstrated for the case with downcomer. The prediction of DHF is 355 kW/ m^2, only a little higher than measured (331 kW/m^2). Figure 3.6 gives the calculation for 355 kW/m^2 and shows the beginning of dryout near the top of the bed. For comparison, the MEWA calculation for the top flooding case without downcomer yields dryout already with about 236 kW/m² (experimental value 222 kW/m^2). Overall, the calculations yield good agreement with the experimental results and also the dryout behavior for natural-circulation-driven flow is accurately captured by the model.

3.2.3.b COOLOCE experiments Takasuo et al. [60] with conical bed

The MEWA code is applied to perform post-test calculations on COOLOCE experiments [60] carried out by VTT in Finland. In these experiments dryout behavior was investigated for two different bed configurations: cylindrical beds and conical beds. Again, the validation of MEWA concerns here more the integral aspects of behavior, related to the water inflow, which here depends on the bed shape, and the resulting flow patterns. The cylindrical debris bed has a height of 270 mm and a diameter of 310mm. The conical debris bed has a height of 270 mm and a bottom-diameter of 500mm. The two bed types are shown in Figure 3.7. Wire nets were used to prevent the particles from leaving the bed during the experiments and to hold the conical test bed in shape. The cylindrical test bed was installed into an inner cylinder and the top of the test bed was also covered with a wire net to facilitate top flooding. The particles are ceramic beads made from zirconia/silica, with diameters between 0.8 and 1.0 mm. The bed porosity was 0.38. The relatively small particles were chosen to reach the dryout with the limited power of the heating system.

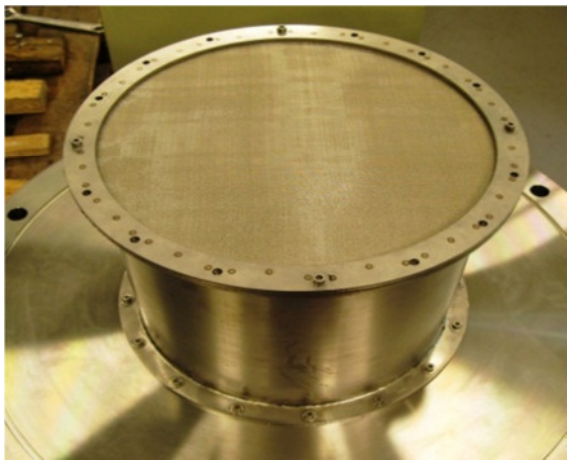

Height 270mm, diameter 310mm

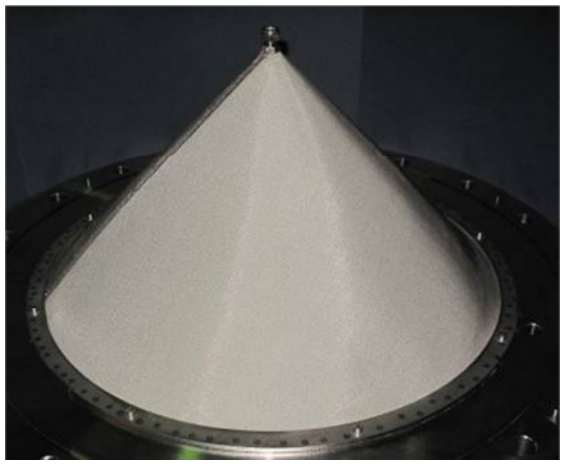

Height 270mm, diameter 500mm

Figure 3.7: Cylindrical (left) and conical (right) beds in the COOLOCE tests ([60], [91]).

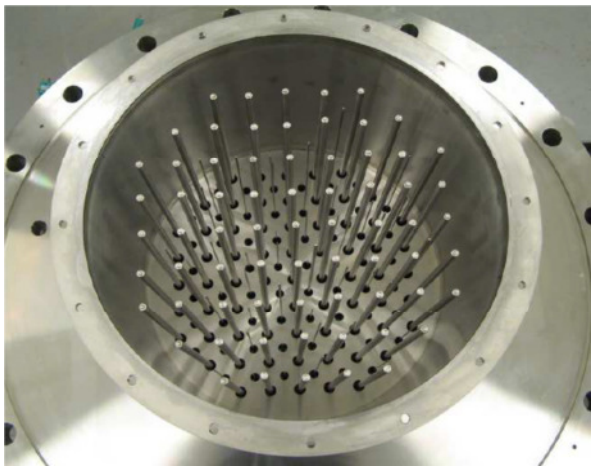

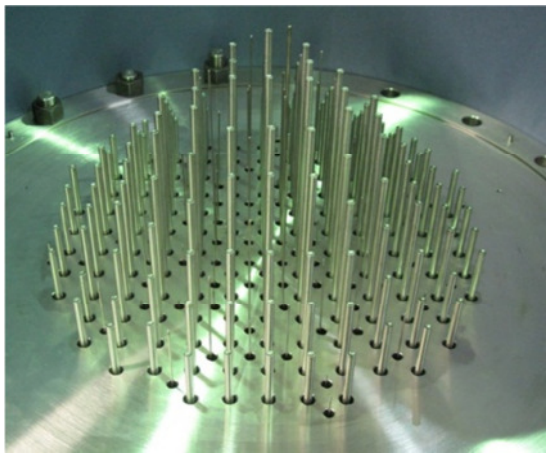

Figure 3.8: Heating bar and thermocouple arrangements of the cylindrical (left) and conical (right) test beds in COOLOCE experiments ([60], [91]).

Pictures of the heating system used for the test with both beds are shown in Figure 3.8. Vertical heating elements penetrating into the debris bed are used to simulate volumetrically heating due to decay heat. The tests were carried out at different system pressures, ranging from1 to 3 bars.

In the experiments the debris beds are submerged in a water pool at saturation temperature. Water can penetrate the cylindrical debris bed only from the top, while penetration via the sides should play a role in the conical configuration.

Figure 3.9 shows a comparison of measured dryout powers at different pressures with MEWA predictions using the MTD friction model. It can be seen that the calculated dryout power agrees well with the experimental measurements. The results suggest that the key phenomena of the dryout behavior are accurately captured by the model for both configurations.

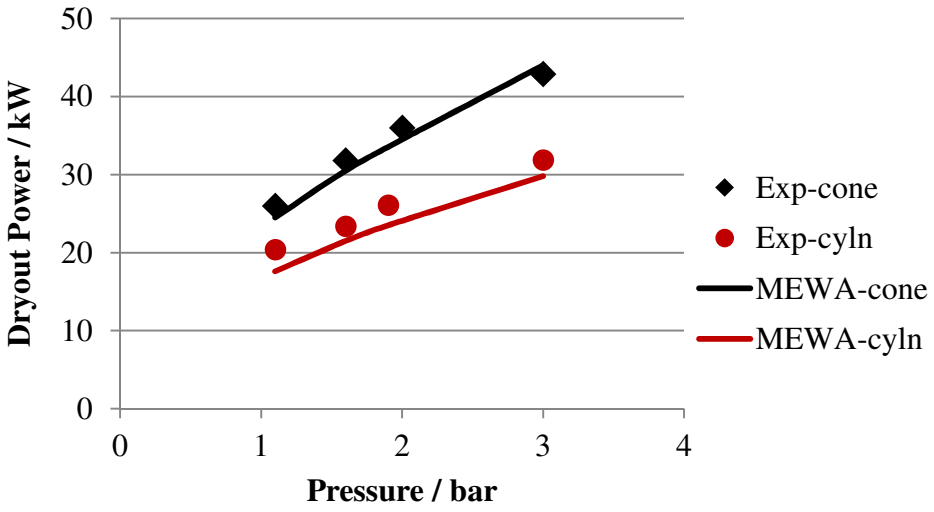

Figure 3.9: Comparison of measured dryout power at different pressures with MEWA predictions using MTD friction model; results for cylindrical and conical bed with same height of 270 mm, bed porosity 0.38 and particle diameter 0.9 mm.

The different flow configurations resulting from the calculations for the different configurations can be seen in Figure 3.10 and Figure 3.11. In the cylindrical test bed, a uniform lateral behavior concerning saturation as well as water down-flow yielded in spite of the rather large diameter of 31 cm. This is probably due to the high friction with the small particles and the resulting small penetration velocities. The counter-current flow situation of water and steam yields limitations to the water inflow from top, already with still significant volume parts of water in the whole bed. At dryout condition, all the water, which infiltrates the debris bed, is evaporated before it reaches the bottom of the bed. Therefore, the first dry zone is formed near the bottom of the test bed as shown in Figure 3.10. The flow pattern resulting from the simultaneous access of water in the conical bed configuration is depicted in Figure 3.11, showing the steady state distribution of saturation and liquid velocities at a power close to the dryout power. It can be seen, that water is entering into lower parts of the bed, supplying the upper parts of the bed which otherwise may already be dry. This is the reason why the dryout power in the conical configuration is about 20 - 30% above that of the cylinder with the same height. It is also indicated in Figure 3.11, that the position with the highest void fraction in the conical configuration is close to the top. Thus, dryout and temperature escalation is predicted at this position, when the limiting power is exceeded. In fact, this was also detected in the experiment.

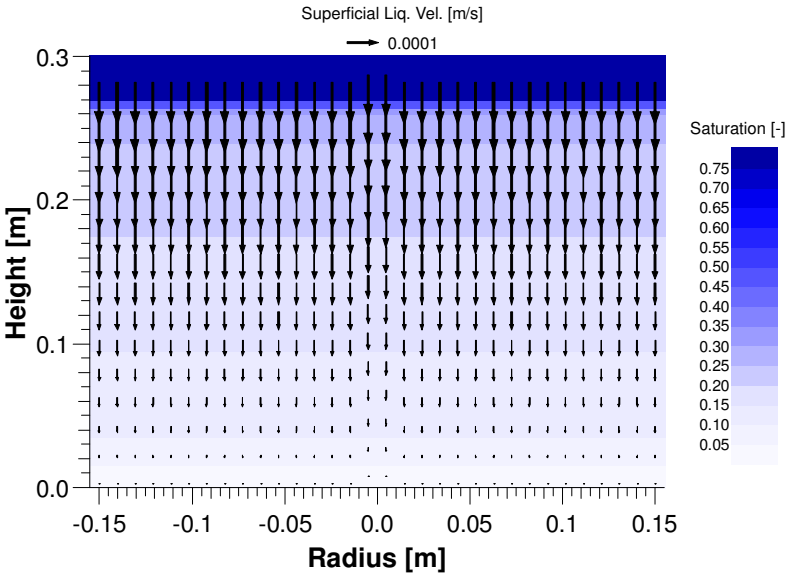

Figure 3.10: Saturation and liquid velocities calculated for COOLOCE test [60] with cylindrical bed close to dryout power.

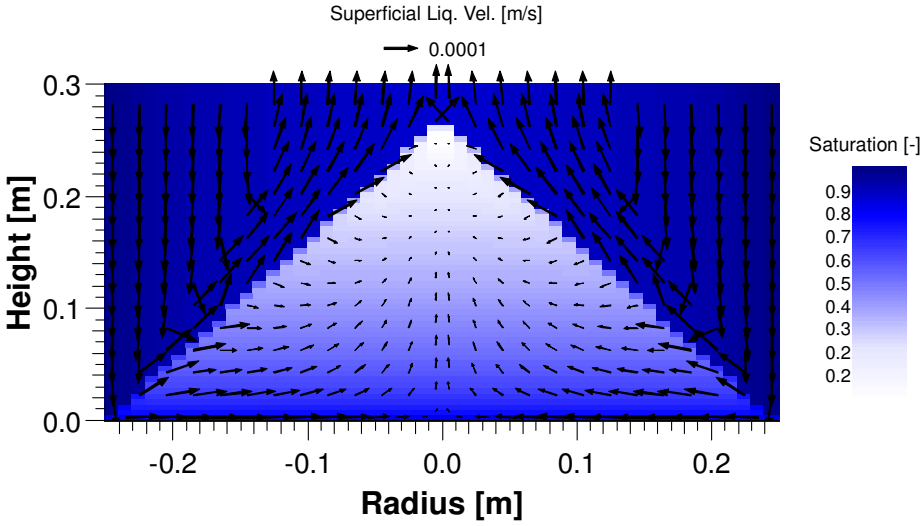

Figure 3.11: Saturation (liquid volume part inside the bed) and liquid velocities calculated for COOLOCE test [60] with conical bed close to dryout power.

3.2.4 Conclusions on validation under boil-off conditions

The validation calculations on the coolability limits under boil-off conditions particularly highlighted the importance of adequate constitutive laws for the friction, especially the explicit consideration of water/steam interfacial friction. The MTD law includes interfacial friction and is considered to be justified for all cases taken here. The significant enhancement of the dryout heat flux due to combined water supply from the bottom and the top of a debris bed which is observed in experiments is consistently also predicted with MEWA using the MTD friction law. This is important for realistic multi-dimensional configurations, where combined top/bottom

flooding is provided either via downcomer-like structures or due to the shape (e.g. mound shape) of the bed.

Further, it is to be remarked that the validation calculations with MEWA cover major experiments with a large range of conditions:

- Debris sizes from 0.8 to 3 mm,
- Spherical mono-disperse/ poly-disperse, irregular shape/ size distributions,
- Flooding modes: top / bottom / downcomer / 2D
- Pressures up to 7 bar

Major quantities measured in the experiments that can be used for the evaluation of the calculation results comprise dryout heat fluxes and dryout locations. From the results presented in this section, it can be concluded that the key phenomena of the dryout behavior are accurately captured by the model. Major experimental trends concerning flooding mode, effect of system pressure and 2D effects are always well reproduced.

3.3 Validation with respect to quenching of hot debris

Quenching experiments are partly more challenging than boiling tests, especially aiming at high temperatures which may be reached in a reactor accident. The experimental data are presently restricted to initial temperatures of the bed below 1000°C. However, the temperatures are high enough to comprise the transition between boiling regimes, from film to nucleate boiling conditions.

Concerning the flooding mode, experiments with imposed injection velocity and experiments with gravity driven inflow of water are available. The gravity driven mode is more relevant for rector situations and also more challenging for the models to correctly predict, since the water inflow rate is a result of the quenching process, not a prescribed fixed boundary condition. Frictions as well as the buildup of counter pressure due to evaporation and water level increase in the bed determines the development of the water inflow. On the other hand, tests with fixed water inflow rates are easier to interpret and control and allow a more detailed comparison of calculations with experimental measurements. Such experiments have been performed in several experiments, earlier experiments, at Brookhaven laboratory (Tutu et al. [61]), PRELUDE (Repetto et al. [62]) at IRSN and DEBRIS (Rashid et al. [64]) at IKE.

3.3.1 Experiments with fixed injection rates from bottom

Several experiments have been performed in the PRELUDE test facility at IRSN in order to investigate the quenching behavior of hot debris with fixed water injection rates from the bottom. The test section consists of a cylindrical bed with internal diameter of 174 mm and bed height 200 mm. The bed is composed of 4 mm steel spheres. The porosity of the bed is about 40%. In order to support the test bed, a quartz particle layer of about 60 mm is placed on the bottom of the test section. The debris bed is heated up to the desired initial temperature by inductive heating and heating is maintained during the test in order to simulate the decay heat. For these tests this heating power is about 200 W/kg. The initial temperature inside the bed is up to 700°C. The experiment is carried out at 1 bar system pressure. The hot debris is flooded from

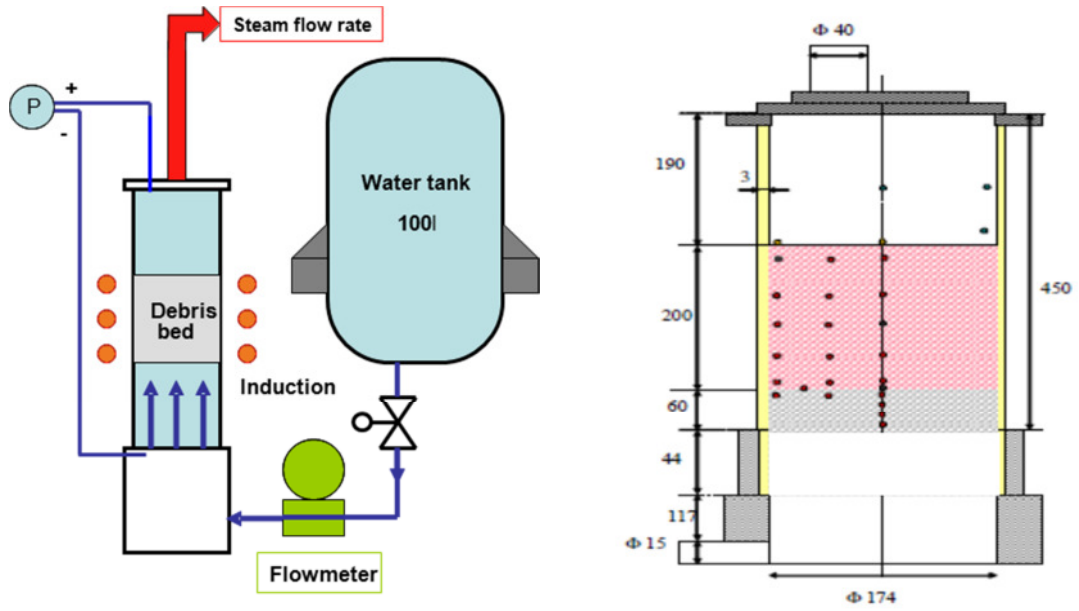

Figure 3.12: Sketch of PRELUDE experiments (all dimensions are in mm) [62].

the bottom with cold water. The temperature of the injected water is about 20°C. Four inlet water velocities have been used, namely 0.55, 1.3, 2.7 and 5.5 mm/s. The temperatures at different positions inside the bed and the steam flow rate generated during the quenching process are measured. A schematic diagram of the PRELUDE test is shown in Figure 3.12.

These experiments are simulated with the MEWA code. The heat transfer model described in chapter 2.2.4 has been applied. In the friction description, the MTD model has been used. The purpose is to validate the integral MEWA model concerning the prediction of the quenching front progression inside the bed for different injection rates as well as the steam outflow rates. The latter gives more insight into the quenching process especially about transitions in heat transfer models.

Results of MEWA calculations concerning the quenching front propagation at the center of the bed together with experimental measurements are shown in Figure 3.13. The experimental quenching front progression appears to be well met by the model. Water first enters the cold, unheated quartz bed. Since no evaporation takes place, this yields a steep slope up to 0 mm. Then the water enters the hot debris of about 700°C. A nearly constant velocity of quenching front then establishes, smaller than the injection velocity, due to the evaporated part of water. With higher injection rates, higher quenching front velocities are calculated by MEWA consistent with the thermocouples reading measured in the experiments.

A further measurement allowing model validation is given by the steam outflow rates. Figure 3.14 shows the comparison of measured and calculated steam mass outflow rates. A transition from a plateau-like steam flow at smaller water inflow rates to a peak type steam flow at higher water injection rates can be seen which is rather well predicted by the model. The difference in behavior is related to a more rapid quenching than water progression (plateau) versus the opposite (peak). This means, in the plateau case the quenching is so rapid compared to water progression that the quenching zone becomes rather thin. A steady progression with constant

evaporation rates according to the progression velocity is the result. However, in case of higher injection velocities, the water progresses more rapidly than quenching, possibly due to film boiling at high bed temperature. Thus, an extended heat transfer (boiling) zone is established behind the water front. This thick quenching region yields rapid evaporation after collapse of film boiling, thus yield peak-like steam outflow rates.

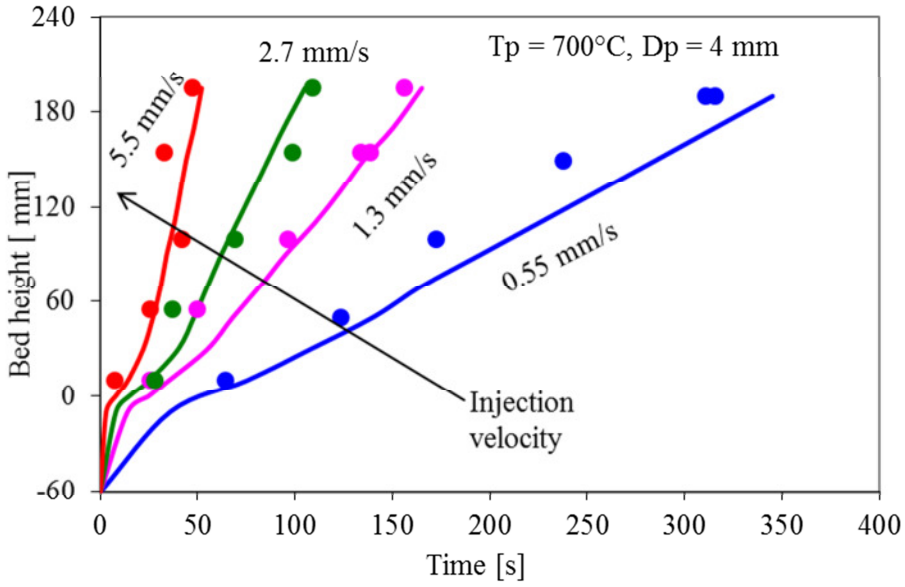

Figure 3.13: Comparison of calculated and measured quenching front progression for PRELUDE experiments with different fixed injection rate from bottom: initial temperature inside the bed up to about 700 °C and particle diameter 4 mm.

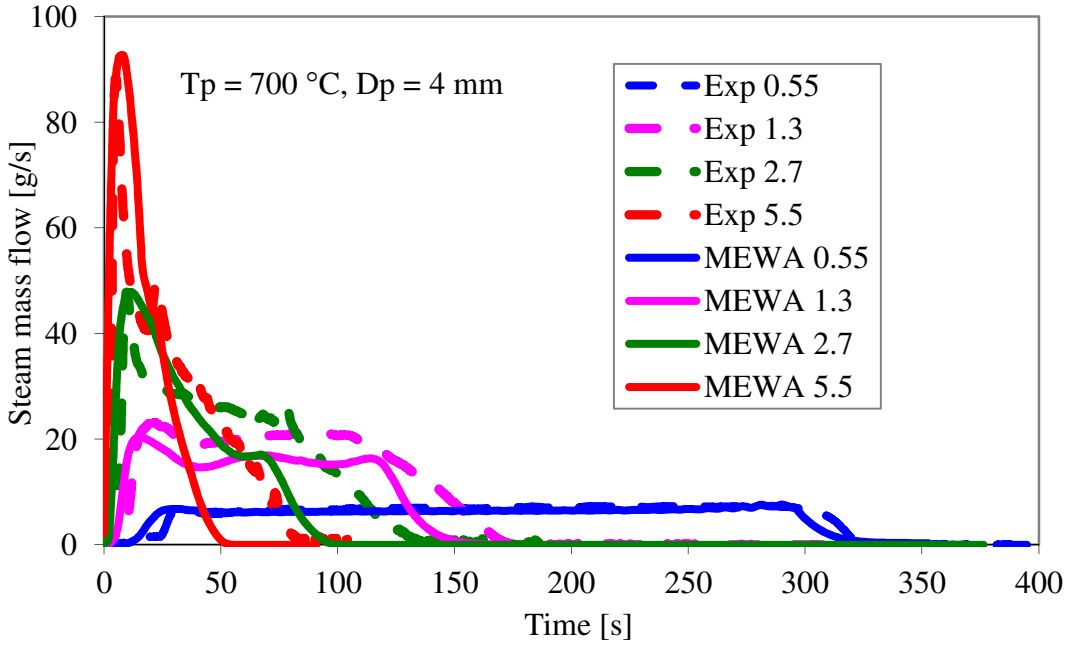

Figure 3.14: Comparison of calculated and measured steam mass outflow for PRELUDE experiments with different fixed injection rate from bottom: initial temperature inside the bed up to about 700 °C and particle diameter 4 mm.

Both the magnitude and duration of steam flow is very well predicted for the two smaller inlet velocities (see the blue and pink curves in Figure 3.14). For the two highest inlet velocities, the experimental observations show a strong peak and no steady-state behavior. The calculations reproduce the magnitude of the experimental peaks, but the total steam outflow time is shorter in the calculation than those observed in the experiments. E.g. in the experiment with inlet velocity of 5.5 mm/s, all thermocouples show quenching at about 50 s which is also reproduce by MEWA calculation (see red point and red line in Figure 3.13) but steam outflow lasts up to 90 s in the experiments in contrast to 50 s in the calculation. Part of the differences may be due to details of the interactions in the extended quenching zone which are not captures by the model, e.g. interactions responsible for propagation of film boiling collapse or on the other hand, partial re-establishment of film boiling or at least reduced quenching.

The question arises which behavior is relevant under rector conditions, plateau or peak i.e. thin or thick quenching zone. In realistic debris configurations, water inflow into the debris beds is driven by the hydrostatic head of external water i.e. by pressure differences, not established as fixed inflow. Additional calculations with a driving water column indicate that only the lowest inlet velocities (< 1.5 mm/s) are realistic under such conditions and a column and bed height of about 20 cm. Thus, a thin quenching front due to slow progression of water in the bed yielding the plateau behavior may be more typical and may also be valid for reactor conditions. This justifies even a simplified approach for the heat transfer model, details in the thin quenching zone are less important. With the present model, satisfactory agreement is obtained for the cases with higher inflow velocities and the transition in behavior between plateau and peak is also quite well met. This further increases the confidence for the evaluation of quenching of hot debris with the model even in case of high water inflow.

3.3.2 Quenching tests with external downcomer

In the DEBRIS quenching tests (Rashid et al. [64]) the cooldown behavior of strongly superheated particles was investigated, also under ambient pressure. As in PRELUDE, the purpose of this experiment is to provide better understanding and support of the modeling of the quenching process. The bed was heated up to the desired temperature (initial temperatures up to 700° C) and, after switching off the heating power, quenched with cold water. The bed is flooded either via an external downcomers. I.e., in these experiments the water inflow from bottom is not fixed, but establishes under feedback with processes in the bed.

In these experiments the test bed is composed of a mixture of 6, 3 and 2 mm steel spheres. The height of the bed is 640 mm and the bed diameter is 125 mm. The measured bed porosity is 0.36 and the effective particle diameter measured from single phase pressure drop is 2.9 mm. The bottom flooding is provided via an external lateral water column and the hydrostatic head of the water column was 950 mm (see Figure 3.15). Experiments were performed for different initial bed temperatures varying from 400 to 700 °C. With the lower particle temperatures higher quench front velocities were obtained in the experiments.

The calculations have been performed with the MEWA code for axisymmetric geometry. The driving head from the lateral water column is considered in the calculation by imposing the pressure corresponding to the system pressure+ hydrostatic head of water column at the bottom

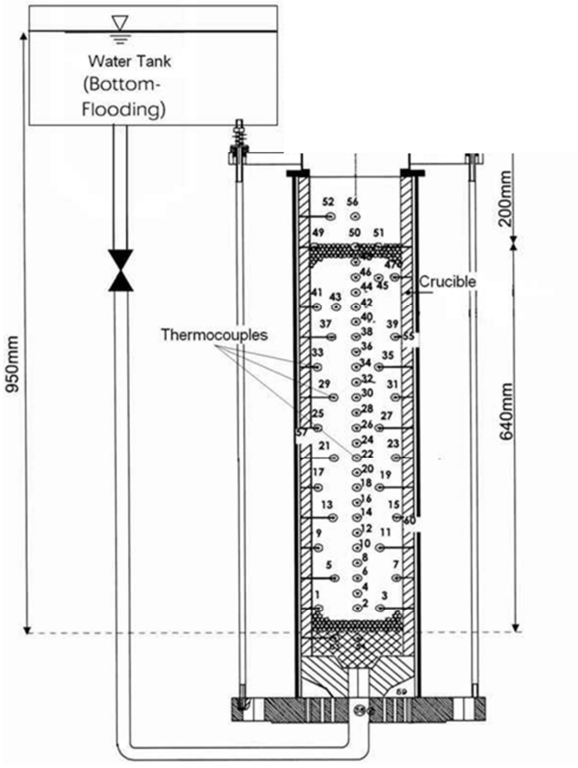

Figure 3.15: Schematic of DEBRIS experiments with external downcomer.

of the bed. This pressure is considered constant assuming no driving head loss due to pipe friction.

As in the experiments, axial and radial temperature profiles have been chosen with lower bed temperatures at the bottom and the outer boundaries (near the wall). Results of the MEWA calculation for the test BF400 are shown in Figure 3.16. In this figure, the status of cooling and water filling inside the bed 75 s after start of water inflow is shown. It can be seen that the quench front progression is not homogeneous; water penetrates preferably at the outer region of the bed (also observed in the experiments). This is due to the lower bed temperature there.

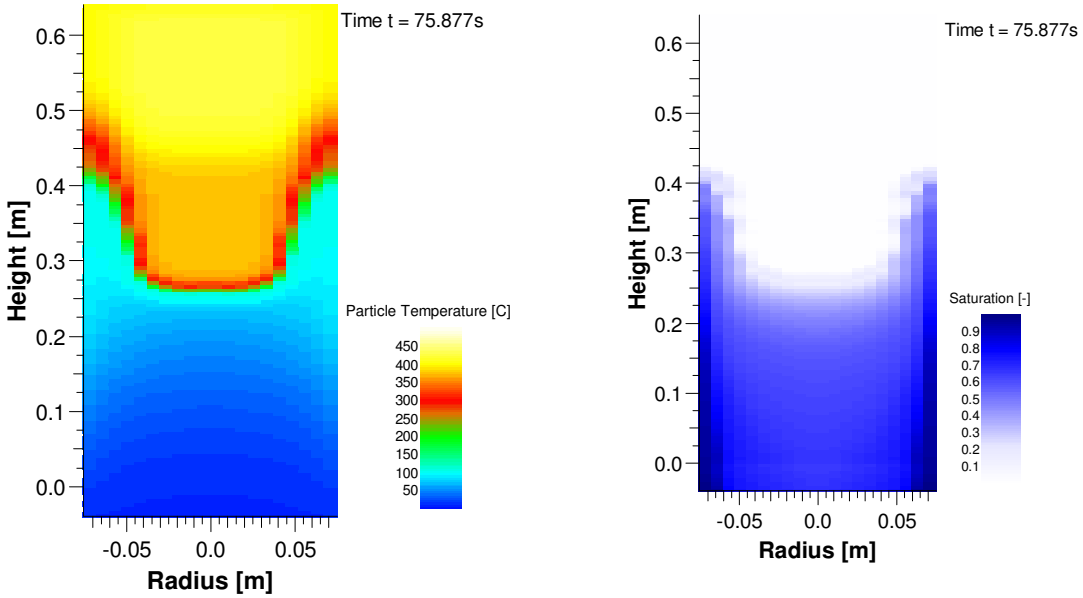

Figure 3.16: Distribution of temperature and saturation (water contained inside the bed) from a MEWA-2D simulation for the test, BF400.

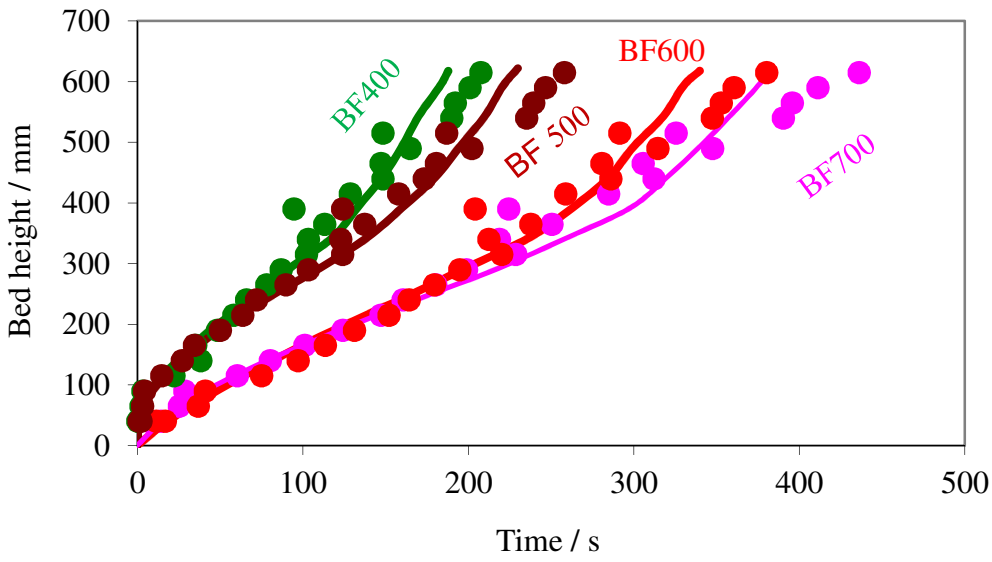

Figure 3.17: Comparison of measured and calculated quench front progression in the center of the bed for bottom-flooding with different initial bed temperatures.

Experimental results for the quench front propagation in the center of the bed with different initial temperatures between 400 to 700 °C are given in Figure 3.17 together with MEWA simulation results. The MEWA results agree well with the experimental results. A thin quenching front due to slow progression of water (average water inflow varies from 1mm/s to 2 mm/s) and rapid quenching results from the calculations. With the higher particle temperatures lower quench front velocities are obtained both in the experiments and in the calculation. This is expectable because a higher thermal energy has to be removed from the bed. However, it is surprising that there is a significant shift between the results of BF400 and BF500 being close together and, on the other hand, BF600 and BF700 being also close together. This can be explained by the initial axial temperature profiles as shown in Figure 3.18 for BF500 and BF600. In the lower bed region, the bed temperature of BF500 is much lower, thus allowing much more rapid quenching and water progression in the lower 5 cm, as also visible in Figure 3.17. Then, the slopes of BF400 and BF500 in Figure 3.17 become closer to BF600 and BF700, i.e. the significant shift disappears.

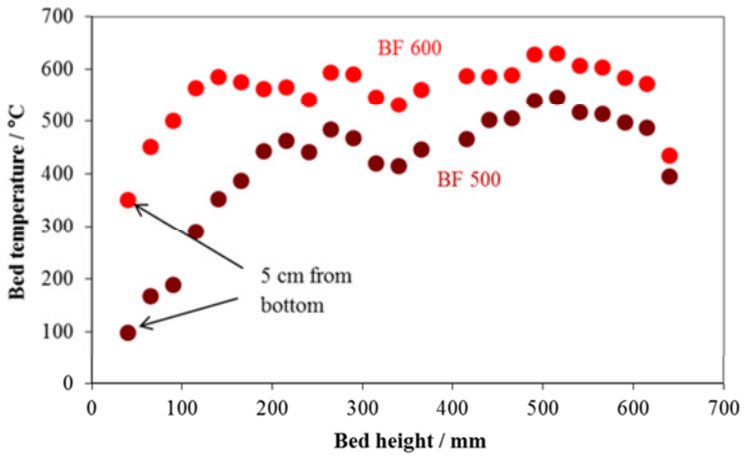

Figure 3.18: Initial temperature profile inside the bed for tests BF500 and BF600 DEBRIS experiments.

3.3.3 Experiments of Tung and Dhir with stratified bed geometries

In the experiments of Tung and Dhir [68] cooling conditions of debris beds with variable permeability in the axial and radial direction were investigated. As a background with respect to reactor conditions, non-homogeneities in a bed and their consequences can be considered. Especially, the question arises whether and to which degree partially higher permeability can contribute to coolability. The experiments used steel particles heated inductively up to 630° C. The beds were flooded either from the top or form the bottom. In the bottom flooding experiments, the water entered through a pipe connected to a large reservoir which provided a constant hydrostatic pressure head.

Figure 3.19 gives the results for an experiment with a vertically stratified bed, where the lower half was composed of spheres of 3.18 mm diameter and the upper half of 6.35 mm spheres. The driving pressure for bottom flooding was provided by a water column of 50 cm. The quench front progression for two different bed temperatures predicted by MEWA lie well within the experimental range measured in the middle(R=0) and the periphery (R=25.4 mm) of the bed. The quench front progression is slightly faster in the upper half of the bed. This can be understood by the smaller friction with the larger particles there.

As a further case, top flooding of a radially stratified bed is simulated. Here, an inner region (55 mm diameter) was composed of spheres of 3.18 mm diameter and the outer region (up to 85 mm diameter) with spheres of 6.35 mm diameter. The radially stratified configuration is especially interesting since it imposes a multi-dimensional behavior which gives the opportunity to check the code also with this respect. The bed was heated up to an initial temperature of 630 °C. Figure 3.20 shows the comparison of measured and predicted quenching behavior. The quench front progresses much faster downwards in the outer region due to higher permeability (larger particles). Part of the inner region is quenched from the bottom after the water has reached the bottom in the outer part. This behavior is well reproduced in the MEWA simulation (see Figure 3.21). MEWA overestimates somewhat the downward quenching progression in the center part (see experimental and calculated points for inner region at 37.0 cm height in Figure 3.20).

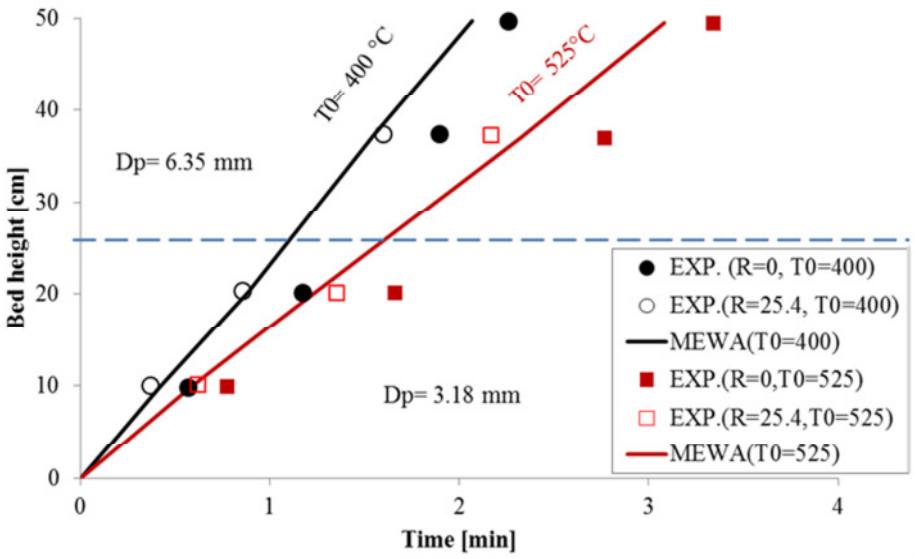

Figure 3.19: Quench front propagation in experiments of Tung and Dhir [68] with bottom flooding of axially stratified bed (initial particle temperatures 400°C and 525°C).

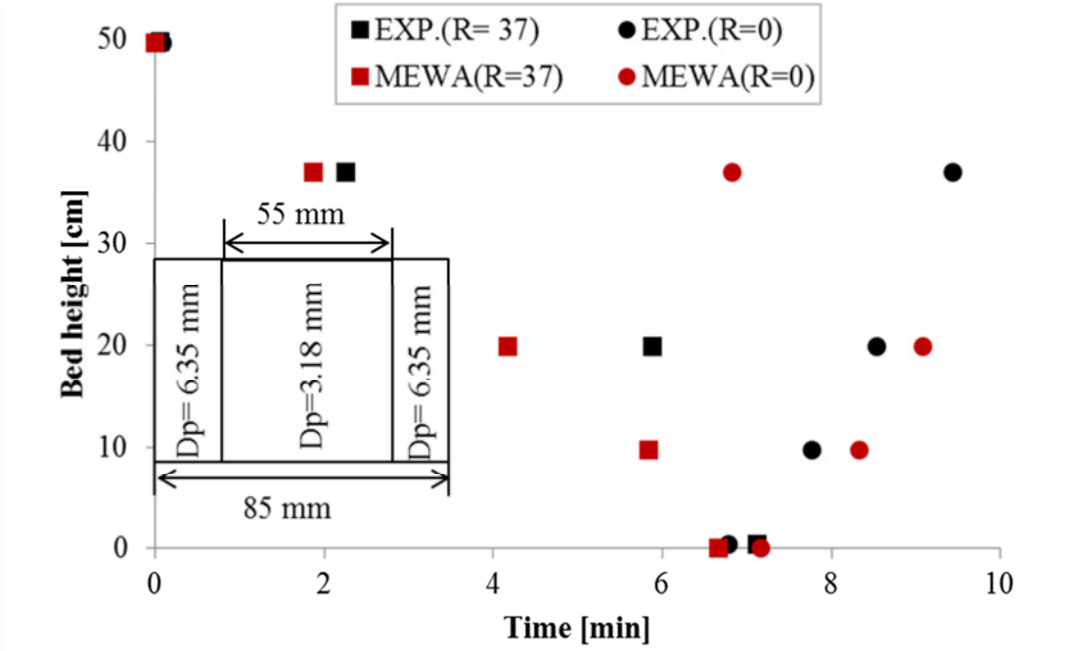

Figure 3.20: Quench front propagation during top flooding in experiment of Tung and Dhir [68] with radially stratified bed at 630°C initial temperature.

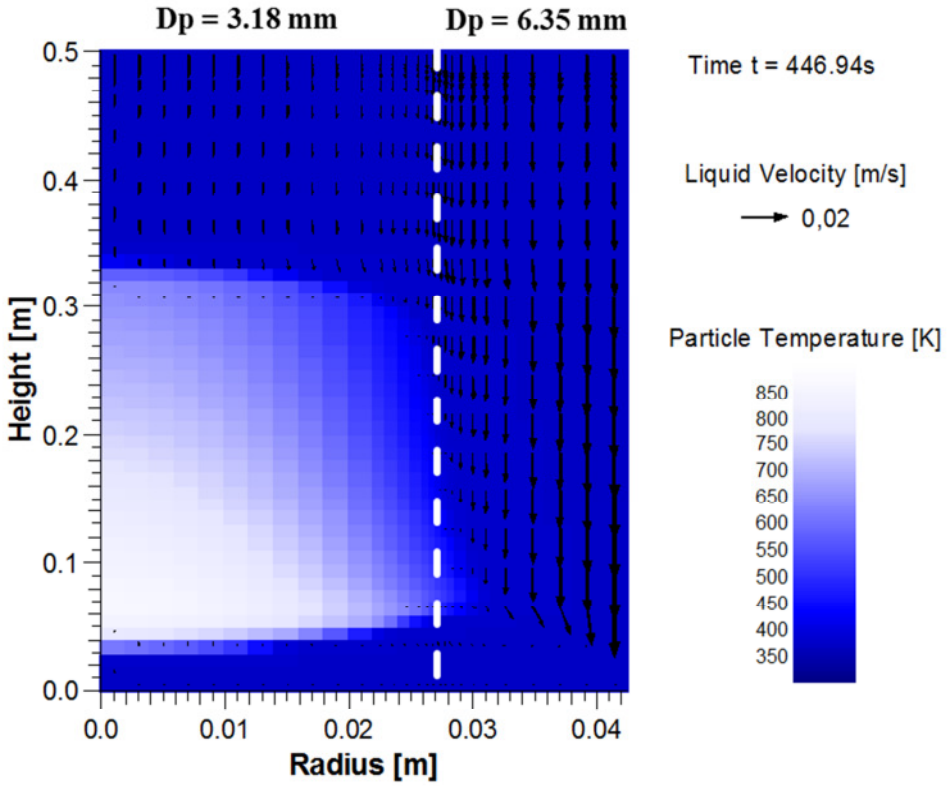

Figure 3.21: Temperature distribution (color shade) and liquid velocities (arrows) from MEWA simulation of Tung and Dhir top flooding experiments with radially stratified bed at 447 s.

3.3.4 Conclusions on validation for quenching

Validation calculations for quenching of superheated, initially dry debris beds were performed for different experiments, addressing various aspects of quenching:

- different flooding conditions with forced water flow from bottom, water flow driven by gravity either via internal or external downcomers and top flooding;
- quenching of particulate debris beds composed of different steel spheres addressing the quenching of non-uniform beds;
- effects of initial bed temperatures on quenching front progression
- effects of vertically and laterally stratified bed configurations;

Major experimental quantities that can be used for the evaluation of the model results are local temperature measurements, which also are used to characterize the quench front propagation, as well as steam and water flow rates, which allow a comparison based on integral features.

In general, it is found that, except in cases with large forced bottom injection, water moves into the debris bed in a slowly propagating front due to high friction, and the quenching is rapid enough to occur in a thin front (“frontal type”). Thus, a detailed modeling of heat transfer regimes is less important, rather an appropriate description for the friction is essential. Even in cases with higher inflow velocities of water still satisfactory agreement is obtained in the cases considered. But it should be remarked that the validation is limited to significantly smaller temperatures in the experiments than to be expected for reactor conditions.

Qualitative trends e.g. top versus bottom quench front progression are generally well reproduced. It is shown that quenching from the bottom is more effective than top-flooding, due to co-current flow of water and steam. In cases with quenching from the top, non-homogeneities (stratification) or downcomers favor the local penetration of water to the bottom, with subsequent quenching of the remaining bed from below, which provides an effective mechanism for faster cooling.

4 Coolability of In-Vessel particulate debris

Key investigation phases and situations of in-vessel cooling concern re-flooding of degraded core and quenching of hot debris beds formed in the lower head. Melt pool formation or coolability of particulate debris is the major issue concerning melt retention in the core and the lower head. Calculations for reactor conditions are carried out to assess the capabilities of the MEWA code as a tool to explore the above issue in general and to draw overall conclusions on coolability of in-vessel particulate debris

4.1 Quenching of a hot, degraded core

Due to loss of coolant in the frame of a severe accident, heating and melting may create a strongly degraded, partly molten core with relocated material and broken parts. The addition of water to this very hot core may produce extended particulate debris in the core region as observed in TMI-2 accident (Reinke et al. [19]). A first goal is to quench the hot core including debris beds to a low temperature in order to establish a steady state of long-term coolability afterwards. Although a hot region may be maintained stable under cooling, a risk remains that poor debris bed quenching can lead to a strong temperature rise and debris bed melting with molten pool formation, growth and possible relocation into the lower head of the vessel. The major question is then, whether a cooled state with continued quenching or formation of a melt pool results by strong increase of temperature in parts of this debris, due to decay heat and insufficient water access. A difficulty of exploration and of concluding about this issue is that the configuration of an in-core particulate debris bed is hardly to be determined from an accident sequence due to significant uncertainties in the debris formation processes. Therefore, calculations are to be carried out with parametrically assumed configurations. The chances to reach coolability by considering the key supporting as well as counter effects are to be considered. A key question for reaching conclusive results is weather strong tendencies in either direction supports such results for a significant range of realistic conditions, thus counting them plausible in spite of the uncertainties.

The experimental studies of Ginsberg et al. [66] show, that cooling can be achieved most effectively if water can enter laterally or from below with sufficient driving head to overcome the friction resistance to penetration through the debris bed. In the reactor core, similar effects are expected from lateral water inflow via the intact core or bypass region. The multidimensional effects of water inflow from the sides and below together with the cooling effects of steam flow through the hot dry zone are considered significantly to facilitate the quenching process. On the other hand, high temperatures and small particle diameters in a debris bed make the quenching more difficult. If quenching of the dry bed is not rapid enough, then heatup by decay heat in still dry regions may again yield melting. Therefore, chances to reach coolability by quenching before reaching the melting temperature are to be explored.

In the following reactor application, a pressurized water reactor with thermal power P_0 = 2700 MW and a total core mass M = 125 tons has been considered. It has been assumed that most of the fuel rods and other core materials are severely damaged and form a particulate debris bed in the core region as can be seen in Figure 4.1. The mass of the debris bed, i.e. the amount of

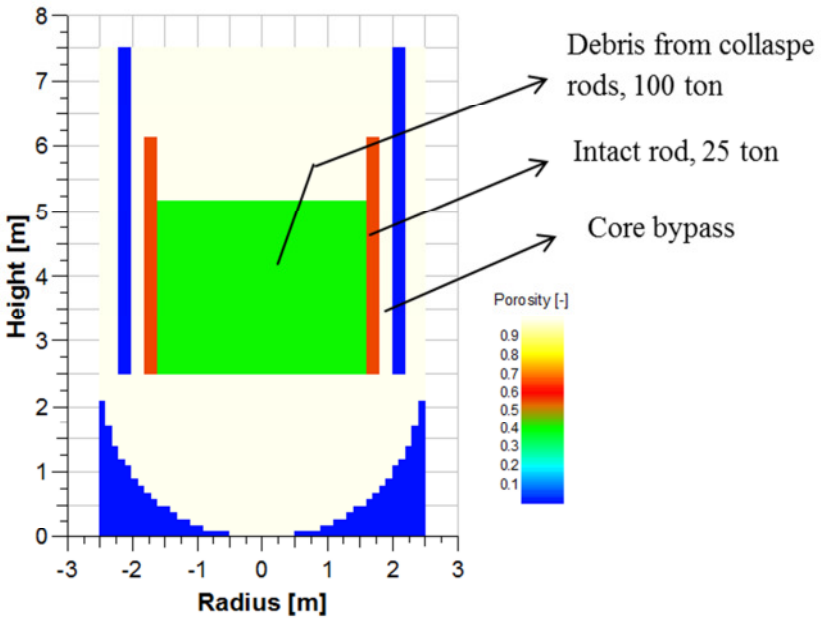

Figure 4.1: Configuration of degraded core as particulate debris surrounded by intact fuel rod and bypass region.

collapsed and damaged rods is considered at about 100 ton. The rest of the fuel rods surrounding the debris bed are assumed to be intact. In the frame of the porosity approach, the intact core part is described by a porosity of 0.55. At the sides of the core significantly increased permeability is assumed to simulate the bypass (see in Figure 4.1)

An average debris bed power q = 220 W/kg is imposed, consistent with the core decay power level reached approximately 2 hours after the reactor scram and this heating power is kept constant during the calculation. In the present analysis a system pressure of 10 bars has been chosen, which is much lower than in the TMI-2 accident (about 100 bars, see Müller [92]). In general, there is an increase in coolability with increasing system pressure due to the higher steam density (see chapter 3). However, in view of depressurization measures established meanwhile, lower pressure is more realistic. Further, in order to get an overall impression about cooling options, as an aim of the present work, more conservative, i.e. less favorable cooling conditions are to be assumed.

During a severe accident with water loss, a significant heatup of the dry core may occur before cooling measure can be re-established (see Sehgal [9]). First attempts may yield a degraded core as assumed here, which is still hot, before continuous water supply may be realized. In order to start with somewhat challenging condition, an initial temperature at this time of beginning water supply is assumed, here a uniform core debris temperature T_p = 1500 K. A coolant mass flux of water of 13.5 kg / (m²s), i.e. a total flow of 60 kg/s, via the downcomer is taken as a realistic choice. Saturated water is assumed under supply via the downcomer (T_{sat} at 10 bar = 452 K).

Bed porosity and particle sizes are the key parameters determining quenching when operating conditions like system pressure and water supply remain constant. Concerning porosities, a standard value of 40% has been chosen, which cover a large bandwidth of debris beds. A uniform effective particle diameter is assumed and varied from 3 mm to 1 mm. The aim is to search for the coolability limit due to too large friction in the debris bed.

The calculations with MEWA have been performed in 2D cylindrical geometry. Calculation results show complete quenching occurs for 3 and 2 mm particle beds but not for 1 mm. Results of MEWA calculation concerning development of saturation (water volume part inside the pores) and water velocity in a 2 mm particle bed are shown in Figure 4.2. Here, successful quenching of the in-core debris due to multidimensional effects is illustrated. Water rises in lateral and intact core regions from flooding via the downcomer. Then, sideway inflows of water into the degraded debris, especially via lower regions, are driven by the external water column head of downcomer. After about 502 s the water level in the external core region is high enough to allow the debris bed flooding from the top. But penetration of water from the top of the bed is limited by the strong steam flow resulting from evaporation of water at the bottom. As a result, a liquid water pool forms above the debris bed and the upper part of the bed remains dry for long time. This region is subsequently quenched by water from below, as water is continuously driven into the bed by the hydrostatic pressure difference.

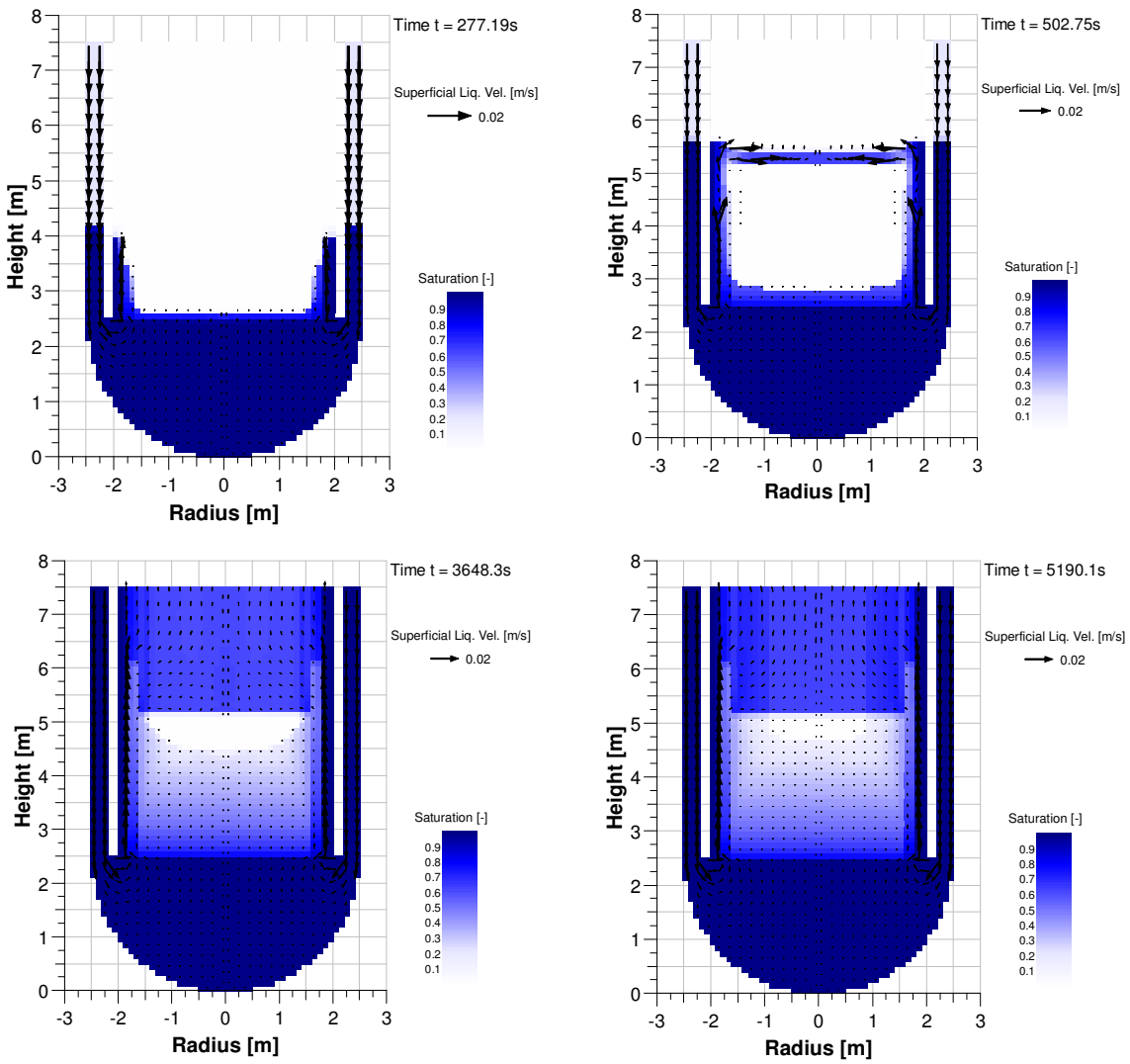

Figure 4.2: Development of saturation and liquid velocity during the quenching of hot debris of initial temperature 1273 K, particle size 2 mm, porosity 0.4 specific power 220W/kg in the core at 10 bar system pressure.

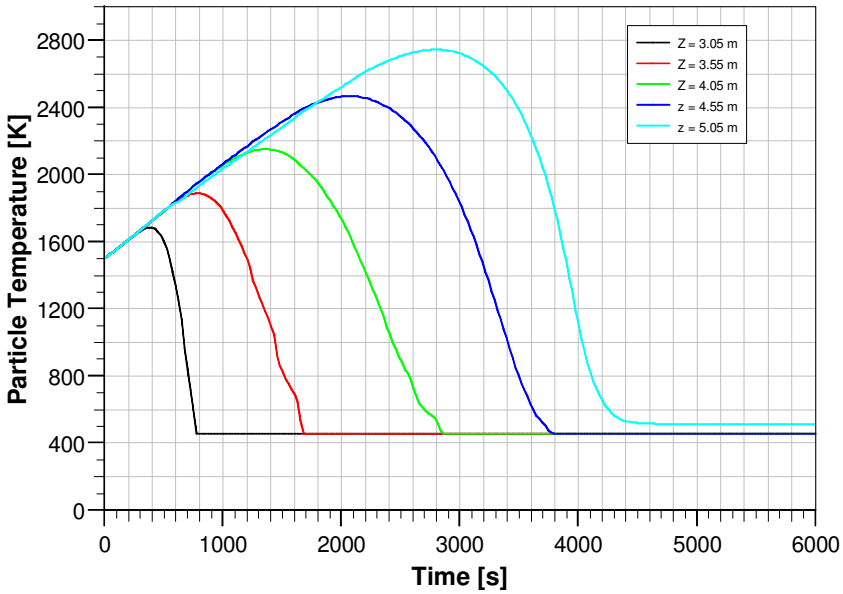

Figure 4.3: Particle temperature versus time at center (radius r = 0) and different elevations (Z) for debris bed of initial temperature 1273 K, particle size 2 mm, porosity 0.4, specific power 220W/kg in the core at 10 bar system pressure.

Complete quenching occurs in this case at about 4400 s as can be seen from Figure 4.3. The penetration of water from below leads to a fast quenching of the bottom part. As a result temperature rise is less in this part. Since quenching from top is limited, water has to fill the bed mainly from bottom. As a result, temperature increases upper parts of the bed due to decay heat and acts against quenching. But quenching from bottom is fast enough that the maximum temperature does not exceed 2750 K (Figure 4.3).

Figure 4.4 shows results of saturation and temperature fields after 478 and 2456 s for 1 mm particle bed. From the calculated results it can be seen that coolability cannot be achieved for 1 mm particle bed. In this case very large friction due to very small particles impedes vapor removal as well as water inflow strongly. As a result, major parts of water coming from the downcomer bypass the debris bed and go through the lateral intact core region, forming a water pool above the bed (Figure 4.4). Since quenching is also limited from top (up-flowing steam prevents water inflow from top), melting temperature is reached in large part of debris bed already after 2456 s, as can be seen from Figure 4.4.

Thus, the quenching calculations performed for a strongly degraded core including a debris bed show that even at a lower system pressure of 10 bar (compared to TMI-2 accident) quenching can be reached for a large debris bed of 100 tons with small particle sizes of 2 mm, porosity 0.4 and initial heat-up to 1500 K. Effective quenching and thus strong trends towards coolability are supported by multidimensional effects: water flooding from the downcomer rises in lateral, intact core regions and then penetrates inside the debris bed driven by the external water column. Smaller characteristic particle diameters (lower permeability of debris) impede cooling, but very small particles, e.g. here1 mm, have to be assumed to yield melting under re-flooding. However,

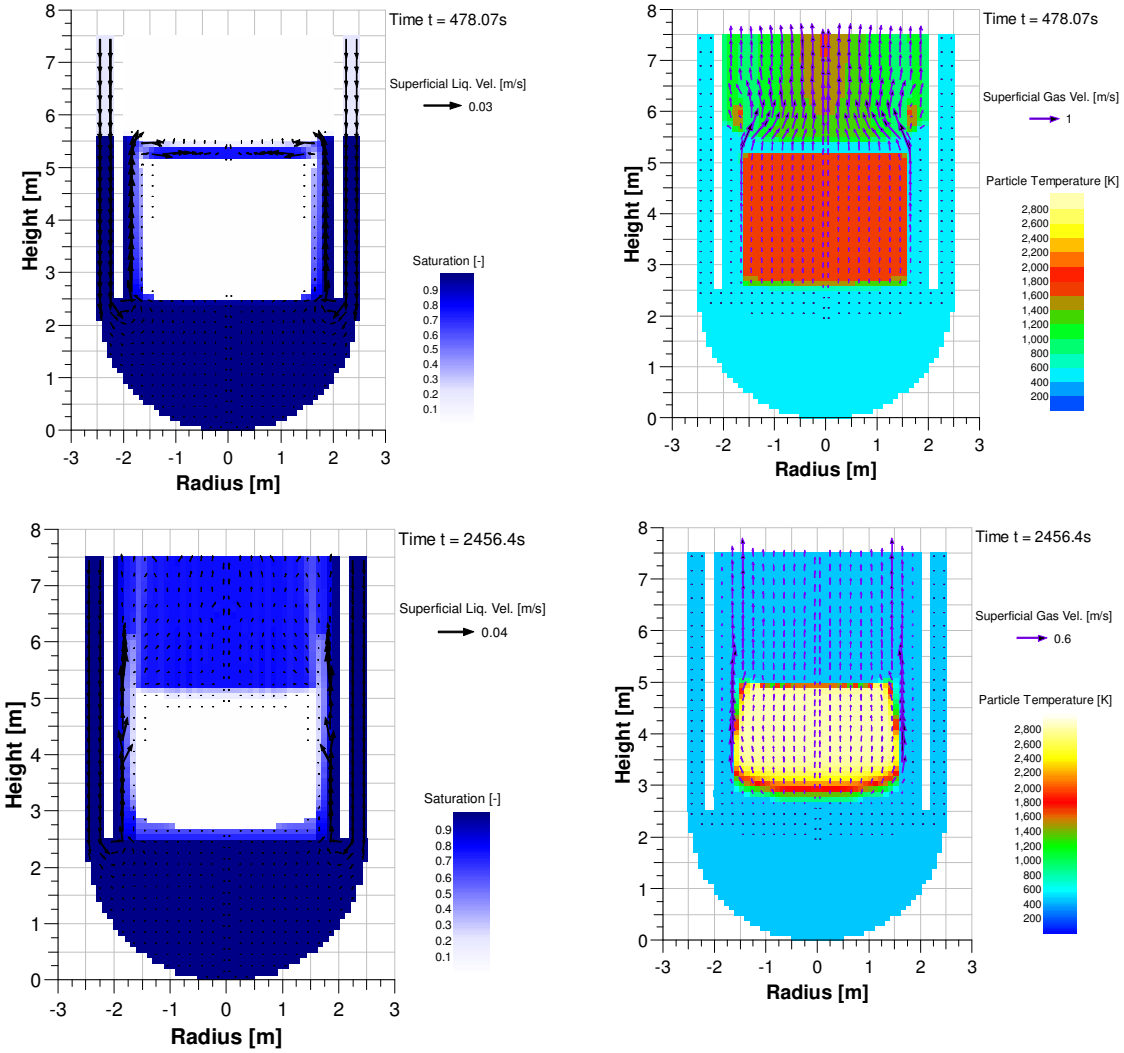

Figure 4.4: Development of saturation and liquid velocity (left column) as well as particle temperature and gas velocity (right column) during the quenching of hot debris (initial temperature 1273 K, particle size 1 mm, porosity 0.4, specific power 220W/kg) in the core at 10 bar system pressure.

extended debris regions with such small particles appear not to be realistic. Therefore, good chances for cooling even of a strongly degraded hot core can be concluded.

4.2 Quenching of hot debris in the lower head

If the core cannot be cooled down due to decay heat and insufficient cooling, core melting and melt relocation to the lower plenum will occur. The melt release from a melt pool in the core may be expected to occur not in a catastrophic mode of large break, but with outflow from holes of limited size (Sehgal [9]). Depending on the accident scenario, but typically in cases with boil-off of water starting from a covered core, the lower head will be filled with residual water. When the melt pours into this water the jet will break up which are partly quenched and solidified during falling in the water and then settle down as particulate debris. The so formed particulate debris will be hot and it is heated by decay heat from the radioactive fission products that are still present in the particulate debris. Then, in addition with decay heat, sensible heat of the hot

particles has to be removed which is much higher for high temperatures than for saturated conditions. If heat removal is not rapid enough, melting of particles will occur and molten core materials will destroy the vessel wall due to thermal load.

Conditions and limits of coolability of such debris beds in the lower head are to be explored, in order to evaluate options and chances of water injection into the vessel, even in such progressed states of an accident. Different possible accident scenarios have to be considered. Certainly, TMI-2 is a key reference, where about 20 tons of corium was relocated into the lower head and quenching was finally achieved at elevated pressure of about 100 bars (Müller [92]). But it must also be considered that its special aspects can not to be extended for all possible cases. Lower system pressures have to be considered, as done here. The question arises how the lower system pressure affects the coolability of debris beds. Such questions have to be explored in order to guide the severe accident management or to investigate measures to keep the melt safely inside the vessel.

Essential effects are to be considered in order to guide the investigations. As outlined in chapter 1.2.2. , lateral water injection from sides and especially via bottom regions due to lateral pressure differences yield a major cooling effect. Even if there would be no heap structure as considered here, the spherical shape of the vessel already yields lower debris heights at the sides and thus pronounced water inflow there.

As in the core, the competition of heatup by decay heat in the dry debris vs. quenching by water ingression decides the final success of cooling. This success of quenching strongly depends on initial conditions. The important conditions considered in this respect are porosity, particle diameter, initial bed temperature, mass of debris bed, system pressure, bed heterogeneities, etc. But, due to the complexity of the bed formation processes, there remain significant uncertainties in these conditions. Therefore, it is required to perform various calculations with variation of these conditions in order to explore up to which conditions and configurations the bed remain coolable.

An emphasis is laid on bed heterogeneities including cake parts. Dense regions appear not to be coolable due to low porosity. Superposed layers of very small particles also hinder cooling. In 1D top feed configuration this yields a significant reduction of coolability (Lindholm et al. [48]). But, in reality multidimensional effects have to be considered. In multidimensional configurations regions with higher porosity or with larger particle size may give water an easier flow path towards lower bed regions, i.e. a downcomer-like structures may be considered to favor supply of water to the lower bed regions. Further, with water access to bottom regions, steam flow from evaporating water through the dry region may strongly support the quenching in the competition with heat-up. Exploring these options for reactor conditions and understanding the underlying physical mechanisms will then give an understanding of resulting chances even with additional handicap (cake parts with low porosity).

4.2.1 Reference calculation: representative case and obtained results

In the following, an accident scenario has been considered, where the melt release from a large melt pool in the core creates a particulate debris bed in the lower head due to breakup of melt during falling in the residual water. It is expected that a debris bed is formed in a mound shape configuration as shown in Figure 4.5. Further, axial symmetry is assumed. For the angle of the cone part, an inclination $\theta = 33°$ has been chosen. Variants of this assumed shape (inclination) may be considered. A typical porosity $\varepsilon = 0.4$ and a uniform effective particle diameter $D_p = 2$ mm is assumed for the bed.

The particulate debris fills the hemispherical lower plenum of radius $R_{LP} = 2.5$ m up to a maximum height $H_b = 1.65$ m. In this geometry about M= 40 tons of debris has been assumed. A decay power q = 200 W/kg has been applied, about twice that assumed by Seiler et al. [29] for TMI-2 accident. An initial temperature $T_p = 1273$ K has been assumed in the initially dry debris bed and a system pressure p = 10 bars.

A larger amount of debris and a lower system pressure have been considered here, compared to the TMI-2 accident, where only about 20 tons of corium relocated into the lower head and quenching was achieved at elevated pressure of about 100 bars. In fact, the aim of this work is not to perform analyses for specific plants and accidents, but to investigate generic reactor situations under challenging (less favorable cooling) conditions. Lower system pressure and higher debris mass are less favorable for cooling. It is assumed that water with saturation temperature is introduced via the downcomer and thus the particle bed is flooded from above.

The aim of this calculation is to check whether quenching is achieved before reaching the melting temperature. Calculations with MEWA have been performed in cylindrical geometry. Results are shown in Figure 4.6 for the development of saturation and liquid velocities and in Figure 4.7 for the development of particle temperature and steam velocity. From Figure 4.6, it can be seen that water ingress predominantly at the sides, along the RPV wall. This kind of water ingression is supported by the shape of the bed. Due to a heap like shape, the bed height additionally decreases from the central bed regions to the outer region of the bed. Because of the lower bed height steam production is less there, so water can more easily penetrate from the side

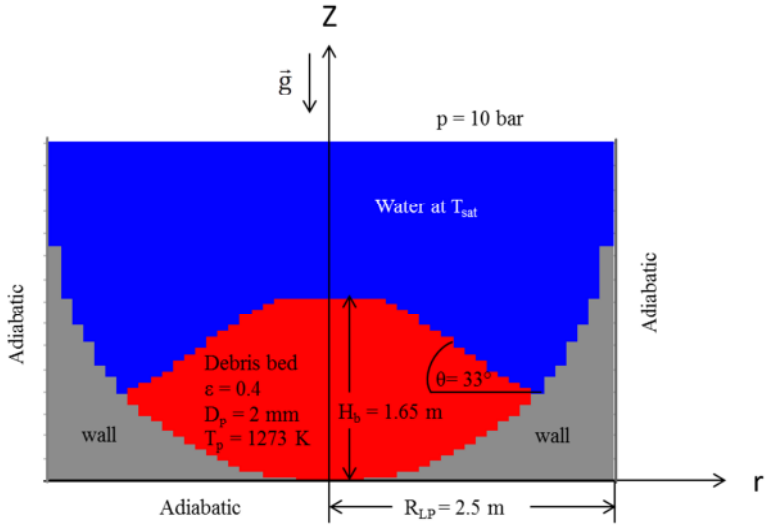

Figure 4.5: Heap-like-bed configuration in the lower head of the RPV: maximum height of the heap of 1.65 m, mean particle diameter 2 mm, porosity 0.4 and angle of slope 33°.

without essential counter-flow of steam. Further, the lower temperatures along the vessel wall allow faster quenching of that region, as can be seen from the saturation development inside the bed.

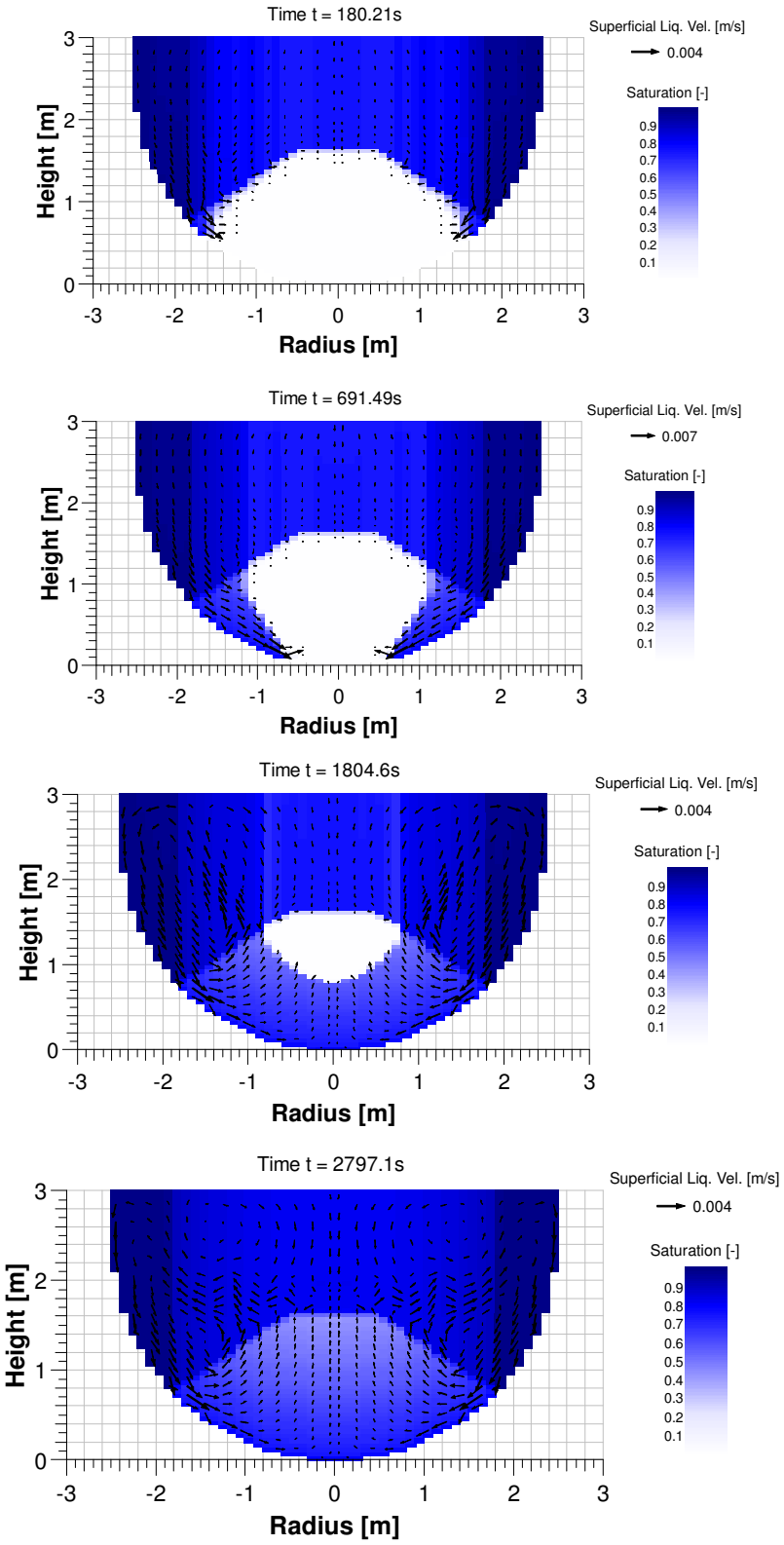

Figure 4.6: Development of saturation and liquid velocity during the quenching of hot debris (total mass 40 ton, initial temperature 1273 K, particle size 2 mm, porosity 0.4, specific power 200W/kg) in the lower head of an RPV at 10 bar system pressure.

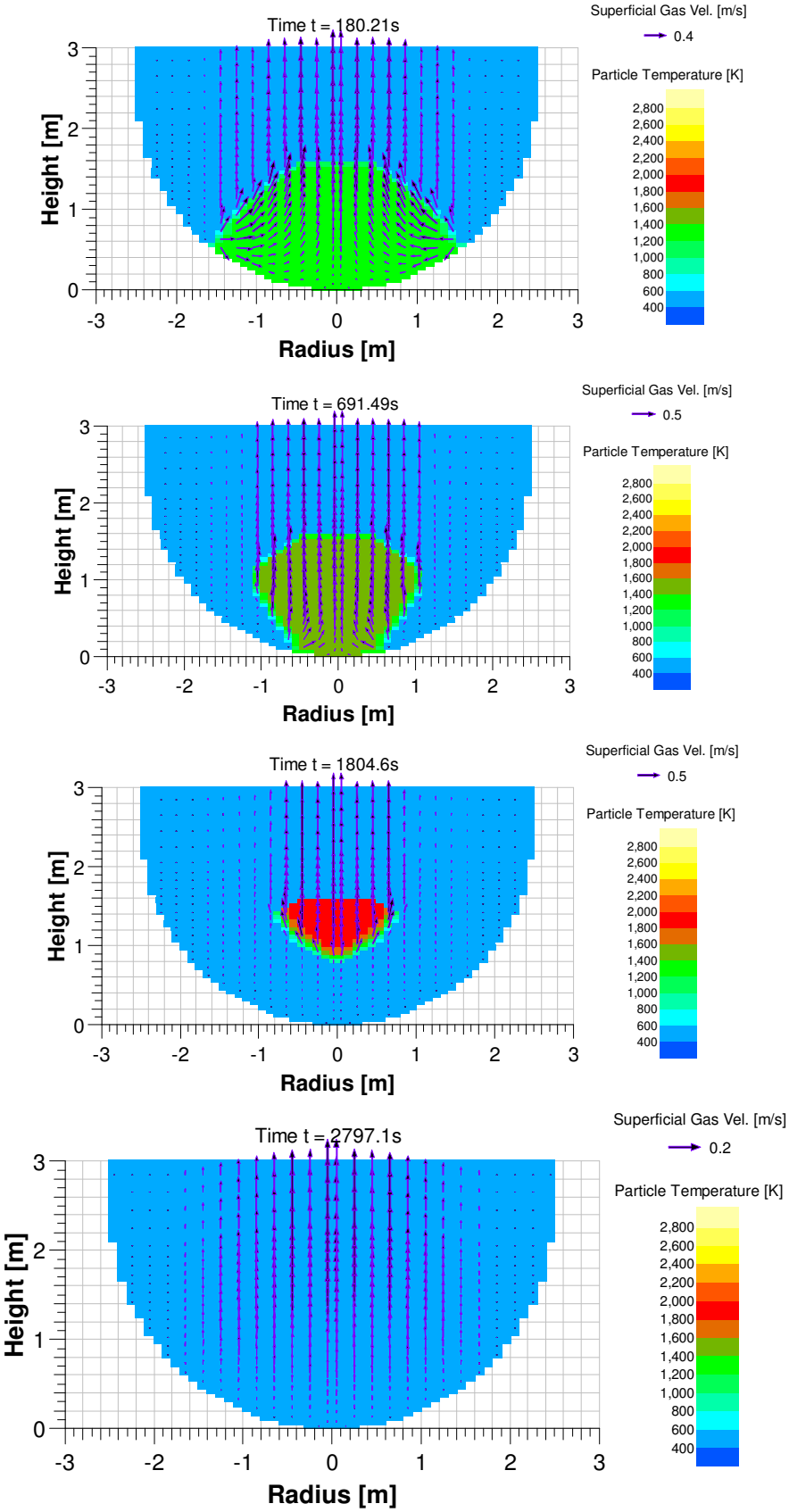

Figure 4.7: Development of particle temperature and steam velocity during the quenching of hot debris (total mass 40 ton, initial temperature 1273 K, particle size 2 mm, porosity 0.4, specific power 200W/kg) in the lower head of an RPV at 10 bar system pressure.

Penetration of water directly from the upper surface of the bed is limited by the strong steam flow resulting from evaporation of water at the bottom. As a result, a dry zone in a central upper region of the bed is maintained for longer time. There, the temperature further increases due to decay heat (see temperature development in Figure 4.7). This zone is finally quenched successively by the surrounding water, flowing into the bed from bottom.

From Figure 4.7, it can be seen that complete quenching to saturation temperature is reached after 2797 seconds. The quenching is fast enough to prevent heat-up due to decay heat above temperatures of 2000 K. Due to the fact that the bottom part is quenched rapidly from the side, the cooling of the upper parts by the gas flow contributes significantly to prevent high temperatures.

Calculations are also performed with 60 ton debris considering the same bed conditions. Results show that complete quenching is not achieved for 60 ton debris. In this case, the temperature in the dry part reaches melting temperature, here taken as criterion of failure of cooling. Continued calculations taking into account melting process, melt pool formation and possible stopping of melt progression under these conditions have not been pursued in the present work. The present modeling does not include these processes. There is some potential for stopping the melting progress and reaching coolability even under such conditions since the dry region where melting starts is located in the upper region of the bed while below water flow in and fills lower parts.

These calculations indicate that coolability is not as effective as in the core case since smaller amount of particulate debris (compared to core debris) have to be assumed to reach coolability. This may be due to the different bed configurations which delayed the establishment of bottom quenching in the lower head as compared to the core, where it starts immediately. Nevertheless, the lower head, as a further barrier for melt release, still yields quite some cooling potential in case of limited melt inflow into remaining water, if water supply can be re-established in time. At least for smaller melt releases (part of the melt still be in the core and may be cooled there), a significant cooling potential in the lower head appears to exist. In order to further explore the chances and limits, additional cases considered as follows. These cases also demonstrate abilities of the code to calculate various variants. The present variations can only give a first perspective about the coolability conditions in the lower head.

4.2.2 Calculations with variations of bed conditions: decay power, initial bed temperature and system pressure

Initial bed conditions e.g. bed temperature, decay heat, system pressure etc. play a significant role to evaluate the quenching against heat up. But depending on accident scenario and reactor type these parameters may vary. Therefore, variations of calculations with these parameters are carried out in order to elaborate under which conditions the hot debris in the lower head remains coolable or re-melting occurs due to insufficient quenching.

The debris bed decay power mainly depends on the elapsed time after the reactor scram, the release of the fission products, the corium composition, etc. The decay power of corium would be reduced from its shut down value as the time goes on. A thumb formula for this reduction of decay power was introduced by Way and Wigner [93]. According to this formula, if a reactor is

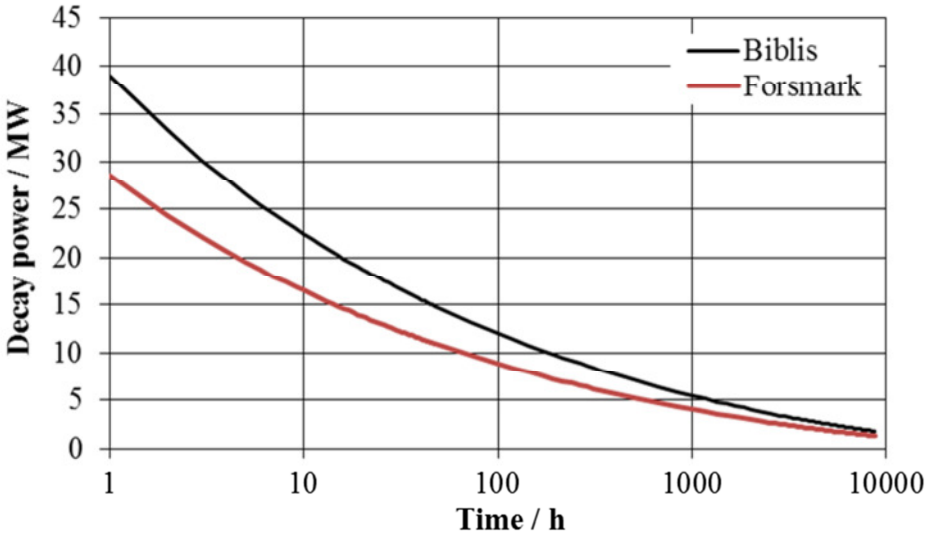

Figure 4.8: Decay power versus time (for two different reactors) after shut down of reactor according to Way-Wigner formula.

operated for the duration T_0 (seconds) with the thermal power P_0 (MW), then the decay power P (MW) at the time t (seconds) after switching off the reactor is

$$P = P_0 \cdot 0.0622\left[t^{-0.2} - (T_0 + t)^{-0.2}\right] \qquad (4.1)$$

Thermal power of the reactor depends on its type and size. For example Biblis, a German PWR is operated with a thermal power of ~3700 MW (1300 MWe). On the other hand Forsmark 1, a Swedish BWR is operated with a thermal power of ~2700 MW (900 MWe). If it is assumed that both reactors operated 36 months with the above mentioned power, then the resulting decay power for the two different after reactor scram according to the Way-Wigner formula is shown in Figure 4.8.

The specific decay power of the debris bed may then vary depending on reactor thermal power and elapsed time. E.g. after 2 hours of reactor shut down a specific decay power q ~300 W/kg may be estimated for Biblis reactor (core mass M= 105 tons). On the other hand, 10 hours after reactor scram this may go down to q ~130 W/kg for Forsmark 1 reactors (core mass M= 120 tons).

Calculations have been performed imposing three different decay powers in order to consider such variations. A specific decay power q= 200 W/kg is considered as reference condition. Two variations, one with q = 300 W/kg and another with q =130 W/kg have been considered in order to cover a plausible range for reactor conditions.

The initial temperature of the bed depends on the cooling history of the falling drops from jet breakup until settling in the lower head. During settling of melt drops quite some quenching can be expected at least at the surface and with crust formation there. More elaborated analyses on the jet break up and debris bed formation are then required in order to get at an approximate result on the initial temperature of the bed. However, as a first step quenching is calculated assuming the whole bed at a given uniform initial temperature. This approach may be considered as conservative since quenching during bed formation is not taken into account.

Three variants of initial bed temperature are considered, here. The bed temperature with 1273K is considered as reference condition. Two variations, one with bed temperature 973K and another with bed temperature 1573K have been chosen in order to get an impression on the influence of initial temperatures.

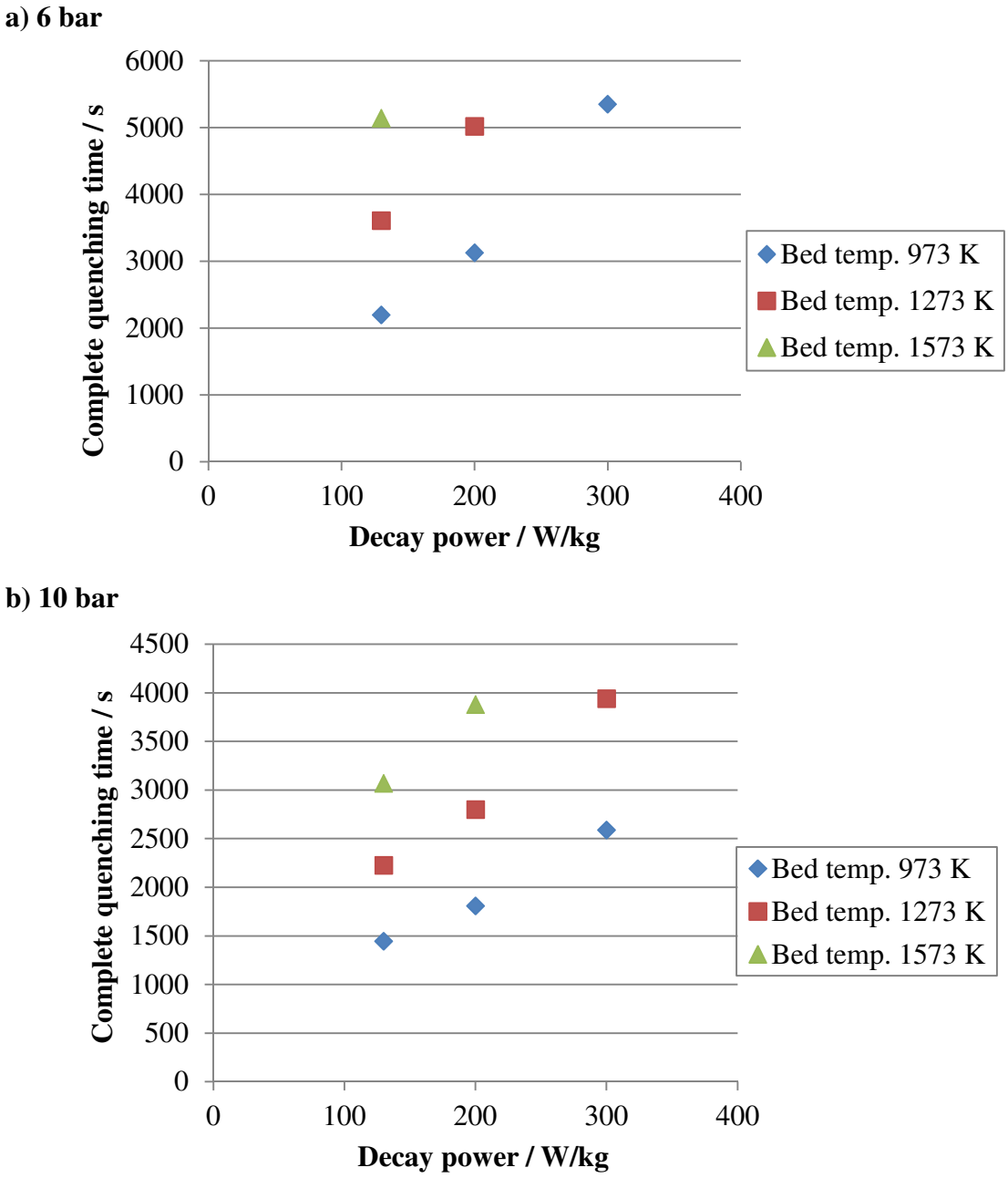

Figure 4.9: MEWA results concerning quenching time of hot debris (40 ton, particle size 2 mm, porosity 0.4) for different specific bed power and initial temperatures: a) at 6 bar system pressure and b) at 10 bar system pressure.

Concerning system pressure, re-flooding scenarios with lower system pressure are of major interest since in case of a severe accident depressurization of the vessel is foreseen as an accident management measure. System pressures of 10 and 6 bars have been considered in order to investigate scenarios with depressurization.

Results of MEWA calculations concerning quenching time for different cases are summarized in Figure 4.9. Points are included in these figures for the cases in which complete quenching are achieved before reaching the melting temperature in any parts of the debris bed. In the conditions with missing points, melting temperatures are reached.

From Figure 4.9 a) it can be seen that even at low system pressure of 6 bar, quenching of 40 ton of 1573 K debris with 2 mm diameter particle and 40% porosity is calculated by MEWA in case with decay power of 130 W/kg.

With decay power of 200 W/kg, complete quenching before reaching the melting temperature can be achieved up to an initial temperature of 1273 K. A lower initial temperature of 973 K has to be assumed for complete quenching in the case of decay power 300 W/kg.

For the two cases with decay power 200 W/kg, initial temperature 1573 K and decay power 300 W/kg, initial temperature 1273K ,part of the bed reaches melting temperature, therefore the cases are not included in Figure 4.9 a). Although the largest fraction of the debris is quenched, the upper central part of the bed heats up further and finally reaches temperatures in excess of 2800 K as can be seen from the calculation result after 3936 s for the first case in Figure 4.10. However, even with this result, coolability is not excluded since a melt pool forming in this region is small and may be stabilized by the water below, i.e. a maintained water flow from bottom around the pool region.

A definite failure limit of coolability is reached only for the case with high decay power of 300 W/kg and high initial temperature of 1573K. In this case, the bed contains already high thermal energy. Further, the density of the steam decreases with increasing temperature. Therefore, the produced steam can only escape slowly through the high temperature bed due its higher specific volume and yields much slower water ingression and quenching. As a result, melting temperature is reached in a large part of the debris bed already after 2343 s as can be seen in Figure 4.11.

However the combination of all less favorable cooling conditions e.g. large debris bed, low system pressure, high decay power and high initial temperature may not be realistic. Change in one parameter to favorable condition e.g. initial bed temperature from 1573 K to 973 K yields a strong trend towards quenching. Therefore, good chances to reach coolability of hot debris in the lower head can be concluded if the debris mass is not too large.

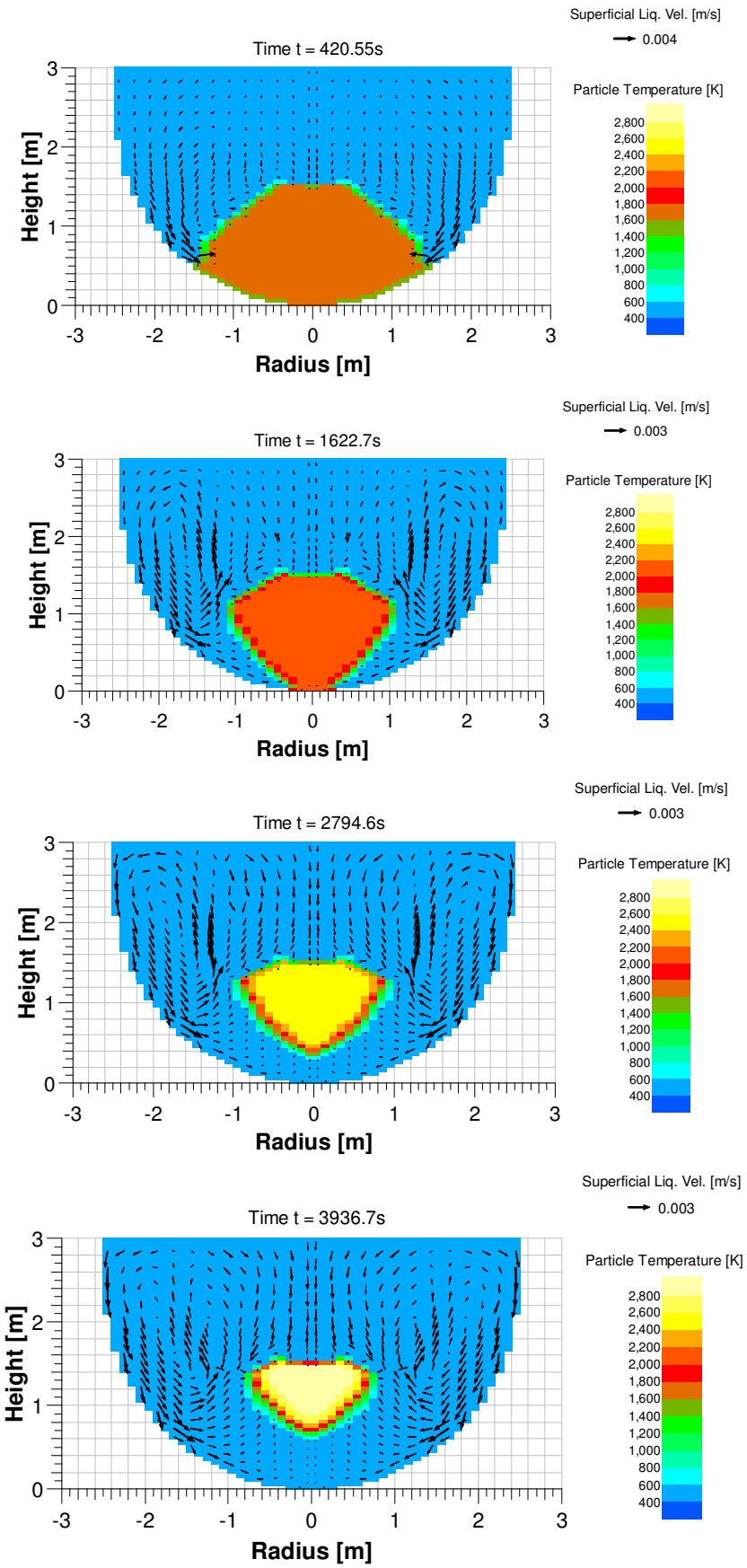

Figure 4.10: Development of temperature and liquid velocity during the quenching of hot debris of initial temperature 1573 K and specific power 200W/kg in the lower head of an RPV at 6 bar system pressure.

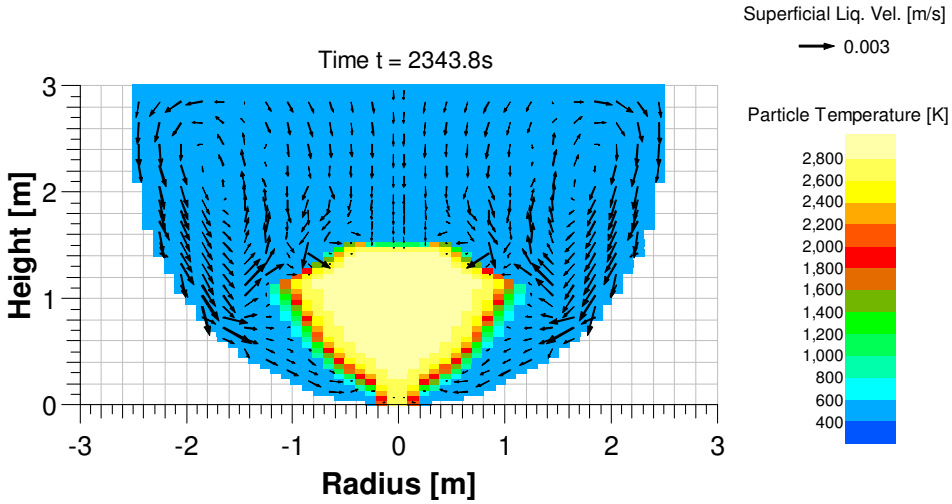

Figure 4.11: Temperature and liquid velocity distribution calculated by MEWA after 2343s during the quenching of hot debris of initial temperature 1573 K and specific power 300W/kg in the lower head of an RPV at 6 bar system pressure.

From Figure 4.9 b) it can be seen that complete quenching is supported by higher system pressure. While partly melting is results for the debris with temperature 1573K and 200 W/kg in case of 6 bar system pressure the similar calculation with 10 bar shows complete quenching before reaching the melting temperature as can be seen from Figure 4.12. Understanding is provided by the specific volume of steam. Produced steam in higher system pressure can escape more rapidly due to its lower specific volume.

With 10 bar system pressure, complete quenching is also achieved for the debris bed with temperature 1273K and decay heat 300 W/kg. Only for the case with temperature 1573K and decay heat 300 W/kg, a small part in the upper center region (Figure 4.13) reaches the melting temperature which may be stabilized by maintained water flow from bottom.

Thus, the limit of coolability increases with increasing system pressure. This means the advantages and disadvantages on depressurization of system in case of severe accident should be generally reconsidered. The advantages of depressurization of the system are considered as auxiliary different alternative means of cooling and to avoid high pressure failure of RPV (rocket). On the other hand the disadvantage of depressurization is that it decreases the coolability due to production of high volume steam which leads slower steam escape and yield slower water ingression inside the bed.

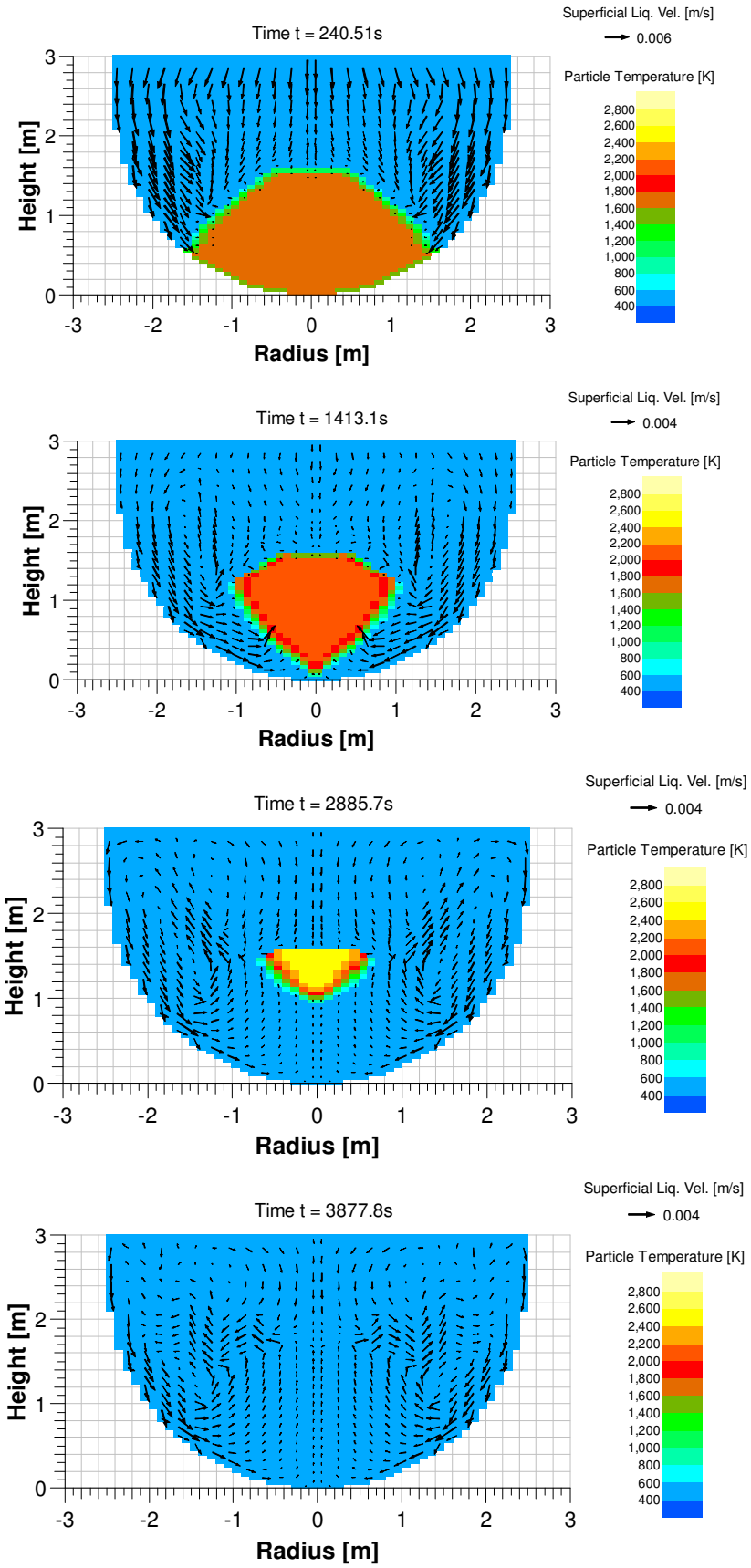

Figure 4.12: Development of temperature and liquid velocity during the quenching of hot debris (initial temperature 1573 K and specific power 200W/kg) in the lower head of an RPV at 10 bar system pressure calculated by MEWA.

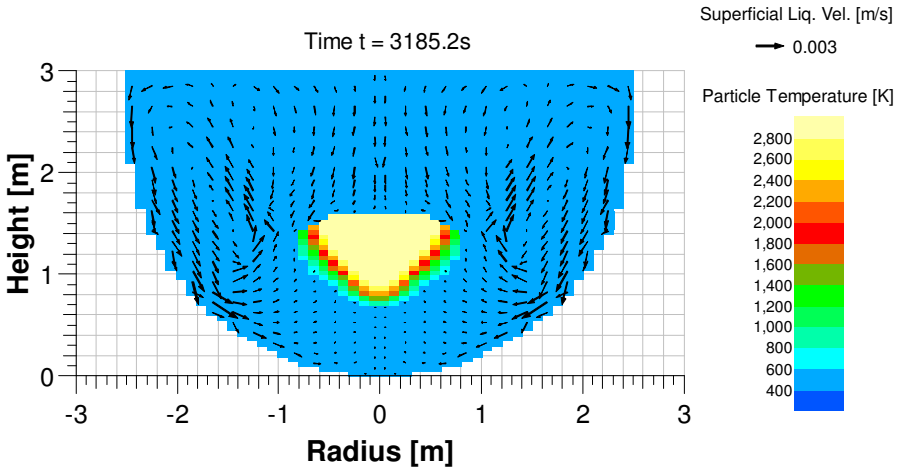

Figure 4.13: Temperature and liquid velocity distribution calculated by MEWA after 3185s during the quenching of hot debris of initial temperature 1573 K and specific power 300W/kg in the lower head of RPV at 10 bar system pressure.

4.2.3 Calculations with dense a region (cake) inside the debris bed

Debris beds which may be formed in a postulated severe accident cannot be expected to have a homogeneous structure. Lateral non-homogeneities of the bed shape are already considered in previous section e.g. by a variation in height as in a heap of debris or due to spherical bottom. Further, internally less porous (less than 30%) or more porous (more than 50 %) region may occur as outlined above. Dense regions appear not to be coolable if the porosity is too low. Superposed layers of very small particles hinder especially water inflow from above. But, in multidimensional configurations, regions with higher porosity or with larger particles may give water an easier flow path towards lower bed regions. Water access to the bottom region due to such multidimensional effects together with resulting cooling of upper region by steam flow may provide sufficient cooling also in denser regions and thus increase the overall cooolability. This is explored here by a MEWA calculation considering a dense region of 40 cm thicknesses inside the debris bed as can be seen in Figure 4.14. Such a dense region inside the bed may e.g. result from melting and relocation process in dry region as obtained above.

A low porosity of 0.22 is considered in this dense region. Surrounding this region, a loose debris bed with porosity 0.4 and particle diameter of 2 mm is considered. A power of 200 W/kg has been applied and maintained during the calculation. An initial temperature of 1273 K has been assumed for the initially dry debris and cake part and a system pressure of 10 bars.

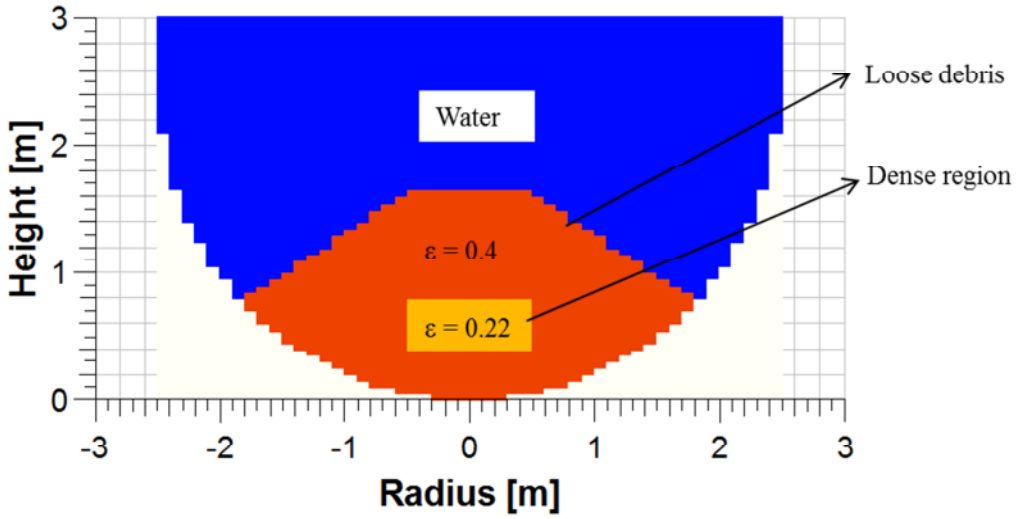

Figure 4.14: Configuration with dense region of porosity 0.22, thickness 40 cm and 1 m diameter inside the loose debris bed (porosity 0.4) in the lower head of RPV bed.

Figure 4.15 shows the development of the saturation and water velocity as well as temperature history inside the bed. The debris with higher porosity is quenched rather quickly due to higher permeability. Quenching in this loose debris part is fast enough that a temporary increase of temperature due to decay heat does not exceed 2130 K. The quenching of the cake region takes a much longer time and temperatures go beyond 2300 K at 3500 s, although in a reduced region (inner top region) in the cake. Complete quenching in the cake part to saturation temperature is reached at about 11371 s.

Steam cooling plays a significant role in the cake region by avoiding rapid heat-up as can be seen from Figure 4.16. The saturation distribution inside the bed at 5007 s indicates that the cake region remains dry at this calculation state. But the temperature development inside the cake region shows no further increase of temperature after 3600s which means the limitation of superheats of the particle is reached by the resulting steam flow from below. This enables slow quenching by water flowing around and partially into the low porosity area.

a)

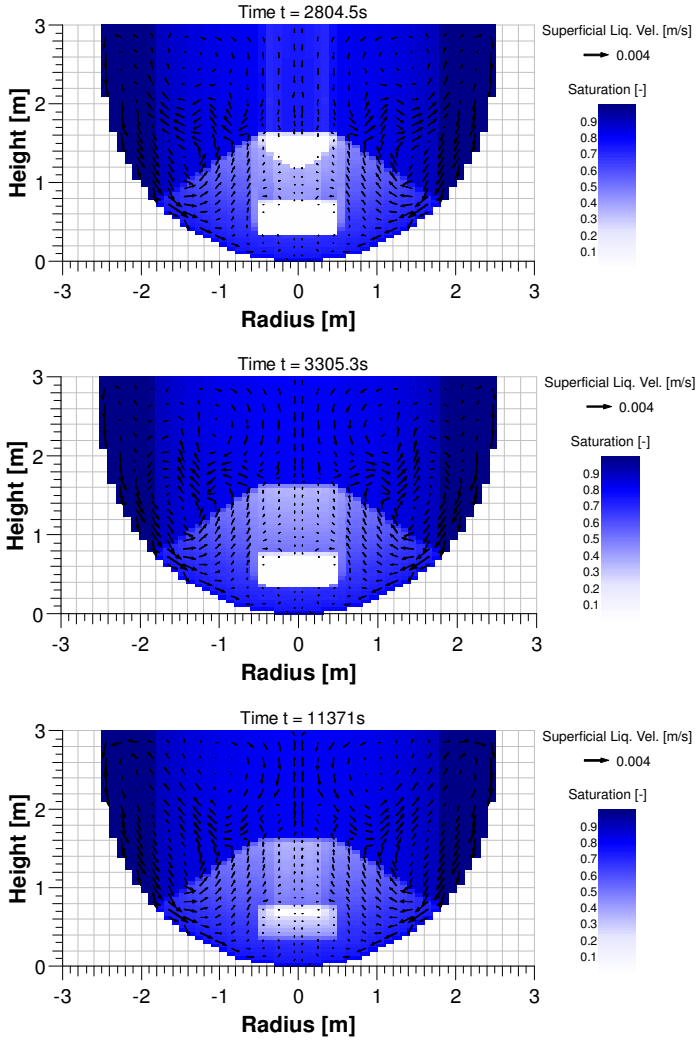

b)

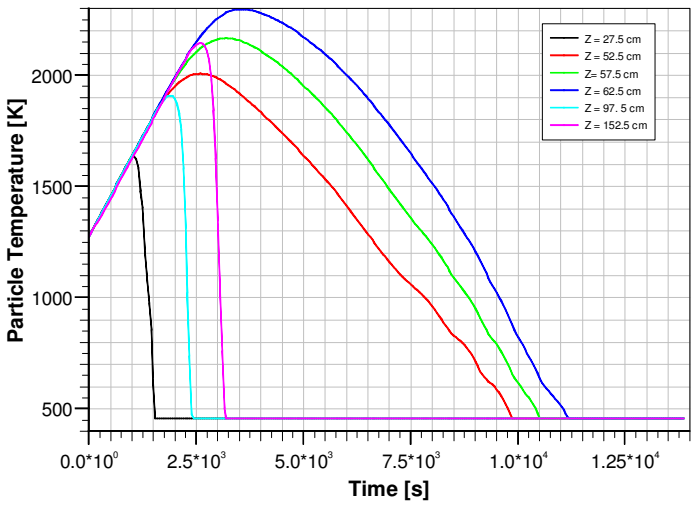

Figure 4.15: MEWA calculation on quenching of hot debris in the lower head with dense region of 40 cm thickness at 10 bar system pressure: a) saturation and water flow field, b) temperature versus time at center (radius r = 0) and different elevations (Z).

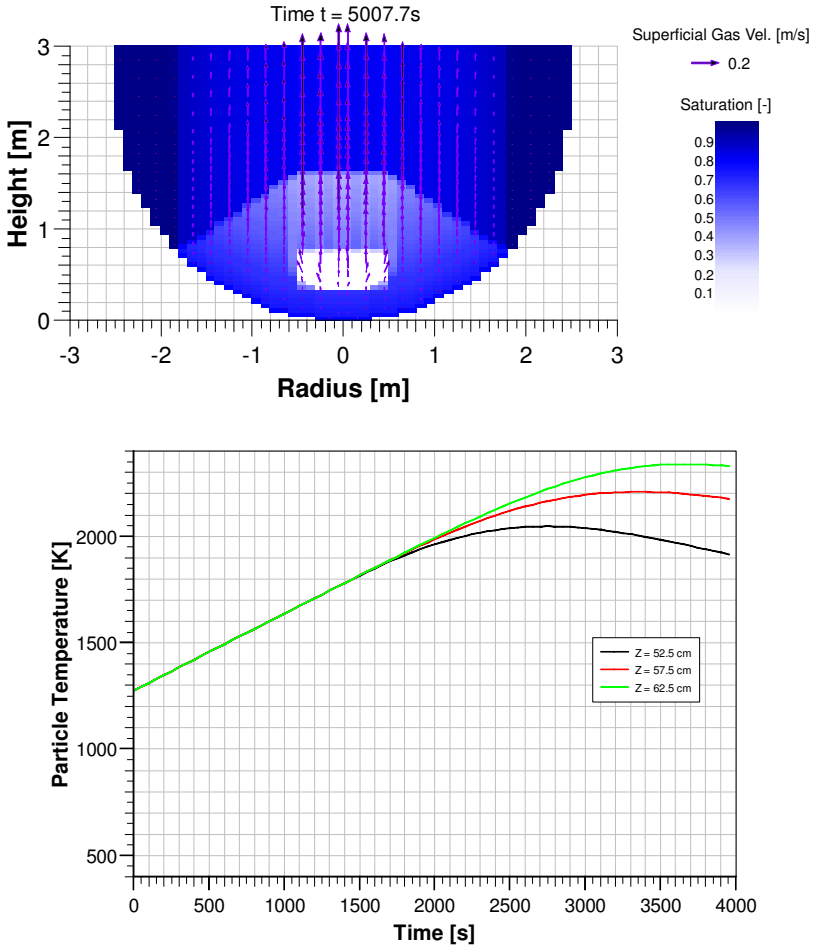

Figure 4.16: Limitation of super heat of the dense part by resulting steam flow from evaporated water below: saturation and gas velocity field at calculation state 5007 s (top) and temperature history inside the cake part (bottom).

Additional calculations have been performed by increasing the thickness of the dense region in order to search the limit of coolability of such configurations i.e. dense regions inside the bed. From various calculations it has been found that a limit of coolability is reached if the region is very thick (more than 40 cm). E.g. a MEWA calculation with a dense region of 50 cm thickness and otherwise the same conditions as in the previous case yield melting temperature inside the cake region already after 6962 s, as can be seen in Figure 4.17. In this case, the steam flow through the cake part is slower since it has to overcome higher friction due to the larger thickness.

Thus, the MEWA calculations give a perspective to evaluate the competition between heat-up by decay heat and quenching with dense regions inside the debris bed, i.e. under conditions with additional handicaps. The calculation results show that quenching can even be reached with a dense region (low porosity of 0.22) if the region is not too thick.

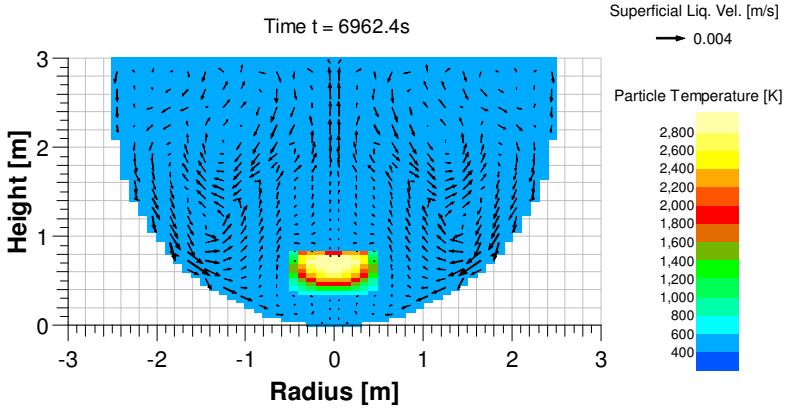

Figure 4.17: Temperature and liquid velocity distribution calculated by MEWA after 6962s during the quenching of hot debris with dense region of 50 cm thickness at 10 bar system pressure.

Coolability even under such more complicated conditions with a dense region is realized due to inflow of water below the dense part via the region with higher porosity, i.e. considering the multidimensional effect. If the cake part is considered alone and flooded from the top only (classical analysis) then quenching of this dense part is severely limited as can be seen in Figure 4.18.

In this configuration quenching is much slower since water has to penetrate against up-flowing steam. The ingression of water into the bed becomes more and more difficult as the quenching front progresses because steam the flow produced from the region being quenched (due to decay heat) gets stronger with increased region under quenching. As a result, only an upper part of the bed (about 20 cm from top) gets quenched but the lower half of the bed remains dry. This region is heated up further due to decay heat and reaches the melting temperature at about 10040 s.

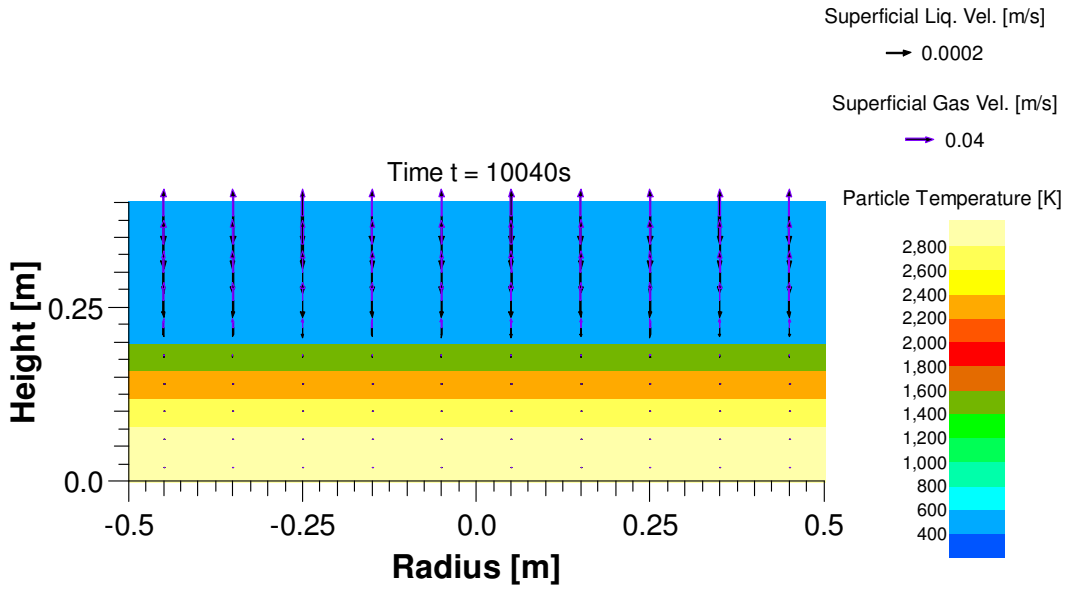

Figure 4.18: Temperature, liquid as well as gas velocity field calculated by MEWA after 10040 s during the quenching of a dense layer of 40 cm thickness, flooded only from top.

5 Coolability of Ex-Vessel particulate debris

In a sequence of a core melt accident, if the corium cannot be cooled inside the reactor pressure vessel, it will settle as a melt pool at its bottom and yield failure of the vessel due to heat-up and thermal stresses. After vessel failure, melt will discharge from the vessel as a jet into the reactor cavity i.e. the volume below the RPV in a LWR. The cavity might be filled with water either as a consequence of the accident sequence or due to accident management measures as considered in Finnish and Swedish BWRs. Depending on vessel breach size (melt jet diameter, D_{jet}) and height of water pool (H_{pool}) different bed configurations may be envisaged. If a thin melt jet (D_{jet} =10-20 cm) falls in a deep water pool (H_{pool} > 5 m), significant break-up of melt and formation of debris bed is expected (Figure 5.1). On the other hand, breakup of melt will be greatly reduced with thick melt jets (D_{jet} > 20 cm) and also with shallow water pools (H_{pool} < 2 m). This may result in bed configurations containing molten parts (Figure 5.1) which are difficult to cool. Therefore, it is required to perform various calculations with variation of conditions in order to gain an overall view on the chances and critical ranges. In this respect, essential effects are to be considered to guide the investigations.

An important consideration with respect to the adequate modeling of the processes is that a debris bed formed by the jet breakup process and subsequent settling of debris. Such debris cannot be expected as fully quenched and filled with water at saturated conditions. Rather, a hot and dry debris bed is to be expected in a first phase. If quenching of this hot debris by water ingression is not rapid enough then heat-up by decay heat in still dry regions may again yield melting. Therefore the major question concerns the chances of quenching of hot debris before reaching melting temperature.

Assuming the whole bed at a uniform initial temperature for analysis of coolability, as done in earlier investigations (Fichot et al. [70], Bürger et al. [77]) may strongly miss the real process in which settling of partly solidified melt drops occurs simultaneously with water inflow and quenching. This real process of continued settling of debris and simultaneous quenching during bed formation is also considered as strongly favorable for cooling. In order to explore this, the jet breakup and particle (debris) settling model, JEMI (Pohlner [81]) and debris cooling model,

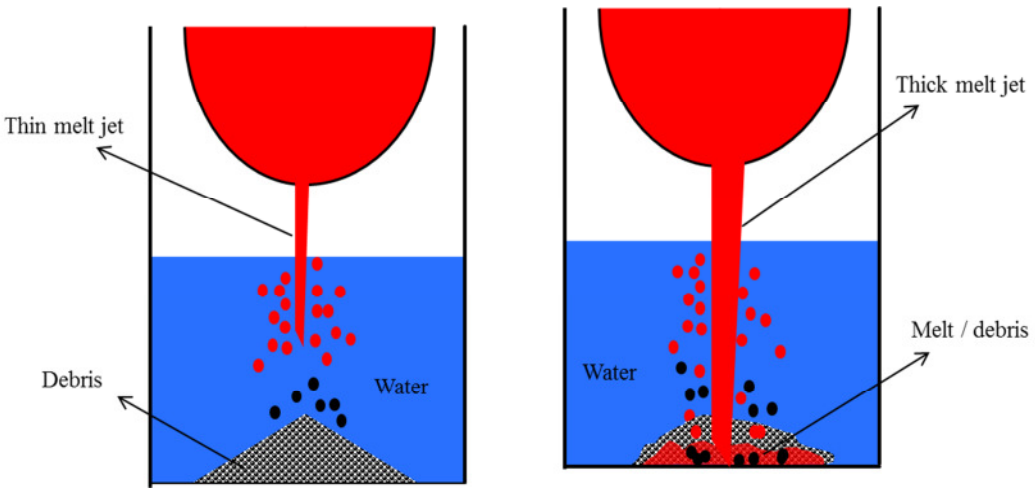

Figure 5.1: Bed configurations in a deep water pool cavity; debris bed formed by breakup of thin melt jet breakup and combined melt / debris formed by breakup of thick melt jet (right).

MEWA (Buck et al. [69]) have been extended to treat these combined processes in the present work (see details in chapter 2.4). Thus, transient formation of debris bed is considered with realistic initial temperatures of the settling particles created from the jet breakup process. With this combined and improved model, analyses of quenching are performed in a more profound way in the present study, with quenching calculated simultaneously during the formation of the debris bed.

Other major effects on quenching of hot debris are expected from decay heat (depending on elapsed time after reactor shut-down), particle size, bed porosity, shape of the bed etc. Approximate results on characteristic particle sizes can be obtained from the jet breakup model whereas conclusions on the global shape of the bed are more difficult and uncertain. Porosities and their distribution in the bed appear to be even more intangible. Concerning the bed shape, a heap like bed is to be expected, but with significant uncertainties concerning the angle of descent, thus the height and spreading. Spreading may be favored by strong convective water flows in the cavity. Concerning porosities, general data on beds with non-spherical particles may be applied, as e.g. 35-40%. Larger values may be expected for strongly deteriorated particle sizes. The DEFOR experiments yield rather high porosities of 50-60%. However, they have not been performed with prototypical material and conditions (especially significantly lower melt temperatures). Thus, due to the uncertainties, these parameters and conditions have to be varied in a reasonable range for reactor applications. The major question is then, whether a general conclusion about quenching can be drawn and under which conditions a limit of coolability is reached.

In case of incomplete breakup of melt (e.g. due to thick melt jet), the resulting bed configurations may contain molten parts at the bottom (see Figure 5.1). For this type of configurations a problem is that depending on the height of this melt layer, the configuration may not be coolable with the present SAM measures i.e. flooding from top only. If a non-coolable configuration is formed, a backup measures may be required to prevent attack of the basement by the melt. As such a measure, injection of water from below may be considered. The COMET experiments at FZK (Alsmeyer and Tromm [12]) have demonstrated that injection of water into a melt layer from below is an option to achieve fast cooling and stabilization, even for melt layers of larger heights (~ 50 cm). An application of bottom injection of water as a backup measure in a wet cavity needs further investigations. It has to be analyzed whether bottom injection of water can avoid or stop this attack by producing porosities and thus a coolable configuration in the molten parts.

5.1 Coolability of particulate debris bed formed in a deep water pool with thin jet diameter

In the following reactor application, a large Boiling Water Reactor (BWR) has been considered which has a thermal power, P_0 = 2730 MW. It has been assumed that a total melt mass, M = 190 tons discharged from the reactor pressure vessel into the water filled cavity. The diameter of the cavity, D_{cav} is chosen as 9 m. Melt has been released as a jet with initial diameter, D_{jet} = 20 cm (15-20 cm jet diameter is considered as most probable in accident scenarios, Sehgal [9]) and an initial jet velocity, V_{jet} = 4 m/s. With the assumed release conditions, the pour of melt from the

RPV has duration time of about, t = 195 s. A water pool height, H_{pool} = 7 m has been considered (7-10 m foreseen in BWR) and a pressure p = 3 bar. In the frame of scenario variations more conservative, i.e. less favorable cooling conditions are to be assumed. Fragmentation will be reduced with a lower height of water pool and a lower system pressure (lower pressure of 3 bars is less favorable for quenching and may exist in the cavity).

The decay power of corium (P) would be reduced from its shut down value as time goes on. After 3 hours the calculated decay power, P according to Way and Wigner formula (equation 6.1) is 22 MW. This corresponds to a specific power, q = 115 W/kg with M=190 tons of corium mass, as considered in the present calculation.

In order to assess the coolability of corium in such an accident scenario, the first checking point is the completeness of breakup of melt when falling in the water pool. JEMI calculations show (see Figure 5.2) with the release conditions mentioned above, i.e. D_{jet} =20 cm and V_{jet} = 4 m/s initial velocity, that the developing coherent jet length, $L_{jet,coherent}$ is 4.5 m which is shorter than the height of water pool (H_{pool} =7 m). As a result, melt jet breakup is complete. Further, the calculation about solidification of the falling drops from breakup indicates that sufficient crust formation occurs until settling to support particulate debris formation on the cavity floor.

However, complete quenching of these particles is not achieved until settling. According to the JEMI calculations, the average temperature of the particles when settling is between 1500 and 1700 K. Due to this high temperature of the particles, water inside the boils off completely in the initial phase of settling. As a result, dry and hot debris is formed. However, quenching of this hot debris by ingression of water from the surrounding water pool also starts immediately after settling of particles and boil-off. Since decay heat is released in the bed there is a competition between quenching and heat-up. If quenching is not rapid enough, then heat-up by decay heat in still dry regions may again yield melting. Thus, the success of quenching against heat up decides

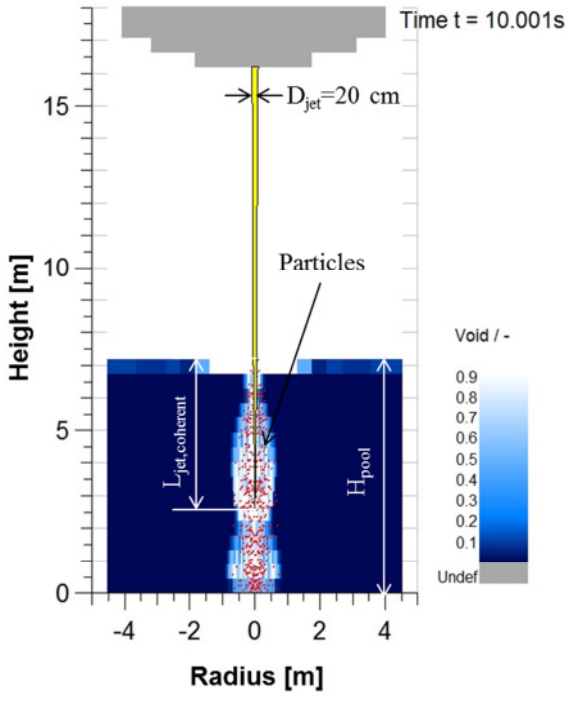

Figure 5.2: Development of void fraction (color shade), coherent jet and particle cloud calculated by JEMI model [81] with D_{jet} = 20 cm.

about the coolablity question in such situations. It has to be investigated whether quenching of the hot debris is reached in a sufficient time, i.e. before heat-up reaches the melting temperature.

In a first approach an established hot debris bed is considered here, as follows. This kind of approach was usually applied in earlier analyses (Fichot et al. [70], Bürger et al. [77]).

5.1.1 Calculation with an initially established hot debris bed

As a limiting case, the whole melt mass of M = 190 tons are assumed to be released into the cavity (D_{cav} = 9 m) and to form there a large particulate debris bed. A conical, axisymmetric shape of the bed is considered. An angle of cone, θ = 30° and a porosity, ε = 0.4 have been chosen which yields a bed height, H_{bed}= 2.36 m with bed diameter, D_{bed} = 8 m at bottom (see Figure 5.3). Regarding particle sizes, MEWA considers an effective particle diameter, which has to be determined from the particle size distribution obtained from the JEMI calculation. Different mean diameters, e.g. mass mean, surface mean, number of particle mean may be used (see equations (1.1) to (1.3) in chapter 1.2.2). Validation calculations with MEWA for different experimental debris beds (see chapter 3.2) suggest that the effective diameter is close to the surface mean diameter. For the present drop size distribution calculated by JEMI the surface mean diameter is about 1.8 mm. A uniform initial temperature T_p=1600 K was assumed as starting condition for the quenching of the hot bed, in this calculation. It is assumed that water with saturated temperature (T_{sat} = 408 K at p = 3 bar) surrounds the initially hot and dry debris bed and is driven into the bed due to the pressure differences from gravity.

Results of the MEWA calculation are given in Figure 5.4, for the development of particle temperatures and liquid velocities. It can be seen that water flows predominantly into the bed at the lower side of the cone and provides quenching there. Water inflow directly from the upper surface of the bed is hindered by the resulting steam up-flow resulting from the evaporation of water penetrating at bottom. Since quenching from top is limited, water has to fill the bed mainly from bottom which occurs very slowly, here. Additional cooling of the upper regions is provided by evaporation of water at bottom and subsequent up-flow of steam. However, in the present case this is not sufficient to avoid that melting temperature (>2800 K) is reached in rather large upper parts of the bed already after 6680 s.

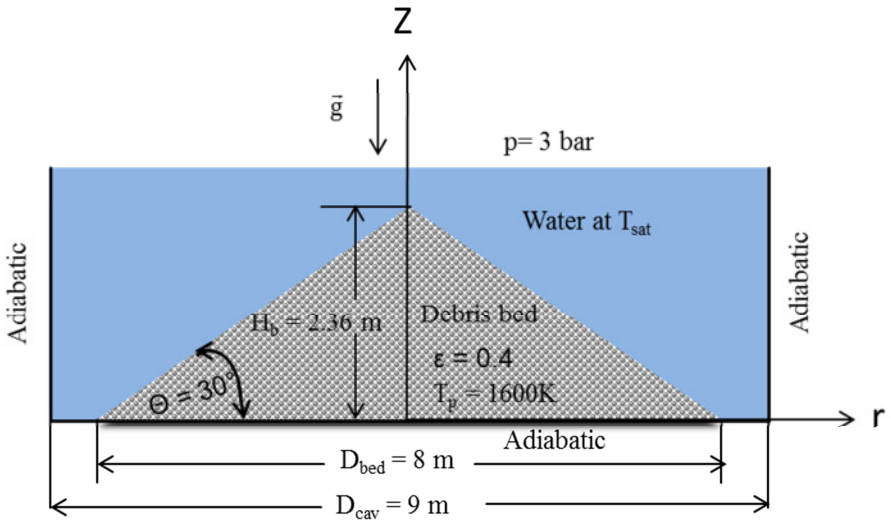

Figure 5.3: Configurations with particulate debris in the reactor cavity.

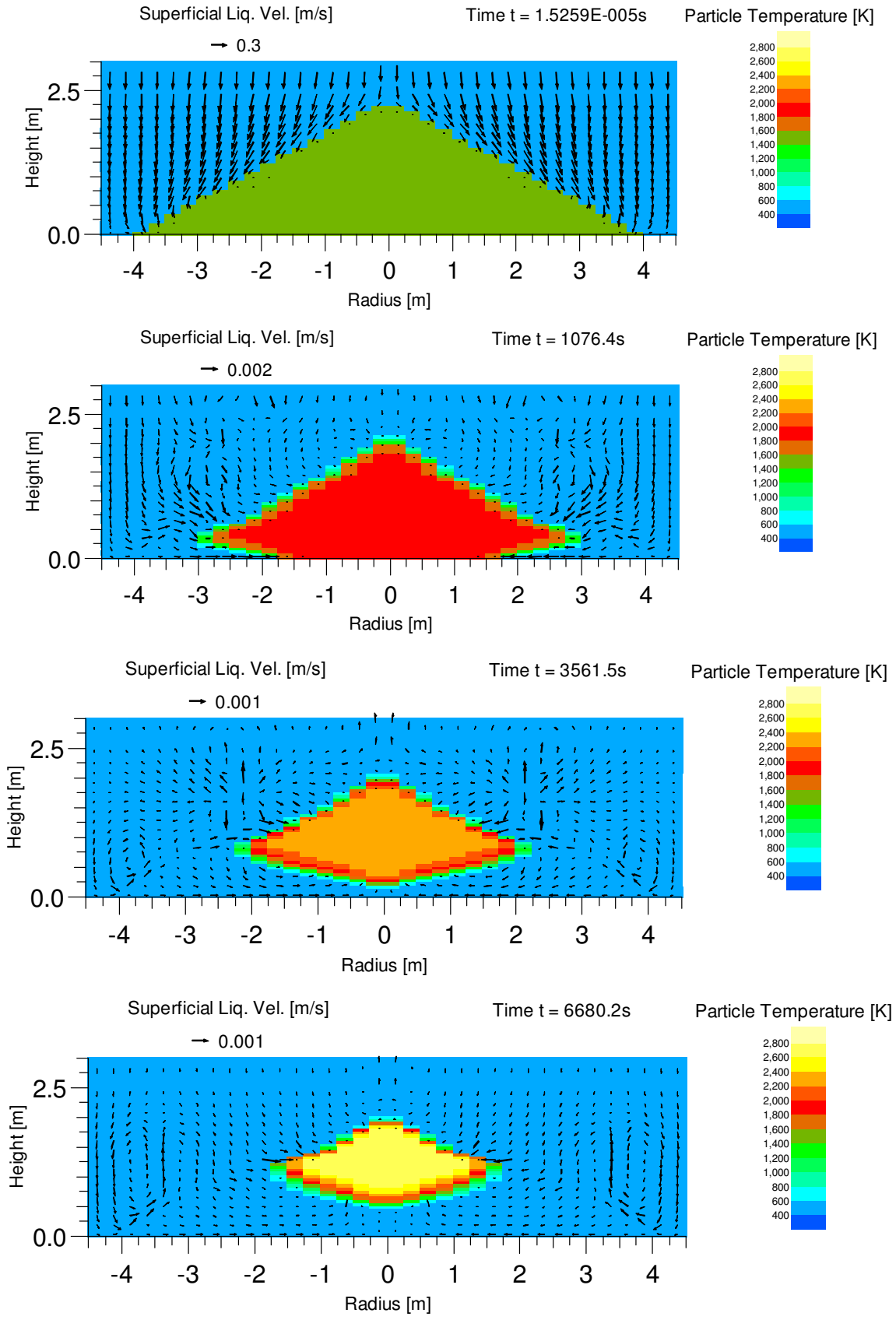

Figure 5.4: Development of particle temperature and liquid velocity during the quenching process for an established hot debris bed calculated by MEWA.

However, the assumption of the whole bed being initially at a uniform temperature is not realistic. In the real process, already settled parts should start to be quenched during the continued build-up of the debris bed. Settling and simultaneous quenching may strongly favor the cooling process excluding a large bed uniformly at high temperature. To explore this, quenching is calculated simultaneously during build-up of the debris bed

5.1.2 Calculation with simultaneous quenching during the buildup of debris

A cone shaped bed structure with angle of cone 30° and a porosity of 40% has been chosen for bed formation. A layer-wise development of the bed is considered in the model. For each layer, average temperatures and mean particle sizes are determined from the temperature of settling particles and their size distribution calculated by JEMI. Surface mean diameter from the calculation yielded particle sizes in the layers ranging from 1.6 to 1.9 mm.

The results of a coupled JEMI/MEWA calculation concerning quenching of debris bed are shown in Figure 5.5/Figure 5.6 and Figure 5.7/Figure 5.8. First two figures show the development of the particle temperature and gas velocity in the developing debris bed. The corresponding developments of void fraction and liquid velocity are shown in later twos. The buildup of the cone from settling particles can be seen in the particle temperature map up to 195s (Figure 5.5; see also the development of a high void fraction region at the bottom in Figure 5.7).

Figure 5.7 and 5.8 show a completely dry bed until 195 s, i.e. the time when bed formation is complete, although some water inflow is seen from the velocity field. Only after that time water is seen to fill the bed by inflow from lateral bottom regions. However, the final results (as compared to the case in previous section 5.1.1) as well as already the temperature history in Figure 5.5 indicate some cooldown (300 to 400 K) in the period of bed formation up to 195 s. This is provided during settling of particles and also by cooling in steam flow from the evaporation of water flowing into the bed. The subsequent development after complete bed formation with quenching and filling up by water from the bottom can clearly be seen in Figure 5.6 and Figure 5.8. In contrast to this process, inflow of water directly from the upper surface is limited. Thus, a dry zone in a central upper region of the bed is maintained for longer time. There, the temperature further increases due to decay heat. This zone is finally quenched successively by the surrounding water, flowing into the bed from bottom.

From the final picture of Figure 5.7, it can be seen that complete quenching to saturation temperature is reached after 11800 seconds. In this case, the quenching is fast enough to prevent heat-up due to decay heat above temperatures of 2400 K. Due to the fact that the bottom part is quenched rapidly from the side, the cooling of upper parts by the gas flow contributes significantly to prevent high temperatures.

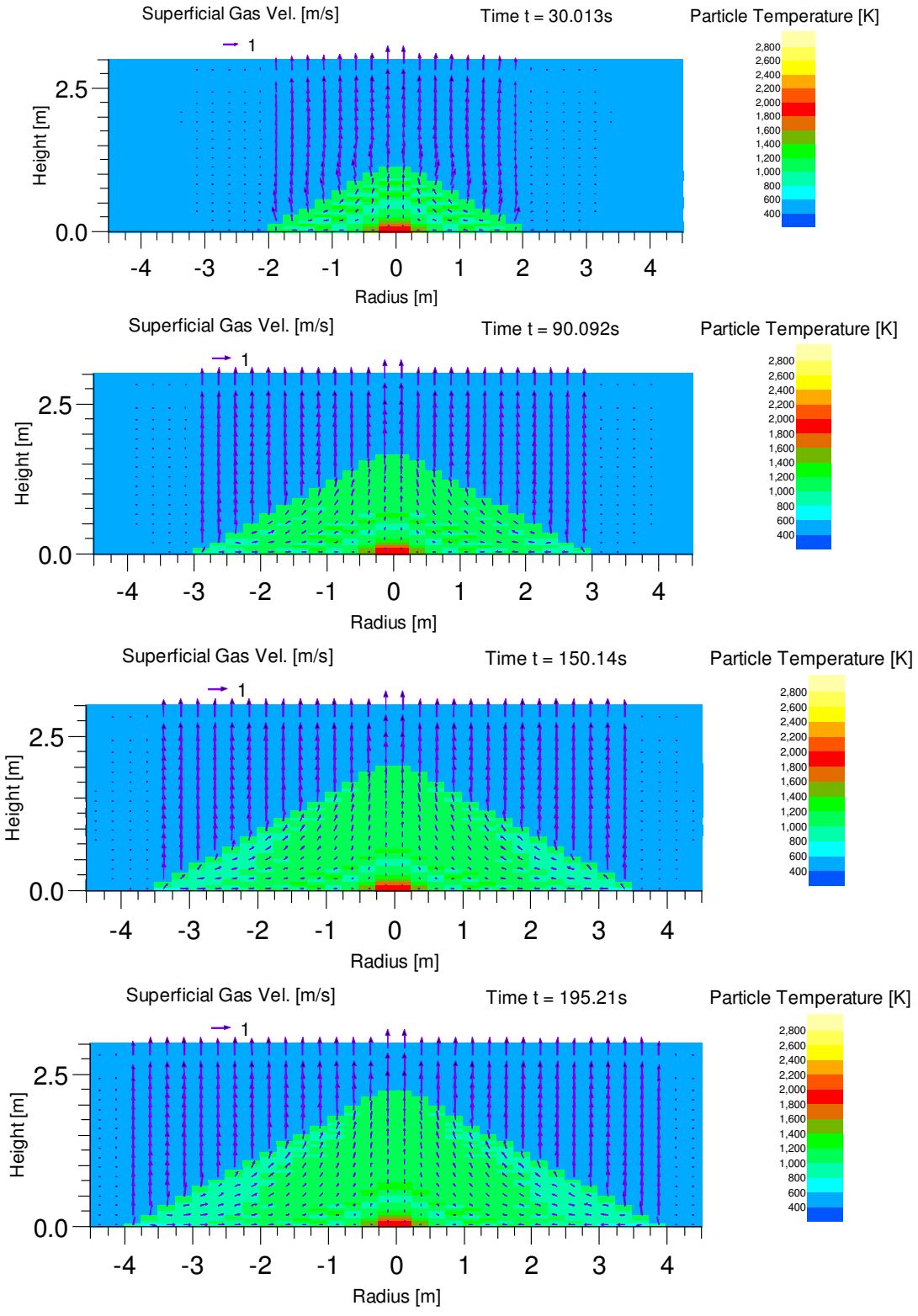

Figure 5.5: Development of particle temperature and gas velocity during the simultaneous processes of bed buildup and quenching calculated by JEMI/MEWA.

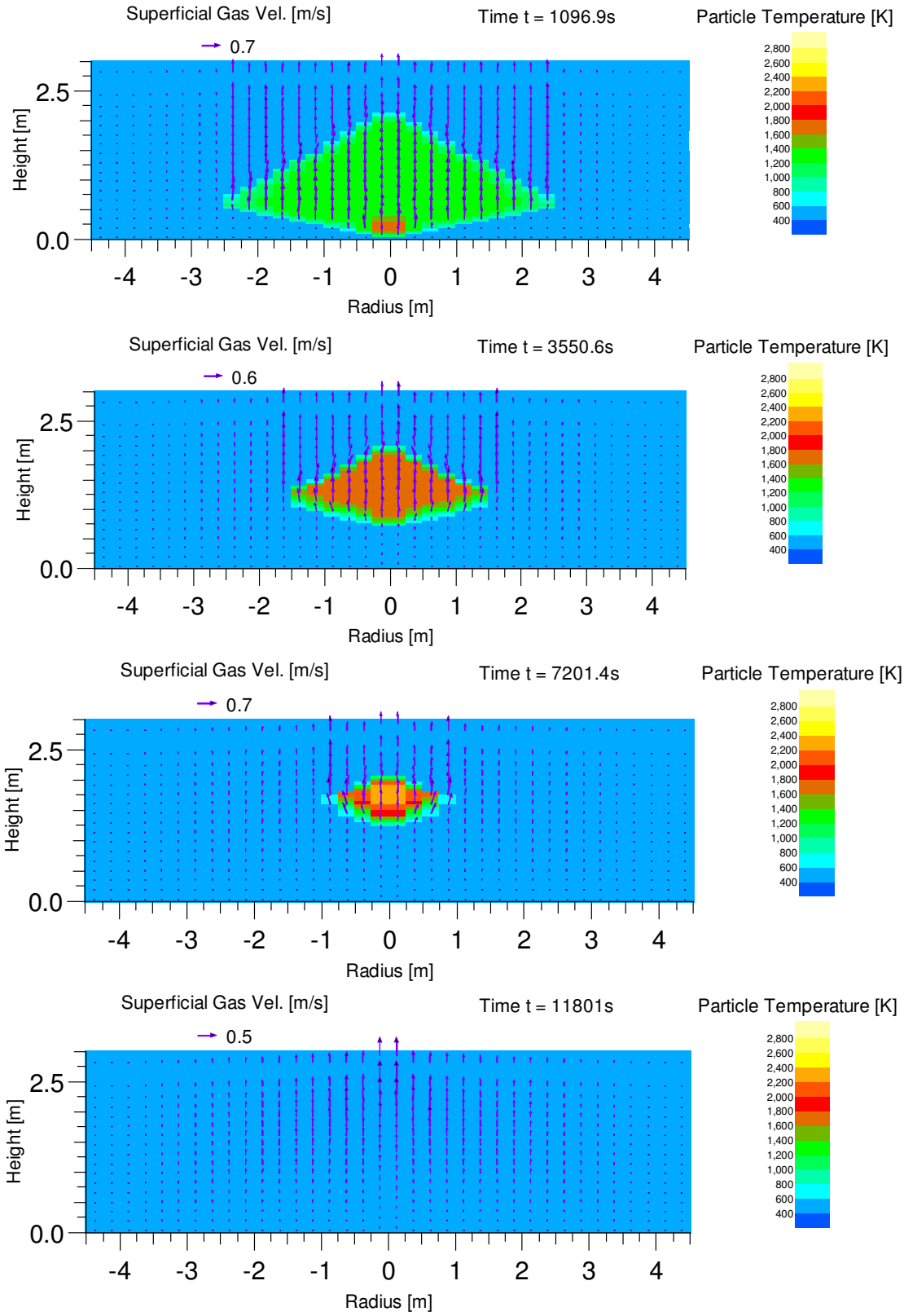

Figure 5.6: Development of particle temperature and gas velocity (continuation from previous Figure 5.5) during the simultaneous processes of bed buildup and quenching calculated by JEMI/MEWA.

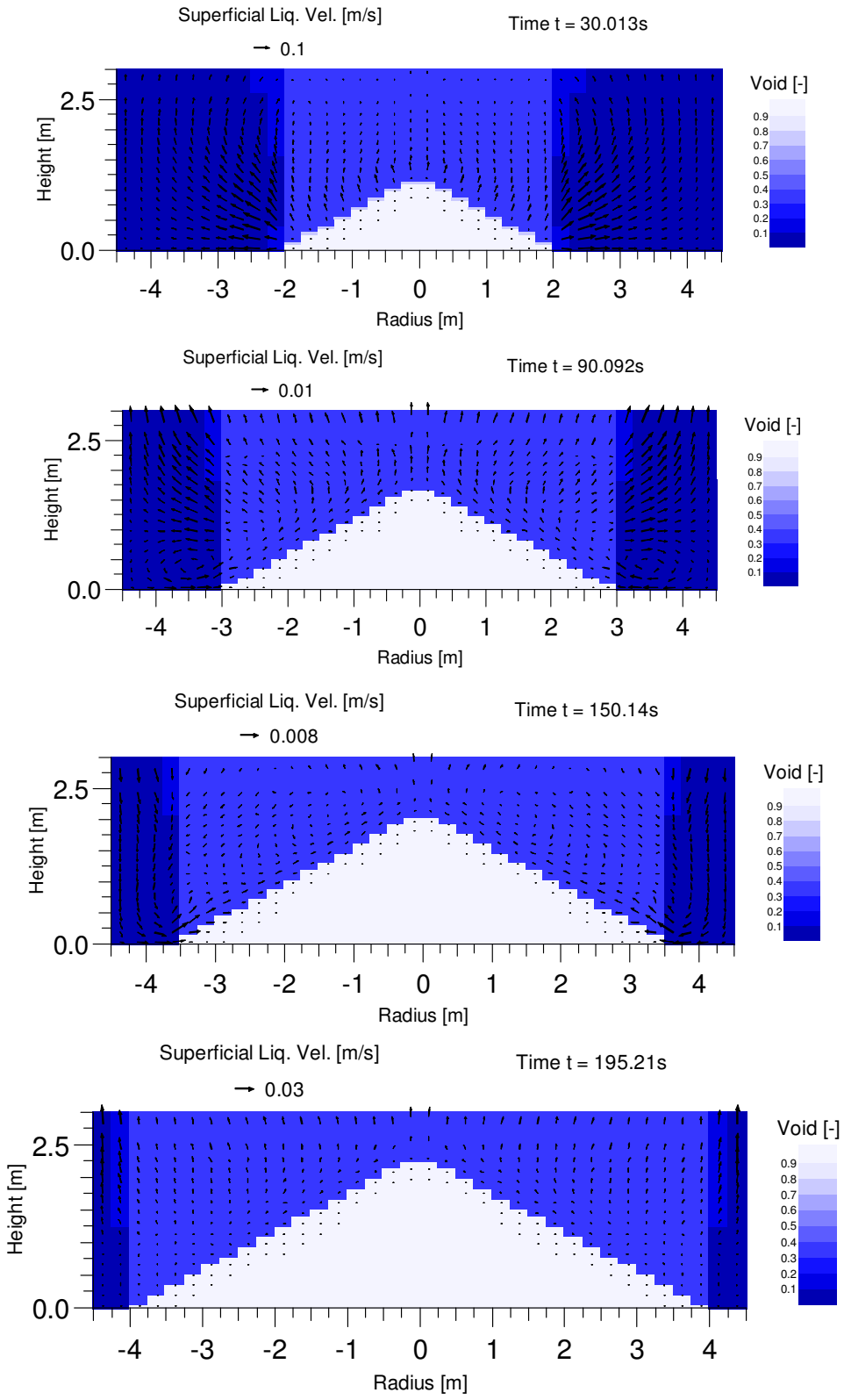

Figure 5.7: Development of void fraction (gas volume part inside the pore) and liquid velocity during the simultaneous processes of bed buildup and quenching process calculated by JEMI/MEWA.

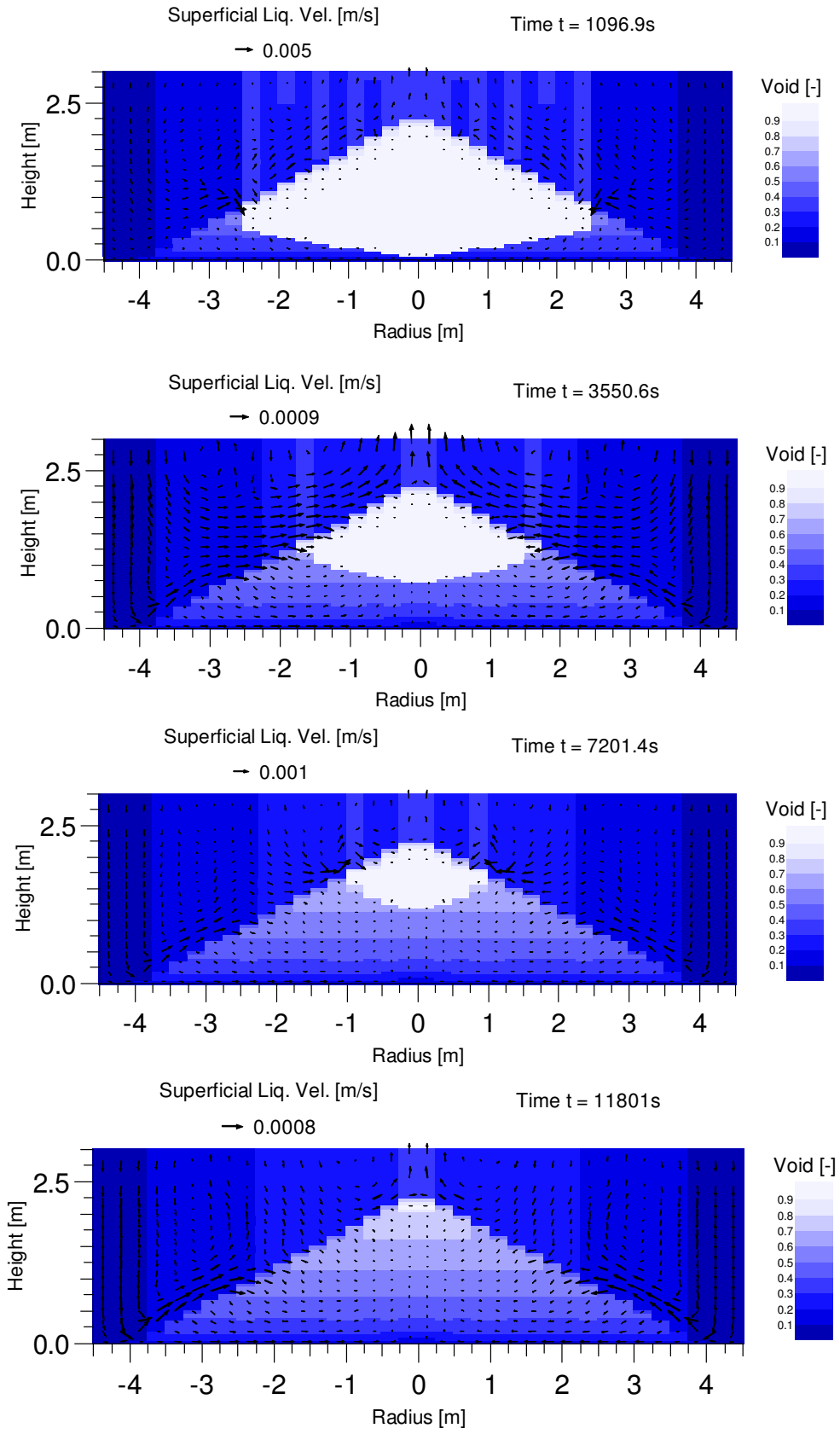

Figure 5.8: Development of void fraction (continuation from previous Figure 5.7) and liquid velocity during the simultaneous processes of bed buildup and quenching process calculated by JEMI/MEWA.

Thus, the quenching calculations performed in one case (section 5.1.1) with an already established debris bed at an estimated uniform temperature and in the other case with simultaneous quenching during bed formation. The results indicate substantial coolability margins in the latter case due to the more realistic modeling. Therefore, in order to get a realistic perspective on the quenching processes, i.e. on coolability in reactor scenarios, it is considered as necessary to apply a coupled treatment of bed formation and quenching as provided with the coupling of JEMI and MEWA. Without consideration of simultaneous quenching during bed formation, i.e. starting with an established debris bed which was usually done in earlier studies, the coolability is significantly underestimated. However, even in this approach, further consideration of possible stabilization of a melt pool, still to be performed with an adequate extension of MEWA for the melt pool model, may yield the conclusion of coolability. Thus, a strong trend to coolability can be concluded for the deep water case with limited (realistic) vessel hole and resulting jet diameter, in view of the large bed and small particles uniformly assumed (extreme case). A weaker point may be the conclusion of sufficiently solidified particles in the whole bed, excluding initial formation of agglomerated particles (“cakes”) or even molten regions. Further, different types of bed shapes and porosities as well as heterogeneous configurations are still to be investigated

5.1.3 Calculation with variations of bed geometry

Regarding bed geometry, experimental evidence is poor especially with corium (only few data from FARO experiments, Magallon [26]) and with inflow of large masses of corium in water. Thus, there remain significant uncertainties regarding the bed geometry. These uncertainties can be considered by variation of bed geometry. The purpose is to get an impression on the overall coolability of the debris bed in possible reactor scenarios.

From FARO (Magallon [26]) and DEFOR (Karbojian et al. [40]) experiments there are indications that at least for fully fragmented melt jet the debris bed formation process will be similar to what is generally known about the formation of heaps of granular materials. When bulk granular materials are poured onto a horizontal surface, usually a conical pile will form. The shape of the pile, higher or flatter i.e. more piled or more spread, depends on the internal angle between the surface of the pile and the horizontal surface which is known as the angle of repose. It is the maximum angle of a stable slope determined by the density, surface area and shapes of the particles, and the coefficient of friction of the material [94]. Material with a low angle of repose forms flatter piles than material with a high angle of repose.

Table 5.1: Typical angle of repose for granular materials.

Material	Angle of repose
Sand with rounded edges	27.5°-30°
Sand with sharp edges	32°-35°
Gravel with wide range of sizes	32°-37°
Salt	40°
Rubble, ore	40°

Here, it has been assumed that corium fragments behave like a typical granular material. Some typical values of angle of repose of granular materials are shown in Table 5.1.

Calculations have been performed with three different conical beds varying the angle of repose. A conical bed with angle of repose 30° is considered as basic configuration. Two variations, one with angle of repose 15° and another with angle of repose 40° have been considered in order to cover the plausible range. Here it should me mentioned that the small angle of repose, i.e. a flatter bed may be considered to be caused by spreading of particles on the large surface of the cavity floor by strong two phase convective flows.

Calculations have been performed with three different conical beds varying the angle of repose. A conical bed with angle of repose 30° is considered as basic configuration. Two variations, one with angle of repose 15° and another with angle of repose 40° have been considered in order to cover the plausible range. Here it should me mentioned that the small angle of repose, i.e. a flatter bed may be considered to be caused by spreading of particles on the large surface of the cavity floor by strong two phase convective flows.

For the configurations considered in this analysis it has always been assumed that the total corium mass of 190 t has been transferred into a particulate debris bed. For all cases, a porosity of 40 % has been assumed. Taking into account the constant corium mass, three different conical beds are obtained, as shown in Figure 5.9with the different shapes.

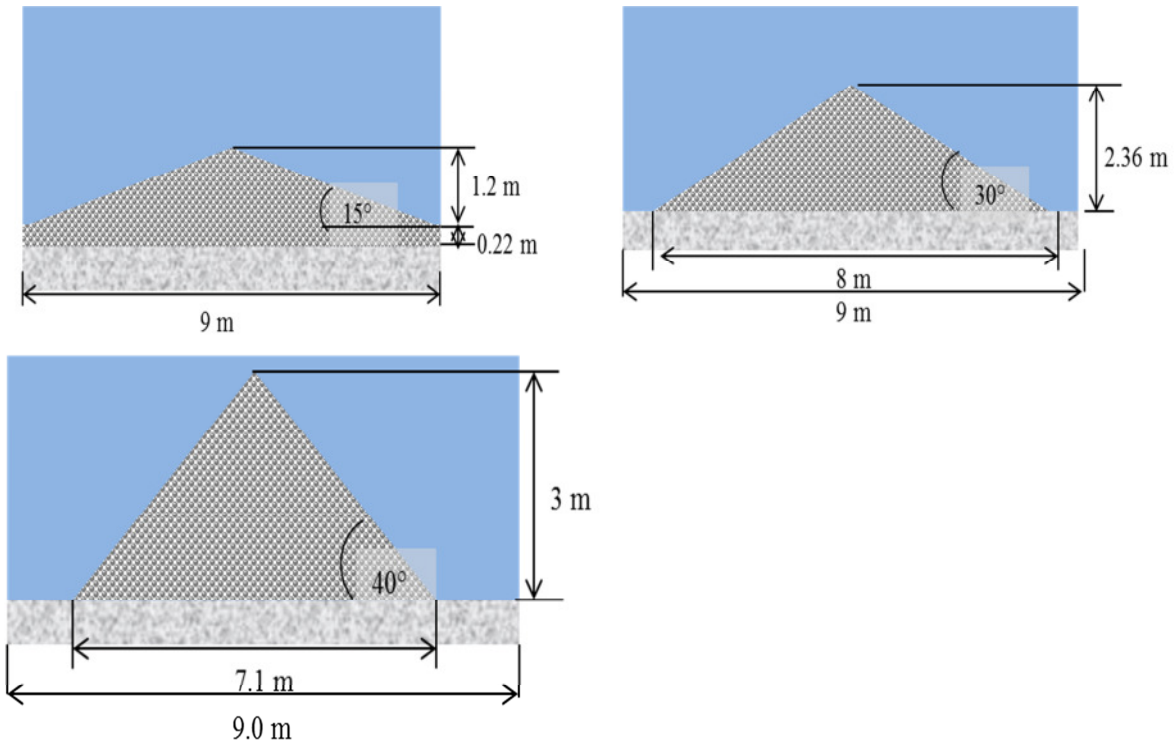

Figure 5.9: Sketch of debris bed shapes used in the calculations for the cases with angle of repose 15° (top left), 30 ° (top right) and 40° (bottom).

All calculations are performed considering simultaneous quenching during the buildup of the debris bed. For the particle size, the surface mean diameter is chosen. The results of the calculation for the basic configuration, i.e. debris bed with angle of repose 30° have already been presented previously (see Figure 5.5/Figure 5.6 and Figure 5.7/Figure 5.8) and therefore not repeated here. The results concerning the development of particle temperatures during the quenching process of the other two configurations are shown in Figure 5.10/Figure 5.11(bed with angle of repose 15°) and Figure 5.12/Figure 5.13 (bed with angle of repose 40°).

The results of the calculations show that complete quenching occurs for the configurations with angle of repose 15 and 30 °. Comparing the total quenching time, faster quenching is observed in the case of the debris bed with smaller angle of repose (see the complete quenching time in Figure 5.6 and Figure 5.11). This is due to the smaller height of the bed in the case of a smaller angle of repose.

Complete quenching is not achieved for the debris bed with high angle of repose (40°) since part of the bed reaches melting temperature as can be seen in the final picture of Figure 5.13. Although the largest fraction of the debris is quenched, the upper central part of the cone heats up further and finally reaches temperatures in excess of 2800 K after about 9271 s. The debris bed with the higher angle of repose forms a cone with taller height. Since quenching is limited from the top (downward inflow of water hindered by the upward steam flow) water has to fill from the bottom. Due to the higher bed in the upper central region, water has to travel a longer distance and thus encounter higher flow resistance there. As a result, quenching is much slower in the upper central region which remains dry for longer time. Due to decay heat this region heats up further and reaches melting temperature in this case. This molten part may be finally stabilized since the region is small. However, more assured results on the coolability of this molten part need further investigations. It has to be clarified whether this region is small enough so that the surrounding water flow is sufficient to stabilize this region by heat transport (super heat +decay heat) or insufficient cooling leads further heat-up and melting. Clarification of the above question is limited with the present modeling of MEWA since heat transfer from melt pools with internal natural circulation is not included.

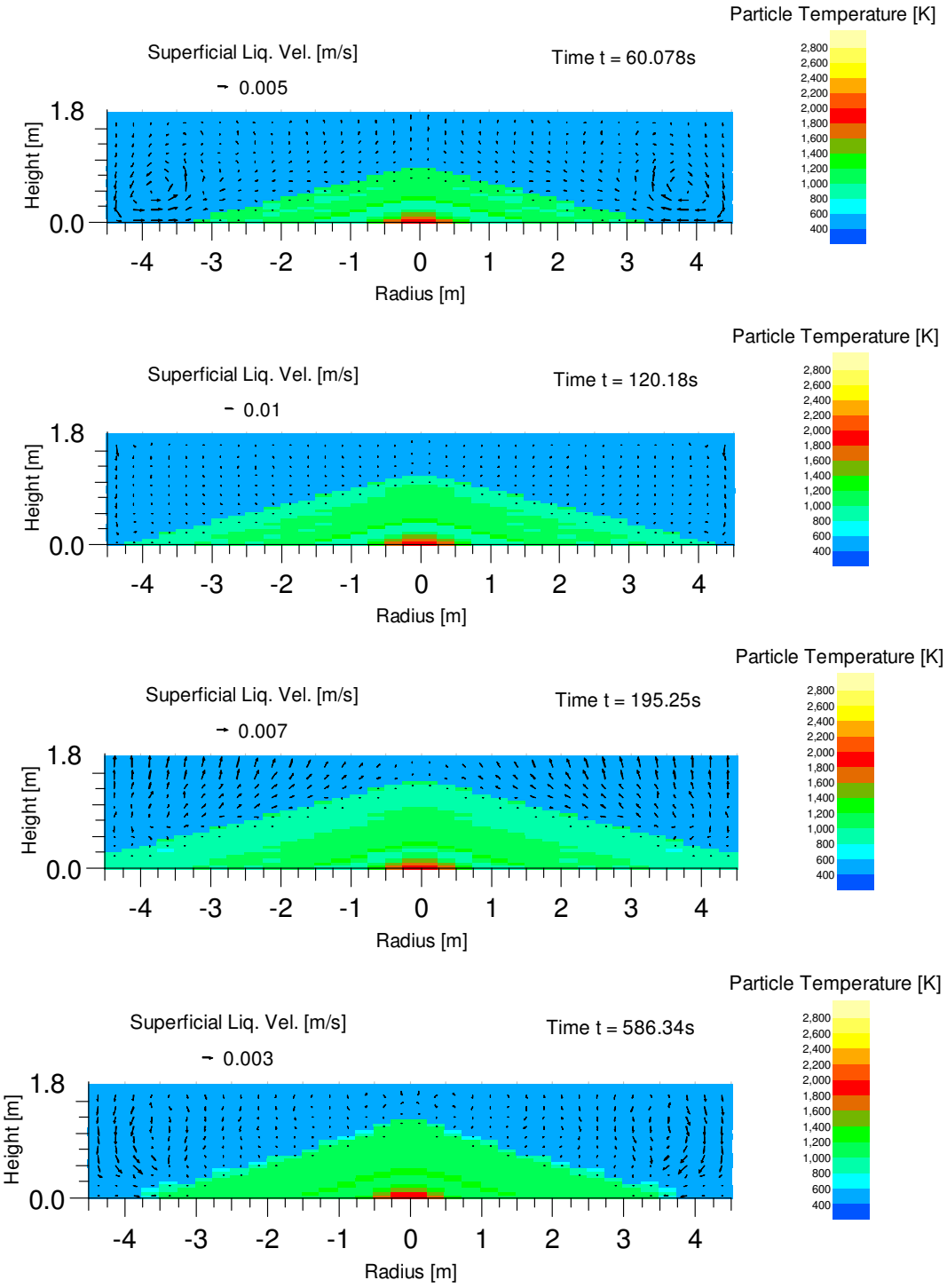

Figure 5.10: Development of particle temperature and liquid velocity during the settling and quenching process for the bed with angle of repose 15° calculated by JEMI/MEWA.

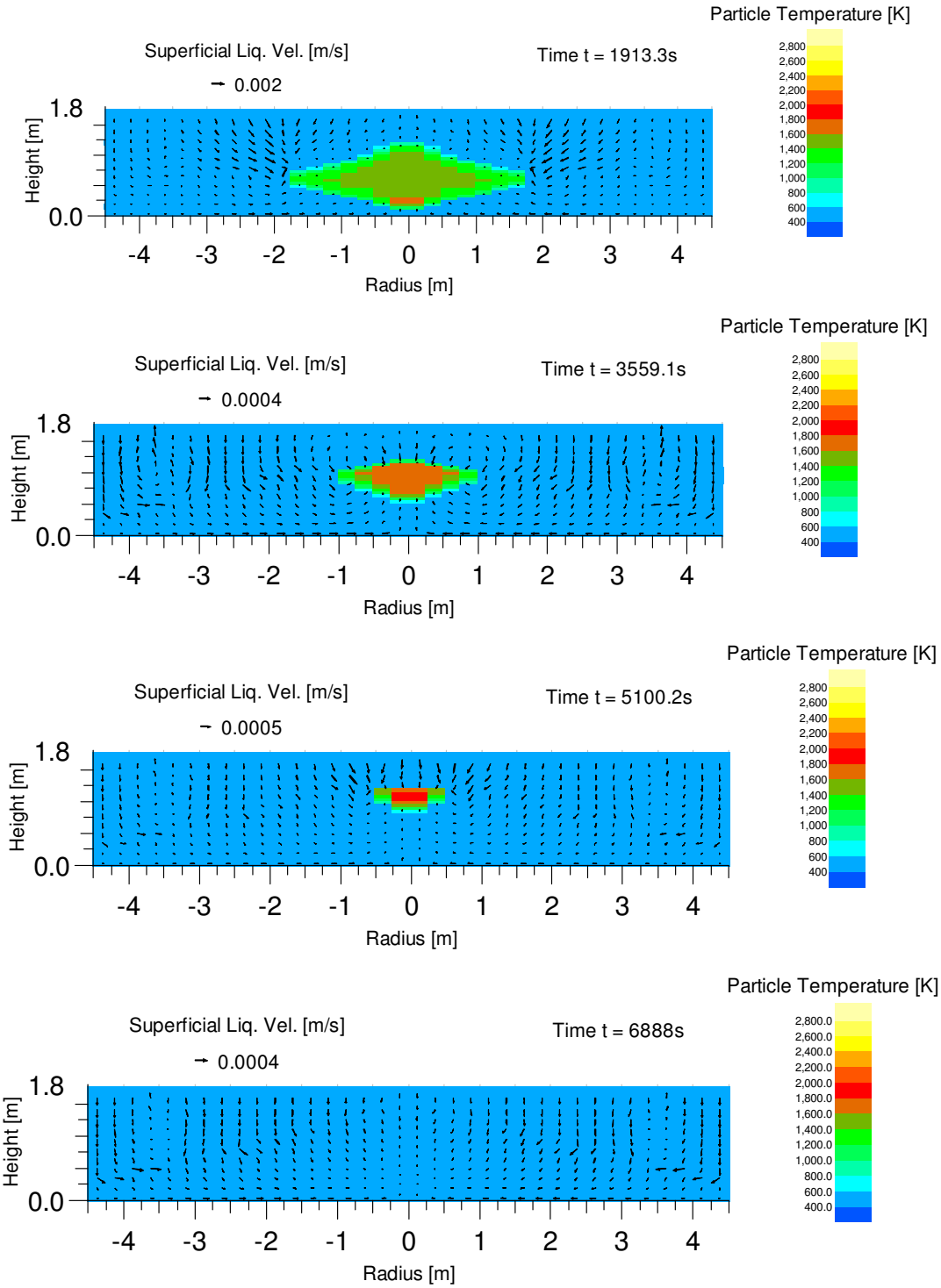

Figure 5.11: Development of particle temperature and liquid velocity (continuation from previous Figure 5.10) during the settling and quenching process for the bed with angle of repose 15° calculated by JEMI/MEWA.

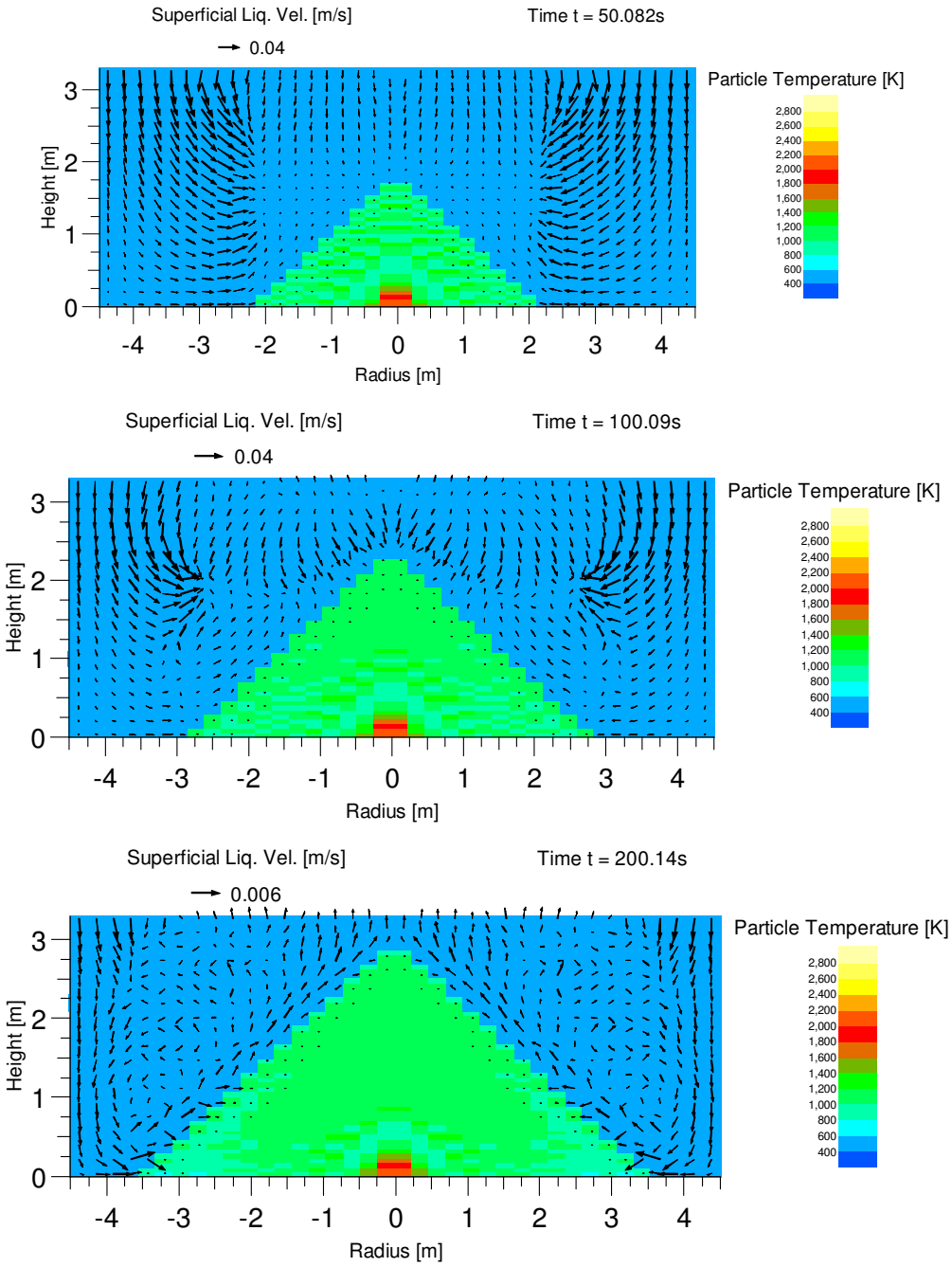

Figure 5.12: Development of particle temperature and liquid velocity during the settling and the quenching process for the bed with angle of repose 40° calculated by JEMI/MEWA.

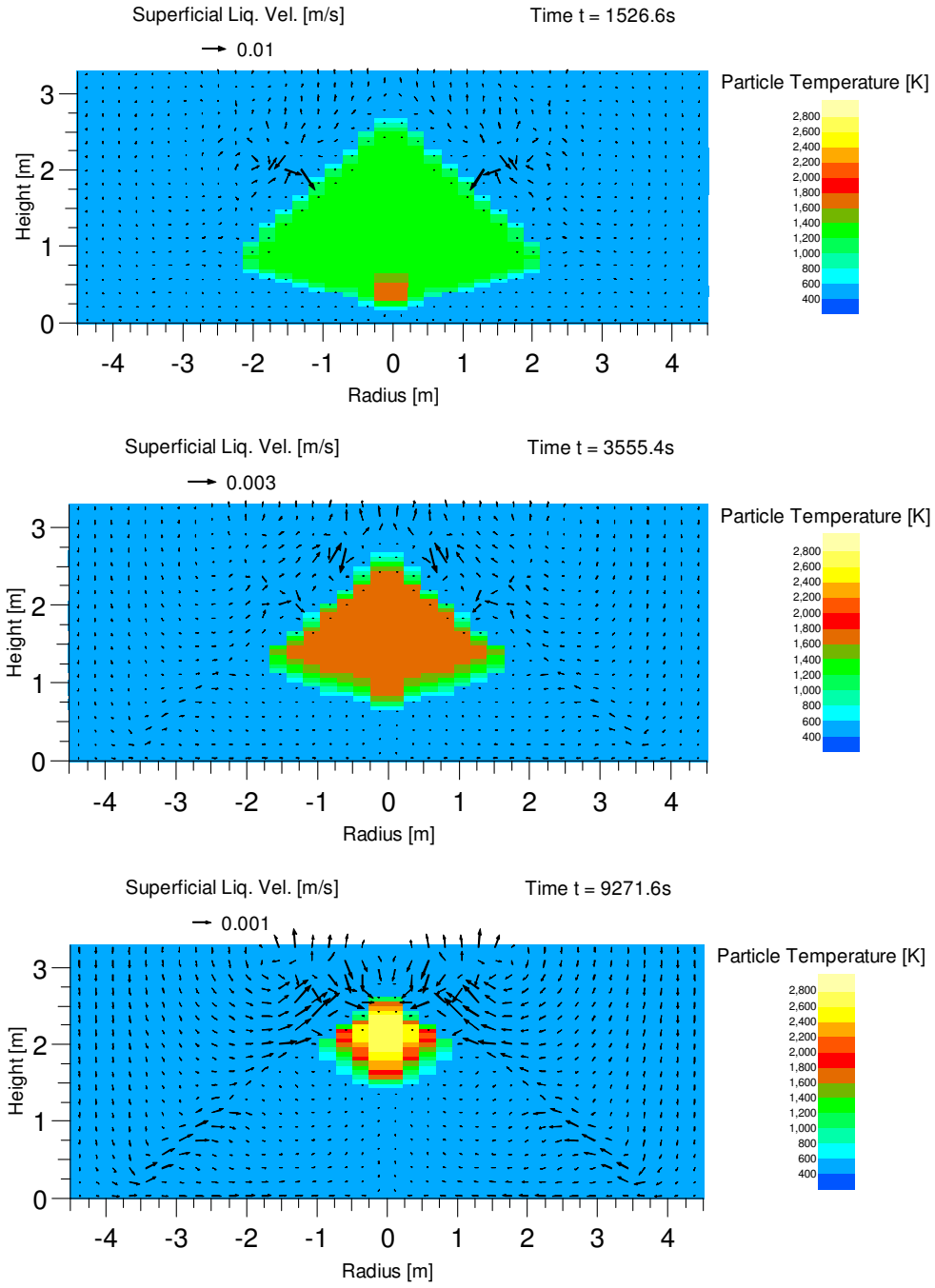

Figure 5.13: Development of particle temperature and liquid velocity (continuation from previous Figure 5.12) during the settling and the quenching process for the bed with angle of repose 40° calculated by JEMI/MEWA.

5.1.4 Calculation with variations of bed porosity

The porosity of the debris bed is highly influential parameter for determining the quenching of the debris bed. It must be selected according to experimental findings. Experiments with several particulate debris beds (e.g. debris bed at IKE, Rashid et al. [47] composed of poly-dispersed spheres, and with particles produced by jet break-up in PREMIX, Keiser et al. [41] or beds composed with FARO-like size distribution at VTT, Lindholm et al [48]) yielded measured porosities are in the range of~ 40%. However, particles have been intensively mixed in these experimental beds. In contrast, under postulated severe accident conditions the bed is formed in a settling process which does not favor mixing. In the DEFOR experiments of KTH (Karbojian et al. [40]) surprisingly high porosities (50 to 60%) resulted which also indicates the effect of settling versus mixing of particles. Thus, there exist uncertainties about the prototypic conditions. Therefore, porosities of the bed are to be varied in a reasonable range for reactor applications. Three different variations of porosities are considered, here. The bed with 40% porosity is considered as reference configuration. Two variations one with 30% porosity and another with 50% porosity have been chosen in order to cover the plausible range.

For all these bed configurations conical beds with angle of repose 30 ° are considered. With the fixed corium mass of 190 ton three different shapes of beds are obtained, as shown in Figure 5.14.

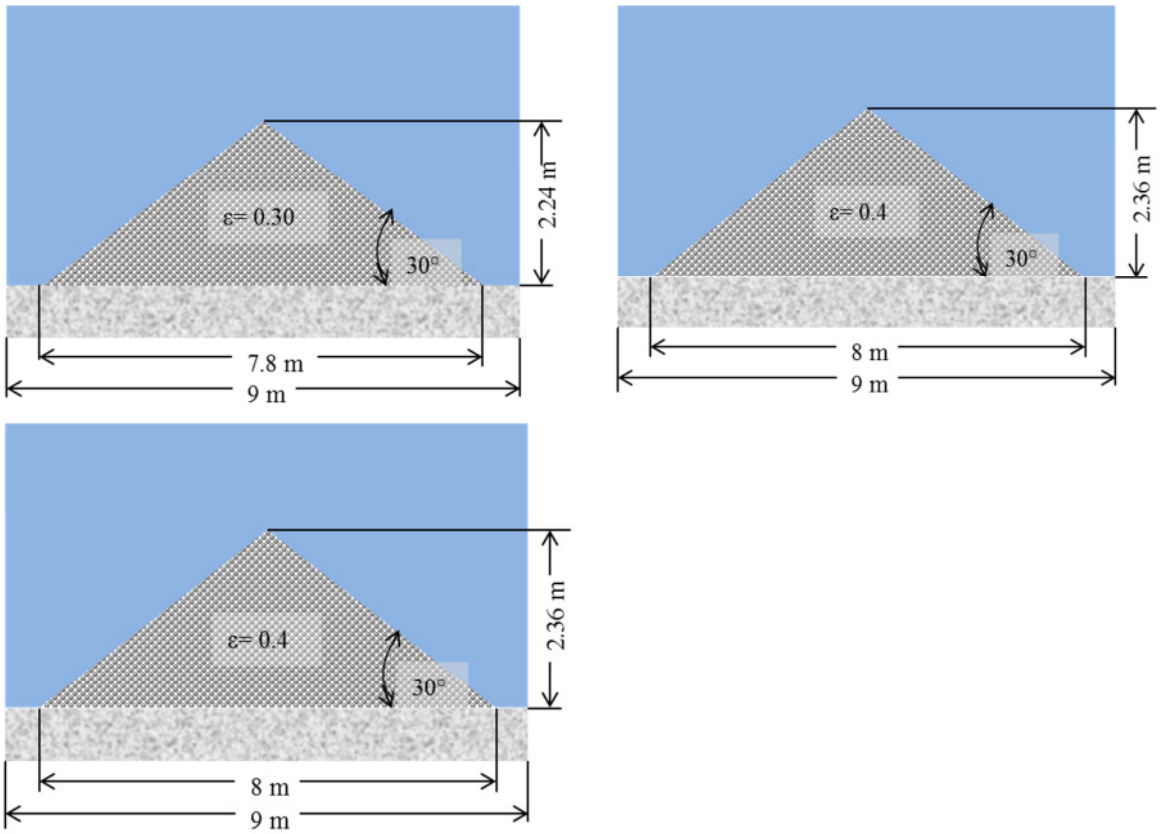

Figure 5.14: Sketch of debris bed geometry and dimensions used in the calculations for the cases with porosity 0.3 (top left), 0.4 (top right) and 0.5 (bottom).

The results of the calculations show that complete quenching occurs for the beds with 40 and 50% porosities (see Figure 5.6 for 40% porosity and Figure 5.15 for 50% porosity). Comparing the total quenching time, faster quenching is observed in the case of the debris bed with larger bed porosity. This can be expected because fluids flow through the bed with larger porosity, i.e. bed with more permeability, encounters less flow resistance. As a result, easier water penetration is obtained for the bed with higher porosity. In the case of 50% porosity, water penetration into the debris bed even starts before the end of the settling process which was not observed for the bed with 40% porosity (see particle temperature map up to 195 s in Figure 5.5 and Figure 5.15).

In case of 30% porosity, the center and upper part of the debris bed remain un-coolable (see Figure 5.16). Water penetration and quenching is significantly slower in this case due to the lower bed permeability. Steam cooling is then also not sufficiently effective in this case.

Thus, calculations have been performed for different bed configurations by varying porosities and the angle of repose of the bed. Average particle sizes obtained from the jet fragmentation process are relatively small. Even with these small particles in the size range of 1.8 mm and a high heap of 2.4 m, complete quenching is obtained for a large debris bed of 190 tons with 40% porosity. A limit of coolability is reached in the case of a bed with very low porosity (30%) or with a rather high heap (angle of repose more than 40 °). However, a very low porosity over the whole bed region or piles of beds in a limited area yielding very high heaps are not realistic. Therefore, it can be concluded that there are good chance for coolability. Faster quenching i.e. better coolability is obtained for the bed with flat-shaped geometry due to its lower bed height and higher heat removal area and with larger porosity due to its higher permeability.

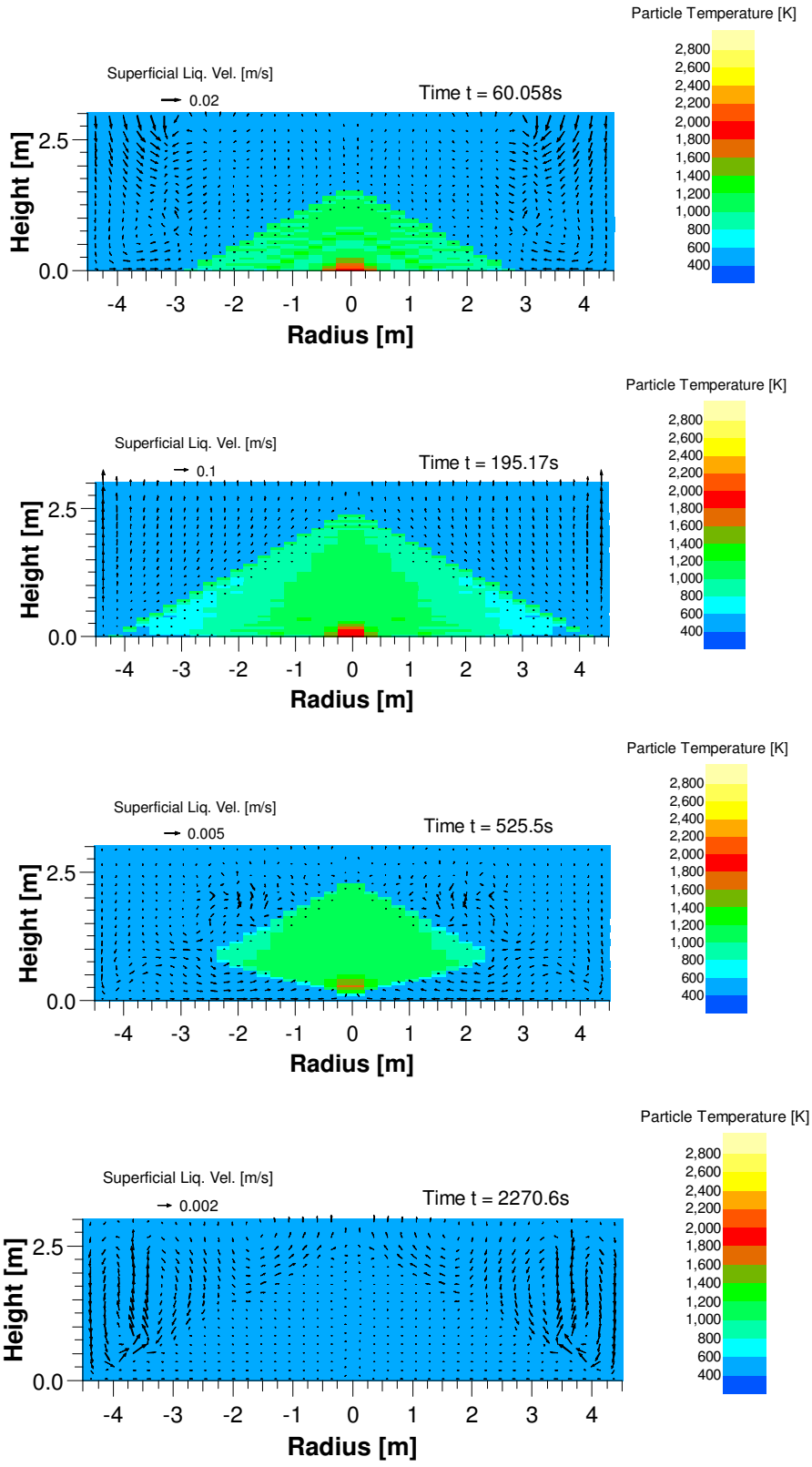

Figure 5.15: Development of particle temperature and liquid velocity during the settling and the quenching process for the bed with 50% porosity calculated by JEMI/MEWA.

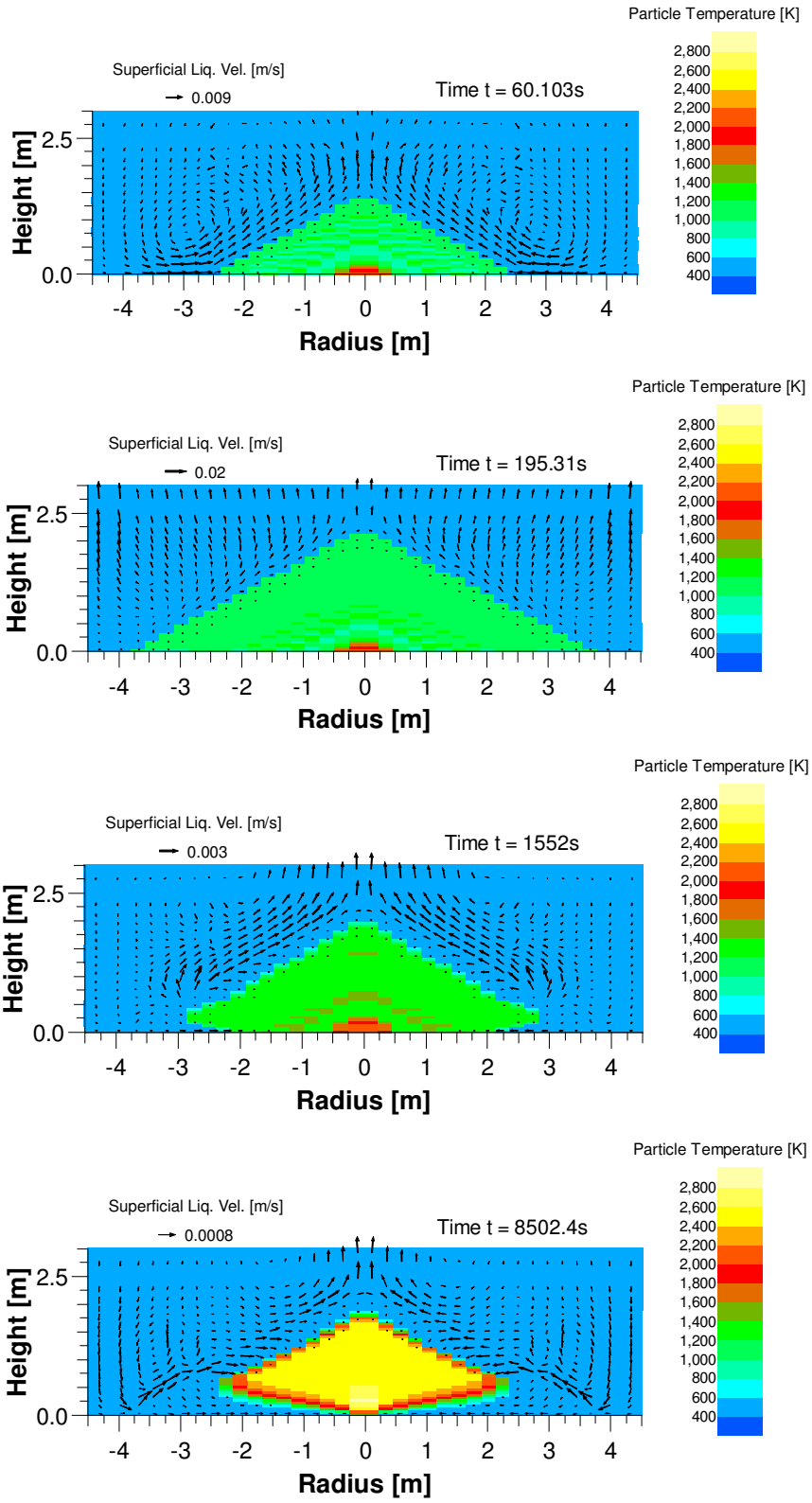

Figure 5.16: Development of particle temperature and liquid velocity during the settling and the quenching process for the bed with 30% porosity calculated by JEMI/MEWA.

5.2 Coolability of combined liquid melt and particulate debris formed due to incomplete breakup of melt with thick melt jet

The previous analysis addressed the case with complete breakup of melt obtained when flowing out from the vessel and interacting with water. However, complete breakup of melt and coolability as a particulate debris bed cannot be achieved for all possible scenarios, even not in the deep water pool concept. With larger vessel breach sizes, significant parts of melt may not be solidified sufficiently when arriving at the cavity floor. E.g. JEMI calculations show that with D_{jet} = 30 cm (all other parameters as system pressure p, water pool height H_{pool} etc. the same as in the previous case) the developing coherent jet length $L_{coherent}$ is longer than the height of the water pool of 7 m (see Figure 5.17). As a result, about 40% of the melt (from a mass inflow of ~2270 kg/s, a mass flow of ~880 kg/s) reaches the bottom without fragmentation according to the JEMI calculations. This non-fragmented part may spread on the cavity floor and form a compact layer of corium. The major question is then whether such a configuration is also coolable with the present severe accident measure (SAM). This issue is also important in the case of existing older pressurized water reactors. In these reactors, breakup of melt jet from vessel failure would be reduced strongly and would be incomplete due to shallow water pools (H_{pool} < 2 m) in the cavity.

The resulting structure form this incomplete breakup process must be highly heterogeneous, composed of fragmented and partly solidified parts and still molten material at high temperature. Liquid parts directly reach the bottom due to incomplete jet breakup and form a liquid layer there which starts to interact with the concrete basement. Solidified particles from the breakup fall into the melt layer may exist there as solid parts for some time, or gather on a crust forming at the top of the melt layer. Coherent jet parts will continue to enter such a structure from above and together with re-melting parts in the bed.

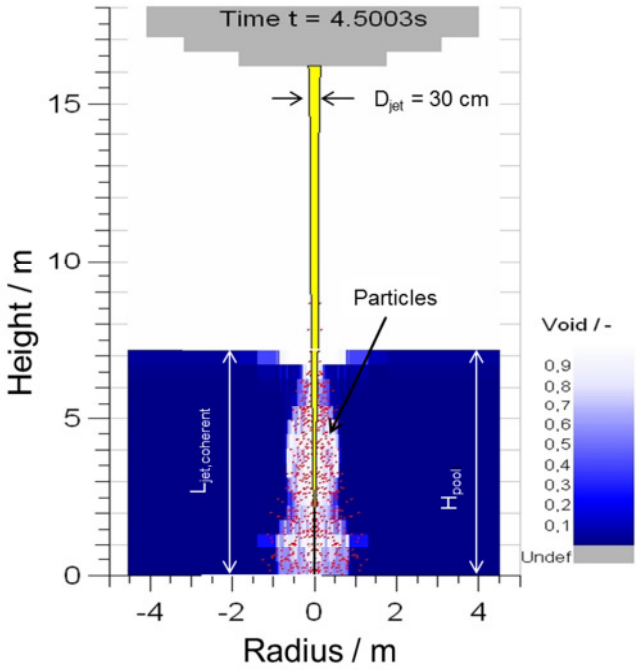

Figure 5.17: Development of void fraction (color shade), coherent jet and particle cloud calculated by JEMI model [81] with D_{jet} = 30 cm.

The coolability of such configurations appears to be limited. Molten layers may be coolable (against decay heat) by water at top if they are thin enough. The low heat conductivity of corium will strongly limit this for a completely solidified state (i.e. without internal convection). Thus additional measures of bottom injection of water, as already indicated in chapter 1.3, are to be envisaged and have to be evaluated with respect to checking coolability option.

In order to get a perspective on coolability on such a complex configuration, a strongly idealized model configuration is considered by partitioning between solidified particulate debris and still liquid melt arriving at the bottom of the cavity. Major questions of coolability of complex real configurations may be analyzed with this model sketched as shown in Figure 5.18.

In this configuration, it is assumed that the fragmented and solidified part forms a particulate debris bed. For the shape of this debris bed, the basic configuration given in Figure 5.3, i.e. an angle of repose 30° and porosity 0.4 was assumed. The non-fragmented part has reached the floor as liquid melt which spreads uniformly on the available cavity area. Thus, there are some regions where liquid melt layer up to a certain height exists in the lower part of the bed which fills the free space in the particulate bed. Taking into account the available cavity spreading area (D_{cavity} = 9 m) and free space inside the debris bed (ε = 0.4), compact melt layers height H_{melt} = 26 cm is obtained from the division of liquid and solid parts calculated with JEMI. This gives the geometrical dimensions shown in Figure 5.18.

Since the quenching of the melt layer is crucial here and decisive for determining the coolability of such configurations, the problem is further simplified by separating the molten part from the debris bed. Now, depending on the thickness of the melt as well as cooling conditions at the top and bottom of the layer, this may be coolable and solidified as a layer, or the melt remains liquid and the corium/concrete interaction will lead to erosion of the cavity floor. As a first possibility, coolability of such melt layer only by heat conduction, i.e. assuming already a solidified state can be checked. This yields maximum thickness for which this is possible.

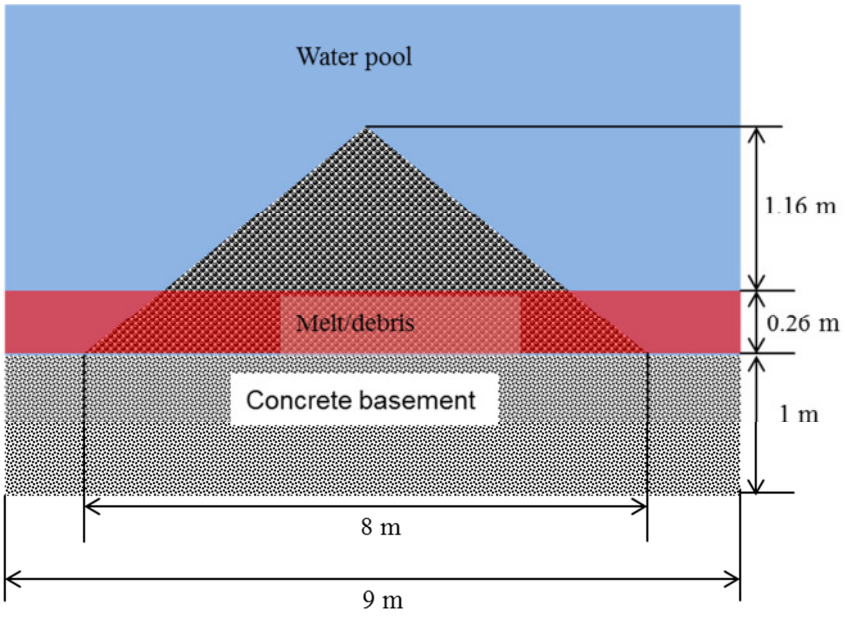

Figure 5.18: Sketch of idealized model configuration to consider coolability for the case with 40% of non-fragmented liquid melt.

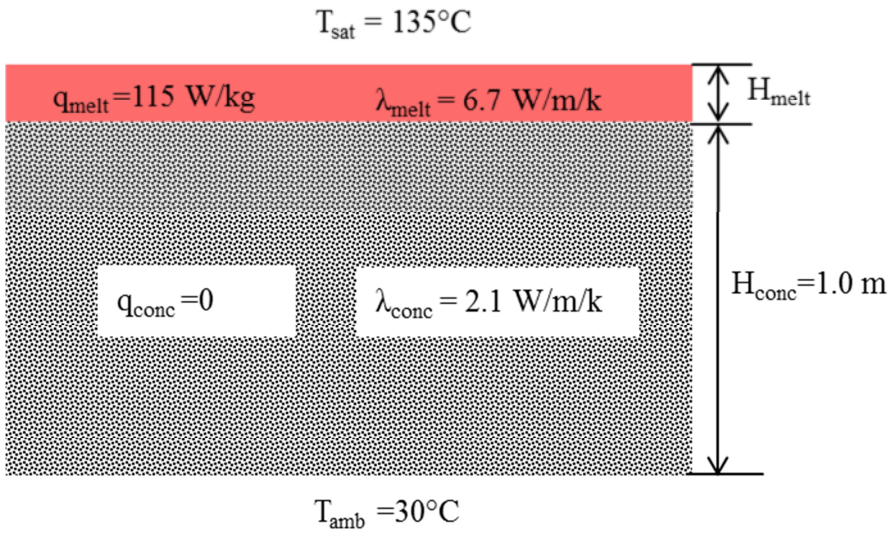

Figure 5.19: Sketch of configuration of melt and concrete layers and properties used in the calculations on coolability of melt layers by heat conduction.

5.2.1 Coolability of melt layer by heat conduction

In order to indicate the limits of coolability given by conductivity alone, two cases have been considered here: Firstly, a case with the melt layer height H_{melt} =10 cm and, secondly, a case with H_{melt} = 20 cm (see Figure 5.19 and Figure 5.20). As in the previous analysis, a decay heat q_{melt} = 115 W/kg is considered. Steady-state conditions are considered, using as boundary conditions saturation temperature of water (T_{sat}) at the top of the compact layer (135°C at 3 bar system pressure) and ambient temperature T_{amb} =30°C at the lower end of the concrete floor. At the bottom a concrete height H_{conc}=1 m is assumed (Figure 5.19). With heat conduction (convection of liquid melt is not considered in this approach), the steady-state temperature profile (T) can be readily calculated.

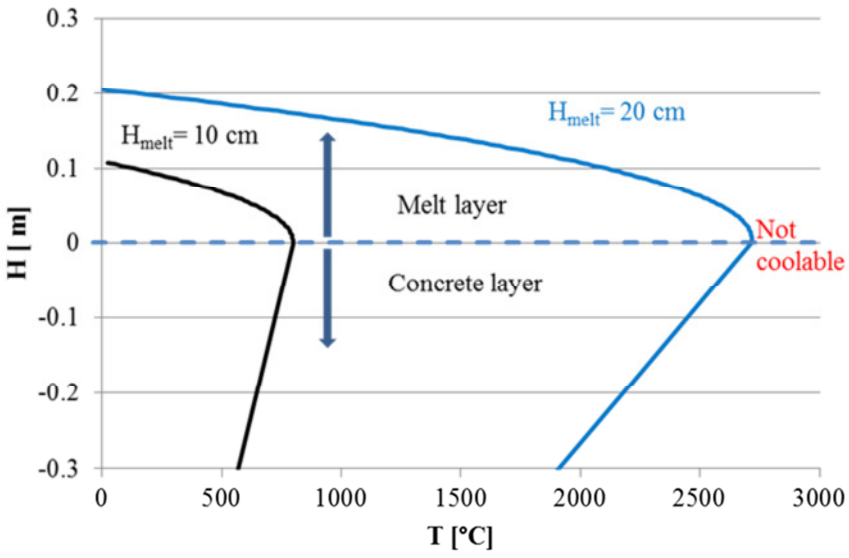

Figure 5.20: Steady-state temperature profile in the melt layer and concrete for the case with H_{melt} =10 cm and H_{melt} = 20 cm thickness.

Figure 5.20 shows the calculated steady-state temperature profile T in the compact melt layer of H_{melt} =10 cm and H_{melt} = 20 cm. For H_{melt} =10 cm , the maximum temperature reaches about 800°C and is obtained very close to the interface to the concrete floor. It remains below the melting or decomposition temperature of the concrete (~1200 °C); also the layer will be solid. This means the layer is coolable if it is thin.

For H_{melt} = 20 cm case, the maximum temperature would be in excess of 2700°C. This is well beyond the melting temperature of concrete (~1200 °C); also the layer would remain liquid. Thus, the layer configuration is not coolable and would yield melt concrete interaction and basement ablation if the liquid parts not surely enclosed by crust, in the EPR concept supported by a cooling circuit close to the concrete surface (see Fischer et al. [31]).

Since only thin layers are coolable at the solidified state, other options are to be envisaged. One option is to consider porosity formation in liquid layer. Studies with top flooding of melt in this respect have been performed in several experiments (Lomperski et al. [95], Sehgal et al. [96]). But effective mechanisms to provide sufficient porosities inside the melt layer by top flooding have not been identified yet. As a possible mechanism, development of ruptures in forming crusts at top has been considered. However, neither by experiments nor by the model it could be shown that such a mechanism of porosity formation based on water ingression into the ruptures, subsequent promoted solidification, again with ruptures, etc. is sufficient to proceed to extended regions into the melt layer.

Therefore, additional measures and improvements of the melt retention concept would be required in this situation to achieve a stable and coolable state. A possible improvement could be injection of water from below via the cavity floor (COMET type concept [11]) as described below.

5.2.2 Improvement of coolability of melt layer/debris configurations by injection of water from below

Injection of water from below is considered as an effective measure to cool and quench the melt. An easy way to provide bottom injection is by bringing the coolant water from the water reservoir at higher level to a bottom region via external downcomer pipe as shown in Figure 5.21. In this measure the melt layer is passively flooded from bottom through multiple flow channels which yields rapid breakup of the compact corium and porosity formation and thus coolability (Alsmeyer and Tromm [12]).

This concept i.e. injection of water from below is originally based on a dry cavity, i.e. without flooding of the cavity with water prior to melt release from the RPV. In principle, bottom injection of water from below can be combined with the wet cavity concept, in order to bring together advantages of both approaches. Bottom injection of water may work as a backup measure for the present deep water concept in case liquid melt arrives at the bottom of the cavity due to insufficient breakup or (partial) melting of the particulate debris. In this case the bottom injection may provide porosity formation in the resulting liquid layer and fast quenching. This is investigated with the calculations presented in this section.

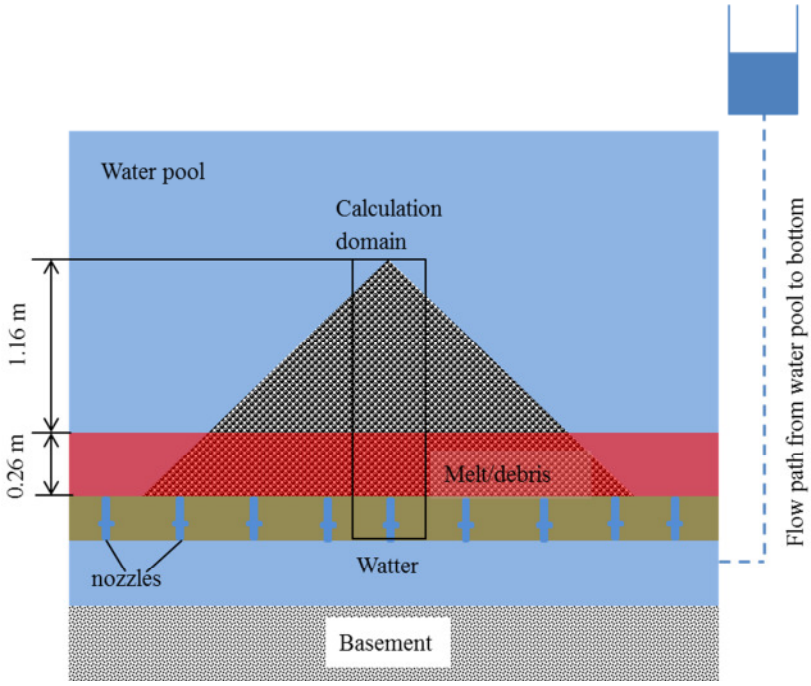

Figure 5.21: Sketch for improvement of the SAM strategy by water injection into melt layer from bottom.

To simulate the processes occurring during bottom injection of water into a melt layer, a special model, MEWA-COMET is also included in the MEWA code (see details of the model and its validation in Appendix A). In this model, especially porosity formation inside the melt and subsequent quenching of the melt are addressed. In this model it is assumed that porosity inside the melt is created due to local pressure buildup with resulting expansion. This is primarily caused by strong evaporation resulting from water injection from the bottom and restriction of the up-flowing steam due to friction (see Appendix A).

For the present investigation, the configuration from the previous analysis with 26 cm thick melt layer has been chosen as a basis (see Figure 5.21). In this case, coolability could not be achieved with top flooding of water (since melt layer thickness higher than 20 cm). Calculations with MEWA-COMET have now been performed with injection of water from below in order to check whether sufficient porosities for effective cooling can be produced in molten parts. In order to evaluate the coolability of remaining molten parts, the region where liquid melts exits inside the debris bed is considered. The height of the liquid layer inside the debris bed is 0.26 m and the debris bed has a total height of 1.42 m (considering the maximum height of debris bed, see calculation domain in Figure 5.21).

It has been assumed that water is injected through nozzles in the cavity floor which are spaced regularly at a distance of 16 cm. A cylindrical approach around an inlet nozzle is chosen in the calculation. A region with a radius of half the nozzle distance is considered as calculation domain area. This area has to be cooled by the water flow through the respective inlet nozzle. The injection overpressure at bottom (i.e. above system pressure + hydrostatic head of the melt) is chosen to 0.15 bar which corresponds the absolute pressure in the inflow region (p_{bottom}) is about 3.5 bars.

It has also been assumed that the debris bed does not change its geometry during the injection. Thus, porosity formation inside the part with melt is only possible up to the porosity of the initial debris (40 %). If porosity (or void) is created inside the liquid layer, the melt level will swell and move upwards inside the debris bed.

Results of the MEWA-COMET calculations concerning porosity production and temperature development are shown in Figure 5.22 and Figure 5.23. Figure 5.22 shows subsequent phases with increasing porosity starting from the inlets. The porosities increase laterally and grow upwards. When porosities are formed, the melt level moves upwards and fills the free space inside the debris bed as can be seen from the porosities distribution field in successive phases of Figure 5.22 (partial decreases of porosity in upper layers by this). From different calculated states it can be seen that the water flow precedes both axially and radially. In the lower region, porosities are formed under the influence of inflowing water and evaporation. In the upper region, porosity is formed in the steam flow. The latter is due to local pressure buildup in the strong steam flow (resulting from strong evaporation in lower regions) which is restricted in removal velocity by friction.

The final result concerning the porosities can be seen in the last picture of Figure 5.22 giving the status at 778 s. Since at that time the temperature in practically the whole layer is below the solidus temperature of 2300 K (see the temperature field in Figure 5.23) no further change of porosities can occur. Thus, the final porosities lie mostly between 0.15 and 0.30. Due to these open porosities inside the melt, quenching is sufficiently rapid and complete. Complete quenching occurs in this case after about 1834 seconds (see the final picture of Figure 5.23).

Thus, the present analyses with MEWA-COMET indicate that combining bottom injection with the wet cavity concept has the potential to improve the core melt cooling and retention capabilities significantly. In cases with melt layers penetrating a debris bed of up to 26 cm height (and most likely also higher), the MEWA calculations indicate sufficient porosity formation and cooling. However, these results require further confirmation, since the present model may not sufficiently take into account effects acting against the porosity formation like plugging of porosity due to melt freezing in contact with cold particles.

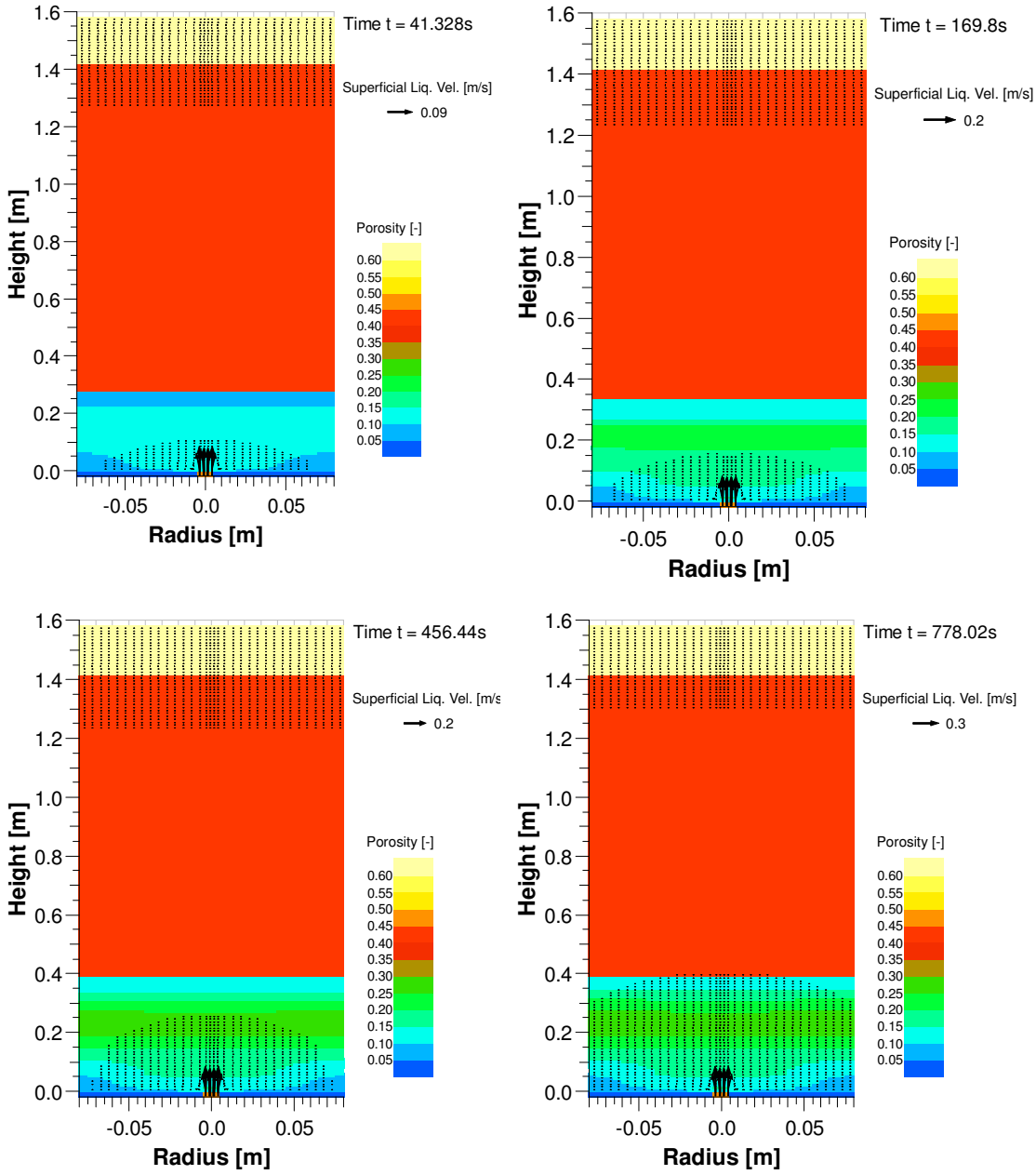

Figure 5.22: Development of porosity and liquid velocity inside the melt calculated by MEWA-COMET.

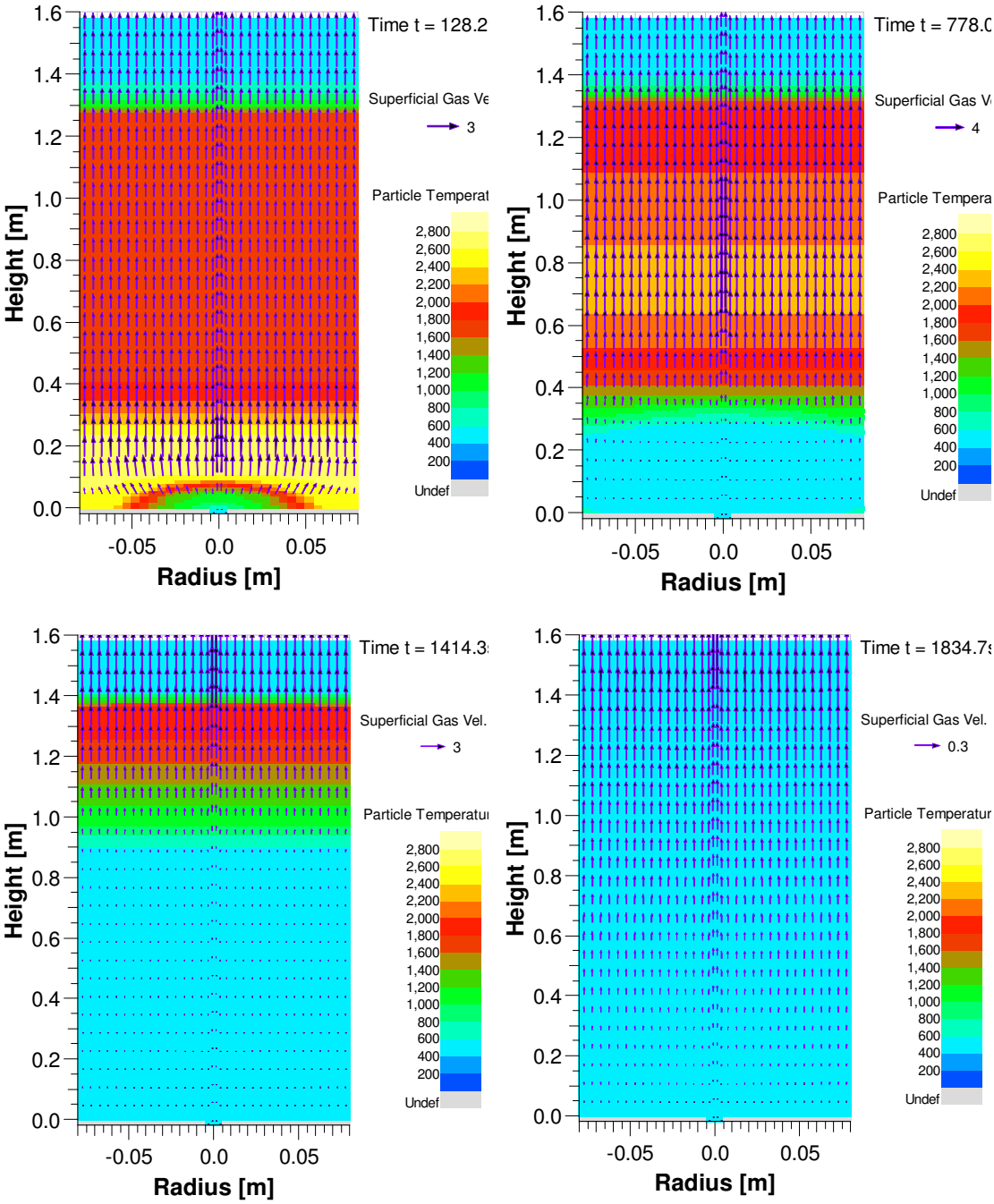

Figure 5.23: Development of particle temperature and gas velocity inside the melt calculated by MEWA-COMET.

6 Summary and Conclusions

The major aim of this thesis was to investigate the options and chances of coolability in key phases of a severe accident with core melting and debris formation. The debris bed formed in different stages of an accident will be hot and dry. In order to establish a steady state of long-term coolability, the hot debris (above saturation temperature) needs to be quenched (cooled to saturation temperature by removing super heat) at first. If quenching by water ingression inside the dry bed is not rapid enough then heat-up (rise in temperature) by decay heat in still dry regions may again yield melting. Thus, chances towards coolability by quenching against heat-up due to decay heat had to be investigated in the context of reactor safety research.

As a basis of the present investigations, models for simulation of two phase flow through porous media were already available in the MEWA code (Buck et al. [69]), being under development at IKE. The objective was to apply the code in essential phases of severe accidents and try to draw conclusions about chances, options and measures of coolability. Thus, the task was both to check the applicability of the MEWA code as a tool to analyze coolability in general and to assess its adequacy for drawing conclusion in such important safety issue. Further, within these tasks, improvement to remove weaknesses in modeling and extension concerning missing parts was also considered. One emphasis with this respect was to qualify the friction and heat transfer models which are considered as decisive for determining the cooling conditions inside the debris bed.

It was identified previously (Schmidt [76], Bürger et al. [77]) that classical models without considering the interfacial friction explicitly, like the model of Reed [74], can predict DHF (Dryout Heat Flux) well under top fed condition but then fail to predict (under-predict) DHF values under bottom flooding conditions driven by a lateral water column. This is because, given an important influence of interfacial friction, counter and co-current flow yield contrary effects which cannot be met by a single adaptation of laws not explicitly including interfacial friction. Tung & Dhir [80] introduced an interfacial friction term in their model, but this model has deficits for smaller particles considered as relevant for reactor conditions (~ 1-6 mm). Schmidt [76] had introduced modifications of the flow pattern transitions depending on particle diameter, as a more rapid transition towards slug and annular flows with smaller particle diameters, physically plausible because of the thinner flow channels. As a further modification, presently gas-particle and liquid-particle drags are also modified here in order to remove the remaining deficits. These modifications concern corrections of relative permeabilities and passabilities which are overestimated in the original law. Moreover, a reduction factor for the interfacial friction term depending on particle size has been introduced to meet the top flooding DHF. In the original law it was too strong.

A significant improvement with the new friction description MTD (Modified Tung & Dhir, MTD) was obtained considering the aim of a unified description for both top and bottom flooding. Good agreement with the experimental DHF results was achieved with the MTD description while the other models fail to reproduce the experimental results either for top or bottom flooding conditions. Further, the MTD model was validated over a broad band width of

conditions with different debris configurations ranging from beds with uniform particle diameters to beds with irregularly shaped particles. From the results, it can be concluded that the key phenomena of the dryout behavior are accurately captured by the model. Major experimental trends concerning the flooding mode, effect of particle size, system pressure and 2D effects are always well reproduced. These extensions and the related validation give also a good basis for the application in quenching analyses.

Validation calculations for quenching of superheated, initially dry debris beds were performed with respect to different experiments, addressing various aspects of quenching: different flooding conditions, non-uniform particles, effect of initial temperature and bed stratification, etc. Results showed that qualitative trends e.g. top versus bottom quench front progression are generally well reproduced. It was shown that quenching from the bottom is more effective than by top-flooding, due to co-current flow of water and steam. In cases with quenching from the top, non-homogeneities (especially lateral differences in permeability) or downcomers favor local penetrations of water to the bottom, with subsequent quenching of the remaining bed from below, which provides an effective mechanism for faster cooling.

In general, it was found that, except in cases with large forced bottom injection, water moves into the debris bed in a slowly propagating front due to high friction, and the quenching is rapid enough to occur in a thin front (few mm). Thus, a detailed modeling of thin heat transfer regimes is less important, rather an appropriate description for the friction is essential. Even in cases with high inflow velocities of water, which yielded extended quenching zones, still satisfactory agreement was obtained. But it should be mentioned here that due to lack of experimental data, the validation is limited to smaller temperatures in the experiments (below 1000 K) than to be expected for reactor conditions (1500 K and more).

In the reactor applications in the present work, quenching of hot and degraded core or trends towards melt pool formation were performed under variation of conditions. Calculations were performed for a strongly degraded core considered as a debris bed. A coolant mass flow of 60 kg/s via the downcomer was considered. The results showed that even at a lower system pressure of 10 bar (compared to 100 bar of TMI-2 accident, Müller [92]) quenching can be obtained for a large debris bed of 100 tons with a small particle size of 2 mm, porosity 0.4 and initial heat-up to 1500 K, uniformly assumed. Effective quenching and thus strong trends towards coolability are supported by multidimensional effects: water is flooded via the downcomer and rises in lateral, intact core regions and then penetrates into the core and debris bed driven by the lateral water column produced in the intact core and bypass regions. Small characteristic particle diameters (low permeability of debris) impede cooling, but very small particles (e.g. 1 mm) have to be assumed to have progressing melting under re-flooding. However, extended debris regions with such small particles appear not to be realistic. Therefore, good chances of cooling even of a strongly degraded hot core can be concluded.

The calculations on quenching of hot debris in the lower head also show a high cooling potential, although with limited mass, i.e. not for the whole core. Coolability is not as effective as in the core case since smaller amount (40 tons) of particulate debris (compared to core debris of 100 tons) have to be assumed to reach coolability. This is due to the different bed

configurations which delayed the establishment of bottom quenching and subsequent steam cooling in the lower head as compared to the core, where it starts immediately. Nevertheless, the lower head still has significant cooling potential for conditions of limited melt release. Other parts of the melt which remain in the core may be cooled there, if water supply can be re-established in time (also happened in TMI-2 accident, Reinke et al. [19]). As shown by the calculations, even at low system pressure of 6 bars, quenching of 40 t of 1273 K debris with 2 mm diameter particles and 40% porosity is obtained in the lower head. Compared to the relocated molten mass of ~20 t in the TMI-2 accident (Sehgal [9]), the amount of coolable debris mass is still significant.

Quenching is supported by a higher system pressure. While partly melting was obtained for a homogeneous bed of 40 t of 2 mm particles in the lower head with temperature 1573K and decay power 200 W/kg in case of 6 bar system pressure, the calculation with 10 bars yielded complete quenching. Understanding is provided by the specific volume of steam. Produced steam in higher system pressure can escape more rapidly due to its lower specific volume. Thus, the coolability increases with increasing system pressure.

The coolability with amounts of dense parts inside the debris bed was also investigated. Such dense ranges at bottom or inside the bed may result from molten parts flowing to the bottom or into the bed, not sufficiently solidified drops sticking together or from melting and relocation processes in a dry region. Such dense regions appear not to be coolable, if the porosity is too low (< 30 %). Superposed layers of very small particles hinder especially water inflow from above and yield significant reduction of coolability especially in 1D configuration (Lindholm et al. [48]). But, in multidimensional configurations regions with higher porosity or with larger particles may give water an easier flow path towards lower bed regions. As shown by the calculations, quenching can even be reached with a rather dense region (low porosity of 0.22) if the region is not too thick (not more than 40 cm). In the calculation, the water inflow to the bottom of the dense region occurs via a region with higher porosity. Thus, water access to bottom regions and resulting steam flow provide sufficient cooling also in a dense region and increase the overall coolability.

For ex-vessel configurations, a large boiling water reactor was considered and a total corium mass of 190 tons was assumed to be discharged from the reactor pressure vessel as a melt jet into the water filled cavity. A deep water pool of 7 m was chosen (7-10 m foreseen in Swedish and Finnish BWR as AMM). Then, the first question is whether the water pool in the cavity is sufficient for breaking up the melt completely, with jet diameters considered as probable for reactor conditions (10-20 cm). JEMI (Pohlner [81]]) calculations showed with the release of a 20 cm diameter jet and 4 m/s initial velocity, that a coherent jet length of about 4.5 m develops which is shorter than the height of the water pool (7 m). Thus, melt jet breakup is complete. Further, the calculation about solidification of the falling drops from breakup indicated that sufficient crust formation occurs until settling to support particulate debris formation on the cavity floor. However, complete quenching of these particles is not achieved until settling. According to the JEMI calculations, the average temperature of the particles when settling is between 1500 and 1700 K. Due to the high temperature of the particles, water boils off completely in the initial phase of settling. As a result, dry and hot debris forms. Quenching of

this hot debris against heat-up due to decay heat is the next challenge and ultimately decisive for the coolability question in such accident scenarios.

Previously, such quenching calculations were only possible for given debris configurations starting from assumed initial temperatures. However, assuming the whole bed at a uniform initial temperature strongly misses the real process in which settling of partly solidified melt drops occurs simultaneously with water inflow and quenching. Therefore, in the frame of this work, the JEMI and MEWA models have been extended to treat the combined process. This combined process of simultaneous quenching during bed formation should strongly favor cooling. To explore this, quenching calculations were performed in one case with an already established debris bed starting from assumed initial temperatures and in the other case with simultaneous quenching during bed formation. In the first case, melting occurred in large parts of the debris bed while simultaneous quenching during bed formation yielded complete quenching with substantial coolability margins, due to the more realistic modeling. Therefore, in order to get a realistic perspective on the quenching processes, i.e. on coolability in reactor scenarios, it is considered as necessary to apply a coupled treatment of bed formation and quenching as provided here with the coupling of JEMI and MEWA. Without consideration of simultaneous quenching during bed formation, i.e. starting with an established debris bed which was usually done in earlier studies, the coolability is significantly underestimated.

In order to sufficiently evaluate the AMM of deep water pools, further major effects on quenching of hot debris i.e. effects of particle size, bed porosity, and shape of the bed were investigated. Results showed that even with the small particles in the size range of 1.8 mm and with 30° angle of repose (high heap of 2.4 m), complete quenching was obtained for a large debris bed of 190 tons with 40% porosity. Partly, melting in the upper region was reached in the case of a bed with very low porosity (30%) or with a rather high heap (angle of repose more than 40 °). However, a very low porosity over the whole bed region or piles of particles in a limited area yielding very high heaps appears not to be realistic. Further, coolability is not finally excluded then, since a small melt pool forming in this region may be stabilized by the water below, i.e. a maintained water flow from bottom around the pool region. Therefore, a strong trend to coolability can be concluded for the deep water case with limited (realistic) vessel whole and resulting jet diameter, in view of the large bed and small particles uniformly assumed.

A problem remains that complete breakup of melt and coolability as a particulate debris bed cannot be achieved for all possible scenarios, even not in the deep water pool concept. With larger vessel breach sizes (thick melt jet), significant parts of melt may not be solidified sufficiently when arriving at the cavity floor. E.g. JEMI calculations showed that with 30 cm jet diameter the developing coherent jet length is longer than the water pool height of 7 m. As a result, about 40% of the melt reaches the bottom without fragmentation. This non-fragmented part may spread on the cavity floor and form a compact layer of corium. With the existing SAM measure i.e. flooding from top only, coolability of such molten layers appears to be highly limited to thin layers. Assuming a solidified state for such layers and calculating steady-state temperature profiles due to conduction, indicated that the melt layers thicker than 10 cm are not coolable in solid state, i.e. by conduction alone, and may yield melt concrete interaction and

basement ablation. Therefore, additional measures and improvements of the melt retention concept would be required in such situations to achieve a stable and coolable state.

A possible improvement could be the injection of water from below via the cavity floor i.e. COMET type concept (Alsmeyer et al. [11]) in which it is considered that the rapid and high volume steam generation at the bottom of the melt will create porosity inside the melt through which water ingression will take place and cool the melt. The COMET concept, i.e. injection of water from below into melt layers to yield quenching via porosity formation, is originally based on a dry cavity, i.e. without flooding of the cavity with water prior to melt release from the RPV. In principle, this concept can be combined with the wet cavity concept in order to bring together advantages of both approaches to cool the melt / debris in the cavity. This was analyzed with the MEWA-COMET model (see Appendix A) considering an idealized configuration for such combined situations, where a liquid melt layer (un-fragmented part) up to a certain height is assumed to exist in the lower part of the debris bed (fragmented and solidified part).

Results of MEWA-COMET calculations performed in this work showed that melt layers penetrating a debris bed of up to 26 cm height (and most likely also higher), can be safely cooled by bottom injection of water. The calculated porosities are in the range of 15 to 30% which are sufficient to quench the melt / debris at about 1834 s. Thus, combining bottom injection, aiming at porosity formation in melt layers, with the wet cavity concept, aiming at particulate debris formation from melt jet breakup, has the potential to improve the core melt cooling and retention capabilities significantly. Bottom injection improves the coolability of particulate debris bed configurations significantly and also provides a backup measure in cases when liquid melt arrives un-fragmented at the cavity floor. However, these results require further confirmation, since the present model may not sufficiently take into account effects acting against the porosity formation like plugging of porosity due to melt freezing in contact with cold particles.

In general, it can be concluded that MEWA is available as a suitable tool for the investigation of coolability in reactor applications. Most important features of the debris cooling dryout and quenching behavior are well captured by MEWA using the improved interfacial friction model. With the coupling of JEMI and MEWA, the quenching of debris can now be evaluated in a realistic way, simultaneously with settling. Applications in reactor conditions highlight the importance of supporting cooling mechanisms, especially the lateral and bottom ingression of water , established in the core region through an intact rod or bypass region, in the lower head through the wall and in the cavity due to the shape (heap) of the bed. These cooling mechanisms together with cooling effects of steam flow through a hot dry zone provide mechanisms to facilitate quenching processes.

7 References

[1] World energy outlook 2012, International Energy Agency (IEA) publications, 9 rue de la Fédération, 75739 Paris, Printed in France by Corlet, November 2012.

[2] A. OMOTO: "Fukushima accident: an overview," International Congress on Advances in Nuclear Power Plants (ICAPP 2011), May 2-5, Nice, France, 2011

[3] R. YOSHIOKA and K. LINO: "Fukushima accident summary", Technical report to Association for the Study of Failure (ASF), August19, 2011.

[4] F. TANABE: "Analysis of Core Melt Accident in Fukushima Daiichi-Unit 1 Nuclear Reactor," J. Nuclear Science and Technology, 48, 1135-1139 (2011).

[5] Fukushima, one year later Initial analyses of the accident and its consequences, Report IRSN/DG/2012-003 of March 12, 2012.

[6] J. M. BROUGHTON, P. KUAN, D. A. PETTI and E. L. TOLMAN: "A Scenario of the TMI-2 Accident," J. Nuclear Technology, Vol. 87, 35-53 (1989).

[7] J. G. KEMENY: "Report of the President's Commission on the Accident on Three Mile Island." Washington, D.C., October, 1979.

[8] M. BUCK: "Modeling of the Late Phase of Core Degradation in Light Water Reactors," PhD Thesis, Institute of Nuclear Technology and Energy Systems (IKE), University of Stuttgart, IKE 2-153, November, 2007.

[9] B. R. SEHGAL: "Nuclear Safety in Light Water Reactors: Severe Accident Phenomenology," Academic Press, Elsevier, Oxford, 2012.

[10] C.C. CHU, J.J. SIENICKE, B.W. SPENCER, W. FRID, G. LÖWENHIELM: "Ex-vessel melt-coolant interactions in deep water pool: studies and accident management for Swedish BWRs," J. Nucl. Eng. Des. 155, 159– 213 (1995).

[11] H. ALSMEYER, G. ALBRECHT, G. FIEG, U. STEGMAIER, W. TROMM, H. WERLE: " Controlling and cooling core melts outside the pressure vessel," J. Nucl. Eng. Des. 202, 269–278 (2000).

[12] H. ALSMEYER and W. TROMM: "Experiments for a core catcher concept based on fragmentation." In: Proceedings of the ARS'94—International, Topical Meeting on Advanced Reactor Safety, April 21–24, Pittsburgh, 1994.

[13] M. BÜRGER, M. BUCK, G. POHLNER , S. RAHMAN , R. KULENOVIC , F. FICHOT , W.M. MA, J. MIETTINEN , I. LINDHOLM , K. ATKEHN : "Coolability of particulate beds in severe accidents: Status and remaining uncertainties," J. Progress in Nuclear Energy, 52 , 61-75 (2010).

[14] N. CHIKHI, N. G. NGUYEN, J. FLEUROT: "Determination of the hydrogen source term during the reflooding of an overheated core: Calculation results of the integral reflood test QUENCH-03 with PWR-type bundle," J. Nucl. Eng. Des. 250, 351-363 (2012).

[15] S. EDERLI, O. COINDREAU, G. BANDINI: "Debris Bed Reflooding Calculations in TMI-2 Core Configuration with ICARE/CATHARE V2.2R1 Code," 4th European Review Meeting on Severe Accident Research (ERMSAR-2010), May 11-12, Bologna (Italy), 2010.

[16] D. W. AKERS, E.R. CARLSON, B.A. COOK: "TMI2 Core Debris Grab Samples, Examination and Analysis." Report GENF-INF- 075, September 1986.

[17] D.W. AKERS and MCCARDELL: “Core Materials Inventory and Behavior.” Nuclear Technology, Vol. 87, 214-223 (1989).

[18] M. BÜRGER, M. BUCK, W. SCHMIDT, G. POHLNER, W. WIDMANN: “Ausbau und Verikation der Spätphasenmodelle und des Gesamtmodels zum Kernschmelzen in KESS und ATHLET-CD.“ Technical report, IKE, Universität Stuttgart, IKE 2-145, Mai 2001.

[19] N. REINKE, T. DRATH, T. V. BERLEPSCH, H.E. UNGER, M.K. KOCH: “Formation, characterization and cooling of debris – scenario discussion with emphasis on TMI-2,” J. Nucl. Eng. Des 236, 1955–1964 (2006).

[20] M. BÜRGER, S.H. CHO, E.v. BERG, A. SCHATZ: “Break-up of Melt Jets as Pre-condition for Premixing:Modeling and Experimental Verification.” Nuclear Engineering and Design 155, 215-251 (1995).

[21] G. POHLNER, Z. VUJIC , M. BÜRGER, G. LOHNERT: “Simulation of melt jet breakup and debris bed formation in water pools with IKEJET/IKEMIX,” J. Nucl. Eng. Des 236, 2026–2048 (2006).

[22] P.T. SPEIS and S. BASU: “Fuel-Coolant Interaction (FCI) Phenomena in Reactor Safety: Current Understanding and Future Research Needs.” In: Proceedings of the OECD/CSNI Specialists Meeting on Fuel-Coolant Interactions, Tokai-Mura, Japan, May 19-24, 1997.

[23] G. FRÖHLICH and H. UNGER: “Investigation of Steam Explosion for Prevention of Severe Accidents in Plants.”Assoc. for Structural Safety and Reliability, pp. 597-601, New York, USA, 1985.

[24] Z. VUJIC: “Improvement and Verification of Steam Explosion Models and Codes for Application to Accident Scenarios in Light Water Reactors,” PhD Thesis, Institute of Nuclear Technology and Energy Systems (IKE), University of Stuttgart, IKE 2-154, December, 2008.

[25] M. SCHRÖDER: “Three-Dimensional Modeling and Simulation of Vapor Explosions In Light Water Reactors,” PhD Thesis, Institute of Nuclear Technology and Energy Systems (IKE), University of Stuttgart, IKE 2-150, August, 2012.

[26] D. MAGALLON: “Formation and Characterisation of Corium Debris Arising From Fuel–Coolant Interaction,” J. Nucl. Eng. and Des. 236, 1998–2009 (2006)

[27] D. MAGALLON and H. HOHMANN: “High Pressure Corium Melt Quenching Tests in FARO.” Nuclear Engineering and Desing, 155, 123-270 (1995).

[28] T. G. THEOFANOUS , C. LIU, S. ADDITON, S. ANGELINI, O. KYMÄLÄINEN, T SALMASSI: “In-vessel Coolability and Retention of Core Melt,” J. Nucl. Eng. and Des. 169, 1-48 (1997).

[29] J.M. SEILER, A. LATROBE, B.R. SEHGAL, H. ALSMEYER , O. KYMÄLÄINEN , B. TURLAND , J.L. GRANGE , M. FISCHER , G. AZARIAN , M. BÜRGER, C.J. CIRAUQUI , A. ZURITA: “Analysis of corium recovery concepts by the EUROCORE group“, Nucl. Eng. Des. 221, 119-136 (2003).

[30] B. R. SEHGAL: “Stabilisation and termination of severe accidents in LWRs“, Nucl. Eng. Des. 236, 1941-1952 (2006).

[31] M. FISCHER : “Main conceptual features of the EPR melt retention concept.” In: Proceedings of the OECD Workshop on Ex-Vessel Debris Coolability, FKK, 15–18 November 1999.

[32] TIAN WAN: “Safety issues of NPP with WWER: research on processes during beyond design basis accidents with core degradation.” In: Proceedings of the Applied Research Workshop, St. Petersburg, 12–14 September 2000.

[33] M. FISCHER, O. HERBST, H. SCHMIDT: “Demonstration of the heat removing capabilities of the EPR core catcher.” Nucl. Eng. Design 235, 1189–1200 (2005).

[34] D. BITTERMANN, U. KRUGMANN, G. AZARIAN: “EPR accident scenarios and provisions,” Nucl. Eng. Des. 207, 49-57 (2001).

[35] W. WIDMANN, M. BÜRGER, G. LOHNERT, H. ALSMEYER, W. TROMM: “Experimental and theoretical investigations on the COMET concept for ex-vessel core melt retention,” J. Nucl. Eng. Des. 236, 2304–2327(2006).

[36] S. K. WANG, C. A. BLOMQUIST, B. W. SPENCER, L. M. MCUMBER, J. P. SCHNEIDER: “Experimental study of the fragmentation and quench behavior of corium melts in water,” J. Transactions of the American Nuclear Society, 60, 26-30 (1989).

[37] B. W. SPENCER, K. WANG, C.A. BLOMQUIST, L.M. MCUMBER, J.P. SCHNEIDER: “Fragmentation and quench behaviour of corium melt streams in water”, NUREG/CR-6133, ANL-93/32, February 1994.

[38] P. KUDINOV, A. KARBOJIAN, C. T.TRAN: “Experimental investigation of melt debris agglomeration with high melting temperature simulant materials,” Proc. of OECD/NEA Workshop on Implementation of Severe Accident Management Measures, October 26-28, Böttstein, Switzerland, 2009.

[39] P. KUDINOV, A. KARBOJIAN, W. M. MA, M. DAVYDOV, T. N. DINH: “A study of ex-vessel debris formation in a LWR severe accident,” Proc. of ICAPP’07, May 13-18, Nice, France, 2007.

[40] A. KARBOJIAN, W. M. MA, P. KUDINOV, T. N. DINH: “A scoping study of debris formation in the DEFOR test facility,” Nucl. Eng. Des., 239, 1653-1659 (2009).

[41] A. KAISER, W. SCHÜTZ, H. WILL: “PREMIX Experiments PM12-PM18 to Investigate the Mixing of a Hot Melt with Water”, Report FZKA 6380, FZ Karlsruhe GmbH, 2001

[42] F. HUBER, A. KAISER, W. SCHÜTZ, H. WILL:“ PREMIX, an experimental approach to investigate the mixing of a hot Melt being poured into water.” Second Int. Conf. On Advanced Reactor Safety, ARS’97, Orlando, USA, June 1-4, 1997.

[43] J. S. MARSHALL and V. K. DHIR:“Effect of overlying liquid layer on dryout heat flux measurements.” Nuclear Science and Engineering, 91,109-113 (1985).

[44] I. CATTON, V. K. DHIR, C.W. SOMERTON:“ An experimental study of debris-bed coolability under pool boiling conditions.”, Technical report, University of California, Los Angeles, 1983.

[45] G.F. STEVENS and R. TRENBERTH: “ Experimental studies of boiling heat transfer and dryout in heat generating particulate beds in water at 1 bar.”, In Proceedings of the Fifth Post Accident Heat Removal Information Exchange Meeting, pages 108-113, Nuclear Research Center Karlsruhe, 1982.

[46] G. HOFMANN: “On the location and mechanisms of dryout in top-fed and bottom-fed particulate beds,” Nucl. Technol 65, 36–45 (1984).

[47] M. RASHID, R. KULENOVIC, E. LAURIEN, A. K. NAYAK: “ Experimental results on the coolability of a debris bed with multidimensional cooling effects,” J. Nucl. Eng. Des., 241, 4537-4543 (2011).

[48] I. LINDHOLM , S. HOLMSTRÖM , M. MIETTINEN , V. LESTINEN ,J. HYVÄRINEN, P. PANKAKOSKI , H. SJÖVALL: "Dryout heat flux experiments with deep heterogeneous particle bed," Nucl. Eng. Des., 236, 2060–2074 (2006).

[49] M. RASHID, R. KULENOVIC, E. LAURIEN: "Experimental results on the coolability of a debris bed with down comer configurations" Nucl. Eng. Des. 249, 104-110 (2012).

[50] P.P. KULKARNI, M. RASHID, R. KULENOVIC, A. K. NAYAK: "Experimental investigation of coolability behaviour of irregularly shaped particulate debris bed," Nucl. Eng. Des., 240, 3067-3077 (2010).

[51] C. ADDABBO, A. ANNUNZIATO, D. MAGALLON: " FARO Test L-24 Quick Look Report." European Commission Joint Research Centre ISPR, Technical Note No. I.97.185, 1997.

[52] R. SILVERII and D. MAGALLON: " FARO LWR Programme Test L-31 Data Report, Technical Note, European Commission Joint Research Centre ISPRA, No.I.99.100, INV-MFCI (99)-D035, 1999.

[53] M. J. KONOVALIKHIN: "Investigation on melt spreading and coolability in a LWR severe accident," PhD thesis of Royal Institute of Technology, Stockholm, November 2001.

[54] V.K. DHIR: " Boiling and two-phase flow in porous media." Annual Review of Heat Transfer, 5: 303-350, CRC Press, Boca Raton, 1994.

[55] M. Kaviany: " Principles of Heat Transfer in Porous Media." Second ed. Springer, New York, 1995.

[56] A. ZEISBERGER, F. MAYINGER: " Heat transport and void fraction in granulated debris." Nuclear Engineering and Design, 236: 2117–2123 (2006).

[57] S. ERGUN: "Fluid Flow Through Packed Columns," J. Chem. Eng. Progress, Vol. 48(No. 29), 89-94, (1952).

[58] L. X. LI, W. M. MA, S. THAKRE : "An experimental study on pressure drop and dryout heat flux of two-phase flow in packed beds of multi-sized and irregular particles," Nucl. Eng. Des. 242, 369–378 (2012).

[59] M.J. KONOVALIKHIN, Z.L. Yang, M. Amjad, B. R. Sehgal: " On dryoutheat flux of a particle debris bed with a downcomer." In: Proceedings of ICONE-8 Conference, Baltimore, USA, April, 2000.

[60] E. TAKASUO, S. HOLMSTRÖM, T. KINNUNEN, P. H. PANKAKOSKI: "The COOLOCE experiments investigating the dryout power in debris beds of heap-like and cylindrical geometries," Nucl. Eng. Des. 250, 687-700 (2012).

[61] N. K. TUTU, T. GINSBERG, J. KLEIN, J. KLAGES, C. E. SCHWARZ: "Debris bed quenching under bottom flood conditions," Brookhaven National Laboratory, NUREG/CR-3850, BNL-NUREG-51788, 1984.

[62] G. REPETTO, T. GARCIN, S. EYMERY, P. MARCH and F. FICHOT: "Experimental program on debris re-flooding (PEARL) results on PRELUDE facility," 14th International Topical Meeting on Nuclear Reactor Thermal Hydraulics (NURETH-14), September 25-29, Toronto, Canada, 2011.

[63] G. REPETTO, T. GARCIN, M. RASHID, R. KULENOVIC, W. M. MA, L. LI: "Investigation of Multidimensional Effects during Debris Cooling," 5th European Review Meeting on Severe Accident Research (ERMSAR-2012), March 21-23, Cologne (Germany), 2012.

[64] M. RASHID, S. RAHMAN, R. KULENOVIC, M. BÜRGER, E. LAURIEN: "Quenching experiments: Coolability of Debris Bed." Nuclear Technology, 181 (1), 208–215 (2013).

[65] P. SCHÄFER, M. GROLL, R. KULENOVIC: "Basic investigations on debris cooling," Nucl. Eng. Des. 236, 2104–2116 (2006).

[66] T. GINSBERG, J. KLEIN, J. KLAGES, Y. SANBORN, C. E. SCHWARZ, J. C. CHEN, L. WIE: "An experimental and analytical investigation of quenching of superheated debris beds under top reflood conditions", Report NUREG/CR-4493, 1986.

[67] D.H. CHO and L. BOVA: "Formation of dry pockets during water penetration into a hot particle bed." Trans. ANS 41, 418-419 (1983).

[68] V. X. TUNG and V. K. DHIR: Quenching of debris beds having variable permeability in the axial and radial directions. Nucl. Eng. Des. 99, 275-284 (1987).

[69] M. BUCK, M. BÜRGER, S. RAHMAN, G. POHLNER: "Validation of the MEWA Model for Quenching of a Severely Damaged Reactor Core," Joint OECD/NEA EC/SARNET2 Workshop on In-Vessel Coolability, October 12 – 14, Paris, France, 2009.

[70] F. FICHOT, F. DUVAL, N. TREGOURES, C. BECHAUD, M. QUINTARD: "The impact of thermal non-equilibrium and large-scale 2D/3D effects on debris bed reflooding and coolability," Nucl. Eng. Des. 236, 2144-2163 (2006).

[71] G. BERTHOUD: "Models and validation of particulate debris coolability with the code MC3D REPO", Nucl. Eng. Des. 236, 2135–2143 (2006).

[72] M. BÜRGER and G. BERTHOUD : "Basic laws and coolability of particulate debris: comments on the status and present contributions", Nuclear Engineering and Design, 236: 2049–2059 (2006).

[73] R. J. LIPINSKI: "A Model for Boiling and Dryout in Particle Beds. Sandia National Laboratories," SAND 82-9765, NUREG/CR-2646, 1982.

[74] A. W. REED: "The effect of channeling on the dryout of heated particulated beds immersed in a liquid pool," PhD Thesis, Massachusetts Institute of Technology, Cambridge, 1982.

[75] K. HU, T. G. THEOFANOUS: "On the measurement of dryout in volumetrically heated coarse particle beds," Int. J. Multiphase Flow 17 (4), 519–532, 1991.

[76] W. SCHMIDT: "Influence of Multidimensionality and Interfacial Friction on the Coolability of Fragmented Corium," PhD Thesis, Institute of Nuclear Technology and Energy Systems (IKE), University of Stuttgart, IKE 2-149, May, 2004.

[77] M. BÜRGER, M. BUCK, W. SCHMIDT, W. WIDMANN : " Validation and application of the WABE Code: Investigations of constitutive laws and 2D effects on debris coolability," Nucl. Eng. Des., 236, 2164-2188 (2006).

[78] N.K. TUTU, T. GINSBERG, J.C. CHEN: "Interfacial drag for two-phase flow through high permeability porous beds", Journal of Heat Transfer, 106, 865-870 (1984).

[79] T. SCHULENBERG , U. MÜLLER: "A refined model for the coolability of core debris with flow entry from the bottom," Proceedings of the Sixth Information Exchange Meeting on Debris Coolability, University of California, Los Angeles, EPRI NP-4455, March, 1986.

[80] V. X. TUNG, V. K. DHIR: "A hydrodynamic model for two-phase flow through porous media," J. Multiphase Flow, Vol. 14 (No. 1), 47–65, 1988.

[81] G. POHLNER: “Modeling of jet breakup and debris bed formation in water pools,” PhD thesis, Institute of Nuclear Technology and Energy Systems (IKE), University of Stuttgart, (in Preparation) 2013.

[82] H.J. ALLELEIN and M. BÜRGER: “Considerations on ex-vessel corium behavior: Scenarios, MCCI and coolability,”J. Nucl. Eng. Des. 236, 2220-2236 (2006).

[83] B.R. SEHGAL: “Accomplishments and challenges of the severe accident research,” J. Nucl. Eng. Des. 210, 79-94 (2001).

[84] C. JOURNEAU, H. ALSMEYER: “Validation of the COMET Bottom-Flooding Core-Catcher with Prototypic Corium,” International Congress on Advances in Nuclear Power Plants (ICAPP 06), June 4-8, Reno, NV, USA, 2006.

[85] K. TRAMBAUER, C. BALS, J. D. SCHUBERT, H. AUSTREGESILO : “Weiterentwicklung des Rechenprogrammsystems ATHLET/ATHLET-CD.”, Report Gesellschaft für Anlagen- und Reaktorsicherheit (GRS), GRS-A-3215, 2004.

[86] W. ROHSENOW: “A method of correlating heat transfer data for surface boiling of liquids,” Trans. ASME 74, 969–976 (1952).

[87] J. H. LIENHARD: “A Heat Transfer Textbook,” 2nd ed. Prentice-Hall, Englewood Cliffs, NJ, 1987.

[88] D. HAGA, Y. NIIBORI and T. CHIDA: “Tracer responses in gas-liquid two-phase flow through porous media,” Proceeding of the World Geothermal Congress, Kyushu, Tohoku, Japan, 2000.

[89] T. STÜRZEL: “Ultraschnelle Röntgen Tomographie zur Untersuchung Zweiphasiger Strömung in Porösen Medium”, PhD Thesis, Institute of Nuclear Technology and Energy Systems (IKE), IKE 8-118, University of Stuttgart, 2013.

[90] S. V. PATANKAR:“Numerical Heat Transfer and Fluid Flow”, Hemisphere Publishing Corporation, New York, 1980.

[91] E. TAKASUO , S. HOLMSTRÖM , T. KINNUNEN , P.H. PANKAKOSKI , V. HOVI , M. ILVONEN , S. RAHMAN , M. BÜRGER , M. BUCK , G. POHLNER: “Experimental and Computational Studies of the Coolability of Heap-like and Cylindrical Debris Beds”, 5th European Review Meeting on Severe Accident Research (ERMSAR-2012), Cologne (Germany), March 21-23, 2012

[92] W. C. MÜLLER: “Review of debris bed cooling in the TMI-2 accident”, Nuclear Engineering and Design, 236: 1965–1975 (2006).

[93] K. WAY and E. P. WIGNER: "The Rate of Decay of Fission Products", in: Physical Review 73, 1318–1330 (1948)

[94] A. MEHTA and G. C. BARKER: “The dynamics of sand,” J. Rep. Prog. Phys. 57, 383-416 (1994).

[95] S. LOMPERSKI, M. T. FARMER, S. BASU: “Experimental investigation of corium quenching at elevated pressure”, Nucl. Eng. Des. 236, 2271-2280 (2006).

[96] B. R. SEHGAL, A. GIRI, U. CHIKKANAGOUDAR, A. KARBOJIAN: “Experiments on in-vessel melt coolability in the EC-FOREVER Program“, Nucl. Eng. Des. 236, 2199-2210 (2006).

A Porosity formation model and its validation

A.1 Porosity formation model

A special model, MEWA-COMET is also included in the MEWA code to simulate the processes occurring during bottom injection of water into a melt layer for situations where melt breakup and quenching until settling of debris is not sufficient to avoid molten parts in the bed.

The crucial process for a successful cooling in the COMET concept is sufficient breakup of the compact corium layer and the formation of a porous structure. Widmann et al. [35] introduced a model to describe the process of porosity formation inside the melt. In this model it is assumed that porosity inside the melt is created due to local pressure buildup with resulting expansion. This is primarily caused by strong evaporation resulting from water injection from the bottom. The restriction of vertical steam removal by friction in the melt then yields a strong local pressure buildup which also produces lateral motion of steam and water and lateral porosity formation. Thus, local porosity formation can be considered as being linked to local pressure buildup in a matrix of low porosity, due to evaporation and resulting flow of steam and water. Finally, porosities can only be stabilized by solidification, linked to water inflow and resulting sufficiently strong heat transfer. Rapid evaporation with resulting pressure buildup, driving porosity formation and water into extended regions, and combined rapid heat transfer are the basis of porosity formation and fixing porosities by solidification.

A heuristic formula approach for a coupling between local pressure buildup (beyond the local surrounding pressure) and a porosity formation rate is presently applied in MEWA. A local porosity production due to the increased pressure is assumed if the local steam pressure is higher than the local static pressure of the melt. For this production rate, the following correlation as proposed by [35] is presently used

$$\frac{d\varepsilon}{dt} = \frac{A}{\mu_M} \cdot \left(p_g - p_M\right) \cdot \frac{\left|\nabla p_g\right|}{\rho_M g} \cdot \varepsilon^{2/3} \tag{A.1}$$

with p_g = gas pressure, p_M = melt pressure, ρ_M = melt density, g = gravity, ε = porosity, t = time, μ_M = dynamic viscosity of melt. A is an adaptation parameter which has been fixed by comparison with COMET-T experiments (Alsmeyer and Tromm[12]) and has a value of 1×10^{-6}. This approach is based on considerations about steam expansion due to the pressure difference of steam and surroundings, required gradient of pressure between neighboring steam regions and counter- effects by viscosity of the melt as well as buoyancy. Calculations start with an initial matrix of small porosity (typically 0.05) which in principle represents the resistance of an initially compact liquid melt against injection of water and steam expansion and flow processes. The increased pressure then leads to porosity formation which should finally be essentially independent of the initial porosity assumption. The matrix is changed during the calculation accordingly. Corresponding to the total increased (or decreased) porosity, the height of the melt layer is increased (or decreased). The temperature development is calculated for the matrix in MEWA. Hereby, the freezing enthalpy is taken into account between liquidus and solidus

temperature. Quasi freezing of porosity formation is determined in the above law by the increase of melt viscosity between liquidus and solidus.

A.2 Validation of the porosity formation model

A.2.1 Important aspects for the validation of the porosity formation model

Local pressure buildup due to strong evaporation resulting from water injection from the bottom and restriction of up-flow of steam by friction is considered as basic process for porosity formation. Presently, a heuristic formula approach for a coupling between local pressure buildup (beyond the local surrounding pressure) and a local porosity formation rate is applied. The local pressure buildup is determined depending on the porosity development by means of the two-phase description of water and steam flows in MEWA including heat transfer and friction as depending on the conditions. An important point in validation is then to reproduce with the model the major processes observed in experiments, notably the strong initial evaporation with resulting pressure buildup, driving porosity formation and water into extended regions, fast cooldown and freezing of porosities by solidification etc.

Within the validation process, MEWA-COMET was especially applied to the COMET experiments of former FZK [12], now KIT (Karlsruhe Institute of Technology), but also an application to an experiment with real core melt has been done, the VULCANO VN-U1 experiment (Journeau et al. [84]). An emphasis concerning COMET-T experiments with simulant materials lay on checking weather major features observed experimentally as initially complete evaporation of injected water, high steam flow at top and lateral porosity formation can be reproduced and understood by the model. VULCANO VN-U1 experiment then yields especially a check weather a quantitative extrapolation to reactor conditions is justified with the model

A.2.2 Validation against experiments performed with corium simulant melt

The COMET-T [12] experiments used around 60 kg of AL2O3 / CaO melt and 5 inlets for water injection from bottom. These basic, transient tests (without decay heat simulation) concern the original COMET concept with an array of plastic tubes provided with water via a lower water filled gap. Initial data are a melt temperature of about 2000 K, melt height of 50 cm, diameter of the melt area 25 cm and water overpressure at bottom of 0.2 bar (above system pressure of 1 bar + hydraulic head of melt). The inlet nozzle diameter is 1 cm.

For the calculation, a representative area around a single inlet nozzle was chosen, in order to be able to simulate the processes in 2D cylindrical geometry. This area corresponds to an equivalent radius of 5.5 cm around one inlet nozzle.

The major experimental features are rapid lateral progression of water in the bottom range of the melt layer, strong evaporation to yield high steam flow rates in the upper ranges and subsequent progression of water through the upper porous ranges with start of solidification. These features are clearly captured by the model as shown by the calculation results presented in Figure A.1. Figure A.1 shows the results of the MEWA-COMET calculation for porosity (top), water fraction (middle) and temperature development (bottom).

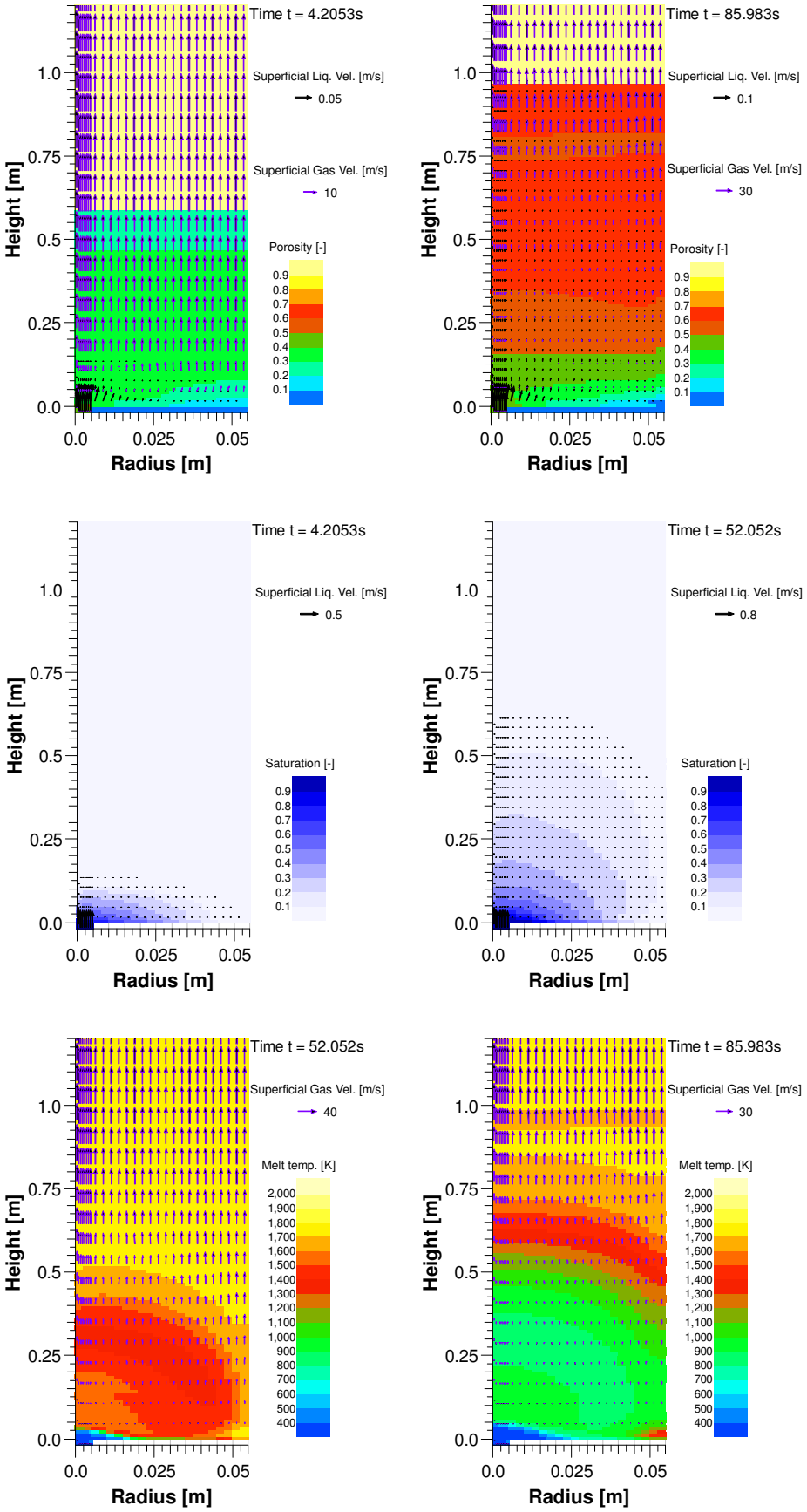

Figure A.1: COMET-T8.6 calculation results for porosity (top), water fraction (middle) and temperature development (bottom).

Firstly the porosity field after 4 s shows that in the bottom region a porosity of 30% has already been formed, uniformly in lateral direction. It indicates that water flows laterally in the lower region due to pressure build up from strong evaporation. Thus, supports the uniform steam upflow over the whole cross section. While the porosity in the lower region is formed due to influence of inflowing water and evaporation, the porosity in the upper region is due to steam flow. This can clearly been seen in the porosity and water fraction (saturation) fields as well as the water and steam velocity fields in Figure A.1. These porosities can only be stabilized by solidification which is linked to water inflow and resulting sufficiently strong heat transfer.

Following the development of the calculation, it can be seen that water progresses further upwards and comes directly in contact with the partly still liquid melt. Thus, the interaction region of porosity formation progresses upwards or at least fixes the porosities by solidification. The results at 52 s (saturation and temperature field) show that water volume parts of about 30% has reached nearly the original height of layer of 50 cm. This is combined with a temperature decrease below the solidus temperature of 1700K. Thus, porosity formation has stopped there but not the evaporation.

The final fixed porosities inside the melt are shown in the porosity distribution field at about 86 s in Figure A.1. The calculated porosities of 50-65% are in good agreement with the experimental result (~50%).The calculated time after which first water reaches the top surface of the melt (~ 86 s) is rather well in agreement with the experimentally given time of about 70 s. At this time, the porosities are already essentially fixed by solidification (see temperature field), as also concluded from the experiment.

Reasonable agreement between the calculation and the experimental result is also obtained concerning the steam outflow rates (evaporation rates), as shown in Figure A.2, also for COMET T8.4. In the latter, a higher overpressure of 0.4 bar was applied which yields a somewhat increased maximum evaporation rate and slightly more rapid quenching, in principle as in the experiments

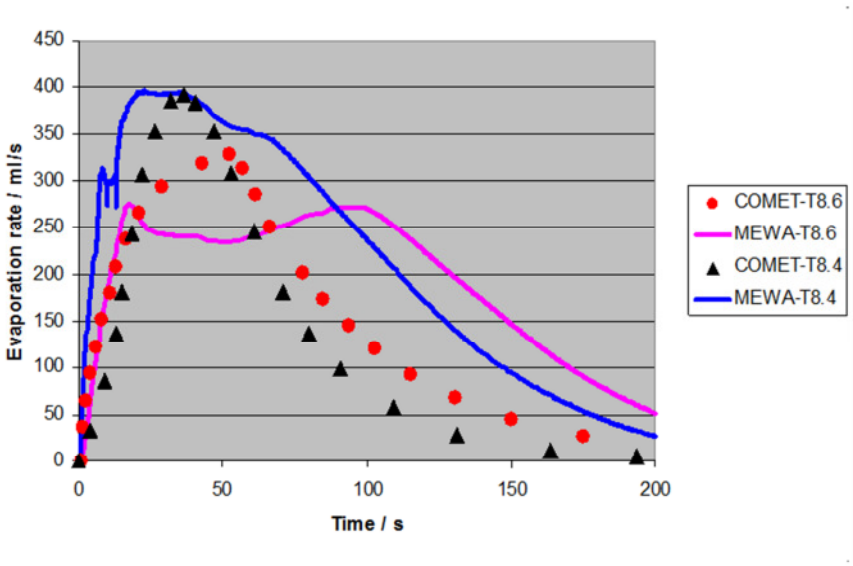

Figure A.2: Development of the rate of evaporated water in COMET-T8.4 and COMET-T8.6 (solid lines: MEWA calculations, points: experiments); results for total number of 5 inlet channels.

A.2.3 Validation against experiments performed with corium melt

The VULCANO VW-U1 experiment has been performed at CEA (Commissariat à l'Energie Atomique, France) to validate the COMET PCA concept (using porous concrete for water inflow) with prototypic corium melt [84]. In this experiment, approximately 40 kg melt (UO2+ZrO2+molten concrete) have been poured into the COMET cooling device at an initial temperature above 2000K. After erosion of the sacrificial concrete layer the bottom flooding was established. The melt was safely arrested, solidified and quenched within approximately 20 minutes.

The MEWA-COMET code is applied to the VULCANOA VW-U1 experiment in order to verify its applicability and to promote better understanding of the experimental results. A planar approach has been used for calculations with the 2D code MEWA-COMET. This approach has been chosen here since the porous inlet are not axially symmetric. Therefore, arrangement should be represented to yield the total mass fluxes. The areas of total inflow (porous inlets) and of melt layer have been taken into account adequately. Figure A.3 shows the geometrical representation and numerical mesh of the experiment in the calculations, with the initial porosity distribution. Inflow of water into the porous concrete layer is in the calculation assumed at bottom. This is in line with the injection inlets towards the melt in this planar approach. The distribution of water towards these injection inlets made of porous concrete occurs via the bottom concrete layer.

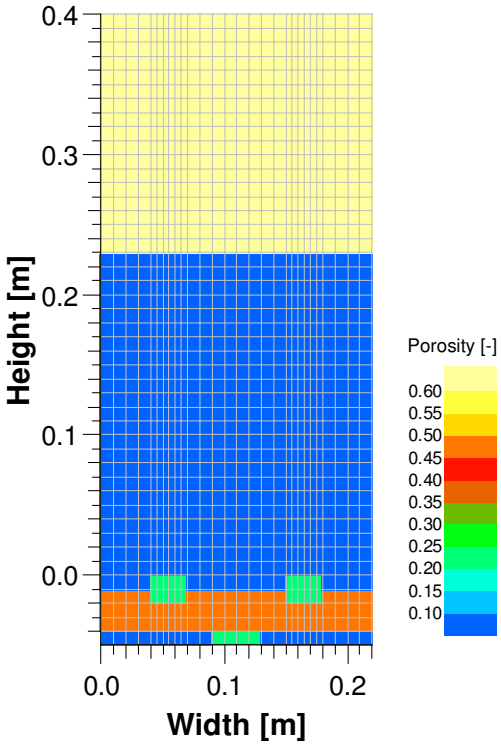

Figure A.3: Geometrical representation of the VULCANO VW-U1 experiment in the MEWA-COMET calculations; initial porosity distribution and nodalisation for plane 2D- case.

As given from the experiment, an initial melt height of 22 cm is assumed and an injection overpressure of 0.1 bar, i.e. about 1.2 bar absolute pressure in the inflow region.

Results of calculations with MEWA-COMET on the VULCANOA VW-U1 experiment are shown in Figure A.4 concerning porosity formation and temperature development as well as the water and steam flow patterns. The calculated porosities are in the range of 35-50% which is smaller than in the above mentioned COMET-T experiments. Nevertheless, rapid cooling still occurs, supported by the lateral distribution of porosities. After 563 s of water inflow as shown in Figure A.4 the porosities are already fixed and solidified but at this time some parts of solid melt where the distance to the injection nozzle is large still maintain with higher temperature (but less than solidus temperature of 1773 K) which ultimately are cooled by water flow from the surroundings and also by conduction

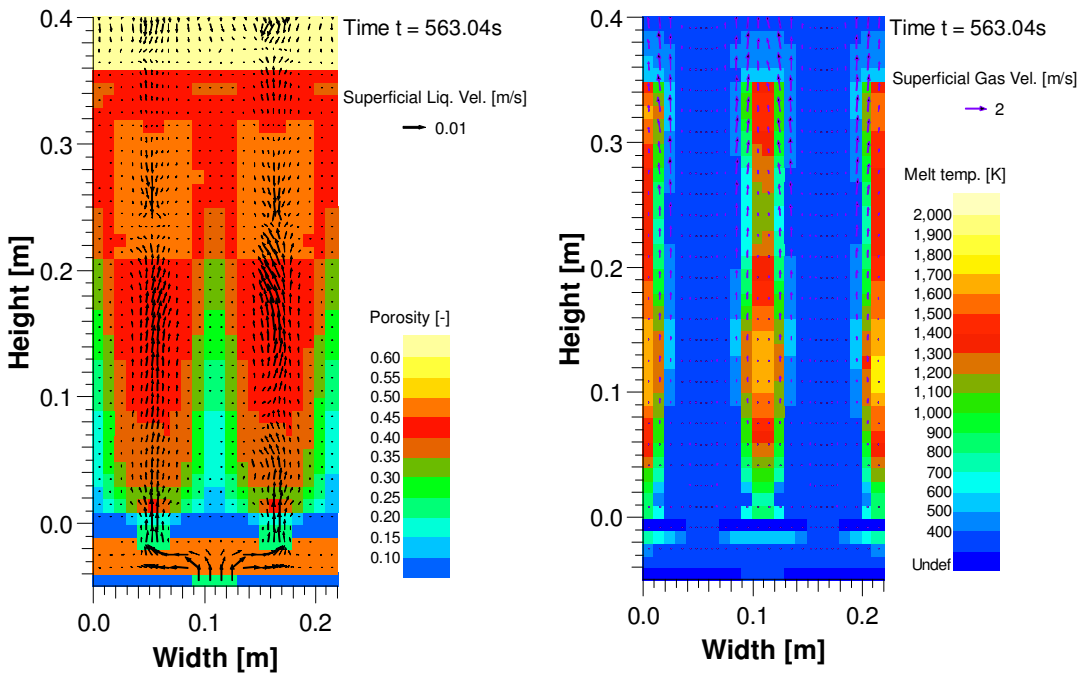

Figure A.4: Porosity (left) and temperature (right) distribution as well as liquid and vapor velocities calculated with MEWA-COMET after 563 s for the VULCANO VW-U1 experiment.

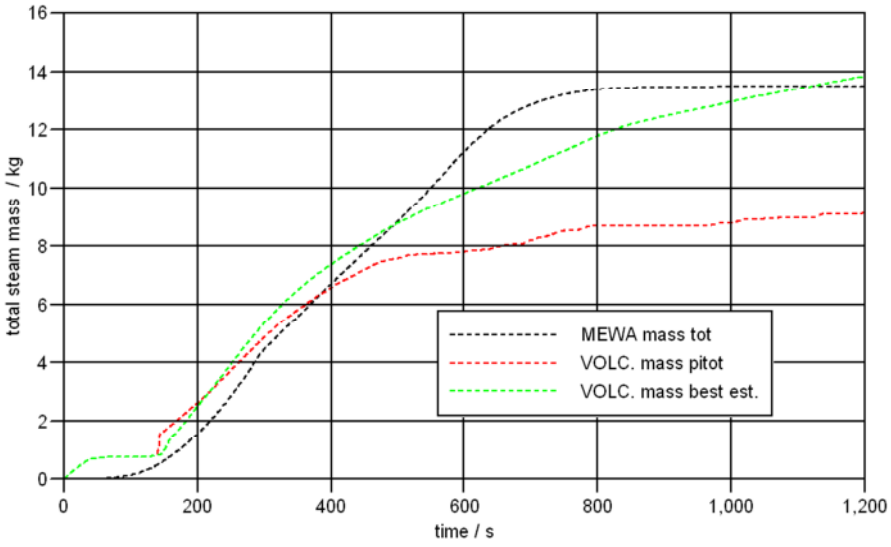

Figure A.5: Comparison of calculated and measured total steam mass for the VULCANOA VW-U1 experiment.

Figure A.5 shows a comparison for the total evaporated steam mass: the red line from a measurement, the green one as a best estimate from experiment. The black line shows the result of the MEWA-COMET calculation. The calculated steam mass development is well within the range of the experimental one.

The successful reproduction of main features and quantitative results of COMET-T experiments supports the understanding of the major processes observed in the experiments, especially the strong initial evaporation, intensive mixing, fast cooldown and freezing of porosities. The amounts and time-scales of porosity formation in melt layers are adequately calculated, especially, the rapid lateral extension of porosity formation in lower regions is reproduced. Good agreement is also obtained with experimental measurements and timing, e.g. concerning water arrival at top, total steam flux etc.

With the same modeling and parameters also the results of the COMET-VULCANO experiment are rather well met. The short quenching times from the experiment as well as the calculation support the present understanding of the underlying physical mechanisms. In view of the complexity of processes, the comparison is quite promising also concerning the quantitative results. This supports the extrapolation capabilities of the model. Since parameters have been adapted to COMET-T experiments and have not been changed for the present application, the results also support this application with extrapolation to different material (corium) as well as to the modified concept (COMET-PCA) using porous concrete for water inflow. Application to reactor scenarios is also encouraged by this.

Acknowledgements

Foremost, I would like to thank most sincerely Manfred Bürger for his continuous and patient support during my PhD study and research at IKE. His guidance helped me in all the time of research and writing of this thesis. He encouraged me to think independently, to see globally and to identify the problem. The experience he shared with me was paramount and I could not have imagined having a better advisor and mentor for my PhD study.

I would also like to express my deepest gratitude to my advisor Professor Eckart Laurien. It has definitely been his invaluable advice, support and encouragement that helped me to accomplish the objective of this study. His broad knowledge provided me with a technical insight and a practical view of the problem. Our discussions were always fruitful and stimulating in advancing my knowledge in the nuclear field. My sincere thanks are extended to Professor Manfred Piesche, my co-advisor, for his interest in my work, his advice and comments.

I am very grateful to Michael Buck, his constant assistance, precious advice and efforts helped me to improve my critical thinking, research methodology and understanding of different numerical challenges. I am also very grateful for the friendly help of Georg Pohlner, with whom I worked closely in resolving many problems.

I would like to convey my heartfelt thanks to my parents for their everlasting love and constant encouragement. Finally and most importantly, I would like to thank my beloved wife Rafat for her patience support during my graduate studies.

Stuttgart, in November 2013

Saidur Rahman